The University Of Sheffield.

Mechanisms of Endosomal Permeability:

A route to enhancing delivery of endocytosed therapeutics

By:

Patrick Shire

A thesis submitted in partial fulfilment of the requirements for the degree of Doctor of Philosophy

The University of Sheffield

Faculty of Science

Department of Biomedical Sciences

January 2021

Abstract

One of the rate-limiting steps for the cytosolic delivery of endocytosed therapeutics is endosomal escape. An increase in endosomal release would increase the therapeutic output of current therapeutics, as well as allowing the use of novel therapeutics that currently cannot be successfully delivered to the correct cellular location. The cellular mechanisms involved in maintaining endosomal integrity and endosomal release are not fully understood and our work here aims to increase our understanding of endosomal release.

During this study I have investigated the mechanisms of endosomal permeability and have identified several novel proteins that are involved in endosomal permeability. We developed and optimised an endosomal release assay in order to perform a kinome wide siRNA interference screen to identify effectors of endosomal release. We were able to identify several proteins that increased endosomal release indicating their involved in maintaining endosomal integrity. We performed a follow up screen using a previously validated LNP uptake assay and were able to identify three proteins (Irak-M, MAP2K5 and Peak1) that consistently increased endosomal release in all the screens performed. We were able to validate these identified hits using alternative siRNA, pharmacological inhibitors and qPCR to confirm the siRNA knockdown efficiency.

After identification of the proteins effecting endosomal release, we attempt to identify a signalling pathway the hits are involved in. We were able to implement the NF-kB signalling pathway as being involved in the endosomal release we observed. We could show the knockdown of our identified hits using siRNA has an effect on the activation of the NF-kB signalling pathway. We speculate on the possible implications of NF-kB signalling in endosomal release and try to elucidate a mechanism of action.

Table of contents

List of Figures

List of Tables

Abbreviations

AAV	Adeno-associated viruses (AAVs)
APC	Anaphase-promoting complex
BSA	Bovine serum albumin
CDRs	Circular dorsal ruffles
CME	Clathrin-mediated endocytosis
CPP	Cell penetrating peptides
Ctbp-1	C-terminal binding protein-1
Da	Dalton
DAB	Diaminobenzidine
DNA	Deoxyribonucleic acid
DOPE	Dioleoylphosphatidylethanolamine
ECS	Elongin BC- Cullin-SOCS-box protein
ECT2	Epithelial cell transforming sequence2
EEA1	Early endosome antigen
EGF	Epidermal growth factor
EGFR	Epidermal growth factor receptor
EIPA	Ethyl-isopropyl amiloride
ERAD	Endoplasmic reticulum assisted degradation
FDA	Federal drug agency
FITC	Fluorescein isothiocyanate
GAPs	GTPase activating proteins
GEFs	Guanine nucleotide exchange factors
GFP	Green fluorescent protein
GILT	Gamma-interferon-inducible lysosomal thiolreductase
GPCRs	G-protein coupled receptors
GTP	Guanosine triphosphate
HIV	Human immunodeficiency virus
HRP	Horse radish peroxidase

IkB	Inhibitor of nuclear factor-kappa B
iNOS	Inducible nitric oxide synthase
LLOMe	L-leucyl-L-leucine methyl ester
LNPs	Lipid nano-particles
MC3-LNP	MC3-Lipid nanoparticle
M-CSF	Macrophage-colony-stimulating factor
MHCI	Major histocompatibility complex 1
MHCII	Major histocompatibility complex 2
mi-RNA	micro-RNA
mRNA	messenger ribonucleic acid
MTMR3	Myotubularin-related protein-3
MTMR4	Myotubularin-related protein-4
NFkB1	p50/p105
NF-kB2	p52/p100
NLS	Nuclear localisation signal
NS	No stimulation/unstimulated
NT	Non-targeting siRNA
OTP	On target plus
PEG	poly(ethyleneglycol)-lipid
PEI	Polyethylenimine
PFA	Paraformaldehyde
PI3K	Phosphoinositide-3 kinase
PIP(3)P	Phosphoinositide-3-phosphate
PIP(4,5)P2	Phosphoinositide-3,4-bisphosphate
PI(3,4,5)P3	Phosphoinositide-3,4,5-trisphosphate
PKC	Protein kinase C
PKCRA	Alpha subunit of PKC
Plk1	Polo like kinase-1
PMA	Phorbol 12-myristate 13-acetate
PTD	Protein translocation domain
PtdIns	Phosphoinositide
RelA	p65

RNA	Ribonucleic acid
RNAi	RNA interference
ROS	Reactive oxygen species
SCF	SKP,Cullin, F-box containing complex
siRNA	small interfering RNA
TAT	Trans activator
TLR	Toll-like receptor
TNF-alpha	Tumour necrosis factor
WASH	Wiskott-aldrich and SCAR homology

Chapter1: Introduction

The internalisation of material into a cell is termed endocytosis and plays an important role in many processes and pathways vital to cell survival. Endocytosis allows the uptake of numerous cargo types by utilising multiple different uptake mechanisms. Ligand activation of a cell surface receptor can trigger internalisation via receptor driven endocytosis or bulk endocytosis can internalise non-specific fluid phase material in large quantities from outside the cell (1,2). There is scientific interest in the regulation of endocytosis as well as the stages after internalisation has occurred. Endocytosed material enters the endosomal system, a series of membrane bound organelles, where cargo sorting can occur in order to regulate internalised material(3).

As endocytosis is the cellular entry mechanism for biological molecules it can be co-opted to aid the delivery of therapeutic molecules. A challenge for designing biologically active therapeutic molecules is the correct delivery at a cellular level. The majority of biological processes occurs either in the cellular cytosol or in membrane bound organelles and therefore usually the transport across the lipid membrane is required before a molecule can function correctly (1). Historically, the molecules utilised as pharmacological compounds were small and had hydrophobic interactions which allowed simple diffusion across the membrane to the correct location (4). To increase the effectiveness of treatments, a wide range of alternative molecules are currently being used as therapeutics, however this introduces the challenge of their correct delivery. Many of these promising therapeutics are large and hydrophilic which prevents passive transport across the lipid membrane (5) . As endocytosis is the cellular internalisation route of native proteins it is an attractive target for delivery of these therapeutic molecules into cells. However, the endosomal system is heavily regulated as internalised proteins require sorting, recycling and potentially degradation in the lysosome. A very small amount of material is released from the endosomal system and a large amount of endocytosed therapeutics are degraded before they can correctly function (6) (Figure1.01).

Our understanding of endosomal release is currently limited, however if we could increase the amount of endocytosed therapeutics being delivered to the cytosol, this would increase the therapeutic output of endocytosed therapeutics, allow the use of additional molecules as therapeutics and decrease the concentration required, which in turn would decrease observed side effects and increase safety. In this project we focus on increasing our understanding of proteins and biological pathways involved in increasing endosomal

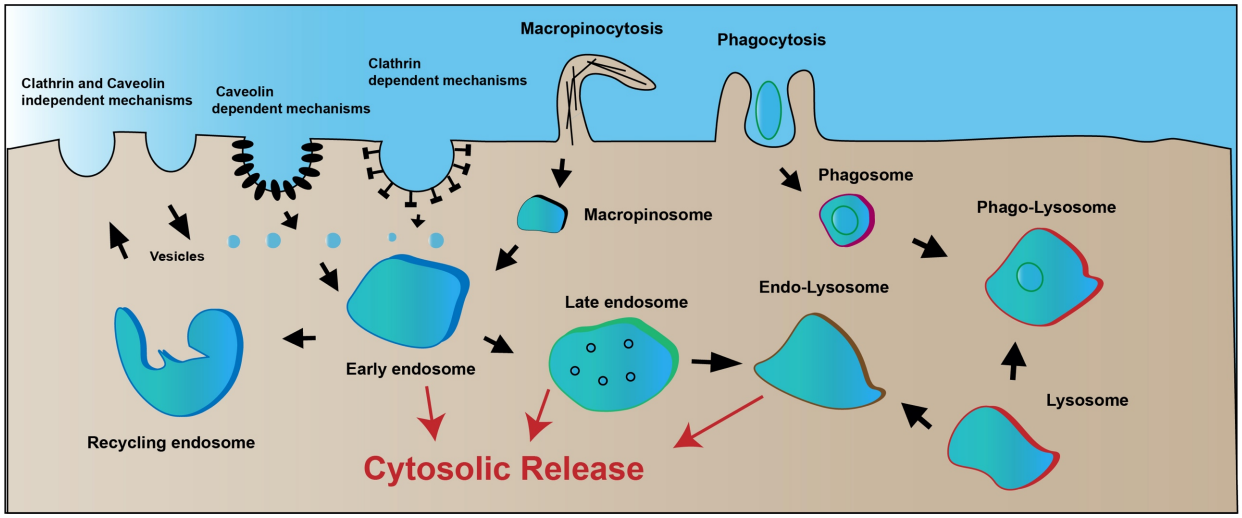

Figure 1.01: A schematic of the endosomal system showing endosomal release of content to the cytosol

permeability that could be utilised in the future to increase the delivery of endocytosed therapeutics.

1.1 Current therapeutic approaches

One method to identify novel therapeutic molecules is high-content screening of compound libraries using a phenotypic assay that is representative of the disease (7), enabling identification of a therapeutics that have a positive effect on disease progression. As our understanding of biological processes involved in disease has increased the use of designed therapeutics to target known proteins has become easier and an effective way at developing novel therapeutics. Both approaches are valid ways of identifying new therapeutics and both methods have benefits as well as limitations. However, the need to target specific proteins in designed therapeutics has increased the diversity of molecules utilized as potential drug candidates.

As a result, current therapeutic approaches utilise a wide range of different types of therapeutic molecules ranging from small molecules to large macromolecules including

antibodies. The chemical and physical properties of a therapeutic determine its ability for cellular uptake and delivery (8–10). Small, hydrophobic molecules can passively diffuse across the lipid bilayer surrounding the cell (11) whereas larger, hydrophilic molecules require a delivery mechanism.

1.1.1 Small molecule inhibitors

The identification of small molecule inhibitors to target proteins has been the traditional way of developing novel therapeutic molecules(7). Small molecule inhibitors are able to diffuse across the cell membrane due to their small size (4,12), allowing the targeting of intracellular proteins. Additionally, many biological systems rely on small molecule interactions with proteins such as receptor agonists and enzyme binding sites. A small molecule inhibitor can be used as a competitive inhibitor in these biological systems as an agonist or antagonist of protein function. With current techniques the development of novel small molecule therapeutics is relatively straightforward by generating libraries of compounds similar to current therapeutic molecules that can be screened for action against new targets. Additional rounds of modification of chemical structures can increase the specificity to a particular target. This same method can be utilised with large chemical library screens using phenotypic assays to identify potential therapeutics. However, the large-scale screening is expensive, and generation of successful targets relies on an appropriate binding site for the small molecule inhibitor. To generate high affinity and specificity the therapeutic molecule has to selectively bind to the target with a dissociation constant (Kd) in the nanomolar region (4). To achieve this level of binding the small molecule usually has to bind in a pocket or groove on the protein to have sufficient contacts that enable this strong interaction(13). Additionally, the specificity of the small molecule depends on the unique binding region on the protein of interest. This limits the use of small molecule inhibitors to proteins with binding pockets that will inhibit function, preventing a large number of proteins being inhibited by small molecules.

As well as being limited by the need for a binding pocket, small molecule inhibitors are not very effective at inhibiting the interaction between different protein due to their small size.
It is becoming more apparent the interaction of proteins is important for the progression of many diseases and can be more effective than inhibition of a target protein (14). As small

molecules are more effective against proteins with defined binding pockets, this limits the types of proteins that can currently be inhibited. A study concluded that currently, we can theoretically target between 10-14% of proteins using small-molecule inhibitors (15). The majority of the druggable proteins are limited to G-protein coupled receptors (GPCRs), protein kinases and proteases etc which highlights the limited proteins that small molecules can inhibit. Although improved delivery mechanisms and the availability of more protein structures will increase the percentage of proteins that can be inhibited using small molecules, this analysis does highlight the requirement for alternative therapeutic molecules to be available to target a more diverse range of proteins and protein-protein interactions more easily (15).

1.1.2 Therapeutic antibodies

Therapeutic antibodies offer an alternative therapeutic approach. Antibodies are proteins produced during an immune response to target a specific antigen sequence. We are able to generate an antibody that can recognise an antigen with high specificity and affinity. Currently we can generate antibodies against many targets, meaning there is large potential to inhibit many different proteins identified to be involved in disease pathogenesis.

As antibodies are also used extensively for research and diagnosis purposes the technology for antibody production is well-developed. The specificity of antibodies has been used extensively in research, but the use of therapeutic antibodies is increasing (16).

The main challenge facing therapeutic antibodies was immunogenicity as a result of the antibody production method in animal cells (17). After increased understanding of antibody structure and encoding gene sequence the process of humanisation allowed the production of antibodies with decreased immunogenicity and related side effects (17,18). This allowed the development of many therapeutic antibodies that are currently on the market today, targeting a wide range of diseases including many involved in cancer treatment. The number of therapeutic antibodies approved by the FDA and European medicines agency on the market is currently >80 (16,19). The highest sale figure ever for a biopharmaceutical product was achieved by Adalimumab (Humira) an antibody targeting TNF-alpha (16). The current

market highlights the usefulness of antibodies as therapeutics and how successful they currently are. However, there are still challenges with the use of antibodies as therapeutics which need to be overcome before antibodies can be used to their full potential. One of the main challenges is access to target intracellular proteins. Due to the large size and hydrophilic nature of antibody molecules they cannot passively diffuse into the cell unlike small molecule inhibitors. This limits the use of therapeutic antibodies to extracellular proteins with the majority targeting transmembrane receptors (20,21). The inability of therapeutic antibodies to target cellular proteins reduces the scope of diseases they can be used to target. If the delivery of sufficient quantities of therapeutic antibodies to the cytosol could be achieved, a wider range of protein targets would become available.

Antibodies can be targeted to receptors and be internalised into the endocytic system but they normally remain trapped, enter lysosomes for degradation or are recycled back to the plasma membrane (22,23). Cytoplasmic delivery through endosomal structures is very inefficient(24,25). If a mechanism of improving the delivery of antibodies to the cytosol could be found, then antibodies could potentially be targeted against intracellular proteins.

The use of therapeutic antibodies would allow the design of novel therapeutics to target specific proteins of interest known to affect disease progression, with high affinity and specificity. There are still other limitations of therapeutic antibodies such as the targeting of antibodies to the correct location in the body and tissue penetration due to their large size however there is ongoing work on reducing the size of the antibodies to overcome these problems(26). Genetic engineering of antibodies to produce antibody fragments that retain the ability to bind protein targets effectively are currently being developed (26).

To demonstrate the efficacy of intracellular delivery of therapeutic antibodies the intracellular expression of antibodies, termed intrabodies has allowed evaluation of effectiveness(26). The intrabodies can be targeted to compartments such as the endoplasmic reticulum or to the cytosol after production inside the cell and can therefore target intracellular proteins and pathways. Intrabodies have been shown to function i*n vitro* via transformation of the cells using expression vectors (26). An example of the therapeutic potential of intrabodies is the inhibition of oncogenic Ras proteins. The Ras family are difficult

to inhibit using conventional small molecular inhibitors due to their high affinity for GTP and lack of deep binding pockets (27,28), however an intrabody targeting Ras was shown to block Ras activation by preventing an important protein-protein interaction (29). The direct use of intrabodies as effective treatments would require gene therapy approaches and delivery of genetic material to cells. The use of genetic modification increases risk associated with off-target effects and has stringent safety regulations (26).

Intrabodies have been shown to be effective at targeting intracellular targets when cells have been transfected. If the delivery of antibodies to the cytosol after endocytosis could be increased to sufficient levels, intrabodies provide evidence that cytosolic antibodies can effectively target proteins and provide therapeutic output (30).

1.1.3 Therapeutic RNA

The nucleic acid sequences in cells control the building blocks of cellular function. The therapeutic molecules mentioned above manipulate the function of proteins involved in disease progression. If the levels of disease-causing proteins could be manipulated at a genetic level, this enables nearly unlimited ability to produce a therapeutic output (31). However, with this powerful tool there are potential risks associated with the manipulation of nucleic acids. The largest risk is long-term changes to the genetic code resulting in unexpected side-effects, especially in germline cells (32). Gene therapy is used to remove a faulty gene in exchange for a functional copy and is mainly performed using a viral vector. The change to the DNA sequence results, especially in stem cells, to long-term therapeutic outcome which is attractive as a therapeutic treatment (33). Gene therapy is a powerful tool but the risks associated with manipulation of the genome means extensive testing is required on gene therapy treatments, potential side effects are dangerous and targeting the correct cells is vital for treatment (33). A different approach to the manipulation of proteins at a genetic level is through the use of therapeutic RNAs (31). In the cell there are two main forms of nucleic acid molecules, DNA and RNA. As mentioned, manipulation of the DNA sequences results in long-term effects, but this increases the risks associated with the treatment. The RNA molecules in cells have a shorter half-life and control the cell through protein expression. The messenger RNA (mRNA) are used in translation of proteins and changes in mRNA levels change the abundance of the protein produced. As a therapeutic, addition of mRNA to a cell

could transiently increase the expression of a protein. Additional functions for RNA were discovered when a micro-RNA (miRNA), called lin-4, was shown to regulate developmental timing in the model organism Caenorhabditis elegans by complementary binding to mRNA (34,35). It was later discovered that exogenous double stranded RNA could regulate RNA levels in cells and was called RNAi (RNA interference) (36). A model was established where miRNA regulated RNA in a cell from endogenously produced double stranded RNA whereas small interfering RNA (siRNA) from exogenous sources such as viruses and transposons regulated genome stability by using foreign RNA to interfere with invading genetic material (35). Both types of interfering RNAi use the same pathway for processing the double stranded RNA. A protein called DICER (37) processes the double stranded DNA to a single strand which then associates into a protein complex called the RISC complex (38). This complex can use the Watson-Crick base pairing of the associated single stranded RNA to target complementary RNA for degradation. The identification of the RISC-complex allowed the manipulation of siRNA to target any protein of interest. The ability to selectively decrease the expression of a protein has been used extensively for research purposes but has also been used as a therapeutic. Before the identification of siRNA and the RISC complex, antisense oligonucleotides were shown to be effective at inhibiting RNA by complementary binding. Antisense oligonucleotides complementary to the RNA of the Rous sarcoma virus was shown to prevent translation and proliferation indicating successful inhibition (39). This led to the first Antisense oligonucleotide therapy called fomivirsen which was used to treat cytomegalovirus rentinitis (40). Current therapeutics are utilising siRNA interference, such as Patisiran which is an approved siRNA-lipid nanoparticle therapeutic that inhibits the production of the transthyretin protein in the liver. This highlights the success of RNA and their potential as therapeutics however there are problems associated with the use of RNA that need addressing before the full potential can be achieved.

Due to RNA being a biological molecule there are mechanisms for removal of RNA present in a biological system. Nucleases are present in the body that cause degradation of therapeutic RNA limiting its delivery to the correct location (41). Additionally, RNA is degraded in cells continuously, shortening the time a therapeutic would remain active. The use of siRNA prolongs the stability of the RNA therapeutics in the cell as RNA associated with the RISC complex have increased stability, especially in non-dividing cells where siRNA could provide

effective knockdown for multiple weeks (42). Modification of RNA structure has enabled an increase in the stability by changing chemical groups of the ribose sugar rings and altering the chemical bonding to make the RNA less prone to degradation (43–45). Some of the modification also decrease the activation of the innate immune system which is an additional problem with RNA therapies (41). As foreign RNA activates pattern recognition receptors in the innate immune response, RNA therapeutics have the ability to activate these receptors also (46). Modifications to the RNA have helped to decrease the immune activation caused by RNA therapeutics to an acceptable level. A main problem associated with the use of RNA therapeutics is cellular delivery. As nucleic acids, such as RNA, have a negatively charged backbone they are difficult to deliver into the cell. The negative charge prevents RNA therapeutics crossing the cell membrane as the plasma membrane also has a slight negative charge resulting in repulsion. RNA therapeutics usually require a delivery mechanism to aid internalisation and entry.

1.2 Delivery of therapeutics

A challenge facing the development of novel therapeutics is the delivery to the correct location. A therapeutic molecule that cannot passively enter cells needs a direct delivery mechanism. Many delivery mechanisms use endocytic pathways as uptake mechanisms with a rate limiting step being endosomal escape (3). The process of endocytosis internalises material into the cell past the cell membrane, however the material enters the endosomal system, which is a series of membrane-bound organelles. Material that has been endocytosed is sorted for recycling, degraded or trafficked through the endosomal system to cellular locations such as via endosome to trans Golgi trafficking (47). Therefore, a limited fraction of endocytosed therapeutics is delivered to the cytosol as the endosomal membrane prevents delivery. To utilise endocytosis as a delivery mechanism, delivery across the endosomal membrane is required.

If the delivery of material to the cytosol could be increased, the therapeutic output of alternative molecules such as antibodies or RNA therapeutics would be enhanced.

There are many challenges facing delivery and promising therapeutic candidates have been withdrawn due to incorrect and inefficient delivery. The correct targeting of therapeutics and

the efficiency of delivery decrease the dose required which has a direct effect on cost efficiency, speed of effectiveness and safety.

1.2.1 Delivery vehicles in use for therapeutics

A delivery vehicle can be utilized to increase the efficiency of delivery of a therapeutic molecule. At a cellular level, some therapeutic molecules require assistance to cross the cell membrane due to the physiological properties of the molecule. Hydrophobicity or size can prevent diffusion across the plasma membrane, thus preventing delivery (11). Different strategies have been utilized to deliver therapeutic molecules across the cell membrane to the correct location. The use of a delivery vehicle can have additional benefits such as protection from degradation and to improve targeting of cell types for therapeutic delivery.

1.2.2 Viral delivery vehicles

As DNA and RNA based therapeutic approaches become more popular, delivery vehicles for nucleic acids are required. Many gene therapy approaches utilise viruses as delivery vehicles. During an infection cycle of a virus, viral nucleic acid is delivered into the cell for reproduction of virus particles. Manipulation of the viral infection allows delivery of therapeutic nucleic acids instead of viral nucleic acids. Viruses have evolved naturally to infect cells making them efficient delivery vehicles for therapeutic nucleic acids. Viruses can be used to stably integrate DNA into the genome, which could be used to cure genetic conditions caused by faulty alleles. Viral vectors can also deliver RNA based therapeutics such as mRNA, siRNA and antisense oligonucleotides. Adeno-associated viruses (AAVs) have been used in gene therapy approaches to deliver therapeutic nucleic acids (48) and virus delivered gene therapies such as Glybera, a treatment for Hyperlipoproteinemia Type I, have been approved for use in humans(49,50). The use of viral vectors for therapeutic delivery does have potential safety implications that need to be addressed before widespread application. The use of viruses to stably integrate DNA into the genome has the potential to cause off-target effects by disruption of functional genes and cause permanent side-effects. The virology of the potential vector would have to be understood fully to prevent off target effects of a virus infection, such as off-target infection of healthy cells. As naturally occurring virus vectors are used, an

immune response can be triggered by viral delivery vehicles causing side effects and immune-toxicity. In the case of Adeno-associated virus a proportion of the population has naturally encountered AAVs and circulating neutralising antibodies lower the efficiency of AAV gene therapies in some patients (51).

1.2.2.1 Nanoparticles

Nanoparticles are loosely defined as particles with size < 100nm and they became attractive candidates for drug delivery vehicles due to their chemical properties. Nanoparticles can absorb proteins and drug molecules to their surface or encapsulate molecules in their interior. The nanoparticles can be used to protect the cargo from degradation, target the delivery to a location using targeting proteins on the surface and can aid with the intra-cellular delivery of cargo (52). The definition of the term nanoparticle is vague and in some cases the size of therapeutic 'nanoparticles' can be up to 1000nm to allow incorporation of a sufficiently large dose of therapeutic and are sometimes referred to as nanomedicines (52). The term nanoparticle therefore is applied to a wide variety of molecules used for an equal wide variety of applications.

For use as a drug delivery vehicle a key aspect is the material used to create the nanoparticle as this determines the immunogenicity and encapsulation efficiency. The nanoparticles can be created from biological molecules such as lipids, dextran's, lectins etc or from chemical molecules such as polymers, metals and inorganic material. The material used for the construction of the nanoparticles will determine their behaviour and ability to function as a therapeutic carrier. The criteria for designing a nanoparticle for therapeutic delivery are: the ability to target delivery of a therapeutic to the correct location, a reduction in immunogenicity and side effects of the therapeutic and nanoparticle stability. Different compositions of material are currently being tested to improve nanoparticle delivery.

1.2.2.2 Lipid nanoparticles

Lipid nanoparticles (LNP) are nanoparticles produced from biological lipids and encapsulate therapeutics for delivery. The initial driver for the use of lipids in nanoparticle formation was

to reduce the toxicity associated with the carrier itself. Lipids are naturally used in membrane structures which is thought to increase biocompatibility for lipid-based nanoparticles. The fusion of the nanoparticle and the cellular lipid bilayers may promote release of content from lipid nanoparticles across the membrane into the cell.

An early example of a lipid nanoparticle was the liposome. Under certain experimental conditions, phospholipids can be formed into membrane structures separating an aqueous core from the surrounding aqueous environment (53). These structures, termed liposomes, were used to study the chemical and physical properties of lipid membranes by researchers. For therapeutic delivery, the structure of the liposomes enabled encapsulation of material inside the inner aqueous space and have been studied extensively as a therapeutic carrier for delivery to cells (54,55). Liposomes allow loading of hydrophilic therapeutics into the inner aqueous space (56–58) and have been approved for use as therapeutics (59). The main problems in the use of liposomes as therapeutic delivery vehicles is the consistency of production and sufficient loading of therapeutics. Variations in the lipid composition, size and shape of liposomes can change their properties affecting the efficiency of therapeutic delivery (60) but could cause additional side effects due to alterations in delivery. To be used as routine therapeutic molecules consistent production of liposomes is required. Additionally, the loading of therapeutics into the liposomes is an important stage of production. The two main approaches developed to load therapeutics into liposomes were passive loading and later active loading. During passive loading the therapeutic molecule and lipid components are mixed before formation of the liposome. The therapeutic is subsequently incorporated into the aqueous space of the liposome upon formation (56,58). Passive loading of liposomes is dependent on a variety of factors such as the solubility of the therapeutic in the aqueous phase but there is a limit on the quantity of therapeutic that can be incorporated via passive loading. To improve loading efficiency active loading was developed where preformed liposomes are loaded with therapeutics, the first example being the use of an ammonium sulphate gradient to drive liposome loading (57).

To increase the delivery capabilities of liposomes, modifications to the lipid structure were altered to manipulate the properties of the liposome. It was discovered the addition of a

PEG head group modification to the liposomes changed their biological characteristics. The PEG surface modification reduced the clearance of liposomes from the blood by phagocytic immune cells in the reticuloendothelial system and therefore significantly increases the blood retention time(61). The incorporation of the PEG modifications was shown to increase the antitumor ability of a liposome carrier(61). Additional modifications on liposomes can also aid liposome targeting to the correct location. The conjugation of antibodies and other ligands have been tested to see if they can increase the delivery of therapeutics to the correct location (62). However, the use of targeting molecules are divisive and more research is require to assess their ability to increase the correct targeting of lipid nano-particles.

The MC3 LNP used during this study is a formulation composed of multiple lipids including DLin-MC3-DMA, 1,2-distearoyl-sn-glycero-3-phosphocholine (DSPC), DMPE-PEG2000 and cholesterol (63). The ionizable lipid DLin-MC3-DMA is a common cationic lipid utilised in LNP formulations to promote endosomal release upon protonation in the acidic endosomal system (64). The lipid DMPE-PEG2000 allows the inclusion of the PEG modification to the nanoparticle.

As well as liposomes, other lipid nanoparticles have been developed. Solid lipid nanoparticle contains a solid lipid centre unlike the aqueous centre of a liposome. The solid centre allows encapsulation of lipophilic therapeutic molecules as well as hydrophilic molecules and allow controlled release of therapeutics to the blood stream allowing a longer effective treatment time without degradation. Solid lipid nanoparticles can be produced without the use of solvents which could decrease the cost and immunogenicity associated with nanoparticle production (65).

1.2.2.3 Delivery of LNP via the endocytic mechanism

Lipid nanoparticles have been successfully used as therapeutic delivery vehicles although the amount of intracellular delivery is still limited by the release of therapeutics to the cytosol. Many liposome formulations and lipid nanoparticles have been shown to be taken up by endocytosis (66,67). The cellular delivery of lipid nanoparticles requires escape from the endosomal system to the cytosol. The translocation of material from the endosome to the

cytosol is a bottleneck in delivery with material being either recycled out of the cell or degraded in the lysosome following endocytosis (68). Increasing the cytosolic delivery of endocytosed therapeutics would increase their therapeutic output and multiple approaches have been implemented to increase endosomal escape of lipid nanoparticles (69). Alterations to the lipid compositions of LNP particles have been successful at increasing the delivery of material. To deliver material from a lipid nanoparticle to the cytosol, one potential route is fusion of the nanoparticle to the endosomal membrane, thereby delivering the material inside the LNP molecule to the cytosol. To increase the fusion of LNPs with cellular membranes, lipids with different properties have been incorporated into the formulation. Different lipid compositions have been shown to form different structures in an aqueous environment based on their physical properties (70). Many different conformations of lipids can occur in an aqueous environment, but rearrangement occurs to provide a low energy environment and sequester hydrophobic regions away from the aqueous environment. A simple structure is a micelle arrangement where hydrophobic regions of the lipid cluster into a circular arrangement (Figure1.02). A common structure in biological systems is the lipid bilayer structure. A key determinant of lipid structure is the ratio of the hydrophobic region to the hydrophilic region. Lipids with small hydrophobic tails form micellar structures and are known to have positive membrane curvature. Lipids with equal hydrophobic to hydrophilic area have a tendency to form lipid bilayers. Lipids with larger hydrophobic regions form structures known as inverted lipid phases such as the inverted micelle or an inverted hexagonal phase (70). These lipids are known as negative membrane curvature lipids. Incorporation of lipids with negative membrane curvature such as dioleoylphosphatidylethanolamine (DOPE) into a bilayer structure such as a liposome has been shown to increase membrane fusion (71,72). Nanoparticles have been composed of different lipid compositions to promote fusion at lower PH. A ratio of PS:DOPE was shown to exhibit increased membrane fusion at acidic pH (71) enabling enhanced release after endocytosis.

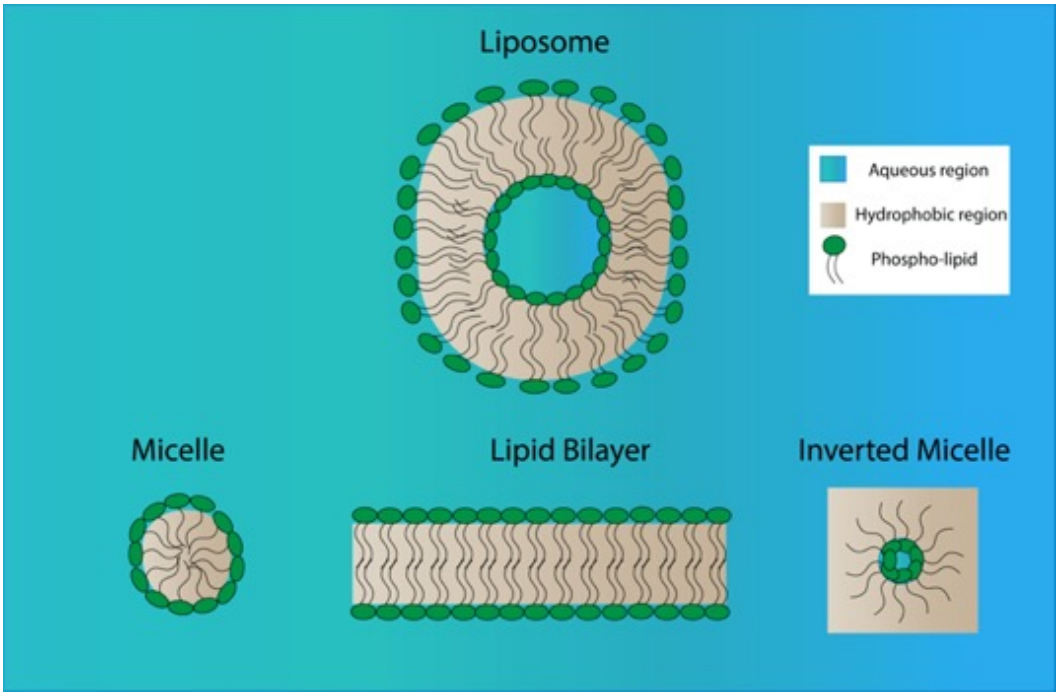

Figure1.02: Different conformations of lipids that can assemble based on their properties

Modifications to nanoparticles have led to advances in triggering release of therapeutics in a controlled manner. Using a carrier such as a nanoparticle offers advantages such as protection from degradation, however in order to function the therapeutic molecule needs to be released from the nanoparticle. The temporal release from the lipid nanoparticle is important for the therapeutic output achieved. Correct triggered delivery would increase the local concentration and reduce side effects in other areas. A wide variety of stimulants to trigger release have been utilised including changes in pH(71), temperature (73), enzyme concentration(74), ultrasound (75)(76) and magnetic fields (77,78).

The location in the endosomal system where LNP's escape has been researched by Gilleron et al (79). They could show that LNP particles are taken up by both clathrin-mediated endocytosis and macropinocytosis in a biphasic manner. Initially, the LNP is taken up via clathrin-mediated endocytosis (CME) for the first ~1.5 hours with a fraction of the total LNP internalised (1%). This phase is followed by the second macropinocytosis driven stage where bulk endocytosis increases the uptake significantly. It was confirmed using inhibitors that both CME and macropinocytosis are important in the process of LNP uptake, but inhibition of both

pathways simultaneously did not have an additive effect indicating that both pathways function together rather than as independent internalisation mechanisms. The research also looked at the localisation of internalised LNP with endosomal markers EEA1, Rabankyrin 5 and LAMP-1. These are markers for the early endosome, macropinosomes and the lysosome respectively and the LNPs were shown to colocalise with these markers after 6 hours internalisation and also the LNP uptake increased the colocalisation of these markers with each other indicating the formation of hybrid organelles. Using microscopy and mathematical modelling they were able to show the endosomal escape of LNPs occurred at specific stages of internalisation rather than a continues release from all compartments.

Lipid nanoparticles have successfully been used to delivery therapeutic molecules and can aid therapeutic targeting, temporal release and even cellular delivery. They have the potential to carry multiple therapeutic types including small molecules and RNA. However, the cellular delivery of lipid nanoparticles is still limited by the delivery of therapeutics to the cytosol after endocytosis. The ability to increase the endosomal release of endocytosed lipid nanoparticles would increase the therapeutic output observed.

1.3 Endocytosis

1.3.1 The Endosomal system and internalisation

The endosomal system is a dynamic series of distinct membrane subpopulations that sort cargo to different compartments of the cell. Trafficking and fusion events between the populations of vesicles and compartments are vital components of the system (80). Endocytic vesicles accumulate and fuse to form early endosome structures that acquire different protein and lipid compositions as they mature into late endosomes and finally become lysosomes. The different pathways of endocytosis feed into the endosomal system and enable processing of newly endocytosed material (Figure1.03).

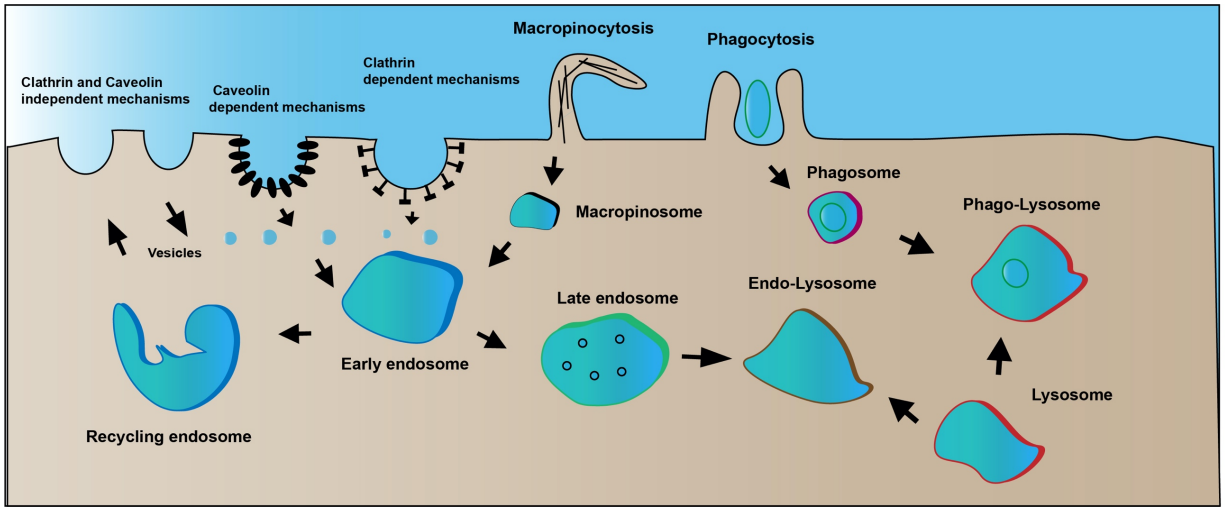

Figure1.03: The endosomal system and the different stages of endosome maturation

1.3.2 Trafficking through the endosomal system

After cargo has been internalised it joins the endosomal system where it can be trafficked to the correct location (80). The early endosome is the first distinct organelle on this pathway. It is formed by fusion of small vesicles from endocytosis and with existing early endosome structures to form a large membrane bound organelle. The GTPase RAB5 is an important protein in early endosome maturation and it is recruited, as well as effector proteins, to the surface of newly formed endosomes enabling the maturation process (81,82). The protein EEA-1 is an important RAB-5 effector recruited to early endosomes structures and aids

maturation and fusion of vesicles (83). The early endosomes accept incoming material for approximately 10 minutes, dependent on cell type, before maturation occurs (1). Cargo can be recycled away from the early endosomes and occurs via tubulation (84,85). Excess membrane is removed via the tubule structures and cargoes that are recycled are included in the tubules. Other cargoes can be targeted for degradation and are sequestered in the endosomes. One of the signals discovered to sort cargo into the degradative pathway is ubiquitinoylation (86,87). Addition of ubiquitin retained cargo in the early endosome eventually resulting in degradation. After recycling of content has occurred, the early endosomes undergoes maturation into late endosomes. The late endosomes marked with a RAB5 to RAB7 switch and no longer undergo tubulation (88).

Material marked for degradation is translocated into vesicles inside the late endosome via the ESCRT machinery to form multi-vesicular bodies (89). Fusion of late endosomes with lysosomes forming endo-lysosomes enable degradation of remaining content.

1.3.3 Phosphoinositides in the endosomal system

Phosphoinositides are lipids that can be modified by phosphorylation and are important signalling molecules in many cellular processes (90). The inositol ring can be phosphorylated at 3 different positions which gives rise to 7 different combinations of phosphoinositides that have been observed (90). One of the roles of phosphoinositides was as membrane identity markers, with different membranes being enriched with different phosphoinositides (90). These phosphoinositide transitions mark intracellular compartment identities and are an important in membrane trafficking (Figure1.04). The control of phosphoinositide (PtdIns) regulation is performed by kinases and phosphatases that specifically target a group of PtdIns. The localisation of these regulatory kinases and phosphatases help to establish the PtdIns compartmentalisation inside the cell.

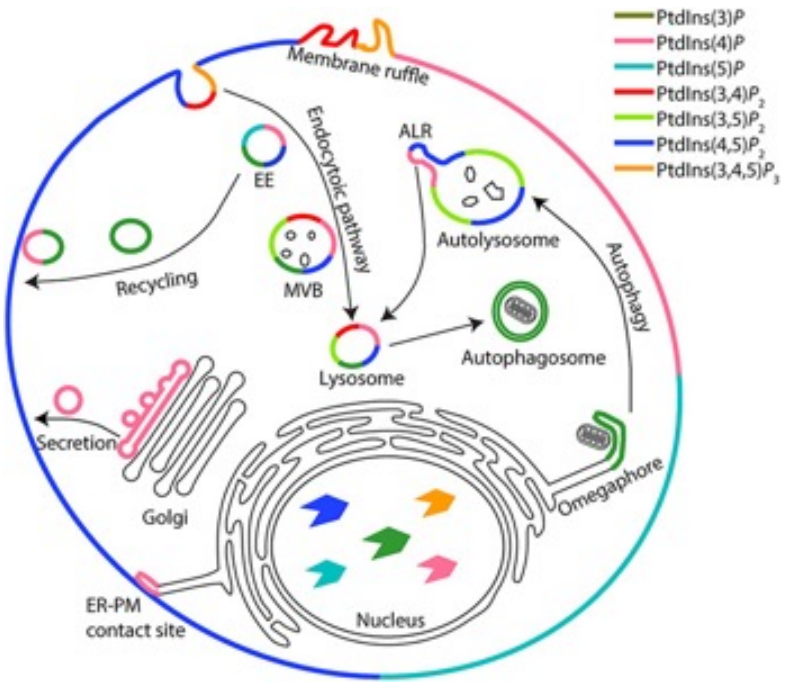

Figure1.04: The localisation of the phosphoinositides around the endosomal system. Figure acquired from BioEssays, Volume: 39, Issue: 12, First published: 04 October 2017, DOI: (10.1002/bies.201700121)

1.3.4 Clathrin-mediated endocytosis

Receptor mediated endocytosis is required to selectively internalise proteins into the intracellular space (91). Clathrin mediated endocytosis is the most studied method of internalisation and requires recognition of cargo by receptors, which allows association of the clathrin triskelion and membrane deformation into coated pit structures using multiple adaptor proteins that confer specificity(91). The CME process is highly evolutionarily conserved (92), involving the recruitment of cytosolic and membrane bound adaptor proteins in a specific order to allow the formation of the coated pit.

Many of these adaptors are recruited to the membrane via interactions with phosphoinositides (93). During clathrin mediated endocytosis PIP(4,5)P2 is involved in the recruitment of important factors such as dynamin which constricts the forming vesicle which results in budding, and the dephosphorylation of PIP(4,5)P2 to PIP(3)P is important after vesicle formation to form the early endosome identity and so subsequent trafficking.

1.3.5 Non clathrin-mediated endocytosis

Other methods of internalisation independent of clathrin have been identified, such as caveolae and lipid raft internalisation (94). Caveolae was first discovered by the observation of flask-like structures at the cell surface. These structures were determined to be formed by the caveolin proteins (95). Not all cells have detectable level of caveolin expression and it has been suggested that caveolae have tissue specific functions (96). The precise mechanism of caveolin endocytosis is unknown, however it is known that caveolin can bind directly to cholesterol. Additional factors important for caveolin endocytosis have been discovered, including the cavin proteins that act as structural components. There are currently four cavin proteins identified and they can act as a marker for detecting sites of caveolin endocytosis(97). Cargo that is dependent on caveolae endocytosis have been discovered, such as: albumin (98), tetanus and cholera toxin (99,100) and some viruses (101). Even though the receptors for some of the cargoes have been identified, the mechanism for the recruitment and concertation of cargo into the caveolae pit is not fully understood.

1.3.6 Phagocytosis

The mechanisms discussed so far have resulted in internalisation of small vesicles, approx. 50-150nm in size. There are mechanisms associated with the uptake of larger cargoes and are distinct from the classical endocytosis model. Phagocytosis is the uptake of large solid particles after receptor activation but instead of invagination the membrane protrudes around the particle, driven by actin polymerisation, until encapsulation and internalisation has occurred (102). The majority of phagocytosis in human cells occurs in immune responses. Professional phagocytes are cells that have evolved to internalise larger bacteria via phagocytosis for degradation.

1.4 Macropinocytosis

1.4.1 The function of macropinocytosis

Macropinocytosis is a pathway that allows the non-selective uptake of extracellular material. It was first discovered in 1931 by Warren Lewis using phase contrast microscopy to study rat macrophage movement (103). He noticed ruffling of the cell surface resulted in capture of phase-bright vesicles. This process requires actin polymerisation to reorganise the plasma membrane resulting in the formation of large intracellular vesicles (0.2-10µm diameter) that contain extracellular fluid (104). As macropinocytosis allows internalisation of large amounts of extracellular fluid, it seems to be an early evolutionary mechanism for nutrient uptake (104). In *Dictyostelium*, a single cell social amoeba used as a model organism for studying macropinocytosis, there is an association between mTOR signalling and macropinocytosis stimulation (105) indicating an early role in cellular metabolism. Macropinocytosis is a non-receptor form of endocytosis but there is regulation in the activation of macropinocytosis. Macropinocytosis can be constitutively active, with continuous uptake of material. Continuous uptake is usually observed in immune cells where it functions to survey the environment. For example, dendritic cells are constantly internalising extracellular fluid in order to monitor for infectious agents which enables a fast activation of the immune response (105,106). In most cells, however, macropinocytosis must be induced by external factors including growth factors binding to receptors, triggering macropinocytosis by the cell and resulting in internalisation of the extracellular fluid. Macropinocytosis can be triggered by different molecules, depending on cell type, and abundance of receptors. A431 epithelial cells from a human squamous carcinoma contain a high level of EGF receptors and macropinocytosis can be triggered by addition of EGF (107). In macrophages, the macrophage-colony-stimulating factor (M-CSF) can increase macropinocytosis (108).

1.4.2 Formation of macropinosomal cups

One of the fundamental questions associated with macropinocytosis is the formation of the cup structure. Unlike with phagocytosis there is not a solid particle to build the leading edge of the cup around. There are different mechanisms by which macropinosomes can form, either by a protrusion folding back on the cell membrane to capture extracellular material or by formation of a cup with actin polymerisation coordinated at either side of a forming cup

to make circular protrusions that meet and form the vesicle (102). To form the cup structure there is a need for localisation of factors that promote actin polymerisation and stability at the edges while at the base of the forming cup, actin polymerisation needs to be inhibited (Figure1.05) (109). It is currently unknown how this spatial separation of actin polymerisation is achieved and the factors that are involved.

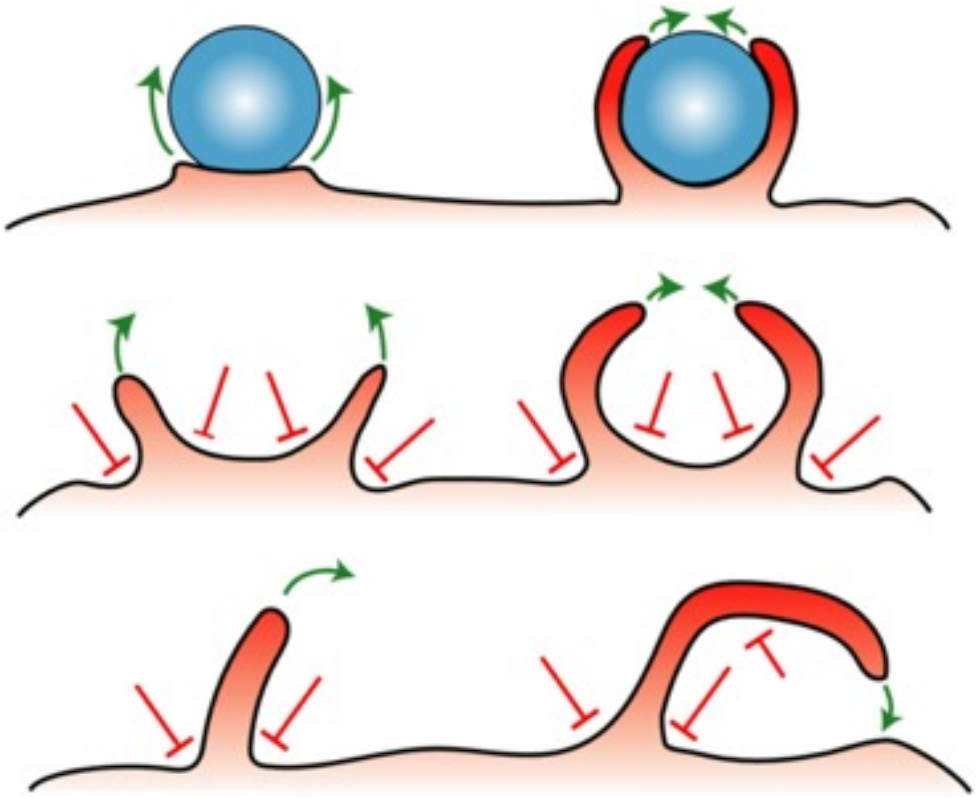

Figure1.05: The required areas of actin polymerisation and inhibition needed to successfully form a macropinosome. Image acquired from The FEBS Journal, Volume: 284, Issue: 22, Pages: 3778-3790, First published: 24 May 2017, DOI: (10.1111/febs.14115)

1.4.2.1 Actin structures and circular dorsal ruffles

There are many different actin structures that have been observed on the cell membrane and are involved in wide variety of functions (110). At the leading edge of the cell during cell motility, actin polymerisation is important in the formation of structures such as lamellipodia and filopodia (111). These structures use the force of actin polymerisation to force the protrusion of the plasma membrane. Additionally circular dorsal ruffles (CDRs) are observed before the peripheral edge of the cell and are formed by actin polymerisation (112) These ruffles are described as actin waves and are believed to have cellular functions, including endocytosis and formation of tubular structures. The endocytosis that has been observed

from CDR is clathrin and caveolin independent but these mechanisms could work alongside other forms of endocytosis at these sites (112). Additionally CDRs are involved in receptor seclusion on the plasma membrane and removal, which could have impacts on macropinocytosis signalling (113). CDRs are activated, by growth factor activation similar to macropinocytosis. They also have similar requirements for formation as both are inhibited due to disruption of phosphoinositide-3 kinase(PI3K) signalling, filamentous actin formation and PAK1 (112). It has been suggested that CDRs can close to form macropinosomes and that macropinocytosis is dependent on CDR's. Phase bright macropinosomes have been observed at the site of CDR in cells (114) but other dextran uptake assays have shown macropinocytosis occurs away from CDRs (115). Additionally, loss of the actin nucleating enzyme WAVE1 was shown to inhibit CDRs but not peripheral membrane ruffles or macropinocytosis. Furthermore, inhibition of WAVE2 inhibited both peripheral ruffles and macropinocytosis indicating that CDRs are not required for macropinosomes formation (115). More research is required to elucidate the roles that CDRs might play in macropinosome formation but with similar regulators and inhibitors there is likely to be some crossover in their mechanisms of formation.

1.4.2.2 Phosphoinositides in macropinosomal cup formation

As PtdIns mark the endosomal system, internalised material by endocytosis undergoes changes in PtdIns levels via phosphorylation or dephosphorylation. During macropinocytosis different levels of PtdIns can be observed, with an initial recruitment of PI(4,5)P2 during ruffle formation (116,117). This is thought to be converted to PI(3,4,5)P3 by the action of PI3Kinase which is required for macropinosome formation. The inhibition of PI3K decreases fluid phase uptake indicating this switch in PtdIns is important for macropinocytosis.

Ras, a GTPase, is linked to regulation of macropinocytosis and membrane ruffling. Ras can be mutated to form a constitutively active form that is prevalent in many types of cancers which have an increased rate of macropinocytosis (28). The RAS protein is activated by growth factor stimulation and helps to activate the production of PIP3 at the site of macropinocytosis (118). Other GTPases such as Rac1 have been shown to play a role in macropinocytosis (119). Expression of oncogenic RAS mutations can increase macropinocytosis and membrane

ruffling and affecting macropinocytosis can be achieved by affecting the regulatory proteins of RAS, the Guanine nucleotide exchange factors (GEFs) and GTPase activating proteins (GAPs). RAS is localised to forming macropinocytic cups which have been observed in macrophages and Dictyostelium (120) (109,120,121).

1.4.3 Stimulation of macropinocytosis

As mentioned previously, macropinocytosis can be constitutively active in cells or inducible by external factors. This could hint at multiple functions of macropinocytosis that depend on the type of stimulation. In dendritic cells, a large volume of extracellular material is taken up by constitutive macropinocytosis and this enables surveying of the environment. This directly correlates to the cellular function where a large volume of material needs to be taken up constantly.

Macropinocytosis can also be stimulated by external factors and receptor activation. The most common method is activation by growth factors. Epidermal growth factor receptor activation by epidermal growth factor results in stimulation of macropinocytosis in some cell types. The A431 cell line has an abundance of EGFR and is a model cell line used to study macropinocytosis due to the high levels of macropinocytosis induced by EGF(122). From the literature, experiments using EGF stimulation in A431 cells are usually performed under serum starvation conditions. This ensures maximum EGFR signal activation and macropinocytosis however it is known starvation can alter cellular activity, including macropinocytosis which may alter the effects observed (123). Additional growth factors have been observed to stimulate macropinocytosis such as the macrophage colony stimulating factor(M-CSF) (108) and the platelet derived growth factor (124). The stimulation of growth factors might be related to energy homeostasis in the cell. Single celled organisms also perform macropinocytosis and is believed to be a mechanism of nutrient uptake. For example, the social amoeba, dictyostelium discoideum uses macropinocytosis for nutrient uptake and can be grown in liquid medium as an energy source but interestingly can also phagocytose bacteria and can be sustained on a solid bacterial lawn (125). This model organism is a valuable tool to study macropinocytosis as it performs constitutively active macropinocytosis and forms large structures that can be easily observed. They are also very genetically malleable enabling easier genetic manipulation and a simplified genome that has

less redundancy while maintaining good homology with human proteins allowing comparisons to be drawn.

1.4.4 PMA activation of macropinocytosis and PKC

Tumour promoting factors such as phorbol myristate acetate (PMA) can induce macropinocytosis, but they usually work by activating downstream effectors of growth factors such as protein kinase C. The signalling pathways that activate macropinocytosis are all involved in growth and proliferation (126). PMA is a small molecule and so can enter cells and directly activate its molecular target. Its activates the classic and novel Protein kinase C sub families by binding to the DAG binding site in the protein resulting in activation (127) There are as many as 12 members of the Protein kinase C (PKC) family of kinases. At the site of a newly forming macropinosome multiple effectors are recruited. The temporal recruitment of effectors is important in the multiple stages of formation. It is known PKCa is an effector that is recruited at or shortly after cup closure indicating it is involved in macropinosome formation (108). As PKCa is a member of the classic protein kinase C family it is sensitive to activation by both DAG and calcium generation (128). It was reported that an inhibitor of the enzyme phospholipase C prevented constitutive macropinocytosis in rat fibroblasts indicating generation of DAG by phospholipase C is required for macropinocytosis (129). When observing the difference between growth factor and PMA induced macropinocytosis, the inhibitor of phospholipase C only functioned to prevent growth factor stimulated macropinocytosis and not PMA induced macropinocytosis (108). These results suggest that growth factor activation generates DAG production by PLC activation, likely due to the high concentration of PIP3 produced in macropinocytosis. PMA activation occurs downstream by directly activating PKC by binding to the DAG binding domain-C1 resulting in activation downstream of PLC. The generation of DAG is important to activate other macropinocytosis effectors, for example RAS-GEF's are known to be DAG activated and the generation of DAG or PMA binding may play a role in activating RAS in macropinocytosis stimulation (108,130).

1.4.5 Inhibitors of macropinocytosis

Multiple inhibitors of macropinocytosis have been discovered. The polymerisation of actin is essential and so treatment with actin depolymerising drugs such as cytochalasin D prevents macropinosome formation (131). This drug blocks F actin formation, preventing polymerisation and so inhibits macropinocytosis by preventing membrane deformation which is required in the formation of the membrane ruffles. Within actin polymerisation there is no force generation to generate the membrane ruffles.

There are several other inhibitors of macropinocytosis and their ability to block macropinocytosis provided early mechanistic insights. Wortmannin inhibits phosphoinositide-3-kinase resulting in multiple effects on endocytosis, including preventing uptake of fluid phase markers (131,132). The control of phosphoinositide signalling is important for the maturation of macropinosomes as well as the initial formation and therefore inhibition of phosphoinositide-3-kinase has an effect on macropinocytosis. Amiloride is the standard inhibitor of macropinocytosis. Amiloride blocks macropinocytosis but other forms of endocytosis can still occur which enables distinction between macropinocytosis and other forms of endocytosis(132). The exact physiological mechanism of how amiloride inhibits macropinocytosis is unknown but the drug inhibits the Na+/H+ exchanger. It was observed by Watts et al (122) that reduction of Na+ in the extracellular media resulted in a drastic reduction in the levels of EGF stimulated macropinocytosis in A431 cells. It was hypothesized that this was due to the requirement of extracellular Na+ for the function of the Na+/H+ exchanger system which is required for cytosolic pH homeostasis in cells. Amiloride was already known to inhibit the Na+/H+ exchange system and was shown to reduce the levels of EGF stimulated macropinocytosis in Na+ free media and regular media. This paper (122) also showed cytosolic pH is important as acidification using NH_4Cl_2 preloading results in complete loss of EGF stimulated macropinocytosis.

1.4.6 Maturation of macropinosomes

After the initial formation of macropinosomes they mature by acquiring and recycling material and undergo changes in the composition of proteins and lipids (Figure1.06). The maturation of macropinosomes is synonymous with the maturation of the endosomal system with the similar stages and proteins involved in their maturation. The maturation of macropinosomes varies from cell type and stimulation methods resulting in different outcomes for the cargo involved (133,134). In macrophages the macropinosomes mature and eventually fuse with lysosome compartments for degradation of the content (135). In contrast A431 cells stimulated with EGF form macropinosomes that recycle back to the plasma membrane and do not progress past the early endosome stage of maturation (122). The differences in maturation between macropinosomes indicate different acquisition of proteins and lipids after formation to drive different outcomes. The exact mechanism involved in determining the fate of macropinosomes is currently unknown. In bone marrow derived macrophages stimulated with CSF-1 the newly formed macropinosomes stained positive for transferrin receptor after 1 minute but transferrin was removed quickly after formation (135). After 2-4 minutes the macropinosomes were positive for rab-7 which is a marker for the late endosomes and finally fused with lysosomes (136). On the other hand, in A431 cells the macropinosomes remain rab-5 positive, a marker for the early endosome and did not show rab-7 recruitment (137). The Rab GTPases are master regulators of endosomal maturation and likely play a crucial role in the maturation of macropinosome and deciding their fate. During the maturation of macropinosomes they undergo a shrinking with a decrease in size as well as volume. The recycling of content away from the macropinosomes is an important step in the maturation process and in EGF stimulated HEK-293 cells, SNX5 positive tubular structures are observed on macropinosomes before acquisition of Rab-7 (138). Internalised content that is not destined for degradation needs to be recycled and trafficked to another part of the endosomal system whereas material for degradation is retained. Plasma membrane components are likely trafficked away after initial formation which has shown to be dependent on the wiskott-aldrich and SCAR homology (WASH) and retromer complexes (139). Both complexes have a role in endosomal sorting and have been shown to be recruited to early endosomes. Changes in phosphoinositides occur during maturation. Recruitment of PI3K by rab5 generates PI3P on the early macropinosomes(116).

The PI3P is converted to PI3,5P2 during maturation. The phosphoinositides can recruit proteins via phosphoinositide binding domains to aid maturation, such as different RAB proteins and recycling complexes such as the retromer complex (140).

The trafficking and maturation of macropinosomes potentially correlates with their function. In macrophages and dendritic cells, internalised material may contain pathogenic material that requires degradation and so the maturation of these macropinosomes ends with degradation to aid pathogen removal and antigen processing. It is known macropinosomes in different cell types can have differing maturation, but the exact mechanism is still being elucidated. It is likely different types of macropinosomes can form and have different trafficking through the cell.

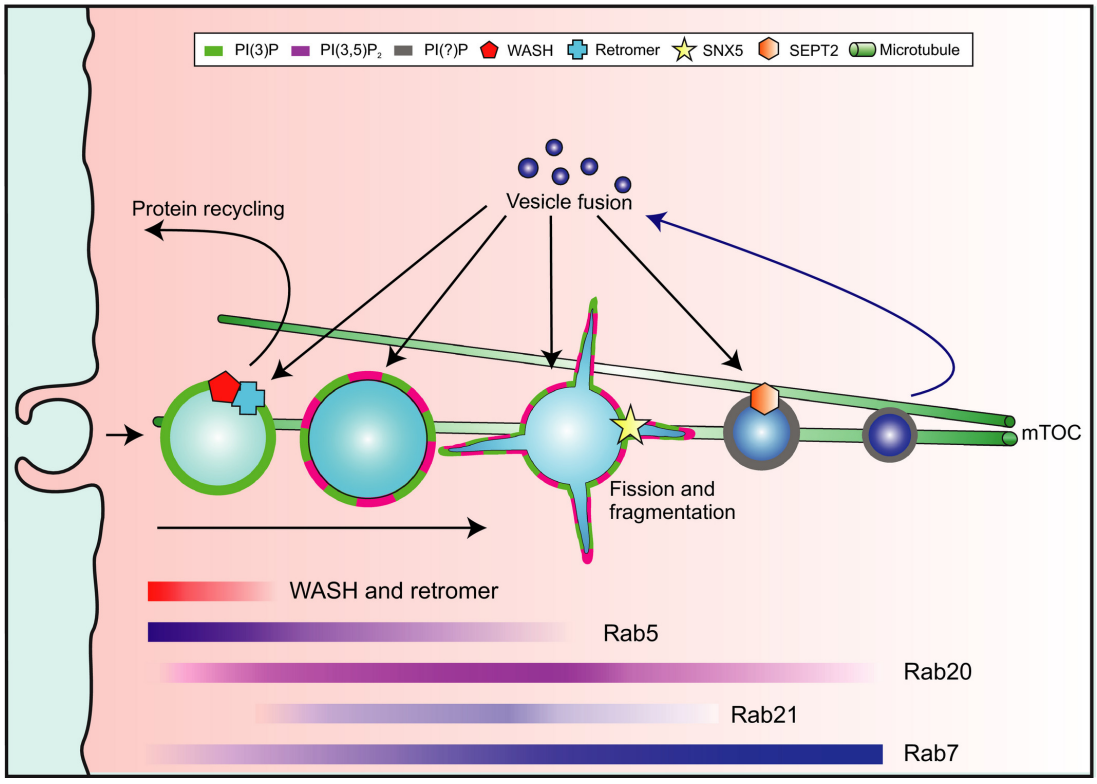

Figure1.06: The maturation of macropinosomes after formation. The diagram shows some of the changes in protein and lipid composition as maturation occurs. The diagram was acquired from The FEBS Journal, Volume: 284, Issue: 22, Pages: 3778-3790, First published: 24 May 2017, DOI: (10.1111/febs.14115)

1.5 Endosomal permeability

Material internalised by endocytosis enters the endosomal system and is trafficked to the correct location, recycled out of the cell or degraded in lysosomes. The endosomal system is a series of membrane bound organelles. The function of the endosomal system relies on the separation of endocytosed cargo from the cytosol. The pH and ion concentration of endosomal populations are also important in the correct function of the endosomal system. Therefore, the basal release of endosomal content to the cytosol is minimal and does not occur under regular conditions. However, for delivering therapeutic molecules into the cytosol of cells via endocytosis, a route out of the endosomal system is required.

1.5.1 Bottleneck for cytosolic delivery of endocytosed therapeutics

One of the rate limiting steps in the delivery of endocytosed therapeutics is the cytosolic delivery and endosomal escape (3,141,142). The endosomal system is heavily regulated with very little endosomal escape under basal conditions(79). Therapeutic molecules of a large size and hydrophilic in nature require active delivery across the cell membrane (143). For most therapeutics taken up via endocytosis a limiting step is crossing the endosomal membrane. Currently there are multiple different approaches to increasing the endosomal escape of endocytosed material.

1.5.2 Current strategies for increasing endosomal permeability

1.5.2.1 Pathogen enhanced endosomal escape

Pathogenic organisms have evolved entry mechanisms into mammalian cells. Many pathogens enter cells via endocytosis and have ways of crossing the endosomal barrier into the cytosol. A potential way of increasing endosomal release is by exploiting the mechanisms evolved by these organisms. Therefore, there has been significant research into the mechanisms involved in pathogen entry into cells.

Bacteria have evolved multiple different entry routes into cells and manipulate host signalling for survival. Many bacteria or bacterial proteins have to cross a lipid membrane during infection and research into different bacterial infection pathways have identified unique ways of solving the translocation of proteins across a lipid membrane. Bacterial toxins are released from bacteria during infection and act on many host cell proteins. Many of these host cell proteins are located in the cytosol and require intracellular delivery. Some bacteria have developed complex secretion systems that act as a needle to directly insert proteins across the plasma membrane. However, many bacterial toxins are taken up via endocytosis and require a delivery mechanism across the endosomal membrane (144). Some toxins such as the diphtheria toxin translocate out of the endosomal system directly by forming a proteinaceous channel triggered by the pH gradient (145). The channel can facilitate translocation of the catalytic domain of the toxin to the cytosol where it can function. Other toxins are known to traffic to the ER and are thought to utilise host cell retro translocation proteins to escape from the ER (146). Understanding of the bacterial mechanisms of escape could be used to enhance endosomal permeability.

Viruses are very effective at invading mammalian cells and have been utilised for nucleic acid transfection in both biological research as well as in the therapeutic area as gene therapy vectors. Viruses have been effective vectors with high efficiency of transfection seen such as with the adeno-associated virus which are often utilized in gene therapy. However as discussed earlier the use of viruses as delivery vehicles has problems associated. Additionally, the exact mechanisms of endosomal escape for many viruses are still being investigated and may be multi-factorial depending on cell type, viral load, receptor activation etc. Viral proteins that promote endosomal escape were identified and their function has led to the development of proteins that promote the endosomal escape of conjugated material called cell penetrating peptides (CPP) or protein transduction domains (PTD) (5).

1.5.3 Adenovirus stimulates macropinosomal lysis

Adenovirus binding results in stimulation of macropinocytosis, indicated by uptake of a fluid phase marker. This stimulation of macropinocytosis is thought to be through grouping of the integrin complexes that are bound to the penton proteins. Integrins have multiple signalling

effectors on their cytosolic region and are involved in other complexes such as adhesion junctions and contact with the extracellular matrix that have a signalling element (22,147). The binding to integrins is not only required for endocytosis, but it is believed to influence endosomal and macropinosomal lysis and stability (24). Adenovirus method of entry is clathrin-mediated endocytosis but there is evidence of virus particles inside macropinosomes as well (24,148). The induction of macropinocytosis seems to play a role in lysis of the endosome containing virus particles.

The K44A mutant dynamin was utilized to observe the effect of adenoviral signalling when the virus was not internalised by clathrin mediated endocytosis (24). The K44A mutation is in the GTPase domain of dynamin preventing GTP hydrolysis and clathrin mediated endocytosis. This mutant allows study of non-clathrin mediated endocytosis. BSA-FITC-NLS is a fluorescent fluid phase marker that translocate to the nucleus following release to the cytosol. Using this assay method, it is possible to determine the amount of macropinosome lysis following adenoviral infection. Adenovirus signalling can still occur with the K44A mutant dynamin but Clathrin mediated endocytosis of the virus is inhibited. Overexpression of K44A mutant resulted in similar levels of macropinosomal lysis as the wild type which indicates viral endocytosis is not required and hints that the signalling from the integrin complexes is important for lysis (24). A lower concentration of the virus did not stimulate similar levels of lysis even though adenovirus was detectable inside vesicle structures indicating that the presence of adenovirus is not sufficient to cause macropinosomal lysis. This indicates a likely role in the signalling pathway from intergrins that results in the lysis of endosomal structures and the potential threshold of viral level required to trigger lysis of vesicles.

1.5.3.1 Cell penetrating peptides and protein transduction domains

The discovery that a protein produced by the Human immunodeficiency virus (HIV), the trans activator (TAT) could stimulate its own uptake and trafficking to the nucleus was the first cell penetrating peptide identified (149,150). A cell penetrating peptide is a peptide sequence that can be taken up into a cell and cross the lipid membrane without assistance. Additionally cell penetrating peptides have been shown to transport conjugated protein into the cell (143). The ability to transport conjugated molecules into the cell would make TAT and other CPP

attractive candidates for increasing therapeutic delivery. Research on the TAT protein identified a region of cationic amino acids that are required for transduction of the protein into the cytosol. This sequence was referred to as a protein translocation domain and was sufficient to induce transduction of proteins into cells. Additional cell penetrating peptides have been identified from many types of organisms with different protein translocation domains. It is believed that the high number of cationic amino acids lysines and arginines located in the protein translocation domain (PTD) allow for increased interaction with the negatively charged plasma membrane. This interaction is important for the transduction of the protein into the cell however the exact mechanism used to cross the cell membrane has yet to be fully elucidated. Crystallography experiments on giant unilamellar vesicles have shown the TAT protein induces a phase change in the lipid bilayer (151) and formation of a pore to allow transition across the membrane. However, computer modelling has shown the protein to lipid ratio to form a pore would need to be 1:8 for successful transduction which is much greater than required in a cell system, indicating an additional mechanism involved in the transduction (152). The ability of PTDs to transduce proteins into cells has been known about for 30 years however they have not been widely accepted as a delivery mechanism due to a lack of understanding of the mechanism involved, the relatively low level of transduction when compared to other available methods and low specificity. There are no FDA approved CPP drug conjugates with reasons stated as stability issues, immunogenicity, lack of delivery and specificity of delivery (153). However, there are CPP drug conjugates undergoing clinical trials which could prove to be effective at increasing the delivery of therapeutics to the cytosol.

1.5.3.2 Endosomolytic peptides

A solution for increasing endosomal escape is the direct disruption of the lipid membrane to damage the membrane or form a pore structure. Virus proteins have been found to disrupt lipid membranes and are believed to be involved in pathogen endosomal escape mechanisms(154). However, lipid membranes are vital for biological function and uncontrolled membrane disruption would be toxic. Endosomolytic peptides selectively perturb endosomal membranes without effecting the plasma membrane (155). As the endosomal membranes are perturbed selectively localised disruption of the membrane can

be achieved which allows endosomal escape. Many endosomolytic peptides use the pH gradient in the endosomal system as the stimulus to trigger endosomal release. The protonation of amino acids in a peptide result in changes to the conformational shape of the peptide that has greater membrane lytic ability (155). Understanding of protein structure has allowed targeted mutations in endosomolytic peptide sequence to increase the specificity of their lytic activity and prevent off target effects. Conjugation of endosomolytic peptides to therapeutic molecules directly or inclusion of these peptides into delivery vehicles such as lipid nanoparticles could increase the endosomal release. The main negative of a lytic peptide is damage to the membrane could increase immunogenicity and side effects in other locations. The correct targeting of lytic peptides is important to reduce these side effects (69).

1.5.3.3 Lipid-Nanoparticles

As mentioned, lipid nanoparticles have been utilised to protect therapeutic payloads, target delivery to the correct location and increase cytosolic delivery of endocytosed therapeutics (8,156). Lipid nanoparticles have been shown to deliver material to the cytosol under basal conditions indicating they have a mechanism of delivering material across the lipid membrane however the efficiency of release is minimal (79). It has been shown only 2% of mRNA delivered using a lipid nano particle was released to the cytosol with the rest being degraded in the lysosome (79). The minimal cytosolic delivery limits the therapeutic output of endocytosed LNP particles. Therefore, ways of increasing the endosomal release of endocytosed therapeutics is an area of ongoing research. Inclusion of endosomolytic peptides onto the LNP particle can increase the endosomal permeability by disrupting the membrane (157). Changes in the lipid composition can increase the fusogenicity of the LNP and promote fusion with the early endosomes to increase delivery (158).

1.5.3.4 The proton sponge effect

Transfection of DNA and RNA into mammalian cell systems commonly use cationic molecules such as polyethylenimine (PEI) to increase transfection efficiency. It is believed the PEI-DNA complexes increase uptake by endocytosis and endosomal escape. The PEI and DNA forms polyplexes where the DNA is condensed into a small complex with the positively charged PEI

by electrostatic interaction (159). The DNA polyplexes were shown to be taken up via different endocytic routes depending on cell type and polyplex used however it is believed clathrin and caveolae mechanisms are common uptake pathways (160,161). The exact mechanism of endosomal escape of polyplexes have not been fully elucidated (162). The hypothesis with the greatest evidence is the proton sponge theory (Figure1.07). The effect was first observed with the observation that polymers with high buffering capacity at low physiological pH had high transfection efficiencies (163). Many of these polymers had amine groups with pKa values at the physiological pH of the lysosome and so it was proposed protonation of the amine groups decreased the concentration of H^+ leading to an influx of H+ and corresponding Cl- ions into the lysosomes via ion channels (164). The polymers acted as a "proton sponge" to absorb H+ ions. The influx of ions increased the osmotic pressure inside the lysosomes leading to bursting and subsequent delivery of material to the cytosol. As well as absorbing H+ ions, protonation of the amine groups expands the polyplex due to increased electrostatic interactions. The expanding of the polyplex into a branched structure increases the volume the polyplexes occupy (165). The effect of increased volume is called the umbrella theory to explain the ability of PEI to increase delivery (165). There is evidence contradicting the proton sponge theory with measurements of pH in PEI positive lysosomes showing no increase in pH (166). It has been argued absorption of protons would increase the pH of the lysosomes which was not observed in some experiments (166) but an increase of pH was seen by other groups (167). The proton sponge effect is still open to debate but understanding the mechanistic details further could increase our understanding of membrane permeability.

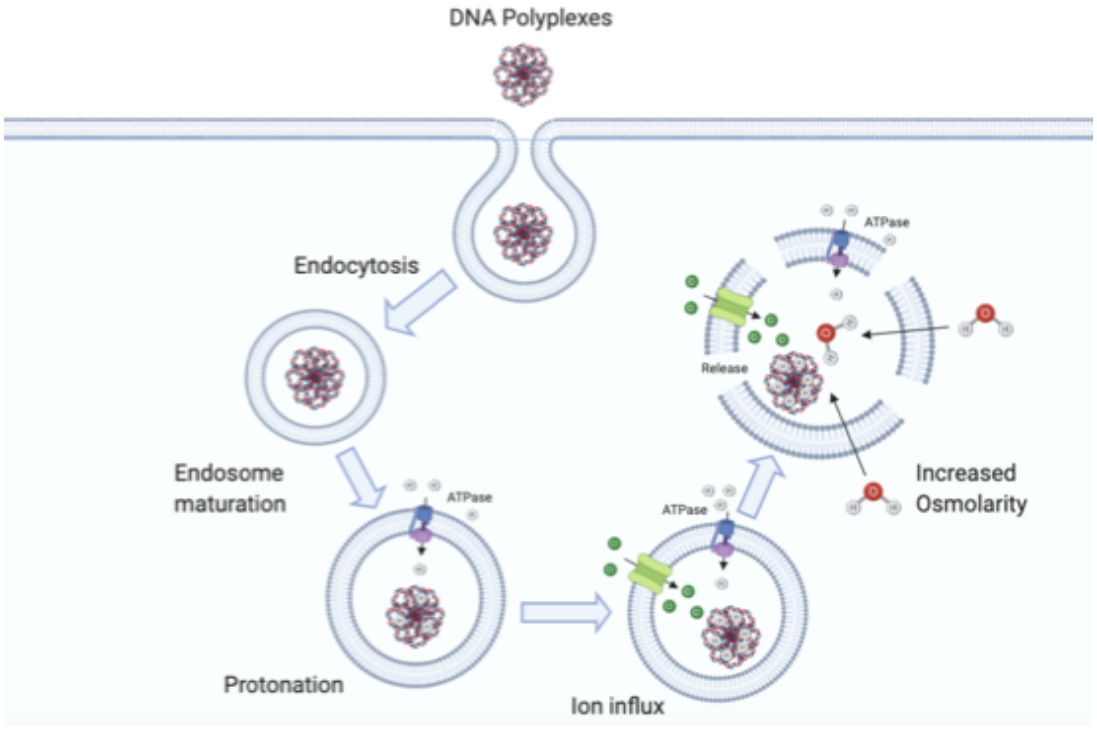

Figure1.07: A figure depicting the proton-sponge effect observed with DNA Polyplexes. The figure was adapted from: Tailoring Iron Oxide Nanoparticles for Efficient Cellular Internalization and Endosomal Escape

1.5.4 Biological pathways in endosomal permeability

There are circumstances when transport of proteins and material across a lipid membrane are important to cellular function. Therefore, mechanisms of transporting material across cell membranes have evolved. As these processes naturally occur in cells, manipulation of these biologically relevant pathways might have reduced side effects compared to damaging the membrane. Several biological processes that can transport proteins across the membrane have been discovered and some are potential therapeutic entry routes into the cell.

1.5.4.1 Reverse Translocation of proteins

Translation of mRNA and protein synthesis occurs at specialised protein complexes called ribosomes in the cytosol. Many proteins require additional processing and post-translational modifications and are inserted into the lumen of the Endoplasmic Reticulum by a process called translocation which either occurs co-translationally or independent of translation (168). A protein called sec61 is the major component of the translocation unit that inserts the protein from the cytosol into the endoplasmic reticulum(169). The sec61 protein forms a pore that allows the protein to cross the ER membrane. Proteins that are misfolded in the ER lumen

need to be degraded and it was discovered a method for removing misfolded ER proteins called ERAD involved the reverse translocation back into the cytosol for degradation in the proteasome (170). It is believed the reverse translocation uses the sec61 protein (171) and some bacterial toxins may utilise the reverse translocation process as a way of escaping the endosomal system (172).

1.5.4.2 Antigen cross presentation

The immune system is constantly surveying the proteins of the body to determine if any non-self-proteins, such as pathogenic material is present (106). Two key signalling systems involved in the regulation of the immune system are the major histocompatibility complex systems 1 and 2 (MHCI and MHCII) (106,173–175). The major histocompatibility complexes present different protein fragments to immune cells to trigger the immune response if foreign material is present. The two complexes have different roles in the presentation of foreign peptides (176). MHC1 present internal cellular peptides from protein degraded by the proteasome. This allows monitoring of internal cellular proteins and signalling by infected cells to the immune system for destruction. Peptides are transported into the ER lumen by the protein TAP and the peptide is loaded onto the MHC1 complex inside the ER lumen (177). The MHC1 complex can traffic to the cell surface and present the peptide to the immune system for monitoring. All nucleated cells present MHC1 on the cell surface (178). On the other hand, MHC2 presents exogenous antigens internalised from the exterior of the cell. The processing of material onto MHC2 signalling is predominantly reserved for immune surveillance by professional antigen presenting cells such as dendritic cells and macrophages (179). These cells internalise material either via phagocytosis or macropinocytosis and survey the environment (106). Internalised proteins are degraded by endosomal peptidases and the peptide fragments are directly loaded onto the MHC2 signalling complex in the endosomes. After loading of the peptide, the complex is trafficked to the cell surface and antigen presenting cells can themselves travel to the lymph nodes and prime the adaptive immune response against specific antigens. MHC1 molecules are important in the innate immune response as they allow identification of infected cells. MHC2 molecules are important to signal to the adaptive immune response. The MHC2 packaging occurs in the endosomal system and internalised proteins are processed in the endosomes. A phenomenon called

antigen cross presentation was shown to occur where peptides internalised by phagocytosis or macropinocytosis were cross presented from the MHC2 pathway onto the MHC1 pathway (175). Exogenous protein peptides were expressed by MHC1 which is believed to be vital for priming cytotoxic T cell response. To cross present material from the MHC2 pathway to the MHC1 pathway material needs to be delivered to the cytosol from the endosomal system. This indicates a biological mechanism for transporting material from the endosomes to the cytosol in a controlled method to allow cross presentation to occur. The pathway of cross presentation could enable greater understanding of endosomal permeability as a route for enhancing cytosolic delivery.

1.5.4.3 Membrane translocation in antigen cross presentation

The research into elucidating the mechanism for cytosolic release of internalised antigens in antigen presenting cells has suggested two possible models. Firstly, it has been proposed that the ERAD pathway and sec61 are involved in the reverse translocation of antigens to the cytosol. The ERAD pathway utilises the protein channel sec61 to translocate proteins across the membrane. Proteins require unfolding to be transported by sec61 due to the limited size of the channel in the protein. Therefore, if retrotranslaocation by sec61 was the main mechanism used in antigen cross presentation the antigens would require unfolding to be properly cross presented. Fixation of the OVA antigen with PFA before internalisation into antigen presenting cells decreased the ability of the cells to activate cytotoxic T cells (180). The fixation reduced antigen cross presentation indicating that protein unfolding might be important to cross presentation. Many proteins contain disulphide bridges and for translocation of proteins using a transporter protein the disulphide bonds would need to be reduced. It was observed that cell types with a high level of antigen cross presentation had constitutive expression of Gamma-interferon-inducible lysosomal thiolreductase (GILT), an endosomal enzyme that reduces disulphide bonds. Knockout mouse models also showed GILT expression was critical for proper antigen cross presentation indicating a role for disulphide bond reduction in cross presentation(181). Direct inhibition of sec61 using the pseudomonas aeruginosa exotoxin (182) showed a decrease in OVA antigen cross presentation with a similar result seen using siRNA silencing of sec61 (183). It is difficult to prove a direct causative link for sec61 being the mechanism of endosomal escape as the sec61 protein is involved in the

translocation of many proteins into the ER, including the MHC1 complex itself, and so the effect on cross presentation could be an indirect effect on the trafficking of other proteins. Experiments using intrabody expression against sec61 as a way of retaining sec61 in the ER and preventing recruitment to endosomes was shown to decrease cross presentation (183). However there are contradicting results with some data indicating long term inhibition of sec61 with an alternative toxin called mycolactone having an effect on cross presentation independently of sec61 (184). As the direct effect of sec61 on cross presentation is difficult to study, there has been a focus on other ERAD adaptor proteins that may have a role in antigen cross presentation. An ATPase protein, p97 is known to be a positive regulator of ERAD and is thought to use ATP hydrolysis to provide the energy required to retro translocate proteins into the cytosol across membranes (185). Addition of exogenous p97 to purified phagosomes resulted in release of luciferase indicating a role in transport across membranes (186).

An alternative hypothesis for the mechanisms of antigen release to the cytosol in cross presentation involves the disruption and rupture of the endosome. Rupture of the endosome is a direct way of releasing content to the cytosol, however there are problems associated with uncontrolled release of endosomal content such as cell toxicity. One mechanism for disruption of the membrane is the production of reactive oxygen species inside the endosomal compartments of antigen presenting cells, which increases antigen cross presentation (187,188). Reactive oxygen species(ROS) production increases lipid peroxidation of the membrane which has been shown to increase permeability of artificial membrane structures (189). The cross presentation of antigens was shown to require the enzyme NOX2 with knockdown of NOX2 decreasing ROS production, lipid peroxidation and antigen presentation (188). If membranes are ruptured to promote antigen release, a mechanism for repair is required. Some work has suggested the member of the ESCRT machinery, TSG101, being required for antigen release however this work implemented TSG101 in poly ubiquitination and not directly in recruitment of the ESCRT machinery (190). ESCRT proteins are known to enhance membrane repair in the endosomal system (191). More work is needed to verify if the ESCRT machinery is involved in repair after membrane rupture in antigen presentation.

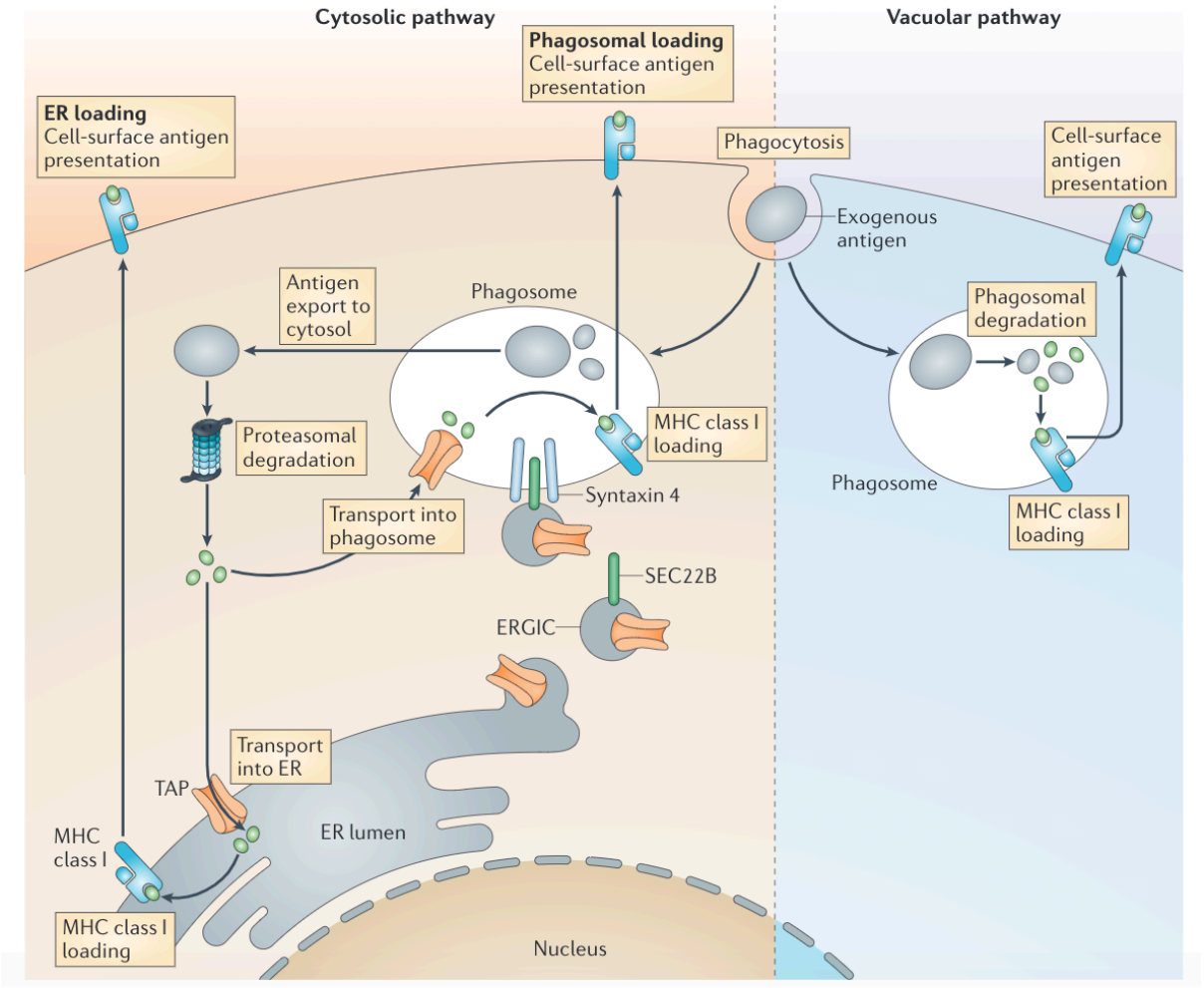

Figure1.08: The pathway of antigen cross presentation in dendritic cells. Image acquired from Joffre, O., Segura, E., Savina, A. et al. Cross-presentation by dendritic cells. Nat Rev Immunol 12, 557–569 (2012). https://doi.org/10.1038/nri3254

1.5.5 Current strategies of detecting endosomal release

To study the process of endosomal permeability, there needs to be a sensitive assay for detecting endosomal permeability and release to the cytosol. An assay to detect endosomal release has several challenges that need to be overcome. The endosomal system has a smaller total volume than the cytosol and therefore any signal molecule that is released from the endosomal system is diluted, reducing the detectable signal. Any signal that remains in the endosomal system has a stronger detectable signal, making it difficult to determine the signal from the cytosolic population. Previous research into endosome permeability and endosomal release to the cytosol has resulted in multiple assays being developed.

1.5.5.1 Direct detection of a delivered molecule

To detect endosomal release, you can directly detect a signal that has been endocytosed and released to the cytosol. Fluorescent molecules allow cellular localisation and fluorescently conjugated molecules have been used to detect endosomal release. For example, fluorescent dextran uptake and subsequent release has been used to detect cytosolic delivery by observing a cytosolic staining pattern of fluorescence (192). Fluorescently tagged LNP and siRNA are routinely used to observe cellular localisation (79). A challenge using direct detection is to distinguish between endosomal and cytosolic fluorescence. To separate these signals the localisation of GFP to the nucleus using a nuclear localisation sequence (NLS) has been used to successfully detect endosomal release (24).

1.5.5.2 Indirect detection of a delivered molecule

Instead of detecting the released molecule directly, many endosomal release assays detect an outcome that is possible only after endosomal release has occurred. The ribosome inactivating drug saporin has been used to detect successful cytosolic delivery as it can only function upon correct delivery resulting in cell death, which is a detectable effect (193). The successful delivery of nucleic acids and the detectable outcome of their delivery has been used to determine the efficiency of cytosolic delivery. Lipid nano-particles that delivery mRNA encoding a fluorescent protein have been used so a fluorescent signal is only produced following successful cytosolic delivery and translation of the mRNA (79,194). Additionally, the delivery of siRNA molecules that target mRNA for degradation in the cytosol has been used as an endosomal release assay, an example being the delivery of siRNA targeting the GFP protein being successfully delivered to a cell line stably expressing a GFP construct and detecting the loss of GFP fluorescence (79).

1.5.5.3 Detecting the delivery of an enzyme

The detection of an enzyme that has been delivered to the cytosol can offer increased sensitivity as the signal is amplified by the enzymatic reaction. An effective enzymatic assay for detecting endosomal release uses the beta-lactamase enzyme. A substrate for beta-

lactamase, CCF2/AM can be loaded into a cell where it is cleaved by cytosolic esterases to form the fluorescent CCF2 molecule that is trapped in the cytosol (195). Cytosolic beta-lactamase enzyme can cleave the CCF2 which results in a shift in the emission spectrum which can be detected. The ratio of cleaved to un-cleaved CCF2 can be deduced and the amount of beta-lactamase can be quantitatively determined (195). This system has low background as signal is only produced upon successful cytosolic delivery of the beta-lactamase enzyme.

1.5.5.4 Complementation assays

The development of complementation assays has allowed detection of cytosolic signal without endosomal background. The signal molecule is split into two proteins that can recombine into a functional protein. A part of the signal protein is expressed or loaded into the cytosol of the target cell and the complementary protein is delivered to the cytosol where complementation results in an active signal. These assays reduce background as the signal is only detected upon complementation which can only occur after cytosolic delivery. The Green fluorescent protein (GFP) can be divided into two peptides that can complement to form the active protein (196,197). The GFP is formed by 11 beta-strands that form a beta-barrel structure which imparts the fluorescent characteristic and allows GFP to be used as a chromophore (5). Removal of a 16 amino acid sequence that make up the 11th beta-strand of GFP prevents it functioning as a fluorescent molecule (5). Co-incubation of the two peptides result in complementation with recovery of the fluorescent protein. These assays are powerful tools as they allow direct detection of cytosolic delivery with low background staining that can be quantitatively measured as each delivered peptide results in a 1:1 ratio of delivered peptide to signal molecules produced (5).

1.6 Signalling pathways

Signalling pathways control many cellular processes and are vital for correct function. A cell needs to be able to respond to external stimuli to react to the local environment. Signalling molecules are used in multicellular organisms to coordinate cellular responses. For example, growth factors encourage cell proliferation and growth in areas where it is required. In order to respond to a signal, usually a receptor is activated at the cell surface and the signal is

transduced across the membrane into the cytosol of the cell. Kinases are important proteins involved in signalling as modification with phosphate groups is used as a reversible post translational modification to switch from an inactive to an active form. Many signalling pathways utilise cascades of kinase signalling to amplify signalling from receptors. If a signalling pathway that increases endosomal permeability could be identified, activation of the signalling pathway in a subset of cells would specifically increase endosomal release in these cells. This would increase specificity, increase effectiveness of the therapeutic and decrease side effects. Additionally, a biological signal is less likely to cause cell toxicity as the delivery mechanism is part of the cellular biology instead of artificial permeabilization of the endosome which is likely to have deleterious effects on the cell.

1.6.1 Epidermal growth factor signalling

Epidermal growth factor signalling is involved in cell growth, survival and proliferation (198). It is one of the most important signalling pathways and has been extensively researched. Because of its role in promoting proliferation and inhibiting apoptosis, it has an important role in the progression of certain cancers (126). The signalling pathway is made up of 4 members of the ErbB family of receptor tyrosine kinases; ErbB1 aka EGF receptor (EGFR), ErbB2 aka HER2, ErB3 and ErB4 (199). Activation of the receptors by ligand activation results in homodimerization or heterodimerisation of two receptors (200). There are currently 15 ligands known to activate the 4 receptors of the ErB2 family and leads to a complex signalling pathway that has some functional redundancy (201,202). Each ligand has a range of specificities for each receptor and different binding affinities. The classical EGF receptor and most widely studied is the epidermal growth factor (EGF). The EGF can bind and activate the epidermal growth factor receptor with a high binding affinity. Activation of the receptor causes homodimerization of two EGFR molecules or heterodimerisation with a different member of the Erb2 family of receptor tyrosine kinases. The different combinations of receptors can change the signalling length and outcome. The Her2 receptor does not have a high affinity ligand and is thought to prolong the signal induced by heterodimerising with one of the other Erb2 receptors (203). After dimerization, a receptor tyrosine kinase domain is activated, leading to phosphorylation of certain tyrosine residues located in the cytosolic domain of the protein. This phosphorylation can recruit a plethora of signalling molecules via

SH2 and PTB domains and acts as a scaffold for signalling. The signalling output will depend on the proteins recruited and modulation of signalling can be achieved through alternative activation and recruitment of downstream effectors. Many additional signalling pathways are activated by EGF including the ERK/MAPK pathway, AKT-PI3K and PLC-y1/PKC(204). The activation of EGFR leads to the activation of the largest number of unique signalling pathways with the other ligands activating alternative pathways and with differing strength of activation. An additional idea in EGF signalling is transactivation of the receptor via activation of different signalling pathways. Activation of Jak2 kinase via its associated ligands has been shown to result in phosphorylation and activation of the EGFR from the cytosol without the need for direct ligand activation. This allows interconnection between different signalling pathways increasing the complexity when trying to understand the effects of ligands.

During this project epidermal growth factor (EGF) was used to stimulate cells. EGF selectively binds to the epidermal growth factor receptor to activate the signalling pathway. We used EGF stimulation to activate macropinocytosis in the A431 cell line. As A431 cells have upregulated expression of epidermal growth factor receptor, they strongly respond to EGF stimulation (122). In order to stimulate macropinocytosis, a high concentration of EGF is required, >50ng/ml (205). At lower concentrations EGF bound to its receptor will enter the cell via clathrin mediated endocytosis (206). At the higher concentration macropinocytosis will be triggered, potentially as a mechanism to quickly internalise large numbers of receptors to downregulate signalling. Growth factors have been shown to activate macropinocytosis and EGF activates macropinocytosis through downstream targets of EGFR. It is known PI3K and phosphoinositides are important regulators of macropinocytosis, and activation of PI3K by EGFR signalling has a role in macropinocytosis activation. Additional signalling pathways such as Ras and PKC are downstream of EGFR activation and have been shown to be involved in the regulation of macropinocytosis. Expression of constitutively active RAS or activation of PKC using the agonist PMA can activate macropinocytosis (207). PMA was used as a macropinocytosis activator for many experiments in this project as it activated downstream of EGFR signalling and activated a strong macropinocytosis response in our A431 cell line.

1.6.2 NF-kB signalling pathway

Nuclear factor kappa B (NFkB) is a transcription factor complex that activates the transcription of a wide variety of genes involved in the innate immune response and inflammation (208,209). The NFkB family of transcription factors contain 5 proteins; NFkB1(p50/p105), NF-kB2(p52/p100), p65(RelA), Rel-B and c-Rel (210). These proteins can form either homodimers or heterodimers with different combinations of proteins having different signalling outputs (211). The NF-kB transcription factors are sequestered in the cytosol in an inactivate form by proteins named inhibitors of kappa B (IkB) (210,212,213) (Figure1.08). There are multiple IkB proteins and they have different affinities for combinations of NFκB proteins in the dimer, likely having a key role in the regulation of signalling. Upon activation of the NFkB signalling pathway the IkB proteins are phosphorylated by the protein complex IKK (214). The IKK complex is a key regulator of NF-kB signalling and two important kinase subunits are IKKalpha and IKKbeta. Phosphorylation of the IkB proteins targets them for ubiquitination and subsequent degradation, leaving the NF-kB dimer to traffic to the nucleus where it can activate transcription(210). The current model has two distinct NFkB signalling pathways called the canonical NF-kB pathway and the alternative NF-kB pathway.

The hyper-activation of NFkB has been linked to autoimmune diseases associated with chronic inflammation leading to the assumption activation of NFkB signalling as a proinflammatory signalling system (215). Upon cell damage or recognition of foreign pathogenic antigens via pattern recognition receptors (PAMPS), there is a release of pro-inflammatory cytokines such as TNF-alpha and interleukin-1 (216). These cytokines have been shown to activate the canonical NFkB signalling pathway. This has led to an interest in NF-kB signalling as a potential therapeutic target for chronic inflammation. Activation of the canonical pathway is associated with the heterodimers containing relA or cRel and is activated in response to proinflammatory signals(217,218). The alternative pathway is activated via alternative signalling molecules such as CD40 ligand, B cell activating factor and the receptor activator of NF-kB. The alternative pathway utilises different NF-kB dimers. The alternative pathway is activated independently of IKKbeta and IKKgamma and utilises a homodimer of IKKalpha instead (219). Differential expression patterns of NF-kB proteins allow differential control of NF-kB signalling in different locations and tissues.

1.6.2.1 Inhibition of Nf-kB

As NF-kB is a central regulator of inflammation and the innate immune system there has been many attempts to find pharmacological inhibitors. There are now ~785 inhibitors of NF-kB signalling characterised highlighting its importance as a signalling pathway(220). There are 3 main areas of NF-kB signalling that these pharmacological inhibitors have targeted as key regulators. Initial activation at the ligand-receptor binding site is the first key target for inhibition. The inhibition of this initial stage will prevent the activation of the signalling pathway, preventing NF-kB activation by preventing the signalling molecules activating the intracellular signalling from the receptor. The next key target for inhibition is the IKK and IkB proteins. The phosphorylation of IkB by IKK is an essential step in NF-kB signalling to allow nuclear accumulation of NF-kB transcription factor. Inhibitors have targeted the kinase activity of the IKK complex directly to prevent degradation of the IkB inhibitory protein. Additionally, maintaining a high concentration of IkB is an effective way of maintaining inhibition of NF-kB (221). Either the degradation of IkB can be inhibited for example by

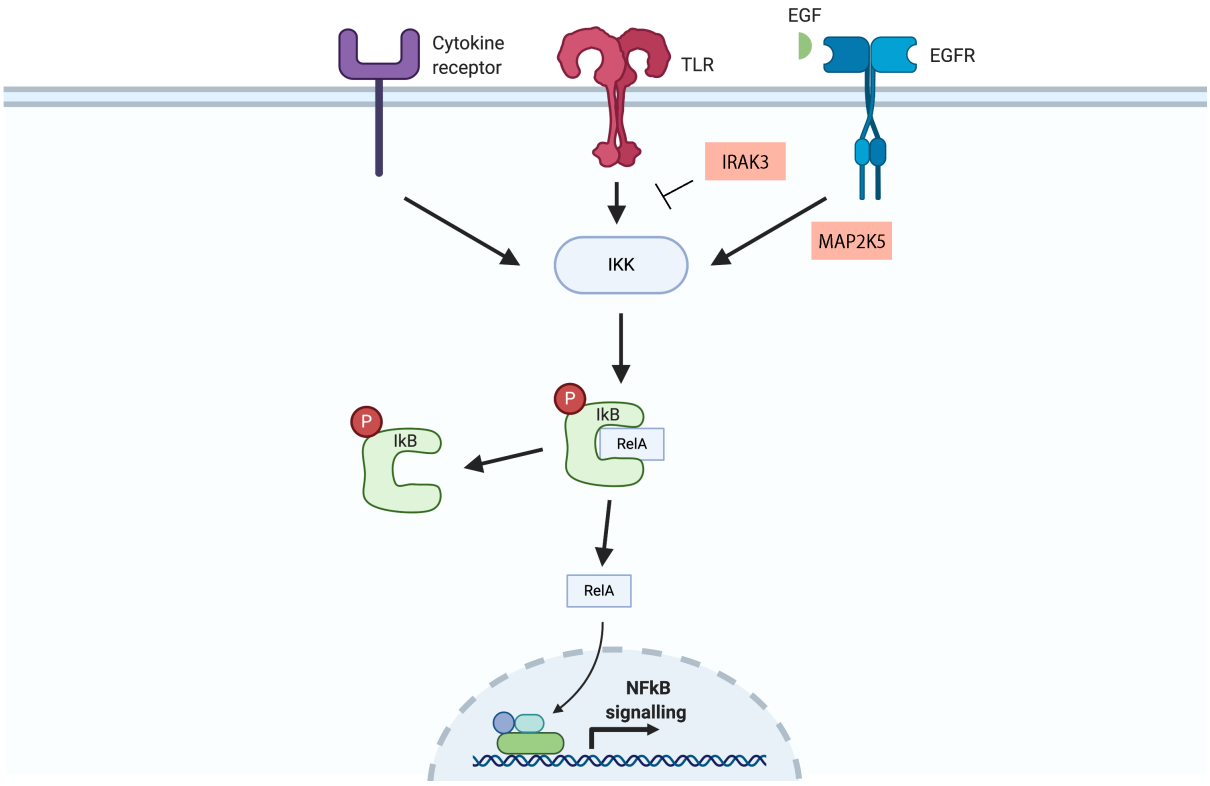

Figure1.09: The activation of the NF-kB signalling pathway

blocking the ubiquitin ligase enzymes to prevent degradation or the IkB protein can be overexpressed to maintain inhibition even when NF-kB is activated. The last key stage is the nuclear translocation and DNA binding of the active transcription factor. If the active NF-kB cannot enter the nucleus or bind to the DNA then no activation of NF-kB transcription can occur.

1.6.2.2 Activators of NF-kB

As discussed, the NF-kB pathway is activated in response to cytokines such as TNF-alpha and Il-1. The activation of NF-kB is part of the immune response to infection and stress. Cytokines can be released to activate the NF-kB pathway in adjacent cells to stimulate a local inflammation response (222,223). Additionally, activation of pattern recognition receptors such as the toll like receptor family have been shown to activate NF-kB. The activation of NF-kB in response to TLR activation induces the transcription of many proteins involved in the immune response. The activation of NF-kB is an important regulatory pathway in the immune response however additional signals have been discovered that activate NF-kB signalling indicating additional roles for the signalling pathway. Generation of reactive oxygen species can active the NF-kB pathway, which could be linked to the immune response to infection, but potentially indicates NF-kB signalling in environmental stress response.

Mitogens, such as the epidermal growth factor, can activate the NF-kB pathway (211,212). This has resulted in an interest in terms of oncology as mutations in growth factor signalling such as EGF that lead to activation of NF-kB provide beneficial survival signals for cancer cells. Many cancers have constitutively active NF-kB providing upregulation of genes leading to pro-survival and anti-apoptotic effects. Activation of EGF in A431 cells was shown to activate NF-kB signalling through degradation of the IkB inhibitory protein (211). This degradation was dependent on the proteasome. Intracellular calcium levels may be important for NF-kB signalling triggered by mitogens as it is known calcium ionophores such as ionomycin that increase intracellular calcium concentration by release of intracellular calcium stores can activate NF-kB signalling (211,224). Activation of EGFR activates Phospholipase C, generating two key signalling molecules in the EGF pathway, inositol 1,4,5 trisphosphate and diacylglycerol (DAG) (225). DAG activates Protein kinase C whereas inositol 1,4,5

trisphosphate activates the release of intracellular calcium stores providing evidence for a mechanism for NF-kB activation in response to EGF stimulation.

1.6.2.3 NF-kB in antigen presentation

The NF-kB pathway has been implicated in the processing of antigens for presentation. NF-kB has a key role in inflammation and is activated by pattern recognition receptors and could have a role in the processing of antigens. Activation of NF-kB in dendritic cells has shown to be important for antigen presentation. Overexpression of IkB to prevent activation of NF-kB in dendritic cells using an adenovirus vector system resulted in decreased antigen presentation indicating a role for the NF-kB pathway (174). Activation of NF-kB has been used as a vaccine adjuvant to enhance the immunogenicity and increase effectiveness (226).

1.7 Project aims

The initial aims of this project were to develop and validate an endosomal release assay that could detect the release of endocytosed material to the cytosol. The assay developed would need to be further optimised for high-content screening to enable us to perform a kinome wide siRNA screen to identify effectors of endosomal permeability. The identified hits would then need to be validated and acquire understanding into their mechanism of action. We wanted to try to identify a signalling pathway that is involved in endosomal release that can be manipulated to increase delivery.

1.8 Hypothesis

A siRNA kinome screen will identify key effectors of endosomal permeability and identify a signalling pathway which can be manipulated to increase endosomal permeability.

Chapter2: Material and methods

2.1 Common Buffers

- PBS: Phosphate buffered saline
  Fisher-BioReagents® tablets (#BPE9739-1)
  137mM NaCl, 10mM phosphate buffer 2.7mM KCl
- PB: Phosphate buffer (0.1M phosphate buffer pH7.2)
  Prepare 0.1M sodium phosphate dibasic and add 0.1M sodium phosphate monobasic until pH7.2
- TBS: Tris buffered saline
  20mM TRIS.HCl pH 7.4, 137mM NaCl
- TBST: Tris buffered saline tween20
  20mM TRIS.HCl pH 7.4, 137mM NaCl,0.1% Tween-20

2.2 Cell lines

- A431
- HT1080
- HEK293
- HEK293-Adeasy
- HeLa
- HeLa-M
- H358 (Medimmune)
- A431 (Medimmune)
- Ad293 (Medimmune)

2.3 Cell culture

2.3.1 Passaging of human cell lines

Cells were passaged upon gaining a confluency of approximately 90%. Media was removed using a vacuum pump aspiration system or manual removal. The cells were washed with sterile PBS, which was gently aspirated and replaced with a dissociation enzyme, routinely trypsin, followed by incubation at 37°C for 5 minutes or until all cells were detached. The dissociation enzyme was neutralized with appropriate cell culture media. A portion of cells were transferred to a new flask containing full media, a 1 in 10 dilution was routinely used and cells were passaged 2-3 times a week when required. Cells were used until they had been passaged between 20-30 times depending on visual and growth characteristics, but no cells were used over passage 30 apart from HT1080 cells. These cells were acquired at P35 and so care was taken not to culture the cells for an extended period.

Different cell lines had optimum growth in different media. The media used and dissociation method used for each cell line are located in table2-01.

Cell lines			
Name	Origin	Dissociation method	Media
A431	Human epithelial carcinoma	Trypsin	DMEM, 10%FBS, L-Glutamine , Pen/Strep
HT1080	Connective tissue Fibrosarcoma	Trypsin	DMEM, 10%FBS, L-Glutamine , Pen/Strep
HEK293	Human embryonic kidney	Trypsin	DMEM, 10%FBS, L-Glutamine , Pen/Strep
HEK293-AdEasy	Human embryonic kidney	Trypsin	DMEM, 10%FBS, L-Glutamine , Pen/Strep
HELA	Human Epithelial cervix carcinoma	Trypsin	DMEM, 10%FBS, L-Glutamine , Pen/Strep
HELA-M	Human Epithelial cervix carcinoma	Trypsin	DMEM, 10%FBS, L-Glutamine , Pen/Strep
H358 (Medimmune)	Non small cell lung cancer	TrypLE trpsin substitute	RPMI, 10% FBS , GlutaMax
A431 (Medimmune)	Human epithelial carcinoma	Acutase	DMEM, 10%FBS, L-Glutamine , Pen/Strep
Ad293 (Medimmune)	Human embryonic kidney	Acutase	DMEM, 10%FBS, L-Glutamine , Pen/Strep

*Table2.01: **Cell lines**: A list of cell lines used with the cell culture conditions and media used.*

FBS used routinely: heat inactivated FBS (Sigma #F4135)

Dulbecco's Modified Eagles' Medium- high glucose: DMEM(Sigma #D5796)

RPMI

L-Glutamine: (Sigma #G7513)

Pen/Strep: (Sigma #P0781)

2.3.2 Long term storage of cell lines

Long term storage of cell lines was achieved using liquid nitrogen cryo-preservation. Cells were grown until 90% confluency and passaged. After neutralisation of trypsin, the cells were transferred to a 15ml tube and spun at 100 x g to form a cell pellet. The cells were resuspended in cryo-storage medium which consisted of 90%FBS and 10% DMSO. After resuspension the cells were placed in cryovials and frozen using the Thermo Scientific Nalgene "Mr Frosty" system. When placed at -80°C, the system results in the optimum rate of temperature decrease for cell viability. After at least 2 days the cells were transferred to liquid nitrogen storage.

2.3.3 Thawing cell lines

Cells were retrieved from liquid nitrogen storage and thawed in a 37°C water bath for the minimum time required to thaw the cells. The cells were transferred to fresh full cell culture media and spun in a bench top centrifuge at 100 x g. The supernatant was aspirated, the pellet was resuspended with cell culture media and cells transferred to an appropriately sized

culture flask. After 24 hours media was replaced to remove any residual DMSO. Cells were left to grow and passaged at least once before use in experiments.

2.3.4 DNA Transfection

DNA transfection was routinely performed using Qiagen polyfect transfection reagent (301105) following the provider's protocol. Briefly DNA was combined with polyfect transfection reagent and incubated in serum free media for 10-20 minutes to allow formation of complexes. Full DMEM was added to the DNA-Polyfect complex and transferred onto cells. Occasionally DNA was transfected using lipofectamine 3000 reagent (ThermoFisher: L3000015) as it obtained a high level of transfection efficiency. The manufactures protocol was followed but was similar to the previously described protocol.

2.4 Molecular biology

2.4.1 Transformation of competent bacteria

Transformation of bacteria was routinely performed by heat shock. Competent bacteria were stored at -80°C and were thawed on ice for 10 minutes prior to transfection. Approximately 50µl of bacteria were transferred to thin-wall plastic tubes to aid heat shock. Plasmid DNA with a concentration between 1ng and 100ng was added to the bacteria and incubated on ice for 30 minutes. Bacteria were heat shocked at 42°C for 30 seconds and placed on ice for 3 minutes. 950µl of liquid broth was added to the bacteria and grown at 37°C in a shaking incubator at 1500RPM. After 1 hour incubation, the bacteria were spun at 1600 x g in a benchtop centrifuge and the pellet resuspended in liquid broth containing the relevant antibiotics to the resistance gene in the transfected plasmid. An appropriate number of bacteria was spread on agar plates to allow for distinct colonies to form after incubated. The plates were incubated inverted at 37°C. Glycerol stocks of transformed bacteria were made where necessary by addition of glycerol to the overnight culture to a final concentration of 15% and stored in -80°C freezer.

2.4.2 Competent bacteria

For general replication of plasmid DNA, the DH5α strain of *E.coli* bacteria that were made chemically competent in the lab were utilised. For expression and production of protein BL21

E.coli strain was utilized. For molecular cloning requiring high competency, XL10 gold (Agilent 200314) were used.

2.4.3 DNA extraction and preparation

Preparation of Plasmid DNA was performed by overnight culture in liquid broth followed by extraction and purification. For transformed bacterial cultures of 1-5ml, a Qiagen miniprep kit(Qiagen#27104) was routinely performed following manufactures instructions. Briefly, the cells were lysed and the genomic DNA precipitated. The lysate was run through a column that binds to plasmid DNA and washed. An elution buffer or water was utilized to extract bound DNA from the column. DNA concentration was determined by absorbance at 280nm using a nanodrop. For preparation of large quantities of plasmid DNA, a greater volume of bacteria was grown and a Qiagen maxiprep kit (Qiagen#12162) was performed following the manufactures protocol.

2.4.4 Expression and production of GFP-NLS

The GFP-NLS sequence had been previously cloned into a pQE9 mammalian expression plasmid by a previous member of the Smythe lab. Amplification of the plasmid was performed in DH5-alpha bacterial strain. Expression of the protein for purification was achieved by transformation of BL21 competent bacteria using the heat shock method described above. The Bl21 bacteria were plated onto agar and incubated inverted overnight at 37°C. Colonies were selected and used to inoculate a larger volume of liquid broth. Up to 400ml liquid broth in a 2L Erlenmeyer flask was grown at 37°C in an orbital shaker at 250rpm until the Optical density at 600nm was between 0.4-0.8. The production of the GFP-NLS was induced using 400µM IPTG for 3 hours at 37°C. The culture was collected by ultracentrifugation to produce a bacteria cell pellet. The pellet was resuspended fully in lysis buffer (25mM Hepes, 400mM KCl, 5% glycerol, 5mM MgCl2, 0.1% triton-x-100, pH7.4) and a spatula of lysozyme (~5g) was added. The solution was sonicated and clarified by centrifugation. The protein was purified using Nickel-agarose beads, the supernatant collect was bound to the beads by incubation for 1 hour in the presence of 25mM imidazole to prevent non-specific binding. The beads were washed, and the protein eluted with 400mM imidazole. The plasmid encoded a FP molecule with a nuclear localisation sequence on the C-terminal end of the protein. The NLS sequence on the GFP construct was a SV40 NLS sequence (Pro, Lys, Lys, Lys, Arg, Lys, Val).

2.4.5 Agarose gel electrophoresis

Agarose gels were prepared by dissolving the required agarose in TAE buffer and heating. DNA stain, 10mg/ml Ethidium Bromide or sybersafe (Fisher Scientific #S33102), was added to the molten agarose and poured into casting frames. The gels were ran at 100v using a Bio-Rad Sub-Cell GT® electrophoresis system until the bands had migrated a sufficient distance to allow separation of fragments.

Gels were imaged using the Gel Doc™ EZ System (Biorad #1708270) to image and capture the position of the bands. Band intensity, if required, were measured using the open-source application FIJI.

2.4.6 Restriction digest of plasmid DNA

Restriction digest was performed on DNA for multiple purposes including quality control and for sub-cloning. DNA (1µg) was incubated with 10 units of restriction enzyme in the appropriate enzyme buffer and milli-Q water up to 50µl. The reaction was incubated at 37°C in a water bath for up to an hour depending on the enzyme used. Reaction products were run on an agarose gel for visualisation.

2.5 Protein analysis

2.5.1 Bradford assay

For protein concentration determination, the BioRad protein reagent (Bio-rad #500-0006) was performed following the manufacturer's instructions. Briefly the 5x stock protein assay solution was diluted to a 1X working stock. A BSA standard curve was created using known protein values of Bovine serum albumin (Melford #A30075-100.0). Between 10µl and 50µl of sample was added to 1ml of 1X BioRad protein assay reagent in a cuvette and inverted until the solution was homogenous. The absorbance of the solutions was read at 595nm in a spectrophotometer. To create the standard curve, each concentration of BSA standard was performed in duplicate and with the sample volume of the unknown samples. The concentrations used for the standard curve were between 0.1 mg/ml and 2 mg/ml as this is the linear range of the assay. Depending on the experiment the samples of unknown protein concentration were diluted in the lysis buffer to decrease the concentration to the linear range, usually 1 in 10 dilution was required.

2.5.2 SDS Page gel electrophoresis and Western blotting

2.5.2.1 Sample preparation

Cells were seeded in 6 well plates and different experimental conditions applied depending on the experiment. Cells were placed on ice and cold lysis buffer was added. Lysis buffer was either RIPA buffer or PBS with 0.5% triton-x-100 and cOmplete™ EDTA free protein inhibitor tablet (Sigma #11873580001) to 1X. A minimal amount of lysis buffer was added to the wells as to not dilute the samples too far. For a 6 well plate a maximum of 100µl was added to each well. After incubation for 5-10 minutes to allow for lysis the cells were disrupted using cell scrapers in order to dislodge cells from the well. The lysates were moved to ice-cold sterile Eppendorf tubes and incubated on ice for 30 mins. Cellular debris was removed by centrifugation at 12,000 G in a bench top centrifuge. The supernatant, containing cellular proteins, was removed from the pellet and transferred to a clean Eppendorf and stored at -20 until use.

Samples for western blot were prepared by addition of Laemmli buffer. 5X stock of Laemmli buffer was added to the protein samples to give a 1X final concentration and a sample protein concentration of between 20-40 ug depending on well size.

2.5.2.2 SDS PAGE (Poly acrylamide Gel Electrophoresis)

To separate proteins via SDS PAGE electrophoresis gels were cast suing the Bio-Rad Mini-Protean Tetra system. A separating gel (Table2.02) was cast initially which allows separation of proteins based on size. The separating gel was covered with 100% ethanol during polymerisation. After sufficient time to allow polymerisation of the separating gel the ethanol was discarded and a stacking gel (Table2.02) was cast onto of the separating gel which ensures the protein samples enter the separating gel simultaneously. Gels were routinely 10% acrylamide as most proteins were standard molecular size. Samples were heated at 100 degrees for 5 mins in a heat block prior to loading. The gel was transferred to a running chamber where gel running buffer was added (25mM TRIS pH 8.3,192mM glycine, 0.1%SDS). A protein ladder of known sizes was added to determine the molecular size of samples,

routinely used (NEB: Colour Protein Standard Broad Range-P7719S). Gels were running at a low voltage (60-80V) until the dye front had entered the separation gel, and then the voltage was increased to (100-120V) until the dye front was almost at the bottom of the gel. The current was stopped, and the gel removed. The dye front was not removed from the gel.

SDS-PAGE gel recipe			
Seperating Gel-10%		Stacking gel	
Component name	Concentration	Component name	Concentration
Bis-Acrylamide	10%	Bis-Acrylamide	4.95%
Tris-HCl pH-8.8	375mM	Tris-HCl pH-8.8	0.1875mM
SDS	0.1% (w/v)	SDS	0.1% (w/v)
Ammonuim persulfate (APS)	0.05% (w/v)	Ammonuim persulfate (APS)	0.05% (w/v)
TEMED	0.05% (v/v)	TEMED	0.05% (v/v)

Table 2.02: SDS-PAGE gel recipe*- The recipe used for casting stacking and separating gels*

2.5.2.3 Blocking and transfer

The gel was removed from the gel running system and the proteins were transferred to a 0.45µm nitrocellulose membrane (GE Healthcare Amersham Protan-10600007) at 100V current for 65 minutes at room temperature. The transfer was performed in transfer buffer (25mM TRIS,192mM Glycine, 20% methanol). The membrane with the proteins were blocked in 5% (w/v) skimmed milk powder in TBST solution(20mM TRIS.HCl pH 7.4, 137mM NaCl,0.1% Tween-20) for 1 hour.

2.5.2.4 Antibodies and imaging

After blocking the primary antibody was diluted in 5% (w/v) skimmed milk powder in TBST solution. The primary antibody was diluted to a concentration specified by the manufacturer and optimised after if required. The membrane was incubated in the primary antibody for 1 hour at room temperature or overnight at 4 degrees Celsius. The membrane was washed 3 times for 5 minutes with 5% (w/v) skimmed milk powder in TBST solution. The correct LICOR secondary antibody that recognised the primary antibody was diluted in 5% (w/v) skimmed milk powder in TBST solution at a concentration of 1 in 10,000. The membrane was incubated

in the secondary antibody for 1 hour followed by three 5-minute washes in TBST. The membrane was left to dry and then imaged using a LI-COR Odyssey® Sa. Data acquired was analysed using the Image StudioTM Lite software.

2.6 Adenovirus production and validation

The Adenovirus used was produced using Agilent's Adeasy viral kit(240243). The adenovirus produced was serotype Ad5 and was replicative inactive. The E1 replicative enzyme had been removed to prevent long term infection as the adenovirus requires the E1 enzyme for successful replication. Adenovirus is a class 2 biological pathogen and so all processes involving adenovirus mentioned were performed under class 2 safety procedures and in an appropriate corresponding laboratory. The adenovirus was inactivated with 24hour treatment with bleach after use.

2.6.1 HEK293 AdEasy cell culture

HEk293 AdEasy cells were obtained from Agilent. The HEK-293 cells stably express the E1 replicative enzyme from adenovirus to allow for virus replication. The cells were kept at a low passage number and low confluency as per manufactures guidance to gain the best titre. The cells were grown in DMEM, 10% FBS, gly, Pen/strep and passaged when cells were approximately 80% confluency.

2.6.2 Adenovirus production

Adenovirus production was carried out using the Agilent AdEasy Virus Purification Kit 2x100. The protocol was followed using the manufactures protocol. Briefly, HEK AdEasy cells were plated in 60mm dishes the day before infection. On the day of infection, cells should be at a confluency of 60-80% to maintain growth phase of the cells. Cells were infected with adenovirus that was previously made in the Smythe lab using the pAdEasy vector system. Described briefly, the shuttle vector (including a gene of interested if applicable) is co-transformed in BJ5183 bacteria with the pAdEasy-1 vector. Homologous recombination occurs resulting in production of a plasmid encoding the desired adenovirus. Pac1 digestion produces linear DNA that can be transfected into HEK293-AdEasy cells which will produce the adenovirus resulting in cell lysis. The corresponding supernatant contains adenovirus and the cells can be collected by manual disruption using a cell scraper. The collected cells and supernatant are centrifuged at 200 x g to separate a cell pellet. Cells were lysed by alternate

freeze, either a -80 freezer or more commonly an ethanol-dry ice bath, and thaw with a 25°C water bath. The temperature should not exceed 25°C as this may lower titre. The lysed cells contain adenovirus and was called the 1° adenovirus stock that was used to infect the cells during subsequent rounds of virus production. After production of the 1° adenovirus stock further amplification was performed using the AdEasy Virus Purification Kit. After the purification protocol the new stock of adenovirus produced was 2°. Only 1°,2° and rarely 3° adenovirus stocks were amplified to reduce the risk of recombination events resulting in replicative active adenovirus. A MOI (Multiplicity of infection) of 10-20 was used for amplification of stocks. After infection, cells were incubated at 37°C for 3-5 days or until cells were showing cytotoxic characteristics and detaching from the surface of the dish. Collection of the supernatant and cells proceeded as previously described but the viral solution was treated with 12.5 U/ml of Benzonase nuclease for 30 mins at 37°C to remove DNA and RNA. Using a system of clamps and tubing the solution was filtered using a 0.45µm filter and then run through a Sartobind filter that specifically binds adenovirus particles. Elution from the filter was carried out using the elution buffer provided. Importantly the rate of fluid flow through the filter can result in loss of viral titre and so the specified rate should be maintained. After elution, the virus was buffer exchanged using a centrifugal concentrator and stored in PBS.

2.6.3 Virus titre

Once produced, the adenovirus was tittered using an adaption of the AdEasy Viral Titer Kit. HEK-AdEasy cells were plated in a 24 well plate and on the same day dilutions of virus was added from 1x10-2 : 1x10-8 as well as a negative control well without addition of adenovirus. The cells were left to be infected for 2 days and fixed with ice-cold methanol taking care not to disrupt the cell monolayers. Higher concentration of the virus might have resulted in cell death. Using the immunofluorescent protocol described in the AdEasy Titer kit cells were stained with a primary antibody against adenovirus and secondary antibody staining with a florescent secondary resulted in staining of cells containing adenovirus. The plate was observed using a fluorescent microscope and the number of cells infected responds to the titre of the virus.

2.6.4 Virus storage

Once produced, the virus was kept in sterile PBS.

Virus was only thawed once after the initial production and flash freezing using liquid nitrogen to prevent the loss of titre and was kept in a lockable -80°C freezer.

2.6.5 Infection of A431 cells

For infection of A431 cells, virus aliquots were removed from the -80 freezer and thawed on ice. If the virus required concentrating or buffer exchange, this was performed using a 100,000 molecular weight centrifugal concentrator to PBS. Virus was diluted in serum free DMEM and added to cells for indicated time periods and at various concentrations.

2.7 Microscopy techniques

2.7.1 Widefield imaging

Widefield microscopy was performed on a Nikon dual camera system. An inverted Ti eclipse with OKO-lab environmental control chamber. Objective lenses

Objective	Description
10X	Plan Apo 10X (NA 0.45)
20X	Plan Apo 20X (NA 0.75)
40X	Plan Fluor 40X Oil (NA1.3)
60X	Apo 60X oil (NA 1.4)
100X	Plan Apo 100x Ph oil (NA1.45)
100X	Plan Apo VC 100x oil (NA 1.4)

Excitation source: SpectraX LED excitation (395nm, 440nm ,470nm ,508nm ,561nm, 640nm)

Detectors: Dual Andor Zyla sCMOS 2560 x 2160 6.5µm

2.7.2 Confocal imaging

Confocal microscopy was performed using a Nikon A1 confocal system.

Objective	Description
10X	CFI Plan Fluor 10X (NA 0.3)
20X	CFI Plan Fluor 20X MI(NA 0.75)
40X	CFI Super Pan Fluor ELWD 40X (NA 0.6)
60X	CFI Plan Apochromat VC 60x oil(NA 1.4)

Excitation source: 405nm, 457-514nm argon laser, 561nm sapphire laser, 642nm diode laser

Emission filters: Single filter for GFP, RFP and DAPI, Quad filter DAPI/GFP/RFP/Cy5

Detectors: 4 standard filter PMTs

2.7.3 Immuno-fluorescence

For immunofluorescence experiments, cells were seeded onto coverslips for large plate formats (6 well and 12 well plates). For high throughout experiments in 384 well plates staining, and imaging was performed in-well without the need of coverslips. However, the technique was performed using the same protocol.

Cells were routinely fixed with 4% PFA for 20 minutes. After fixation two 10-minute washes with 50mM NH4Cl was added to quench any remaining fixative. Cells were washed with PBS two times prior to the IF protocol. Cells were first blocked in blocking buffer (PBS-0.5% Fish Skin Gelatine) for 20 minutes. Following this, cells were permeabilised using PBS-0.5% FSG-0.1% Triton-x-100 for 10 mins. Primary antibodies were diluted in blocking buffer at a concentration dependant on the antibody being used, manufacturers specifications and optimisation considered. Primary antibody was incubated at room temperature for 1 hour followed by three 5-minute washes using blocking buffer. Secondary antibodies were also diluted in blocking buffer and protected from light. SA was incubated for 1 hour followed by three 5-minute washes using blocking buffer. Coverslips were mounted onto cover glass using prolong gold antifade reagent following a brief ddH20 wash to remove excess salts. Samples were incubated on a flat surface in the dark overnight before imaging.

2.7.4 Dextran uptake assay

Uptake of 70kDA dextran was used to mark macropinosomes as due to its size the majority of 70kDa dextran is endocytosed via macropinocytosis rather than other forms of endocytosis. The co-localisation of transferrin was used to confirm uptake of dextran by macropinocytosis as little colocalisation was observed between 70kDa dextran and transferrin indicating distinct populations in the endosomal system (Figure3.02) . Other size dextran's were occasionally used depending on the experiment. Dextran is water soluble and

was dissolved in ddH20 to form a stock solution at a concentration of 20mg/ml. The dextran was dissolved fully and centrifuged at around 10,000g to remove any large, undissolved dextran. The dextran was aliquoted and stored at -20℃. The number of freeze thaw cycles for each aliquot was kept to a minimum. Multiple dextran conjugates were used, including: Dextran-Tetramethylrhodamine 70kDaMW lysine fixable (Invitrogen D1818), Dextran-Fluorescein 70kDa Anionic lysine fixable (Invitrogen D1822) and Dextran Oregon Green 488 70kDaMw Anionic Lysine Fixable (Invitrogen D7173).

Cells were serum starved in DMEM for a minimum of two hours prior to the experiment. Dextran was diluted in serum free-DMEM with 0.2% Bovine serum albumin added. The final concentration of dextran was 0.125 mg/ml cells were incubated with the dextran at 37℃. After incubation at 37°C for the specified time, cells were placed on ice and washed 2 times in ice cold DMEM-BSA, then washed with an acid wash followed by PBS-BSA-0.2%. The acid wash was repeated, followed by PBS-BSA washes four times. Cells were fixed with 4% paraformaldehyde for 20 minutes followed by NH4Cl to quench any remaining PFA. DAPI (1µg/ml) was added either separately in PBS or diluted in either the PFA or NH4Cl steps but was always followed by 2 wash steps before imaging. If coverslips were used, they were mounted onto cover glass using prolong gold mounting reagent.

2.7.5 HRP uptake assay

HRP uptake was used to detect the release of endosomal content to the cytosol. HRP powder (Sigma P8250) was dissolved in DMEM BSA-0.2% to a final concentration of 10mg/ml unless stated otherwise. Cells were serum starved for at least 2 hours prior to the experiment and then incubated with HRP. After 10 minutes the HRP was removed and the cells were washed with DMEM-BSA-0.2%. The cells were incubated for 90 minutes at 37°C. After the 90 minutes the cells were placed on ice and washed 3-4 times with ice cold DMEM-BSA-0.2%, followed by 4 washes with ice cold PBS. Cells were fixed for 10 minutes in 4% PFA. The length of fixation was optimised to be a critical stage in the process to develop effective HRP staining. Excess PFA was quenched with 50mM NH4Cl for 2 x 10-minute washes. The first NH4Cl wash contained Draq-5 nuclear stain(5µM). After quenching the cells were washed twice in phosphate buffer. A diaminobenzidine reaction was utilized for HRP localisation. DAB was dissolved in Phosphate buffer (0.1M phosphate Buffer pH7.2) to a concentration of 0.5mg/ml. Hydrogen peroxide was added to the DAB solution immediately prior to staining to a final

concentration of 0.003%. The cells were incubated with DAB for 10 minutes followed by washing twice with PBS. As DAPI staining is not compatible with DAB, DRAQ-5 was used as an alternative nuclear stain. The product of the HRP reaction with DAB results in an insoluble product that seems to quench the fluorescence of DAPI making them unsuitable to be used together. This was discovered after optimisation and so initial experiments used DAPI staining. After DAB staining was performed there was an accumulation of non-specific DAB background, likely produced by non-internalised HRP. To limit the impact of this non-specific background plates were washed three times after DAB staining with phosphate buffer and plates were imaged as soon as possible, usually on the same day as DAB staining.

2.7.6 LNP uptake assay

Cells were reverse transfected in a PerkinElmer cell carrier ultra 384 (black wall, clear bottom) plate. The siRNA was transferred either using a multi-channel pipette or using a Labcyte Echo555 liquid handling unit. The siRNA transferred was in a volume of 5µl and 150nM concentration. The transfection reagent, 6µl RNAi-Max at a concentration (1/100), was added to the siRNA to form a complex. The complex was left to form for 10 minutes before the cells 30µl were seeded into the plates. The final siRNA concentration in the well was 18.75nM. The plates were incubated at 37°C for 3 days to allow sufficient knockdown to occur. Any pharmacological inhibitors used and the EGF stimulation was transferred to the cells via ECHO liquid transfer. This process allowed rapid transfer to all the wells requiring EGF addition. Following addition of EGF, the MC3-LNP was also added by ECHO liquid transfer to disperse 20ng per well(or 40ng in certain control wells). The plates were sealed and incubated at 37°C for 24 hours. The cells were fixed using 4% PFA and the nuclei stained with Hoechst staining. The plates were washed 3 times with PBS using a BioTEK plate washer. The cells were imaged using a Yokogowa CV8000 high-throughput microscope and the images analysed using the PerkinElmer Columbus analysis software (Described in 2.8.4)

2.7.7 Flow cytometry

When preparing cells for flow cytometry analysis, the cells were dissociated into solution using a EDTA based enzyme free dissociation buffer (Gibco-13151014). The cells were collected by centrifugation at 1000g. The cells were resuspended in ice-cold PBS-0.5% BSA in 1.5ml Eppendorf tubes and incubated with the Primary antibody for 30 minutes at 4°C. The

cells were washed 3X by centrifugation at 1000g for 5 minutes and the supernatant exchanged with PBS-0.5% BSA. The cells were incubated with a complementary fluorescent secondary antibody. The cells were washed 3 times as performed previously and the cells were resuspended prior to analyses by flow cytometry. The analysis was performed using a BD-LSRII flow cytometry system, with 10,000 objects being detected per condition. The forward scatter and side scatter were detected for each object to detected size and granularity respectively. A gate was selected based on the forward vs side scatter to select objects that are likely to be cells. The objects fluorescent intensity was detected using a laser to detect the secondary antibody fluorescence. The fluorescent signal was gated based on the background signal obtained from a secondary antibody control, where samples were incubated without the primary antibody.

2.8 High throughput screening techniques

2.8.1 384 well plate assays

384 well plate assays were carried out either in the SRSF screening facility at the University of Sheffield or at the Darwin building, AstraZeneca. The high throughput plate format used were the Perkin Elmer black 384 well View plates or PerkinElmer cell carrier ultra 384 (black wall, clear bottom)

Seeding

Cells were either seeded by hand using a 96 well multichannel or via a multidrop automated system, the ThermoFisher Scientific Combi Reagent Dispenser (5840300). Cells were passaged as previously described and diluted to the correct volume in Full DMEM. A standard multidrop cassette was soaked in 70% ethanol for 30 minutes prior to use with cells. The feed tubes were primed with ethanol followed by autoclaved distilled water and then placed into the cells for dispensing.

Aspiration

Aspiration was performed using either a BioTek ELx405 plate washer automated unit or using a 384 aspiration wand (VP189LP) from V&P scientific, INC. To ensure the correct volume of

liquid remained after aspiration to prevent disruption of the cells, O-rings were added to the wand to increase the liquid left after aspiration. The wand was optimised to leave approximately 10µl (Figure2.01). The pins were regularly cleaned using a metal cleaning rod and flushed with dH20 and ethanol. Additionally, a low concentration bleach solution was used to disinfect after use with adenovirus.

A

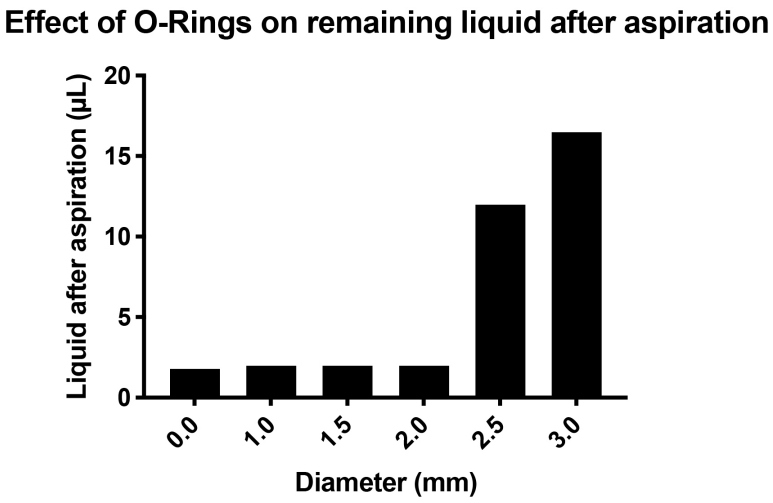

Figure2.01: The effect of O-rings on remaining liquid after aspiration- *Liquid was aspirated from 384 well plates using the 384-aspiration wand (VP189LP) from V&P scientific, INC. The volume of liquid in the well was measured after aspiration with different diameter O-ring attachments which increased the hight of the pins and therefore increased the volume remained.*

2.8.2 RNA reverse transfection

To transfect cells in a high throughput manner, reverse transfection of cells was utilized. The Hamilton Microlab STAR robotic dispenser was used to seed plates from a siRNA collection or siRNA was transferred manually. Each well normally contained 150 nM siRNA and stored at -80°C until use. Plates were thawed before use and transfection reagent was added using a multidrop system. Plates were incubated at room temperature for 10-15 minutes to allow complex formation. Detached cells were then seeded on top of the complex to give a final concentration of 30nM siRNA. Cells were left to settle for 30 mins in the tissue culture hood before transfer to 37 °C. Plates were sealed with a PlateLoc system or using a manual seal.

2.8.3 High-throughput microscope

Imaging of high-throughput plates was performed using a molecular devices, image Xpress micro system to capture widefield fluorescent images.

Additionally, an InCell analyser 1000 was utilized for high throughput brightfield imaging that was required for DAB staining images.

For LNP uptake assays performed at AstraZeneca a YOKOGAWA Cellvoyager CV8000 was utilised for high-throughput imaging of multi-well plates.

2.8.4 High-throughput image analysis

Analysis of high-throughput images was performed using molecular devices software package, MetaXPress. Automated nuclei counting detected cell number and depending on the assay different custom module editors were utilized during the analysis.

Images acquired using the InCell analyzer system were transferred into MetaXpress using the Xchange software and then processed using the same CME modules.

For images acquired on the YOKOGAWA microscope, Columbus imaging software (**PerkinElmer Columbus v2.8.3)** was utilized, and previously developed scripts by AstraZeneca scientists were used to analyse the results.

The following analysis pipeline was used for image analysis of LNP uptake assays:

1. Input Image – default settings
2. Find Nuclei – find all nuclei based on Hoechst staining
3. Calculate Intensity Properties – of all nuclei
4. Calculate Morphology Properties – of all nuclei
5. Select Population – refine nuclei identification using results of steps 2-4
6. Find Cytoplasm – based on Hoechst staining and nuclei identified in step 5
7. Calculate Morphology Properties – of cells (using cytosol from step 6)
8. Select Population – remove border objects based on cytosol
9. Select Population – refine cell population using cytosol size
10. Calculate Intensity Properties – of mCherry fluorescence
11. Define Results – export data as well means + standard deviation

2.8.4.1 High throughput macropinocytosis assay analysis

To analyse the level of macropinocytosis after automated imaging, the number of macropinosomes per cell were calculated. A nuclei count was performed using the DAPI stain.

A prebuilt nuclei detection algorithm was utilized that could be optimised with size and intensity and create a nuclei mask. The nuclei mask was expanded to give an approximation of the cell area. The dextran signal was thresholded and large dots detected were counted as macropinosomes (Approx. size 1-5µm). Very large dextran background (Size:40-200µm) was substituted from the final macropinosome mask. The number of nuclei could be counted to give an overall cell number. The number of macropinosomes inside the cell area mask was calculated and divided by the overall cell number to give the average number of macropinosomes per cell. For each well 9 images were acquired, and the nine data points were averaged to acquire a single value for each condition. (A full analysis script is located in the appendix-Section 8.2).

2.8.4.2 NF-kB nuclear translocation assay

To measure Nf-kB nuclear translocation an automated pipeline using CellProfiler was developed. The pipeline detected the nuclei mask using the nuclei fluorescent dye used. The number of cells per image was counted from the number of masks identified and the fluorescent intensity from the NF-kB antibody was detected for each nuclei mask. The nuclei were filtered based on a fluorescent intensity threshold to determine cells with nuclear translocation. We were then able to determine the percentage of cells with nuclear translocation of NF-kB.

2.8.4.3 HRP release assay analysis

To measure the number of cells with cytosolic DAB staining a similar approach was used. The images from the Incell Analyzer were imported into the MetaXpress software and analysis was performed. The nuclei mask was obtained and expanded as before. The DAB stain was thresholded using a Metaexpress module called 'Find Dark Holes' that detects local pixel regions of low intensity when compared to the local pixel environment. The module was found to be very effective at locating cells with cytosolic DAB staining. The cells were filtered based on the intensity of the threshold mask produced by the 'Find Dark Holes' module and positive cells were counted. A total cell count allowed the calculation of the percentage of cells showing endosomal release. The full analysis method can be found in the appendix(Section8.1).

2.9 Gene expression and RNA analysis

2.9.1 RNA extraction

RNA extraction was performed using TRI-Reagent. For a 6 well plate, 1ml of tri-reagent was added to each well. Incubation for 10 mins resulted in lysis of cells while inhibiting RNAase activity. The contents of the wells were transferred to sterile RNAase free Eppendorf tubes. Addition of 200µl of chloroform and vortexing for 20s was followed by 5-minute incubation at room temperature. The samples were centrifuged for 15 minutes at a speed of 17,000 x g at 4°C. This results in separation of the sample into 3 phases. The top, colourless phase contains the RNA content and this phase was carefully transferred to a new sterile Eppendorf, avoiding contamination from the other layers as this effects further processes. Addition of an equal volume of isopropanol was added to the RNA sample and vortexed for 20s and an incubation for 10 minutes at room temperature. Samples were additionally centrifuged at 17,000 x g for 10 minutes at 4°C. This step results in an RNA pellet forming at the bottom of the tube. The supernatant is removed carefully from the pellet and replaced with 75% ethanol as a wash step. Centrifugation at 17,000 x g for 5 minutes at 4°C was followed by removal of the supernatant again. The sample was air dried for 10 minutes with care to make sure all contaminating ethanol has been removed as this effects nanodrop RNA concentration analysis. The RNA pellet was resuspended in RNAase free water. Nanodrop analysis by measuring the absorption at A270 was used to get a concentration of the extracted RNA.

Alternatively, RNA was extracted using the RNeasy Mini Kit from Qiagen (74104), following the manufactures instructions.

2.9.2 RT-PCR

The High-Capacity RNA – cDNA kit (ThermoFisher Scientific # 4388950) was used to convert the RNA to cDNA for use in q-PCR. The reaction was carried out using the manufactures instructions. Briefly the same amount of RNA was used for each sample and made up to 20µl following the table.

Component	+RT reaction	-RT reaction(control)
2X RT Buffer mix	10µl	10µl
20x RT Enzyme Mix	1 µl	0 µl
RNA sample	Up to 9 µl	Up to 10 µl
RNAase free water	Up to 20 µl	Up to 20µl
Total volume	20µl	20µl

The reverse transcription reaction was run in a thermocycler using the following parameters.

Step1: 37°C for 60 minutes

Step2: 95°C for 5 minutes

Step3: Hold at 4°C

cDNA was stored at -20°C until used. The cDNA was diluted 1/10 in distilled water as components of the reverse transcription reaction can affect the following qPCR reaction.

2.9.3 qPCR

The qPCR reactions were performed using an Applied Biosystem QuantStudio 12K Flex system using SYBR green. A 10µl reaction was setup per well:

2µl of template cDNA

1µM Forward primer

1µM Reverse primer

RNase free water up to 10µl

5µL SYBR Green JumpStart Taq ReadyMix (Sigma S4438)

The reaction was performed in a qPCR applied biosystems MicroAMP optical 384-well reaction plate-(4309849)

2.10Primers

qPCR primers		
Gene name	Sequence- Forward 5'-3'	Sequence- Reverse 5'-3'
GAPDH	GTC TCC TCT GAC TTC AAC AGC G	ACC ACC CTG TTG CTG TAG CCA A
IRAK-M	ATG CTC GGT CAT CTG TGG CAG T	CTC TGA TGT TCT AGG TGG GAC C
MAP2K5	CCT TCC AGT TGG AGA GTT CTC G	CGG CAT TTC CAT CAT TGA ACT GC
PEAK-1	GCA TTA CTA CAG GAC TCA GAG AAG	CCT GCC ATC TTG CTT CCC AAC A

Table2.03: qPCR primers

2.11 Antibodies

Antibodies		
Target	Catalogue number	Concentration used
Adenovirus	151-9004	1 in 1000 dilution
GFP antibody	ab290	1µg/ml
Anti-intergrin alphaV	ab179475	0.921 µg/ml
Anti-tubulin	11224-1-AP	1 in 1000 dilution
B actin	A1978-200ul	1 in 1000 dilution
NF-kB p65	sc-8008	1 in 1000 dilution
IKB alpha monclonal	MA5-15132	1 in 1000 dilution
Phospho-nfkb	MA5-15160	1 in 1000 dilution
anti-galectin	PA012887YA01HU	3µg/ml
anti-ova-sinfekly-human	GTX14318	5.02µg/ml
MHC class 1 antibody (W6/32)	sc-32235	1 in 1000 dilution

Table2.04-Antibodies

Chapter3: Assay development

The aim of my project was to identify the mechanisms involved in endosomal release. To help understand these mechanisms of release, we wanted to identify the signalling proteins that are involved in endosomal permeability and macropinocytosis. We decided to use an siRNA screen to identify the relevant molecules and to do this we first needed to establish robust assays for macropinocytosis and endosomal release which could be used in a high throughput format. Previous studies had shown that uptake of 70KDa dextran can be used to selectively mark macropinosomes(116,134,227,228). Due to its large size, 70kDa dextran is excluded from clathrin coated pits (diameter ~ 100nm) and exclusively taken up via macropinocytosis. Different fluorescent molecules can be conjugated to the dextran which enables the use of fluorescent microscopy to observe macropinocytosis in cells.

Developing an assay for endosomal release is a harder prospect. The use of a fluorescent signal, such as a conjugated dextran, has been used previously to detect endosomal release and subsequent cytosolic fluorescent staining (192) but this requires a very high concentration of dextran to enable sufficient uptake for enough signal to be detectable in the cytosol following endosomal release. Additionally, any fluorescent signal observed from within the endosomal system will produce a higher signal prior to endosomal release because the relatively large volume of the cytosol will result in dilution of delivered fluorescent probes. This limits the use of fluorescent molecules in detecting endosomal release which usually requires sustained uptake for a long period of time to generate a detectable cytosolic stain. An alternative assay was thus required to detect endosomal release and so initially several different assays were tested.

We wanted to validate assays for detecting both macropinocytosis as well as endosomal release.

3.1 A 70kDa Dextran uptake assay in A431 cells

The process of macropinocytosis is used extensively in immune cells, such as dendritic cells, to internalise large amounts of extracellular material (2,106). These cells perform macropinocytosis constitutively without needing external stimulation. Many other cell types have the ability to perform macropinocytosis but requires an external factor in order to stimulate uptake (122). The initial cells selected for this project were A431 human epithelial cells and previous work (122) had shown they macropinocytose in response to growth factors such as EGF or the addition of Phorbol 12-myristate 13-acetate (PMA), which directly activates protein kinase C (PKC) to activate macropinocytosis.

3.1.1 Stimulation of macropinocytosis in A431 cells

As a first step to optimize a macropinocytosis assay, A431 cells were treated with 70kDa dextran for 15 minutes either in the absence (no stimulation control) or presence of PMA. Macropinosomes were detected using fluorescence microscopy and the number quantified using automated detection using the ImageJ software. Treatment of A431 cells with PMA resulted in an increase in the number of macropinosomes observed per cell after the 15-minute treatment (Figure3.01). The dextran puncta formed did not colocalise with fluorescent transferrin that was delivered to the cells at the same time as the dextran. As transferrin is selectively endocytosed via clathrin mediated endocytosis (122) and is excluded from macropinosomes, the absence of colocalisation between the dextran and transferrin validates that the dextran is being taken up specifically via macropinocytosis and not via a clathrin mediated route. During automated detection of macropinosomes, only particles above 0.5µm in diameter were detected. Macropinosomes are large structures and the detection of particles above 0.5µm enables confidence in detection of macropinocytosis selectively rather than endosomal dextran. Additionally, the use of 70kDa dextran promotes uptake via macropinocytosis as the dextran is too large to be incorporated into conventional endocytosis machinery.

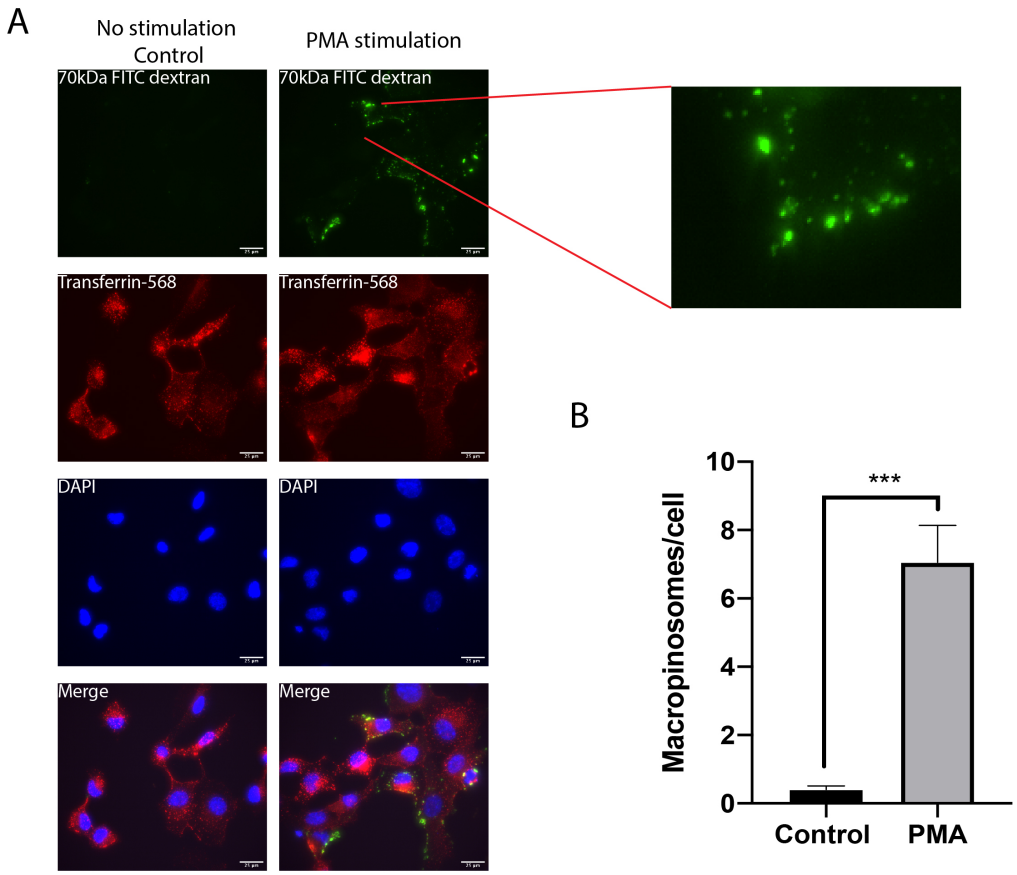

*Figure3.01: **Stimulation of A431 cells with PMA increases macropinocytosis**. A431 cells seeded onto coverslips 2 days prior to the experiment were preincubated in serum-free media for at least 2 hours before being incubated with 5ug/ml alexafluor 588 transferrin, 0.25mg/ml 70kDa FITC dextran in the absence or presence of 1uM PMA. After incubation at 37℃ cells were placed on ice, washed and stained with DAPI. Coverslips were imaged using an inverted widefield system and analysed using imageJ as described in the methods. Data shows mean + SEM from 4 independent repeats. Number of images acquired, No stimulation = 10, PMA stimulation = 19. An unpaired two-tailed T test was performed with ****p≤0.0001, *** p≤0.001, ** p≤0.01 , * p≤0.05*

3.1.2 The time course of PMA stimulation of macropinocytosis

We next measured the time course of macropinocytosis in A431 cells stimulated with PMA to determine the lifetime off macropinocytosis. A431 cells were treated with 70kDa FITC-dextran and PMA for a range of times up to 20 minutes. The number of macropinosomes per cell increased with time up to 20 minutes post stimulation (Figure3.02). This indicates that PMA stimulation of macropinocytosis is sustained for at least 20 minutes, with new macropinosomes still being formed.

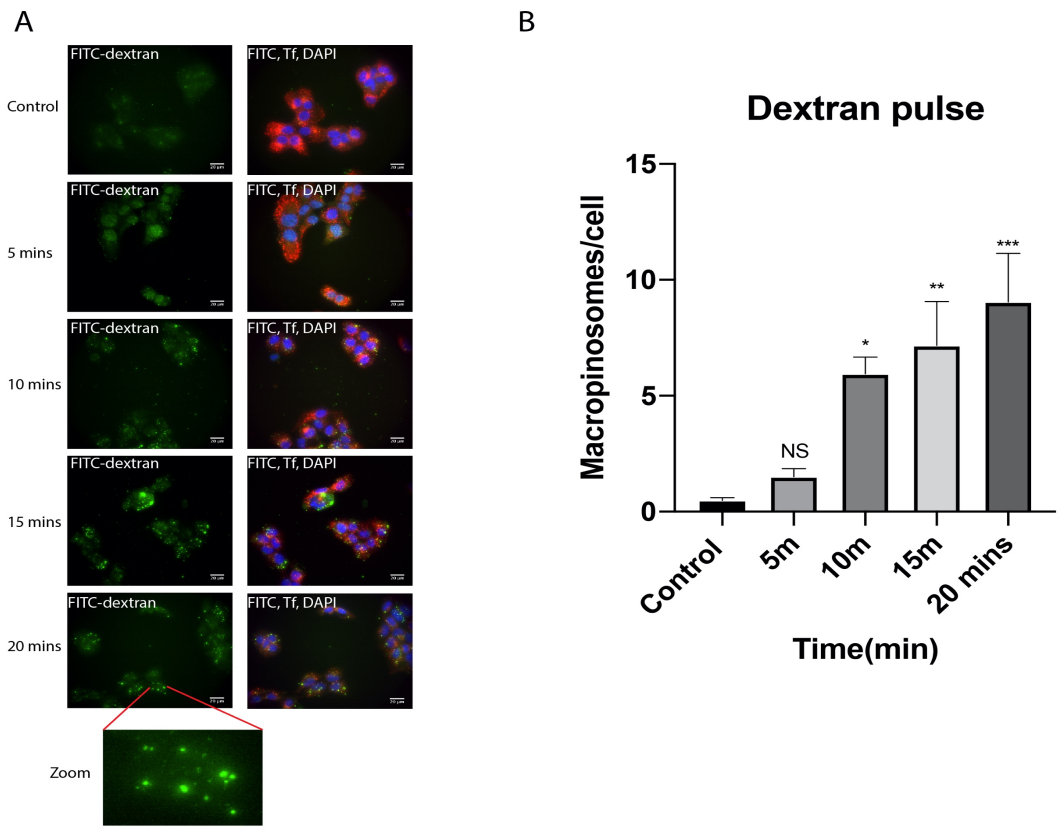

Figure3.02: ***Increasing time of PMA stimulation increases macropinocytosis in A431 cells.*** *A431 cells seeded onto coverslips 2 days prior to the experiment were preincubated in serum-free media for at least 2 hours before being incubated with 5ug/ml alexafluor 588 transferrin, 0.25mg/ml 70kDa FITC dextran in the presence of either 1uM PMA or a DMSO carrier control. Control cells were incubated for 15 minutes and PMA treated cells were incubated for the times shown. Coverslips were imaged using an inverted widefield system and analysed using imageJ as described in the methods. Data shows mean + SEM at least 3 independent repeats. A one-way ANOVA with Dunnett's comparison test was performed with ****p≤0.0001, *** p≤0.001, ** p≤0.01 , * p≤0.05, 'NS' p >0.05 and markings on graph above bars represent significance to the control*

3.1.3 The macropinosomes formed after PMA treatment are stable

After internalisation of material via macropinocytosis there are two possibilities for the macropinosomes formed. They are either recycled to the plasma membrane and released or they fuse with a lysosome and are degraded(229). As the trafficking of macropinosomes in these cells was not understood, we next wanted to investigate the stability of the macropinosomes formed in A431 cells. To investigate the lifetime of the macropinosomes, cells were treated with 70kDa FITC dextran and PMA for 15 mins. The dextran was removed and replaced with fresh serum-free media and the cells were then further incubated for different lengths of time. The number of macropinosomes observed per cell did not decrease significantly for up to 15-minute chase time (Figure3.03). This indicates that the

macropinosomes formed are relatively stable and exist for at least 15 minutes post formation without their cargo being degraded or recycled.

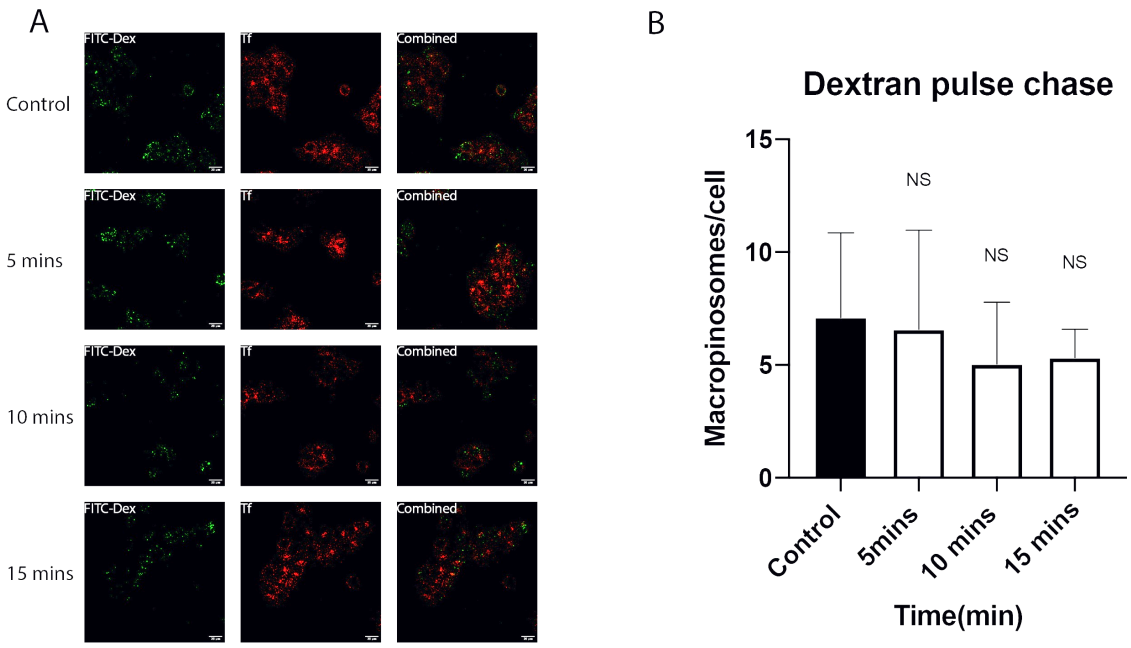

*Figure3.03: **PMA stimulated macropinosomes are stable for at least 15 minutes in A431 cells**. A431 cells seeded onto coverslips 2 days prior to the experiment were preincubated in serum-free media for at least 2 hours before being incubated with 5ug/ml alexafluor 588 transferrin, 0.25mg/ml 70kDa FITC dextran in the presence of either 1uM PMA or a DMSO carrier control for 15 minutes. Cells were washed with serum-free media and chased with serum-free for the indicated time. The control samples were fixed at 0 minutes of chase. After the chase period cells were placed on ice, washed and stained with DAPI. Coverslips were imaged using an inverted widefield or a confocal system. Images acquired were analysed using imageJ and automated macropinosome counting was performed. Data shows mean + SEM at least 2 independent repeats. A one-way ANOVA with Dunnett's comparison test was performed with ****p≤0.0001, *** p≤0.001, ** p≤0.01 , * p≤0.05, 'NS' p >0.05 and markings on graph above bars represent significance to the control*

3.1.4 Macropinosome formation is unaffected by a collagen matrix

The formation of macropinosomes requires the ruffling of the plasma membrane to encapsulate extracellular fluid. This ruffling is driven by actin polymerisation and the ability of the cell to reorganise its plasma membrane is vital for macropinocytosis (230). In our initial experiments, cells were seeded directly on glass coverslips. The next question we addressed was whether including extracellular matrix components might have an effect on macropinocytosis. Cells were seeded onto collagen coated coverslips and a dextran uptake assay was performed. The cells still responded to PMA stimulation with a maximum number of macropinosomes being observed at 10 minutes but there was an increase in the variability in the number of macropinosomes detected per cell (Figure3.04). The collagen matrix could

result in the formation of less stable macropinosomes, but further experimentation would be required to determine the effect of a collagen matrix. We decided to continue to use glass coverslips as the collagen coating did not result in an increase in macropinocytosis.

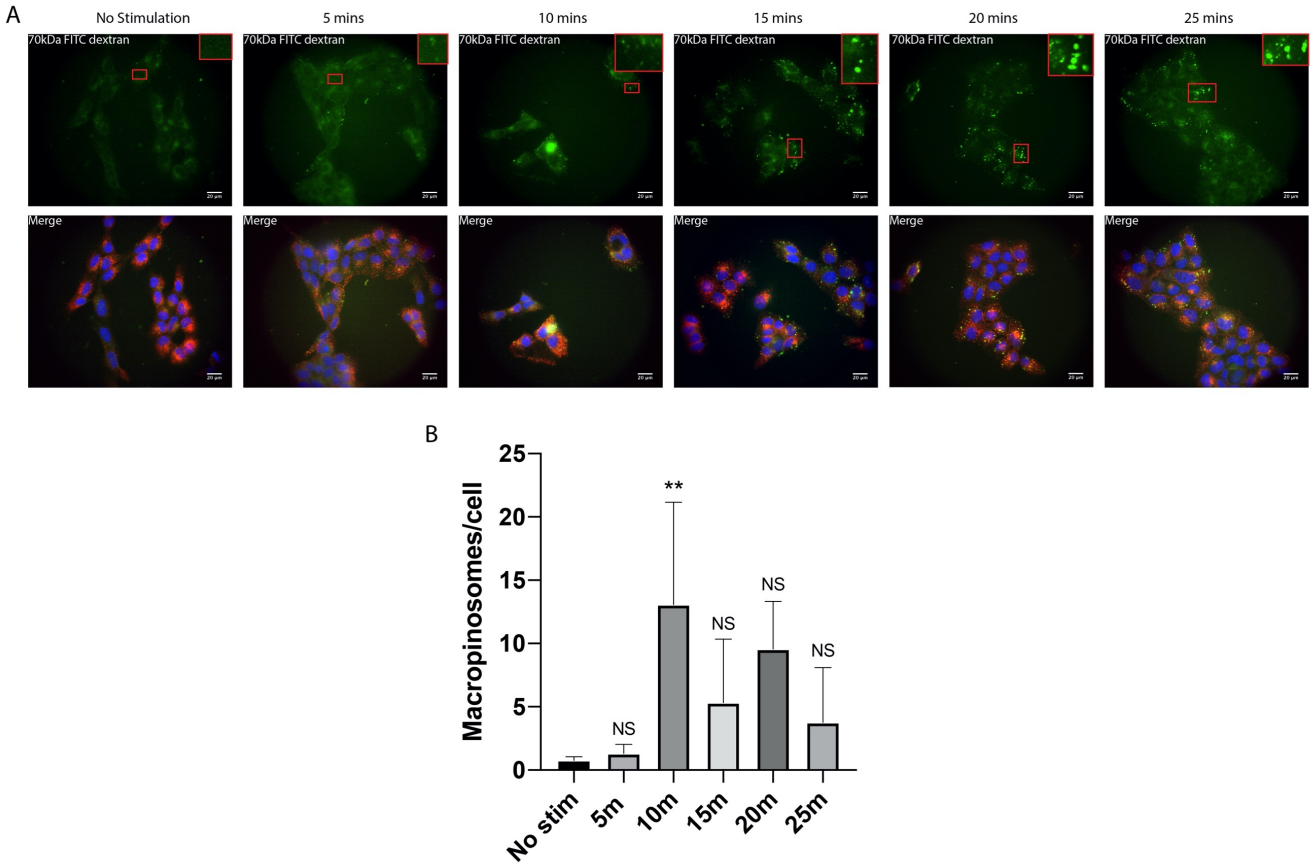

*Figure3.04: **Collagen coating coverslips does not increase PMA stimulation of macropinocytosis in A431 cells**. A431 cells were seeded on collagen coated glass coverslips 2 days prior to the experiment. Media was exchanged to serum-free media for at least 2 hours prior to performing the experiment. The cells were stimulated for the variable time shown, with 5ug/ml alexafluor 588 transferrin, 0.25mg/ml 70kDa FITC dextran and with 1uM PMA. The control, no stimulation, samples were treated with 5ug/ml alexafluor 588 transferrin, 0.25mg/ml 70kDa FITC dextran and a DMSO carrier control for 15 minutes. After incubation at 37℃ cells were placed on ice, washed and stained with DAPI. Coverslips were mounted imaged using an inverted widefield system. Images acquired were analysed using imageJ and automated macropinosome counting was performed. Data shows mean + SD from 1 experiment, Number images acquired: No Stim= 3, 5m =4 , 10m = 4 , 15m = 5 , 20m=4, 25m = 6. A one-way ANOVA with Dunnett's comparison test was performed with ****p≤0.0001, *** p≤0.001, ** p≤0.01 , * p≤0.05, 'NS' p >0.05 and markings on graph above bars represent significance to the control*

3.1.5 Cell confluency impacts the levels of macropinocytosis

To further understand the process of macropinocytosis in A431 cells, we next wanted to observe the effect of confluency on the number of macropinosomes formed. We hypothesized that increased confluency would result in less macropinocytosis due to the inability of the membrane to remodel. As the cells become more confluent and more cell contacts form, the ability to reform the membrane also decreases(231). To test the hypothesis, we plated cells at different densities and performed a dextran uptake assay. Figure 3.05 shows that as the number of cells seeded increased there was a corresponding decreased ability to perform macropinocytosis. This experiment also highlighted some of the growth characteristics of A431 cells. When cells were seeded at lower confluency, they grew in small independent clusters and no single cells were observed. More macropinosomes are located in the periphery of these cellular clusters which indicates that the cells with more edges, and so ability to reform their membrane, have the greatest ability to perform macropinocytosis (Figure3.05 arrows in 90,000 cell condition).

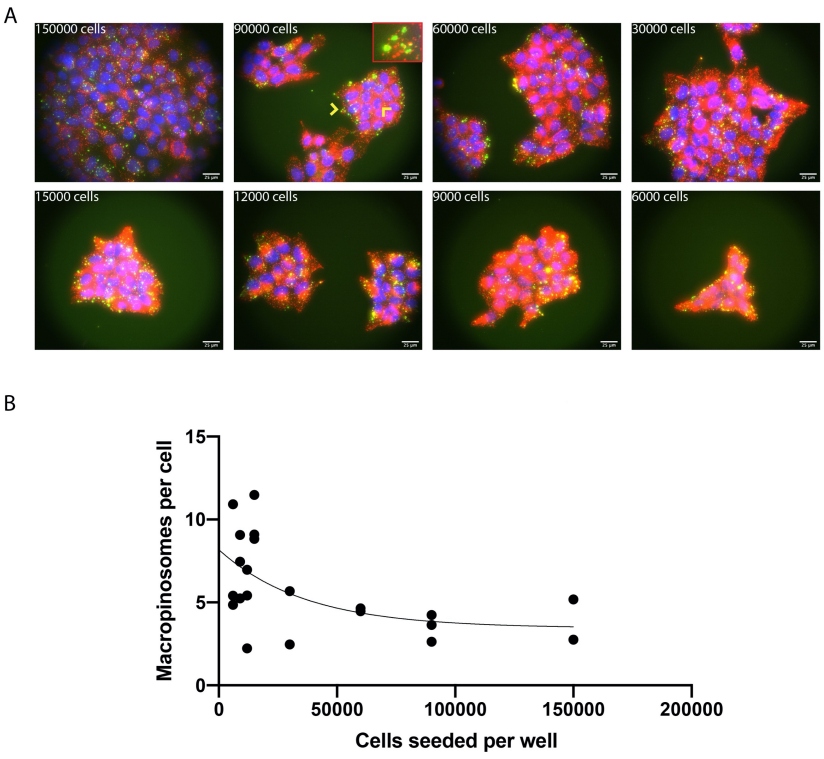

*Figure3.05: **PMA stimulated macropinocytosis increases at lower confluency**. Different numbers of A431 cells were seeded onto on glass coverslips 2 days prior to the experiment. Media was exchanged to serum-free media for at least 2 hours prior to performing the experiment. The cells were stimulated for 15 minutes with 5ug/ml alexafluor 588 transferrin, 0.25mg/ml 70kDa FITC dextran and with 1uM PMA. After incubation at 37℃ cells were placed on ice, washed and stained with DAPI. Coverslips were mounted imaged using an inverted widefield system. Images acquired were analysed using imageJ and automated macropinosome counting was performed. Data shows a scatter graph of cells seeded vs the number of macropinosomes per cell from 1 experiment.*

3.1.6 Live cell macropinocytosis in A431 cells using a PI(3,5)P2 probe

We could observe the stimulation of macropinocytosis by PMA in fixed A431 cells using the dextran uptake assay, but we also wanted to observe the effect in live cells. In order to perform live cell imaging of dextran uptake, we used a novel probe for PI(3,5)P_2, which is a marker for macropinosomes. This probe is a px domain from a *Dictyostelium discoideum* protein, which was developed in Jason King lab (UoS) which is believed to selectively bind PI(3,5)P2 and can thus be used to follow formation of macropinosomes in live cells. Following expression in A431 cells using transient transfection, I performed a dextran uptake assay. In the unstimulated cells a basal level of macropinocytosis was seen with formation of dextran positive vesicles and the PI(3,5)P2 probe located to sites of active membrane ruffling at the cell surface (Figure3.06). This highlights the ability of these A431 cells to form membrane ruffles under basal conditions which might explain their ability to perform a higher amount of macropinocytosis then other cell types. The stimulation of cells with PMA resulted in an increase in the number of dextran positive vesicles formed as previously observed in PFA fixed samples. The PI(3,5)P2 probe was seen at active membrane patches and coating newly formed macropinosomes but there was limited colocalisation on smaller, older macropinosomes. The difference between newly formed macropinosomes and older ones can be seen in the difference in size observed. After internalisation, macropinosomes are processed, with material being removed and recycled which results in shrinking (133). The material that is not removed, such as the 70kDa dextran, is condensed which can be seen as an increase in fluorescent signal due to the increase in local concentration. The early macropinosome are large and have low fluorescent signal. They are not normally seen in the fixed cell assays which could be due to their weaker dextran signal and highlights a weakness of the fixed-cell assay at detecting early macropinosomes.

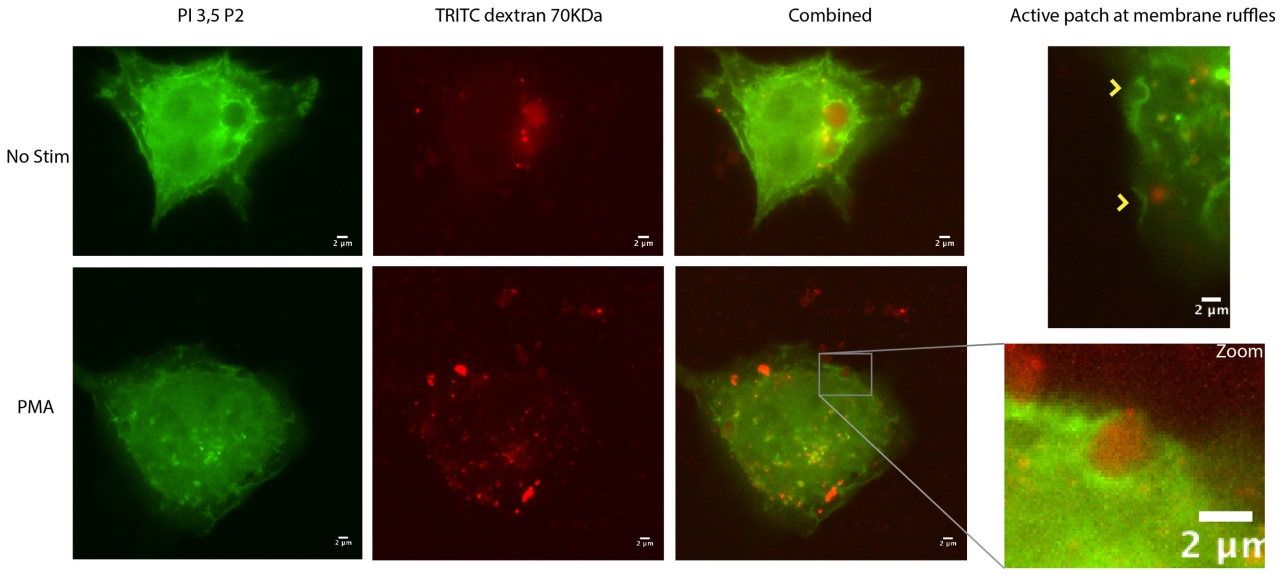

Figure3.06: ***Live cell imaging of macropinocytosis in A431 cells****. A431 cells were seeded in glass bottomed live cell microscopy dishes 2 days prior to the experiment. Cells were transfected with the PI(3,5)P2 probe 24 hours before and the media was exchanged to serum-free media for at least 2 hours prior to performing the experiment. The cells were either stimulated with 1uM PMA or a DMSO carrier control (No stim) in the presence of 0.25mg/ml 70kDa TRITC dextran for 10 minutes. Cells were washed and immediately imaged at 37℃*

3.2 Adenovirus as a stimulator of macropinocytosis and endosomal release

Our studies on macropinocytosis were directly connected to our aim of stimulating release of endosomal content which normally occurs with very low efficiency. There was some evidence in the literature that Adenovirus binding to a cell surface receptor could trigger a signalling cascade that increased the infectivity and endosomal release of adenovirus particles (232). The activated signalling pathway is known to subsequently stimulate macropinocytosis(24). The understanding of a signalling pathway and the key component that increased endosomal release would increase our understanding of the maintenance of endosomal stability and how endosomal release might be increased as a route to enhancing therapeutic delivery. We therefore wanted to test the ability of adenovirus to trigger endosomal release in the A431 cell line.

3.2.1 Generation of adenovirus using the AdEasy virus kit

The production of adenovirus was performed using the Agilent AdEasy virus system to generate active adenovirus particles (see material and methods). Initially we performed an adenovirus titre assay to measure the quantity of virus produced. An adenovirus titre was performed after most virus preparations to quantify the amount of active virus produced. A serial dilution of the viral preparation was performed and subsequent infection of HEK-Ad cell that could support Adenovirus replication. An immunofluorescent assay, using an Anti-adenovirus antibody, was used to stain infected cells (Figure3.07) and a viral titre could be calculated from the number of infected cells. The viral titre assay confirmed the presence of replicatively active virus, but we also confirmed the presence of adenovirus by SDS page gel electrophoresis. The virus particles were disrupted in detergent and the proteins were separated on a protein gel. The identification of protein bands that corresponded to adenovirus proteins validated our production of adenovirus particles.

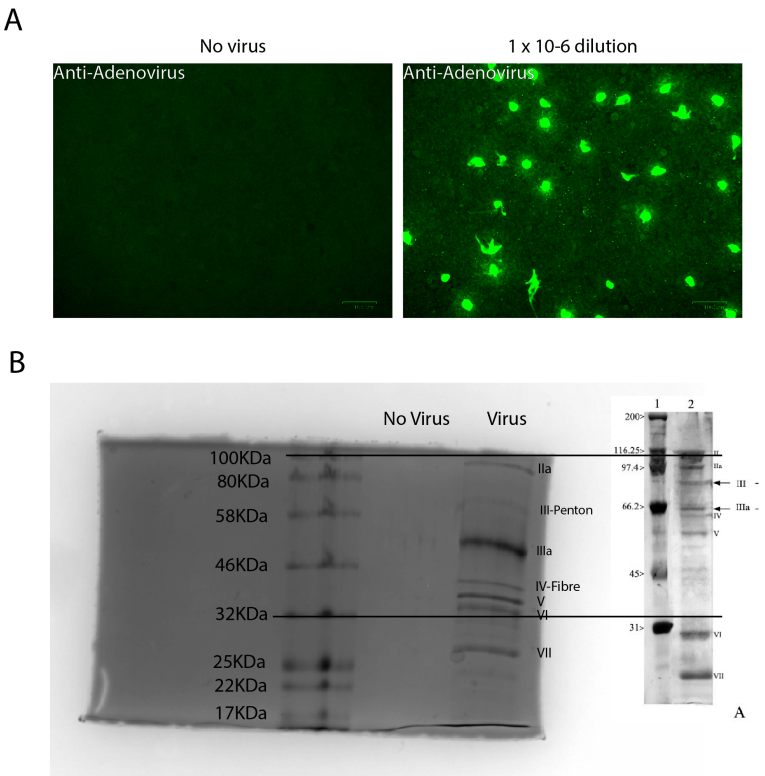

*Figure3.07: **Viral titre and adenovirus western blot**. Adenovirus was produced and purified following the AdEasy virus purification kit (see materials and methods section) After purification a virus titer was performed using a modified AdEasy virus titre assay kit. **A)** A serial dilution of the adenovirus stock was prepared, and each dilution was used to infect HEK-Ad cells. After 48 hours of infection cells were fixed via methanol fixation. Immunofluorescence using an antibody against adenovirus proteins identified infected cells and a titer of the original stock could be calculated. **B)** Adenovirus was denatured by addition of SDS and boiling at 95 ℃. The sample was separated using SDS page gel electrophoresis and visualised using comassie blue stain. Reference gel from (Bovine Lactoferrin Inhibits Adenovirus Infection by Interacting with Viral Structural Polypeptides: Pietrantoni)*

3.2.2 Adenovirus incubation did not increase macropinocytosis in A431 cells

Adenovirus triggers clathrin-mediated endocytosis by binding to receptors at the cell surface, which is the canonical route of infection. However it has previously been reported that adenovirus can also trigger macropinocytosis (148,232). It is currently unknown if macropinocytosis is directly triggered by the adenovirus to increase infectivity or if it is a side effect of adenovirus signalling. We wanted to see if adenovirus particles could trigger an increase in the levels of macropinocytosis observed in A431 cells (Figure3.08). The dextran uptake assay was performed in the A431 cells following incubation with adenovirus. Although there was a slight trend suggesting an increase in the average number of macropinosomes per cell following Adenovirus treatment (0.35 macropinosomes formed per cell in the absence of virus to 1.945 in the presence of virus), this increase was not significant due to high variability which might indicate that the virus can only trigger macropinocytosis in a subset of cells. The increase in macropinocytosis induced by the virus was also much lower than that observed when cells were stimulated with PMA, which resulted in an approximately 18-fold increase in the number of macropinosomes formed per cell when compared to the unstimulated condition.

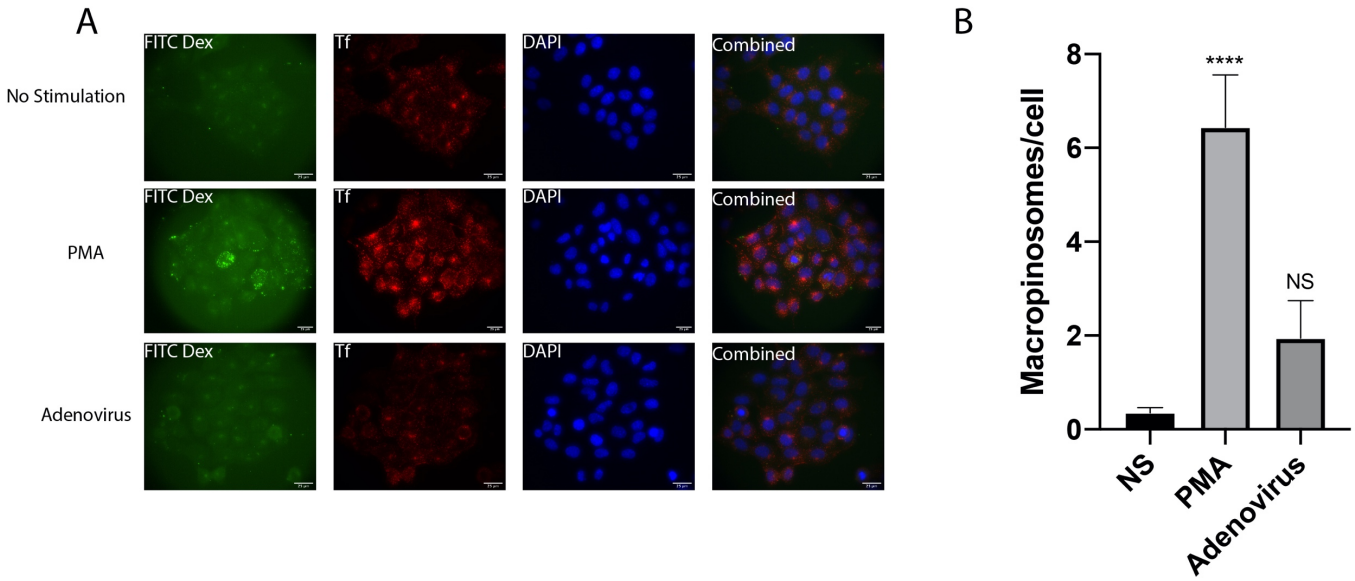

Figure3.08: ***Adenovirus does not increase macropinocytosis in A431 cells.*** *A431 cells seeded onto coverslips 2 days prior to the experiment were preincubated in serum-free media for at least 2 hours before being incubated with 5ug/ml alexafluor 588 transferrin, 0.25mg/ml 70kDa FITC dextran and either a DMSO carrier control in No stimulation conditions, 1uM PMA or Adenovirus. After incubation at 37℃ cells were placed on ice, washed and stained with DAPI. Coverslips were imaged using an inverted widefield system. Images acquired were analysed using imageJ as described in the methods. Data shows mean + SEM from 3 independent repeats. Number of images acquired No stimulation = 10, PMA stimulation = 13, virus =14. A one-way ANOVA with Tukey's multiple comparison was performed with ****p≤0.0001, *** p≤0.001, ** p≤0.01 , * p≤0.05*

3.2.3 Macropinocytosis in different cell lines

In contrast to the published data(232), incubation of A431 cells with adenovirus did not result in an increase in macropinocytosis. To test if the stimulatory effect of adenovirus was cell-type specific, we tested the ability of the virus to trigger macropinocytosis in other cell lines. A dextran uptake assay was performed in HeLa, HT1080 and ARPE cells comparing PMA stimulation, adenovirus incubation or both PMA and adenovirus incubation simultaneously (Figure3.09). The HeLa cells did not show increased macropinocytosis under any conditions and in general showed very low levels of macropinocytosis. The HT1080 cells showed increased macropinocytosis in the presence of PMA but not in the presence of adenovirus. When HT1080 cells were treated with both PMA and adenovirus there was a slight increase in the number of macropinosomes per cell, but this increase was not significantly different to PMA stimulation alone. ARPE cells had slightly lower overall levels of macropinocytosis compared to HT1080 cells but neither PMA nor adenovirus caused a significant increase in macropinocytosis. However, both PMA and adenovirus together caused a significant increase in macropinocytosis when compared to no stimulation. These results indicate that the adenovirus might potentially be having a small effect on macropinocytosis in the ARPE cells and HT1080 cells but none of the cell lines tested showed strong induction of macropinocytosis in response to adenovirus incubation.

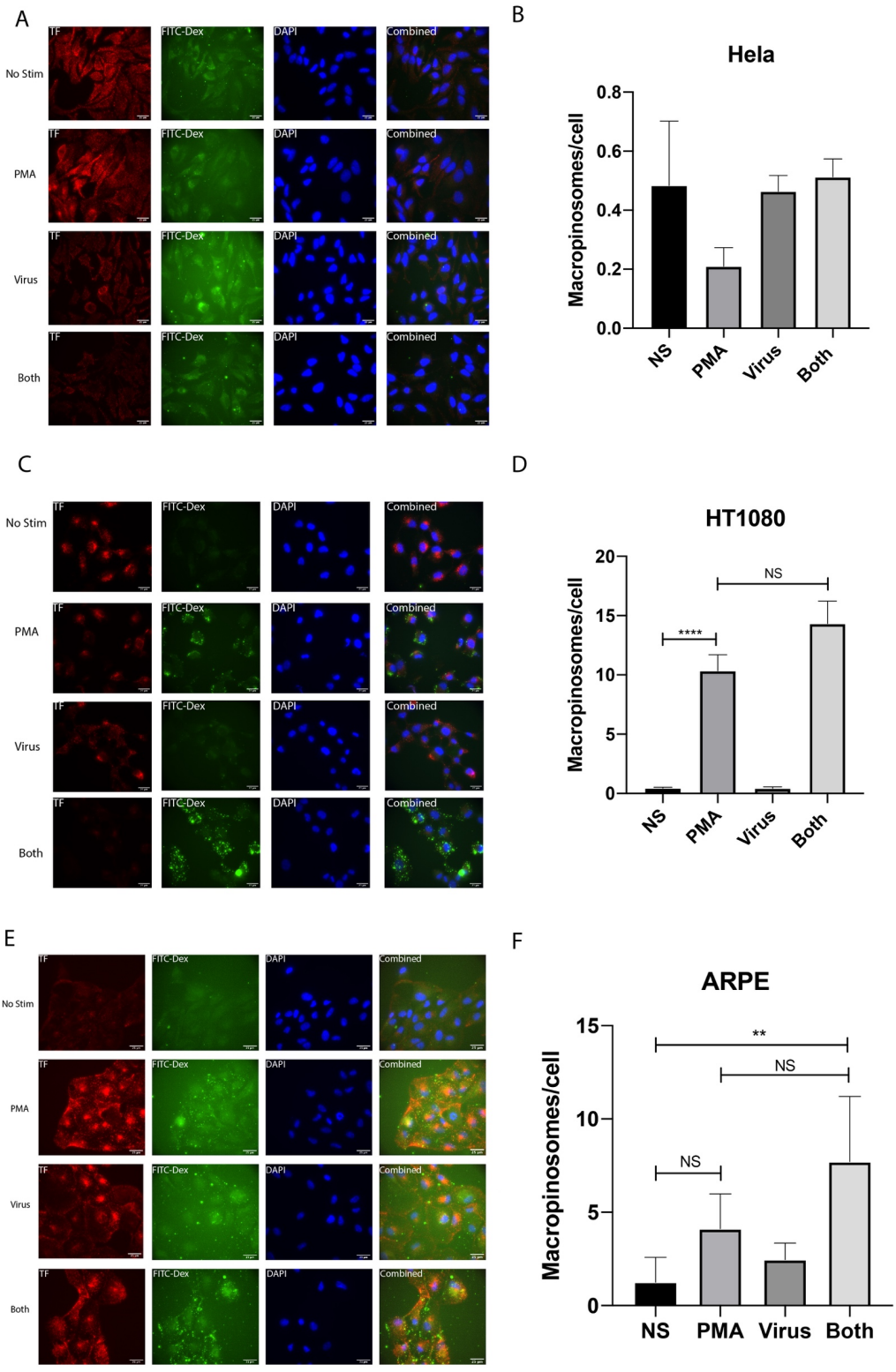

Figure3.09: ***Adenovirus does not stimulate macropinocytosis in other cell lines****. Hela, HT1080 or ARPE cells were seeded onto coverslips 2 days prior of experiment. Media was exchanged to serum-free media for at least 2 hours prior to performing the experiment. The cells were stimulated for 15 minutes with 5ug/ml alexafluor 588 transferrin, 0.25mg/ml 70kDa FITC dextran and either a DMSO carrier control in No stimulation conditions, 1uM PMA, Adenovirus or both 1uM PMA and adenovirus. After incubation at 37℃cells were placed on ice, washed and stained with DAPI. Coverslips were mounted imaged using an inverted widefield system. Images acquired were analysed using imageJ and automated macropinosome counting was performed. Data shows mean + SD from 1 independent repeat for each cell line. Images acquired ≥3 for each condition. A one-way ANOVA with Tukey's multiple comparison was performed with ****p≤0.0001, *** p≤0.001, ** p≤0.01 , * p≤0.05*

3.2.4 A431 can internalise adenovirus

One possibility for the absence of a stimulatory effect on macropinocytosis in A431 cells could be that these cells are unable to bind/internalise the virus. The ability of adenovirus to enter A431 cells was assayed by immunofluorescence stain using an anti-adenovirus antibody to observe the cellular location of adenovirus. As can be seen in figure3.10 there is positive staining with the antibody only when adenovirus is added to the cells. The staining seen was believed to be intracellular, observed by acquiring Z stack images, indicating successful internalisation of the virus into A431 cells.

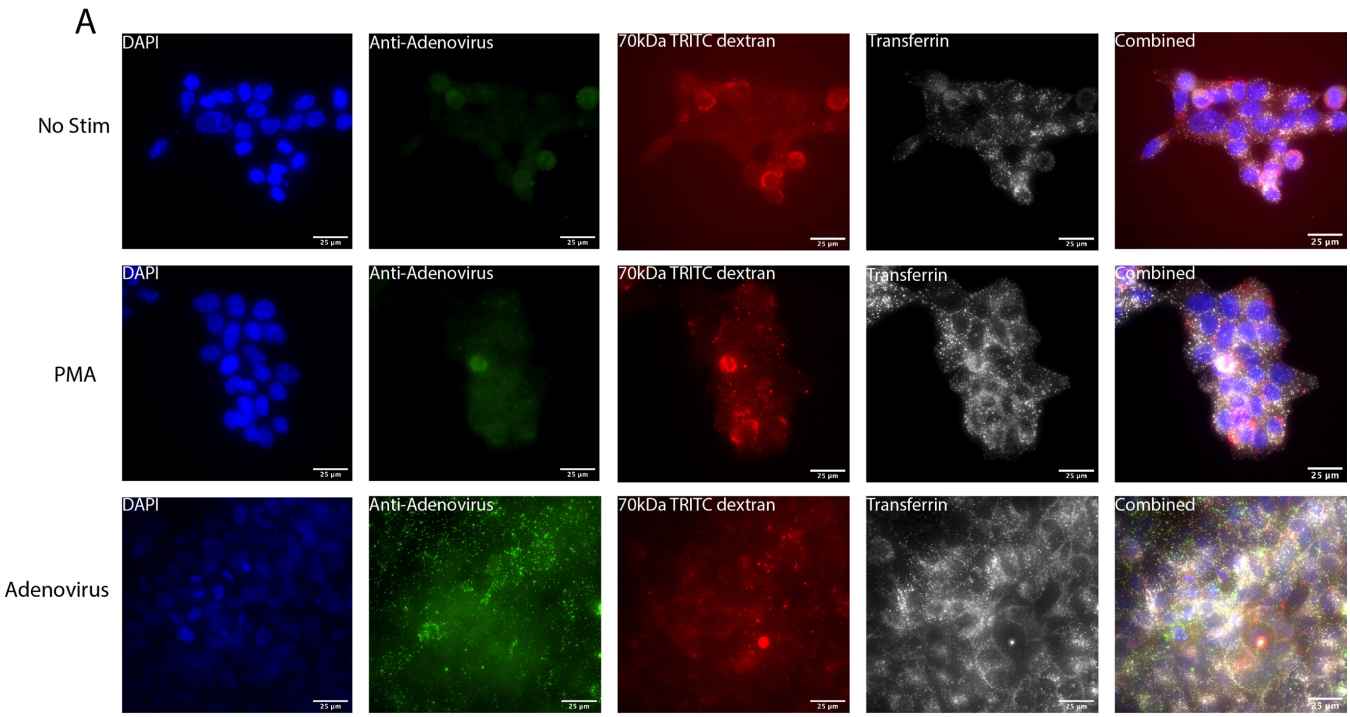

Figure3.10: ***Cells incubated with adenovirus show positive Anti-Adenovirus immunostaining****. A431 cells seeded onto coverslips 2 days prior to the experiment were preincubated in serum-free media for at least 2 hours before being incubated with 5ug/ml alexafluor 588 transferrin, 0.25mg/ml 70kDa FITC dextran and either a DMSO carrier control in No stimulation conditions, 1uM PMA or Adenovirus. After incubation at 37℃ cells were placed on ice, washed and stained with DAPI. Cells were immunolabeled with Anti-Adenovirus primary anti-body and a Alexa-fluor488 secondary using a standard immunofluorescence protocol. Coverslips were mounted imaged using an inverted widefield system. Images shown are representative images from two independent experiment.*

3.2.5 Adenovirus stimulation of macropinocytosis does not occur at earlier time points

A potential reason for the observed lack of adenovirus stimulated macropinocytosis could be explained by virus-induced endosomal release. If the virus was stimulating macropinocytosis and stimulating release to the cytosol, then this disruption to the macropinosomes could potentially decrease the number of dextran positive vesicles. We therefore tested the effect of short incubations of adenovirus on macropinocytosis. However, there was no increase in dextran positive vesicles at earlier time points from 2 minutes up to 15 minutes adenovirus stimulation (Figure3.11). Thus, eliminated the possibility that we were missing macropinocytosis stimulation because of endosomal release.

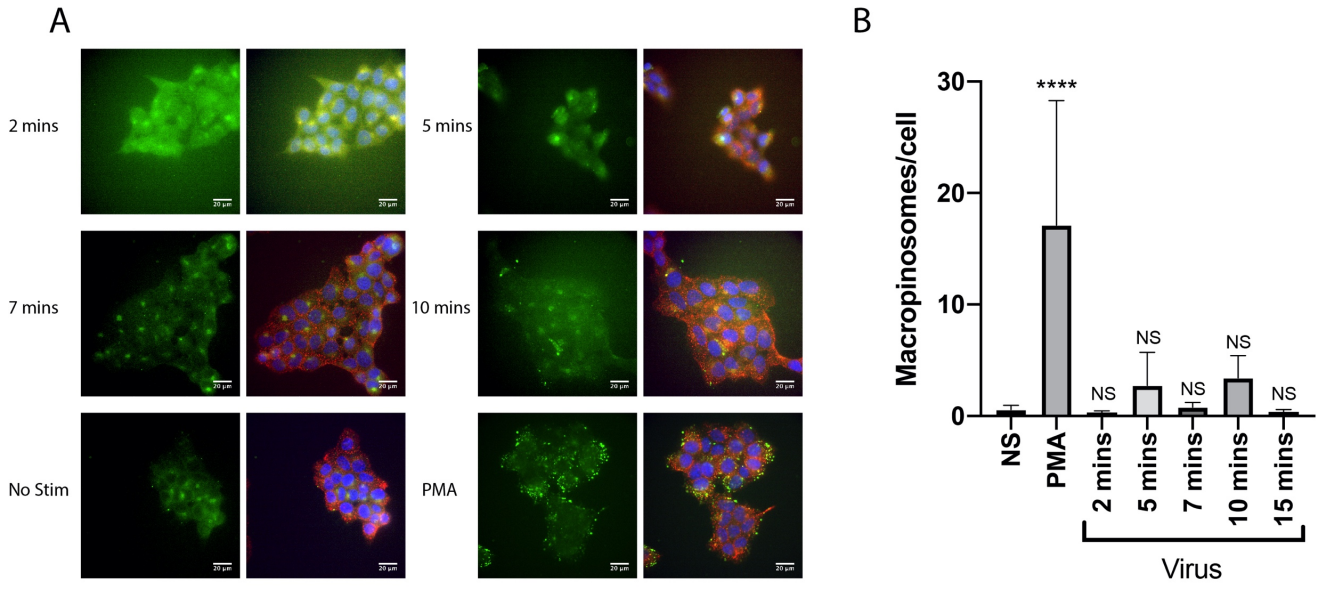

Figure3.11: ***The effect of variable virus incubation time on macropinocytosis****. A431 cells seeded onto coverslips 2 days prior to the experiment were preincubated in serum-free media for at least 2 hours before being incubated with 5ug/ml alexafluor 588 transferrin, 0.25mg/ml 70kDa FITC dextran and either a DMSO carrier control in No stimulation conditions, 1uM PMA or Adenovirus. NS and PMA conditions were stimulated for 15 minutes were as adenovirus was stimulated for the time shown. After incubation at 37℃ cells were placed on ice, washed and stained with DAPI. Coverslips were imaged using an inverted widefield system A)Images acquired were analysed using imageJ and B) automated macropinosome counting was performed. Data shows mean + SD from 2 independent repeats. Images acquired NS=8, PMA=6, Virus time points ≥3. A one-way ANOVA with Tukey's multiple comparison test was performed with ****p≤0.0001, *** p≤0.001, ** p≤0.01 , * p≤0.05, 'NS' p >0.05 and markings on graph above bars represent significance to the no stimulation (NS) control*

3.2.6 A GFP-NLS uptake assay to detect endosomal release

My next step was to investigate whether adenovirus triggered detectable endosomal release in A431 cells. In order to detect endosomal release, we needed an assay that was sensitive enough to detect release in a short time period. The initial work on adenovirus signalling performed by Meier et al utilized a nuclear localisation signal (NLS) conjugated to BSA and FITC (24). This molecule would traffic to the nucleus after cytosolic release due to the NLS and accumulated fluorescence could be detected in the nucleus. This assay enables sensitive detection of endosomal release as the nucleus has a smaller volume than the cytosol and so less material needs to be delivered to observe a positive result. I attempted to establish a similar system using a GFP construct with an NLS that had previously been created in the Smythe lab.

3.2.7 GFP-NLS did not show nuclear staining with adenovirus stimulation

The purified GFP protein was used as a fluid phase marker and cells were stimulated, in the presence of the GFP-NLS, with either PMA or adenovirus. The addition of adenovirus did not result in increased nuclear accumulation of GFP signal indicating no detectable release (Figure3.12). The GFP staining observed in cells was weak and so after performing the GFP-NLS uptake assay, cells were immuno-stained using an Anti-GFP antibody and a green, fluorescent secondary antibody to enhance the signal. As can be seen in Figure3.13 this did successfully enhance the signal, but the staining was punctate and not nuclear indicating no detectable endosomal release was observed. The punctate staining of the GFP-NLS did not colocalise with the transferrin signal indicating separate endosomal compartments, which could potentially be macropinosomes. However, the size of the puncta were small and larger puncta were seen in the PMA treated cells indicating macropinosomes.

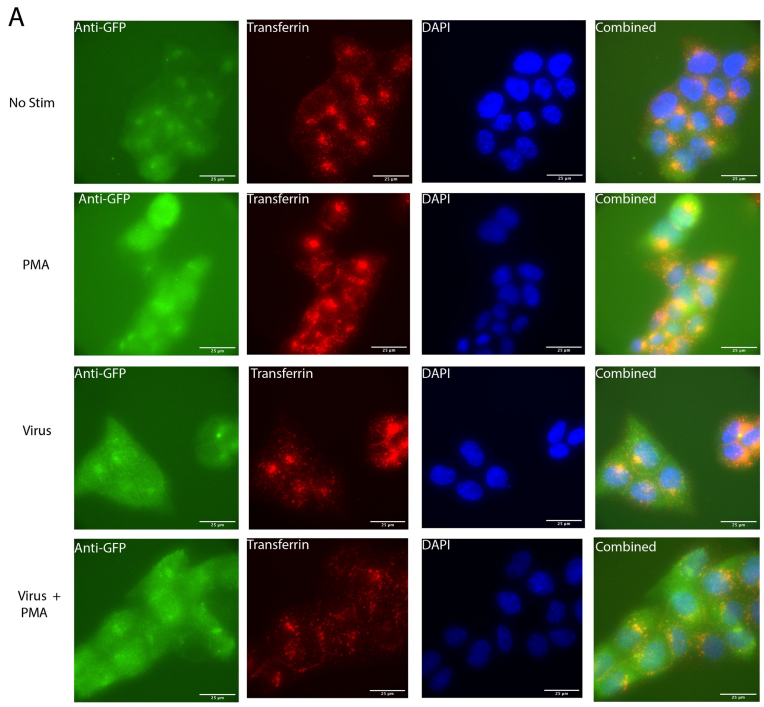

Figure3.12: ***Adenovirus does not trigger nuclear accumulation of GFP-NLS*** *. A431 cells were seeded onto glass coverslips 2 days prior to the experiment. Media was exchanged to serum-free media for at least 2 hours prior to performing the experiment. The cells were stimulated with 5ug/ml alexafluor 588 transferrin and 0.15mg/ml GFP-NLS plus a stimulation for 1 hour. The No stimulation control was treated with a DMSO carrier control, PMA samples were treated with 1uM PMA, Virus samples were treated with Adenovirus and Virus + PMA were treated with both 1uM PMA and adenovirus simultaneously. After incubation at 37℃ cells were placed on ice, washed and stained with DAPI. Coverslips were mounted imaged using an inverted widefield system. Images acquired were analysed using. Data shows representative images from 3 independent repeats.*

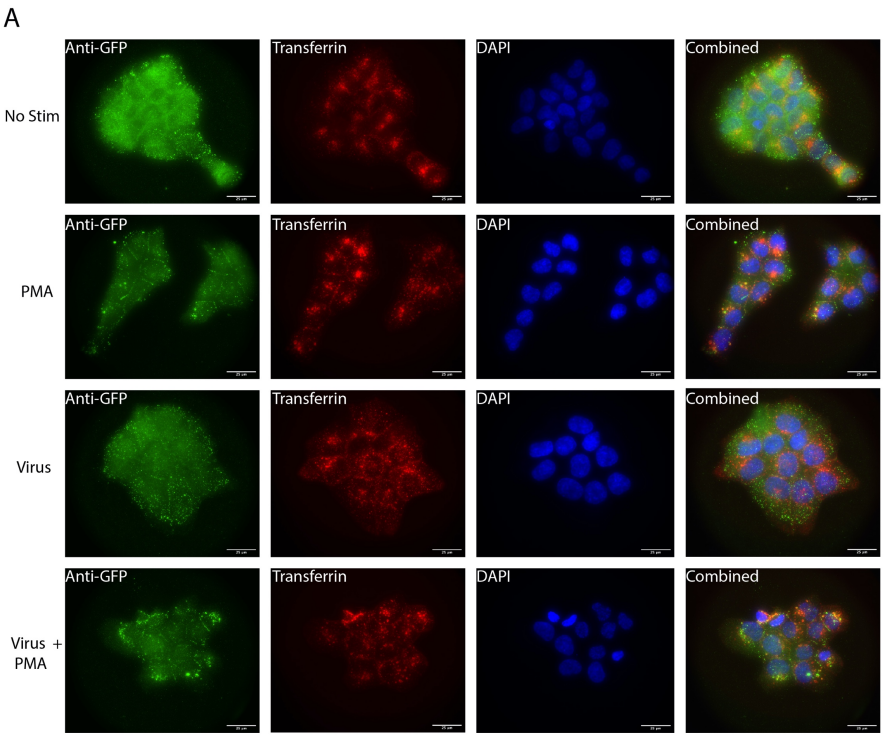

Figure3.13: ***Anti-GFP immunostaining amplifies GFP-NLS*** *. A431 cells were seeded onto glass coverslips 2 days prior to the experiment. Media was exchanged to serum-free media for at least 2 hours prior to performing the experiment. The cells were treated with 5ug/ml alexafluor 588 transferrin and 0.15mg/ml GFP-NLS plus a stimulation for 1 hour. The No stimulation control was treated with a DMSO carrier control, PMA samples were treated with 1uM PMA, Virus samples were treated with Adenovirus and Virus + PMA were treated with both 1uM PMA and adenovirus simultaneously. After incubation at 37℃ cells were placed on ice, washed , fixed with 4% PFA and stained with DAPI. Cells were immunolabeled with Anti-GFP primary anti-body and an Alexa-fluor488 secondary using a standard immunofluorescence protocol. Coverslips were mounted imaged using an inverted widefield system. Images acquired were analysed using. Data shows representative images from 3 independent repeats.*

3.3 HRP uptake assay

As we were unable to detect successful endosomal release using GFP-NLS, we decided to develop an alternative method to detect release. Horse radish peroxidase (HRP) has been used as a fluid phase marker previously and was used as a way of marking the endosomal system before the widespread use of fluorescent microscopy (107,233,234). The enzymatic reaction of the HRP is used to convert a substrate into a visible signal. To visualise the location of endocytosed HRP we used the HRP substrate 3,3'-diaminobenzidine which is a colourless solution but can be converted by HRP to a brown insoluble product. The insoluble product precipitates and stains the local area around the HRP molecule enabling localisation.

3.3.1 HRP uptake in A431 cells

We initially tested HRP uptake in A431 cells by addition to the fluid phase of A431 cells which were stimulated for 30 minutes with PMA or adenovirus. Cells were washed extensively to remove any extracellular HRP and fixed with PFA. The location of intracellular HRP was detected using DAB staining and visualised by brightfield microscopy. In the absence of HRP, there was no staining indicating the DAB substrate was stable and was not reacting with any cellular enzymes to produce a background signal. Therefore, I was confident that any DAB staining in the test conditions was due to the presence of HRP. In the absence of stimulation, there was a basal uptake of HRP into the endosomal system and some punctate staining was observed (Figure3.14A). As HRP is smaller in size then the 70kDa dextran, it can be taken up via clathrin mediated endocytosis, as well as other forms of endocytosis. Hence a greater degree of HRP uptake is observed in the non-stimulated condition compared to basal dextran uptake. Stimulation of cells with PMA resulted in a greater amount of punctate HRP staining indicating a larger amount of fluid phase macropinocytosis, validating the dextran uptake results shown previously. We initially thought adenovirus stimulation had little effect on HRP uptake as we did not observe punctate staining as seen with PMA stimulation, since we saw a staining pattern similar to unstimulated cells. However, upon further observation we noticed a subsection of cells were displaying cytosolic HRP staining. Instead of punctate staining where the HRP is trapped in the endosomal system, the entire cytosol of some cells had been stained with DAB. These cells were clustered together, and they were not found in

all cells incubated with adenovirus. This could indicate the adenovirus incubation could only result in release in a small subset of A431 cells for reasons that are unknown. On the other hand, the cells observed with cytosolic staining may be unhealthy and dying which results in breakdown of the membrane and therefore allows entry of the HRP to the cytosol. However, these results validated the use of the HRP assay at detecting cytosolic release of endosomal content.

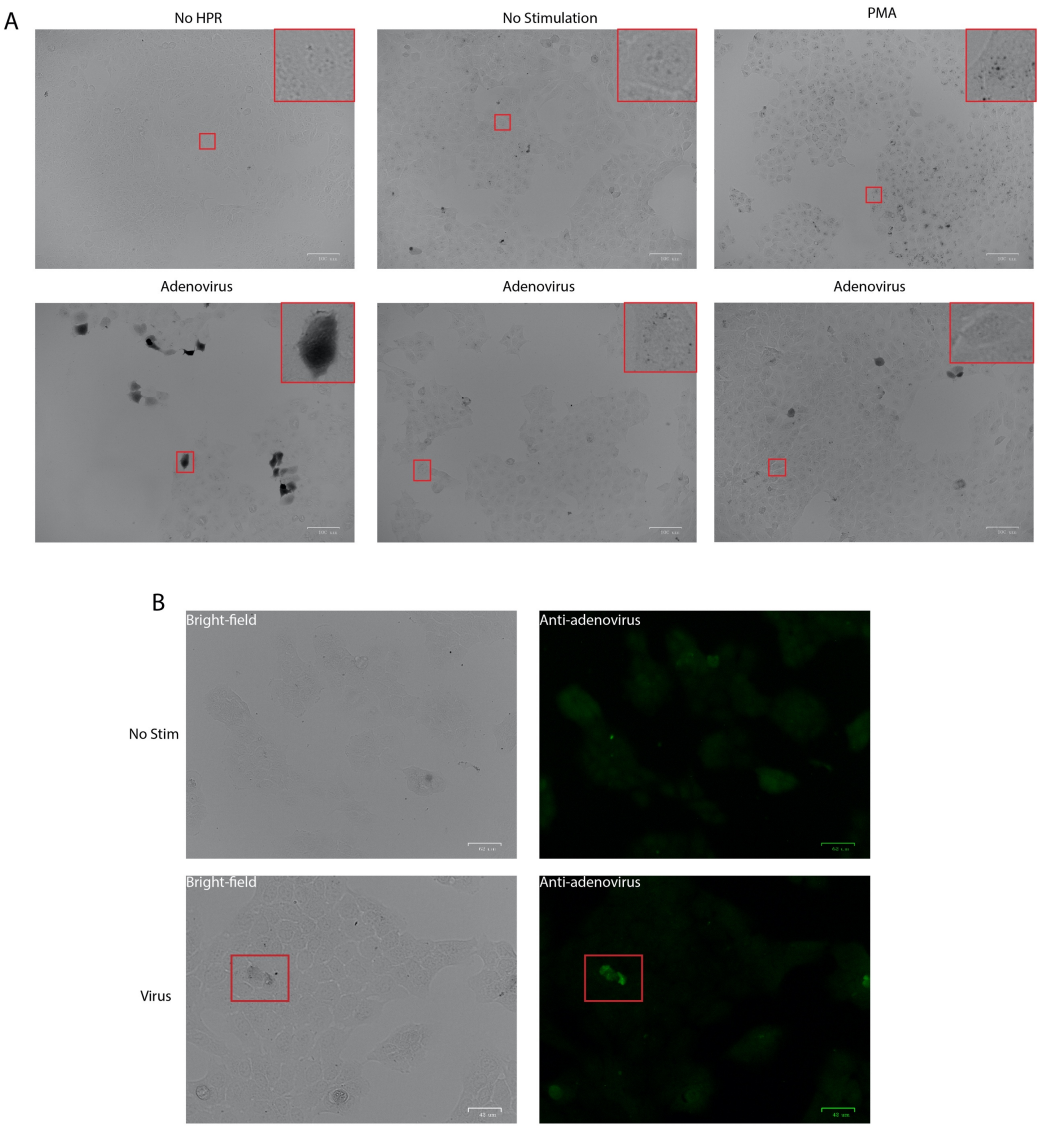

Figure3.14: ***Adenovirus incubation results in cytosolic HRP staining in a subset of A431 cells.*** *A431 cells seeded onto coverslips 2 days prior to the experiment were preincubated in serum-free media for at least 2 hours before being incubated with 4mg/ml HRP plus a stimulation for 1 hour. No HRP conditions were treated without HRP. The No stimulation control was treated with a DMSO carrier control, PMA samples were treated with 1uM PMA, Virus samples were treated with Adenovirus. After incubation at 37°C cells were placed on ice and washed to remove external HRP. Cells were fixed with 4% PFA, DAPI stained and Dab staining was performed. B) Some cells were antibody stained using an Anti-adenovirus antibody and an alexafluor 488 secondary antibody. Images were acquired using a ZOE Fluorescent cell imager. Data is representative from 3 independent experiments for HRP staining and from 1 experiment for the antibody staining.*

3.3.2 Cells showing cytosolic HRP staining were adenovirus positive

To test if the cells showing cytosolic staining was linked to adenovirus, we performed immunofluorescence using anti-adenoviral antibodies after DAB staining to visualise which cells had intracellular adenovirus particles. There seemed to be colocalisation between cells showing cytosolic staining and adenovirus staining indicating that the release was due to adenovirus internalisation into the A431 cells (Figure3.14B). It was challenging to locate cells showing endosomal release due to clustering of positive cells which complicated analysis of the effect adenovirus was having. The immunofluorescence protocol performed interfered with the DAB stain which resulted in a much weaker staining then the previous experiment and less cells were seen to be positive. Though there was some evidence to suggest released cells had antibody staining, this result would need further validation and possibly a different assay to conclusively prove the release was due to the adenovirus.

3.3.3 The lysosomal disrupting agent LLOMe does not result in cytosolic HRP staining

To identify a positive control for cytosolic delivery and validate the HRP release assay, we decided to see if disruption of the lysosomal membrane using L-leucyl-L-leucine methyl ester (LLOMe) resulted in cytosolic HRP uptake. LLOMe is taken up via endocytosis and traffics to the lysosomes where it is processed by lysosomal enzymes (235). This processing results in increased osmotic pressure in the lysosomes and subsequent loss of lysosomal membrane integrity. HRP was added to the fluid phase in the presence of 2.5µM LLOME for 60 minutes. Following uptake of HRP, cells were fixed and DAB stained. The treatment of cells with LLOMe did not result in an increase in the cytosolic staining of HRP (Figure3.15). Interestingly, from the literature, LLOMe treatment was seen to disrupt the proton gradient and release lysosomal markers below 10,000 kDa to the cytosol but was seen to not release cysteine cathepsins (235). The size of HRP (~35kDa) may explain the lack of cytosolic staining with LLOMe.

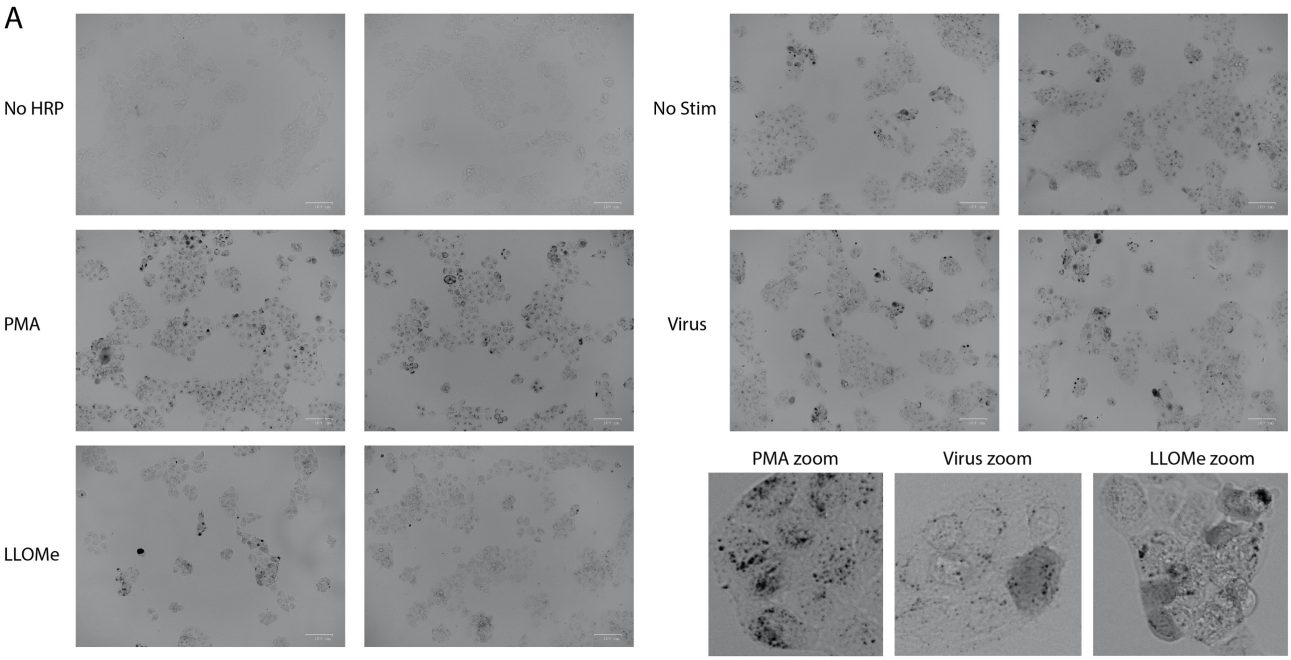

*Figure3.15: **Treatment of cells with LLOME does not result in cytosolic HRP staining**. A431 cells seeded onto coverslips 2 days prior to the experiment were preincubated in serum-free media for at least 2 hours before being incubated with 4mg/ml HRP plus a stimulation for 1 hour. No HRP conditions were treated without HRP. The No stimulation control was treated with a DMSO carrier control, PMA samples were treated with 1uM PMA, Virus samples were treated with Adenovirus 10,000 MOI and LLOMe samples were treated with 2.5uM LLOMe . After incubation at 37℃cells were placed on ice and washed to remove external HRP. Cells were fixed with 4% PFA for 10 minutes and stained with DAPI. Dab staining was performed using 0.5mg/ml DAB with 0.003% hydrogen peroxide for 10 minutes. Images were acquired using a ZOE Fluorescent cell imager. Images are representative from one independent experiment*

3.3.4 Increasing the multiplicity of infection does not increase release

To see if the limited release with adenovirus stimulation was due to low concentrations of virus particles per cell, we incubated A431 cells with virus of increasing multiplicity of infection (MOI). The MOI indicates how many particles of adenovirus are present to infect a single cell. For example, an MOI of 10 indicates that there are on average 10 adenovirus to infect each individual cell. This value was estimated from the number of cells seeded and so the actual MOI is probably less due to the expansion of cell number between seeding and performing the experiment. To produce reproducible data the same amount of time between seeding and the experiment was maintained, and the same number of cells were seeded every time. Increasing the MOI did not seem to result in increased cytosolic release and due to the quantity of virus required to perform these experiments limited optimisation could be performed (Figure3.16).

A

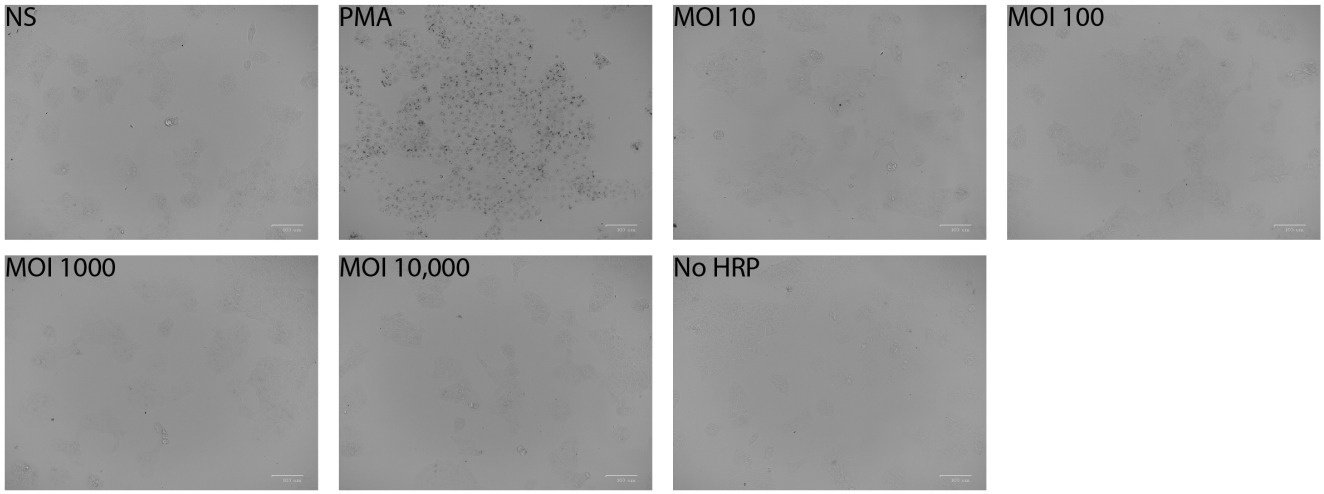

*Figure3.16: **Treatment of A431 cells with increasing concentration of adenovirus**. A431 cells seeded onto coverslips 2 days prior to the experiment were preincubated in serum-free media for at least 2 hours before being incubated with 4mg/ml HRP plus a stimulation for 1 hour. The No stimulation control was treated with a DMSO carrier control, PMA samples were treated with 1uM PMA, Virus samples were treated MOI as shown. After incubation at 37℃, cells were placed on ice and washed to remove external HRP. Cells were fixed with 4% PFA for 10 minutes and stained with DAPI. Dab staining was performed using 0.5mg/ml DAB with 0.003% hydrogen peroxide for 10 minutes. Images were acquired using a ZOE Fluorescent cell imager. Images are representative from two independent experiments*

3.3.5 A J774.2 macrophage cell line shows basal endosomal release

As the adenovirus was only stimulating release in a very small population of cells, we validated the HRP endosome release assay in a cell line that was known to release endosomal content. A publication from A.Rust et al highlighted the ability of a specific macrophage cell line, J774.2, to be affected by the ribosome inactivating drug saporin without addition of any delivery mechanism (193). As saporin is not normally released to the cytosol these results indicated the J774.2 cells had semi permeable endosomes. We performed a HRP uptake assay on the J774.2 cells and stained for the HRP cellular location using DAB staining. We observed that there was cytosolic DAB staining under basal conditions and with PMA stimulation (Figure3.17). Interestingly stimulation of cells with adenovirus resulted in a significant increase in cytosolic DAB staining indicating an active effect of the virus on endosomal release. Potentially the semi-permeable endosomes were affected more by adenovirus stimulation then the other cell lines tested previously. Additionally, these results further validated the functionality of the HRP assay to detect endosomal release.

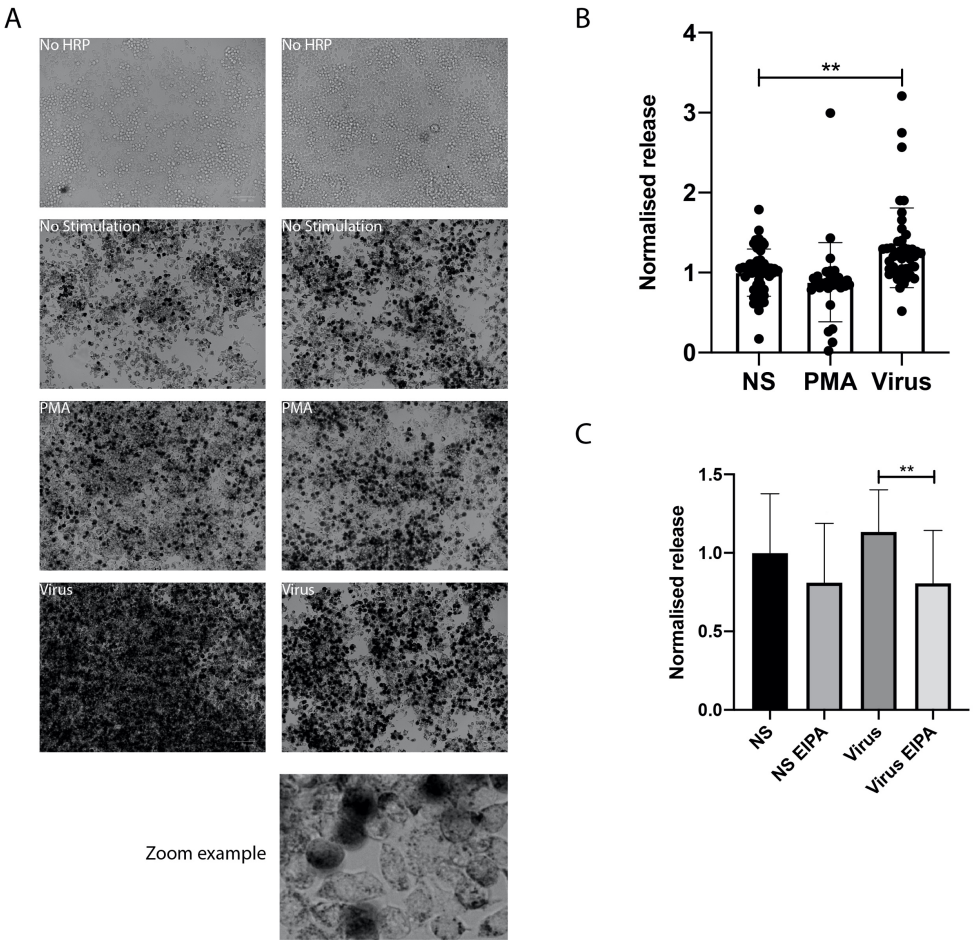

Figure3.17: ***Treatment of J774.2 cells with adenovirus results in increased cytosolic staining:*** *A431 cells seeded onto coverslips 2 days prior to the experiment were preincubated in serum-free media for at least 2 hours before being incubated with 10mg/ml HRP plus a stimulation for 1 hour. The No stimulation control was treated with a DMSO carrier control, PMA samples were treated with 1uM PMA, Virus samples were treated with 1ug/ml adenovirus. After incubation at 37℃, cells were placed on ice and washed to remove external HRP. Cells were fixed with 4% PFA for 10 minutes and stained with DAPI. Dab staining was performed using 0.5mg/ml DAB with 0.003% hydrogen peroxide for 10 minutes. A) Images were acquired using a ZOE Fluorescent cell imager. B) Release was measured in imageJ by thresholding and measurement of total intensity of the threshold area. Data was normalised to the average No stimulation control. Data shown is Mean + SD from 4 independent experiments. N>30 for all conditions. A one-way ANOVA with Tukey's multiple comparison test was performed with ****p≤0.0001, *** p≤0.001, ** p≤0.01 , * p≤0.05, 'NS' p >0.05. C) Cells were either pretreated with EIPA or a DMSO carrier control for 30minutes Cells were stimulated with either a DMSO carrier control or Virus in the presence of 10mg/ml HRP and EIPA. Data is Mean + SD from 2 independent experiments with images acquired >20 for all conditions. A one-way ANOVA with Tukey's multiple comparison test was performed with ****p≤0.0001, *** p≤0.001, ** p≤0.01 , * p≤0.05, 'NS' p >0.05*

3.3.6 J774.2 cells have lower levels of Intergrin alpha V

In an attempt to elucidate the reason for the increased ability of the adenovirus to trigger endosomal release in the J774.2 cell line we looked at the expression of alpha V intergrin.

As integrin alphaV is one of the possible secondary adenovirus receptors required for internalisation, a lack of the alpha V intergrin might explain the different response to adenovirus incubation.

Initially we observed the localisation of alpha V intergrin in A431 cells upon incubation with PMA or adenovirus. We observed cellular staining of intergrin alphaV at the cell surface but also intracellularly in the cytosol (Figure3.18A). There was no detectable difference in the localisation of the integrin after treatment with either PMA or adenovirus, suggesting no response to the adenovirus incubation. If the alpha V intergrin was utilized to trigger endocytosis, the incubation of cells with adenovirus may result in loss of membrane alpha V intergrin staining which was not observed during our experiment.

Adenovirus had previously been shown by us to increase endosomal release in the J774.2 cell line but not in the A431 cells. Additionally, we showed adenovirus did not increase macropinocytosis in multiple different cell lines. Next, we wanted to discover the difference in the J774.2 cell line that enables increased endosomal release with adenovirus incubation. As alpha V intergrin is the secondary receptor for adenovirus, changes in its abundance could affect the adenovirus internalisation. To quantitatively compare the protein levels of alpha V intergrin in cell lines, western blot analysis of cell lysates from A431, J774.2, HT1080 and Hela-M cells was performed. Hela-M cells are a standardised Hela cell line that was characterised due to the variability observed within different laboratory HeLa cell lines. The A431 cells used during this project were chosen due to their ability to “ruffle” at the plasma membrane and were designated A431-Ruff for this experiment. Additionally, an A431 cell line that had less membrane ruffling (designated A431-master) was tested to see if the A431-ruff cells had observable differences in alpha V intergrin levels to the A431-Master cell line.

The western blot band intensity values were firstly normalised to the protein loading control and then to the levels of intergrin alphaV in the A431 cells (A431-Ruff). As can been seen from the blot and quantification, the J774 cells have lower levels of intergrin alphaV then the A431-ruff cells (Figure3.18B). The lack of this receptor in J774 cells could explain their ability to release more endosomal content in response to adenovirus infection. An alternative secondary receptor might result in greater signalling or an alternative route of internalisation that is shown by the increase in endosomal release. In the J774 blot there is another band of lower molecular weight that is positive for alphaV integrin. This band could be degraded

protein or an alternative splice variant which could explain the differences between the cell lines.

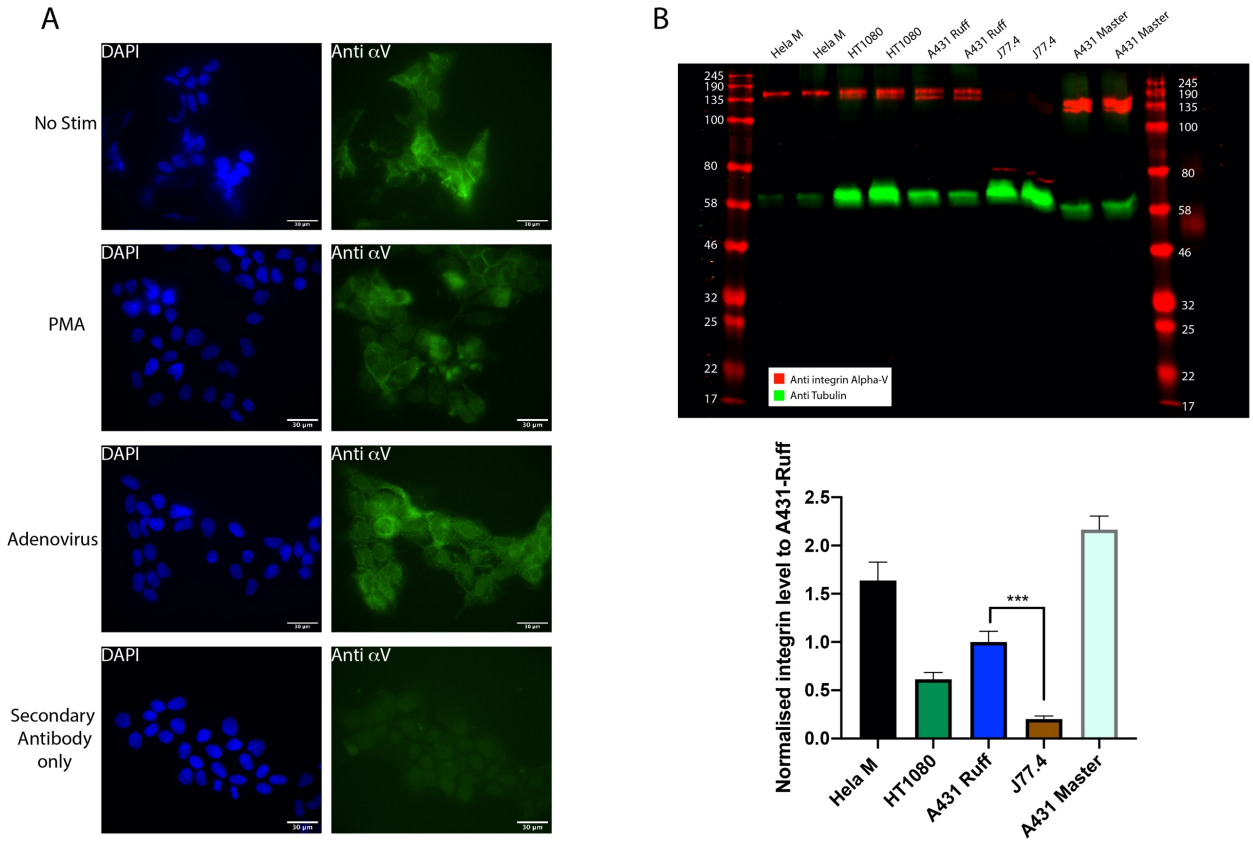

Figure3.18: **Assaying the localisation and quantity of intergrin alphaV in multiple cell lines**. **A)** A431 cells were seeded 2 days prior to the experiment. The cells were fixed with 4% PFA and an immunofluorescence staining protocol was performed using an Anti-Integrin Alpha-V antibody and an alexafluor 488 fluorescent secondary. Coverslips were mounted and images acquired using an inverted widefield system. The images shown are representative from 1 independent experiment **B)** Protein samples were acquired by cell lysis. Protein concentration was quantified using a Bradford assay and equal amount of protein was loaded onto an SDS page gel. A western blot was performed using the Anti-Integrin Alpha-V antibody (Red) and an Anti-Tubulin loading control (Green). The gel was visualised using a Licor imager and band intensity was measured, Normalised to the loading control. These values were normalised to A431-Ruff from each experiment. The Data shown is mean + SD from 2 independent experiments for A431-Ruff and J77.4 samples. Other samples were acquired from one independent experiment. A one-way ANOVA with Tukey's multiple comparison test was performed with ****p≤0.0001, *** p≤0.001, ** p≤0.01 , * p≤0.05, 'NS' p >0.05

3.3.7 J774.2 cells show greater cytosolic staining with HRP under all stimulation conditions

A drawback of the HRP staining is the quality of DAB stain can be variable between experiments. We believe this is due to the stability of the DAB in solution and can vary between experiments. Therefore, we tested the A431 cells and the J774.2 cells in the same experiment to observe the differences in HRP DAB staining directly between the two cell lines. The J774.2 cells showed greater amount of cytosolic staining under all conditions (Figure3.19).

The J774.2 cells consistently showed high levels of cytosolic staining but the mechanism behind the endosomal release were unknown. Other variants of J774 macrophages do not show similar release characteristics indicating the semi-permeable endosomes in the J774.2 cells are probably due to an alteration due to genetic mutation of the cell line rather than a stimulation of a biological mechanism of endosomal release. Additionally, although the increased release observed with adenovirus infection was significant, the signal to noise ratio was low due to the high basal release seen in the absence of stimulation. We ideally wanted a system with inducible endosomal release using a biologically relevant molecule that had a high signal relative to background release.

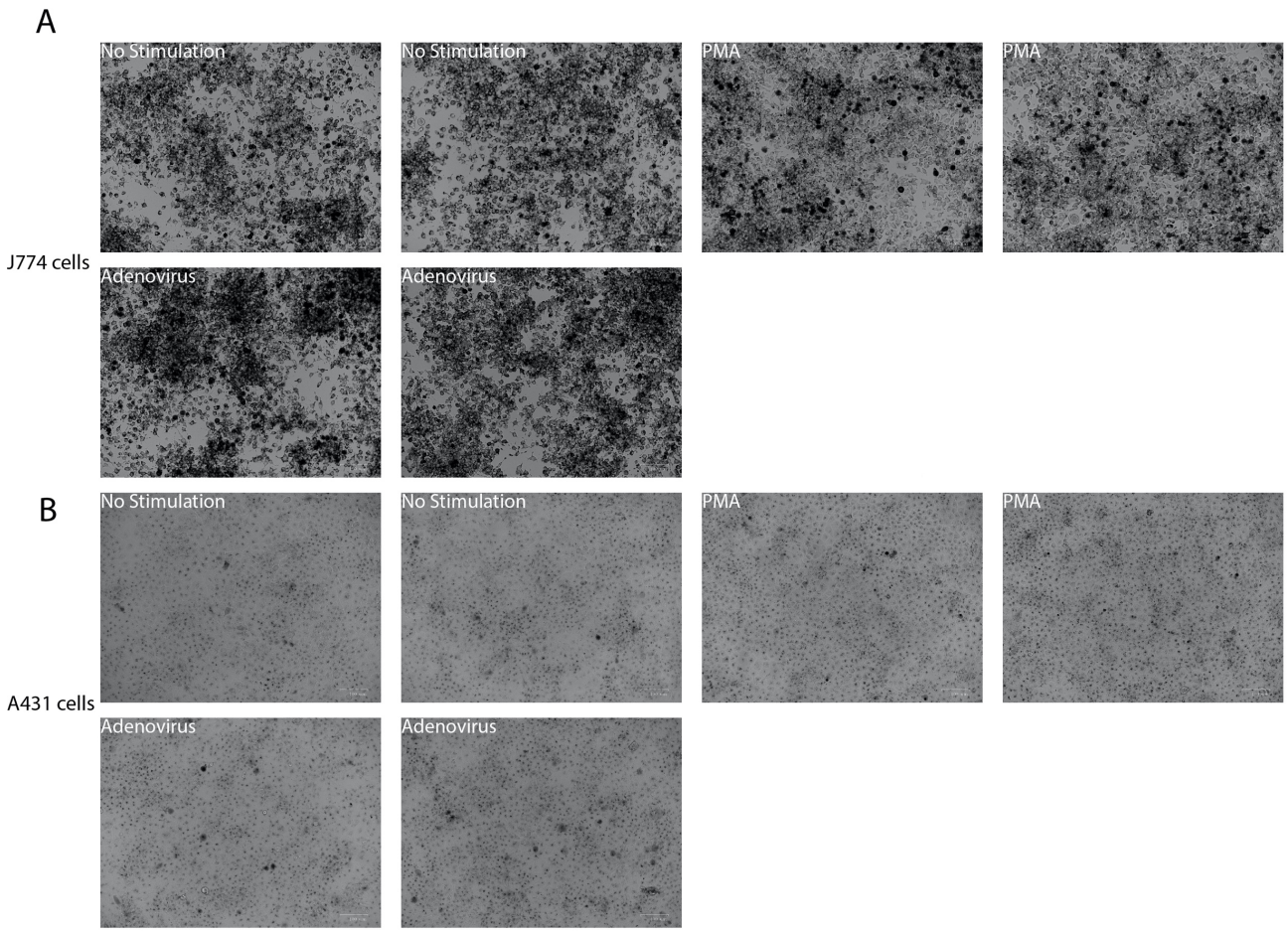

*Figure3.19**: HRP staining in J774.2 cells compared to A431 cells**. J774 and A431 cells were seeded onto glass coverslips 2 days prior to the experiment. Media was exchanged to serum-free media for at least 2 hours prior to performing the experiment. The cells were treated with 10mg/ml HRP plus a stimulation for 1 hour. The No stimulation control was treated with a DMSO carrier control, PMA samples were treated with 1uM PMA, Virus samples were treated with 1ug/ml adenovirus. After incubation at 37°C, cells were placed on ice and washed to remove external HRP. Cells were fixed with 4% PFA for 10 minutes and stained with DAPI. Dab staining was performed using 0.5mg/ml DAB with 0.003% hydrogen peroxide for 10 minutes. A) Images were acquired using a ZOE Fluorescent cell imager for A431 cells. B) Images were acquired using a ZOE Fluorescent cell imager for J774.2 cells.*

3.4 EGF as a ligand for endosomal release

In order to study a more biologically relevant system we looked for alternative stimulants of endosomal release. Work from C.Watts had identified a phenomenon in the A431 cells where stimulation of the cells with EGF resulted in cytosolic HRP staining (173). It was postulated that EGF induced release might reflect a physiological role for endosomal release in cross presentation. Antigen cross presentation is a biological process whereby endosomal antigens can be released to the cytosol for presentation onto the MHC1 pathway. We decided to test EGF stimulation in our A431 cell line to reproduce the endosomal release seen in the original work.

3.4.1 EGF stimulation result in cytosolic HRP staining indicating endosomal release

In order to assess the ability of EGF to stimulate endosomal release, an HRP uptake assay was performed with 100ng/ml EGF stimulation. It has been previously reported that high concentration(~100ng/ml) of EGF is known to stimulate membrane ruffling (236) and therefore macropinocytosis, whereas lower concentrations of EGF (<10ng/ml) stimulated only clathrin-mediated endocytosis. A431 cells were stimulated with EGF for 10 minutes and then chased with serum free media for 90 mins before fixation and DAB staining as described (173). The treatment of A431 cells with EGF resulted in cytosolic staining of HRP in our cell line as described (Figure3.20). The HRP stain was cytosolic but was excluded from the nucleus indicating the cells were still viable. The endosomal release triggered by EGF was also sensitive to inhibition with EIPA, an inhibitor of macropinocytosis, implying that the release could potentially be dependent on macropinocytosis and occur from macropinosomes. As no release was observed under basal conditions, there was a robust and sensitive signal for the released HRP. This would enable us to perform further inhibitory or stimulatory experiments with greater certainty to identify the effectors.

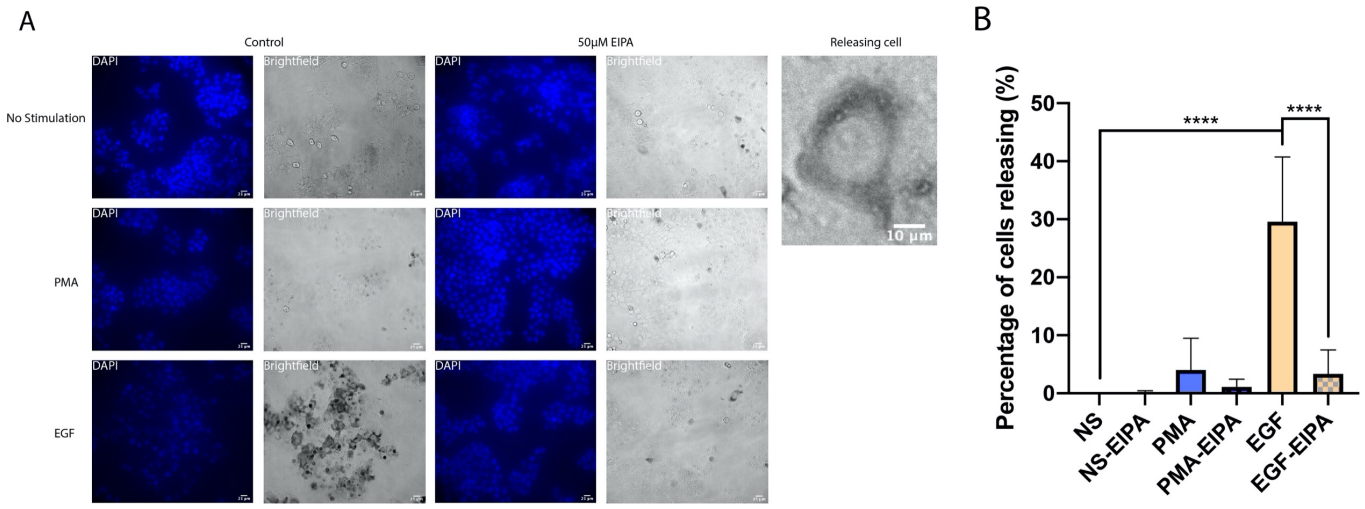

Figure3.20: ***Treatment of A431 cells with EGF results in cytosolic HRP staining.*** *A431 cells were seeded onto glass coverslips 2 days prior to the experiment. Media was exchanged to serum-free media for at least 2 hours prior to performing the experiment. The cells were treated with 10mg/ml HRP plus a stimulation for 10 minutes followed by a chase with serum-free for 90 minutes. The No stimulation control was treated with a DMSO carrier control, PMA samples were treated with 1uM PMA or EGF samples were treated with 100ng/ml EGF. Conditions with EIPA inhibition shown were pretreated with 50uM EIPA for 30minutes and non-EIPA treated cells were treated with equivalent DMSO carrier controls. EIPA was additionally included in the stimulation for each condition if EIPA is shown. After incubation at 37°C, cells were placed on ice and washed to remove external HRP. Cells were fixed with 4% PFA and stained with DAPI. Dab staining was performed using 0.5mg/ml DAB with 0.003% hydrogen peroxide for 10 minutes. A) Images were acquired using an inverted widefield microscope. B) Release was measured in imageJ by manual counting of released cells and a total cell count was performed using automated analysis. Data shown is Mean + SD from 2 independent experiments. Images acquired > 15 for all conditions. A one-way ANOVA with Tukey's multiple comparison test was performed with ****p≤0.0001, *** p≤0.001, ** p≤0.01 , * p≤0.05, 'NS' p >0.05.*

3.4.2 EGF stimulates release in the HT1080 cell line

We wanted to see if the effect of EGF stimulation was specific to A431 cells, and so performed the HRP uptake assay in the HT1080 cell line. In the A431 cells, endosomal release was only observed upon EGF stimulation and not with PMA or under no stimulation conditions. In the HT1080 cells EGF stimulation also resulted in cytosolic release of content (Firgure3.21). Interestingly PMA stimulation was also seen to increase the release of endosomal content in the HT1080 cells. The cells under basal conditions had some cytosolic HRP staining, more than observed in the A431 cells indicating increased basal endosomal permeability in this cell line. As stimulation with PMA is known to increase fluid phase uptake in this cell line, as seen previously with the dextran uptake assay (Figure3.09), the increased endosomal release could be explained by the increase in fluid phase HRP uptake by PMA stimulation. This would mean the effect of PMA stimulation is not seen in the A431 cells as there is less basal endosomal release and so an increase in fluid phase uptake does not correlate to increased endosomal release. On the other hand, the data could suggest there are different sub-populations of macropinosomes that are formed under different stimulatory conditions. The stimulation of

cells with EGF might result in the formation of permeable macropinosomes in the A431 cells whereas the PMA stimulation forms a different, less permeable sub type of macropinosomes. However, in the HT1080 cells both PMA and EGF stimulation results in the formation of the permeable endosomes due to differences in signalling pathways in each cell type.

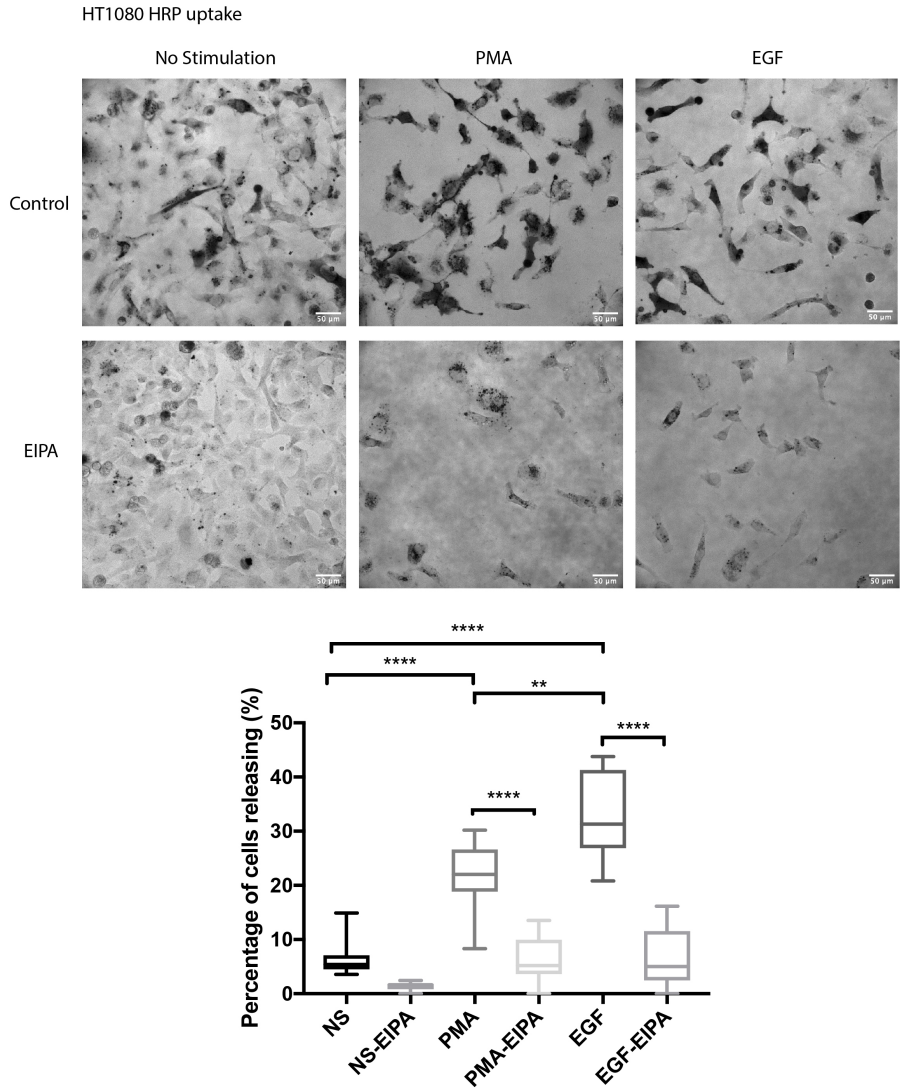

Figure3.21: ***Treatment of HT1080 cells with EGF results in cytosolic HRP staining.*** *HT1080 cells were seeded onto glass coverslips 2 days prior to the experiment. Media was exchanged to serum-free media for at least 2 hours prior to performing the experiment. The cells were treated with 10mg/ml HRP for 10 minutes followed by a chase with serum-free for 90 minutes . The No stimulation control was treated with a DMSO carrier control, PMA samples were treated with 1uM PMA and EGF samples were treated with 100ng/ml EGF. Conditions with EIPA inhibition shown were pretreated with 50uM EIPA for 30minutes and non-EIPA treated cells were treated with equivalent DMSO carrier controls. EIPA was additionally included in the stimulation for each condition if EIPA is shown. After incubation at 37℃, cells were placed on ice and washed to remove external HRP. Cells were fixed with 4% PFA and stained with DAPI. Dab staining was performed using 0.5mg/ml DAB with 0.003% hydrogen peroxide for 10 minutes. A) Images were acquired using an inverted widefield microscope. B) Release was measured in imageJ by manual counting of released cells and a total cell count was performed using automated analysis. Data shown is Mean + SD from 1 independent experiments. Images acquired ≥7 for all conditions. A one-way ANOVA with Tukey's multiple comparison test was performed with ****p≤0.0001, *** p≤0.001, ** p≤0.01 , * p≤0.05, 'NS' p >0.05.*

The endosomal release in the HT1080 cells was sensitive to EIPA inhibition, as seen previously with the A431 cells indicating that the endosomal release was from macropinosomes directly.

The HT1080 cell line showed more nuclear staining and less of a distinct absence of HRP staining in the nucleus as can be clearly seen in the A431 cells. This could be a difference in the physiology of the cell line but could suggest differences in the response to EGF. The cell shape of the HT1080s made identification of releasing cells harder as there are many small protrusions as well as a smaller cell body. Some cells showed many large vesicles that were HRP positive which made quantification of cells where release had occurred more challenging.

An important note on the HT1080 cell line is the mutation in the RAS protein. RAS is a major signalling pathway in cells and is additionally activated by EGF signalling. Mutations in RAS can result in oncogenic transformations due to constitutively active signalling. The HT1080 cell line contains a constitutively active N-RAS mutant form which could potentially explain the difference between the A431 cell line and the HT1080 cells (237).

3.4.3 Optimisation of the HRP release assay for a high-throughput format

To perform a high throughput screen using the HRP release assay it would require optimisation for a 384 well plate format. We tested the HRP release assay in a 384 well plate using a range of different HRP concentrations. One enzymatic HRP molecule can perform multiple DAB reactions which results in amplification of the signal. The enzymatic nature of the assay gives increased sensitivity as HRP can continuously generate reaction product at least for a limited time. However, this limits the information on the total amount of endosomal release as the HRP delivered is not directly proportional to the signal observed. In order to observe the sensitivity of the assay and to obtain the amount of HRP that is required to see endosomal release, we performed an HRP concentration curve. Different concentrations of HRP were used for the uptake assay with EGF stimulation or under basal conditions. As the concentration of HRP decreased, so did the amount of endosomal release that was observed (Figure3.22). Using 10mg/ml HRP with EGF stimulation resulted in an

increase in endosomal release approximately 7x greater than under basal conditions. As a lower concentration of HRP was used, the difference between unstimulated and EGF decreased until 1mg/ml HRP only showed a 2X increase in endosomal release. This experiment showed the release of HRP to the cytosol is proportional to the concentration of HRP in the fluid phase. From the experiment we could select the optimal HRP concentration to observe endosomal release without introducing background staining. As there was no difference in the unstimulated conditions between the HRP concentrations, 10 mg/ml HRP was selected as it gave the best separation of signal.

The actual percentage of cells showing release decreased in the 384 well plate assays then compared to the equivalent in a larger well format. The reason for this difference was not known but the assay still showed consistent and large separation of signal enabling a screen to be performed using this assay.

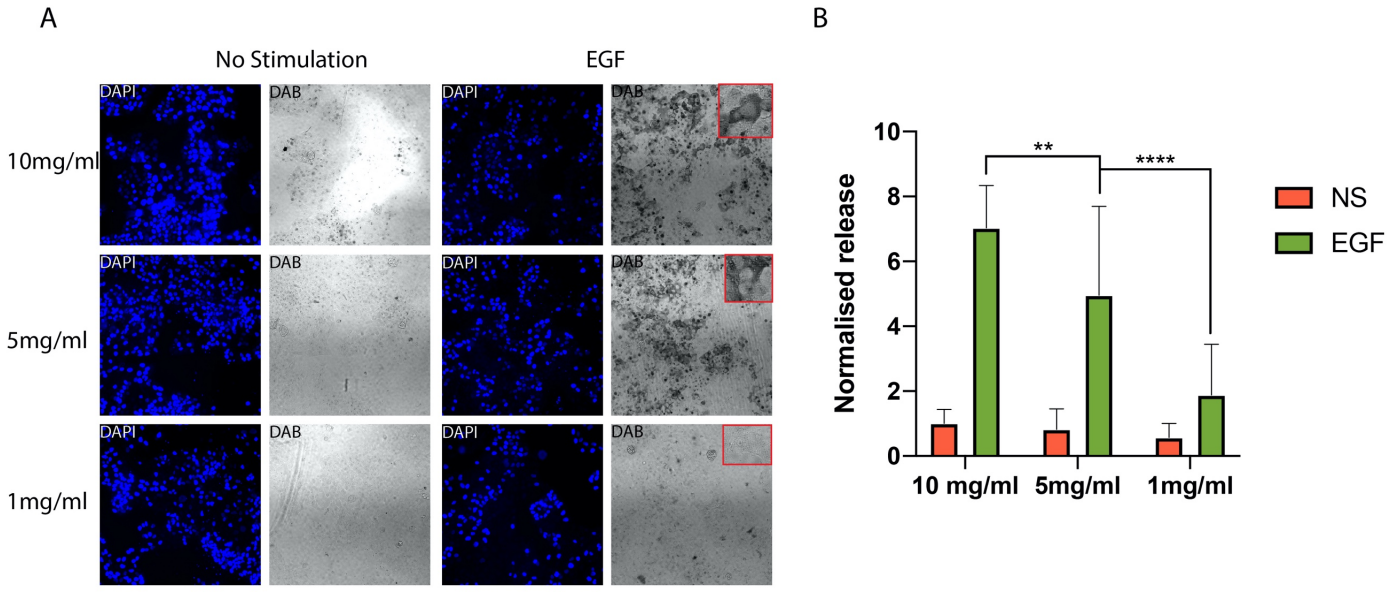

*Figure3.22: **The effect of HRP concentration on EGF stimulated HRP release.** A431 cells were seeded into a 384 well plate 3 days prior to the experiment. The seeding density was 1000 cells/well. Media was exchanged to serum-free media for at least 2 hours prior to performing the experiment. The cells were treated with the shown concentrations of HRP plus a stimulation for 10 minutes followed by a chase with serum-free for 90 minutes. The No stimulation control was treated no stimulation and EGF samples were treated with 100ng/ml EGF. After incubation at 37℃, cells were placed on ice and washed to remove external HRP. Cells were fixed with 4% PFA and stained with DAPI. Dab staining was performed using 0.5mg/ml DAB with 0.003% hydrogen peroxide for 10 minutes. A) Images were acquired using an automated plate microscope. B) Release was measured using the MetaXpress high throughput imaging software using a custom module. Data shown is Mean + SD from 3 independent experiments. Images acquired = 12 for all conditions. A two-way ANOVA with Tukey's multiple comparison test was performed with ****p≤0.0001, *** p≤0.001, ** p≤0.01 , * p≤0.05, 'NS' p >0.05.*

3.4.4 DAB staining interferes with DAPI signal

In order to perform a siRNA screen, the analysis to identify the number of cells showing endosomal release needs to be automated. In order to automate the analysis a software package from Molecular Devices, MetaXpress, was utilized. A custom module editor (CME) was used to design an analysis pathway. The CME would need to detect the cells showing cytosolic DAB staining and count the total number of cells releasing content as well as the total number of cells. The full CME developed is described in the appendix (Section8.1) but briefly the nuclei of cells were identified from the nucleus stain and a mask was expanded from the nuclei to identify the whole cell. If the DAB signal in the whole cell mask was above a threshold level, the cell was counted as having cytosolic DAB staining. In order for this CME to function correctly identification of nuclei from the nuclear stain was very important. However, it was noticed the DAB product quenched the DAPI signal from cells showing cytosolic release (Figure3.23). The absorption spectra for the DAB product shows a peak at 465nM (238) and DAPI has an emission peak at 461nM (239) which indicates quenching of the DAPI signal. As the detection of nuclei is an important stage in the automated analysis an alternative dye was required. We therefore tested the far-red DNA dye, Draq-5. As can be seen (Figure3.23B) the draq5 stain is not affected by the DAB stain and similar nuclei intensity is observed in cells showing cytosolic staining as non-cytosolic stained cells.

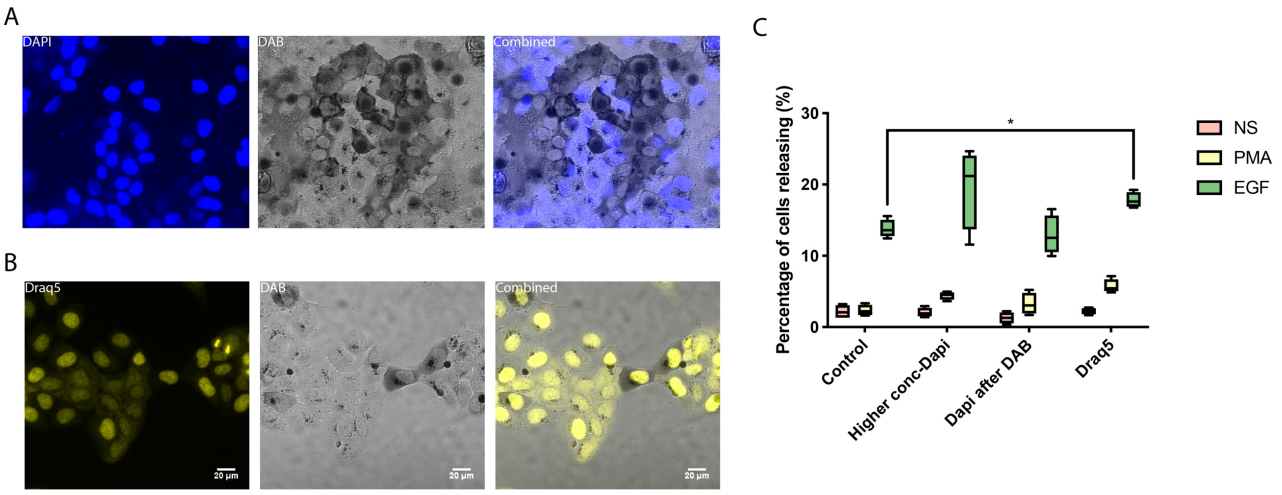

*Figure3.23: **The use of Draq5 nuclear stain during the HRP release assay.** A431 cells were seeded into a 384 well plate 3 days prior to the experiment. The seeding density was 1000 cells/well. Media was exchanged to serum-free media for at least 2 hours prior to performing the experiment. The cells were treated with the shown concentrations of HRP plus a stimulation for 10 minutes followed by a chase with serum-free for 90 minutes. The No stimulation control was treated with a DMSO carrier control, PMA samples were treated with 1uM PMA and EGF samples were treated with 100ng/ml EGF. After incubation at 37℃, cells were placed on ice and washed to remove external HRP. Cells were stained with either DAPI or Draq5 . Dab staining was performed using 0.5mg/ml DAB with 0.003% hydrogen peroxide for 10 minutes. A) Images were acquired using an automated plate microscope. B) Release was measured using the MetaXpress high throughput imaging software using a custom module. Data shown is Mean + SD from 1 independent experiments. Images acquired =4 for all conditions. A two-way ANOVA with Tukey's multiple comparison test was performed with ****p≤0.0001, *** p≤0.001, ** p≤0.01 , * p≤0.05, 'NS' p >0.05.*

The use of Draq5 resulted in more accurate quantification of the data. Multiple methods to increase the accuracy of nuclei detection were tried including using higher concentrations of DAPI, applying the DAPI stain after DAB staining rather than before or using the new Draq5 nuclear stain. Draq5 resulted in more consistent identification of releasing cells and less variability in the data (Figure3.23C). Draq5 also detected more cells with cytosolic staining then the original DAPI method.

3.4.5 The time of chase and EGF concentrations do not affect endosomal release

Before performing an siRNA screen, we wanted to understand the EGF triggered endosomal release. Initially a chase period of 90 minutes in serum-free media was performed following 10 minutes incubation with HRP. This was performed following previous reports in the literature (173) but we wanted to see if this chase step was necessary to see endosomal release. When no chase was performed, we still observed release of content (Figure3.24) and a similar number of cells showed cytosolic HRP staining compared to the full 90 minutes of

chase. From these results it looks like the chase is not required but the variation in the data was smaller with the 90 minutes chase and so was kept for future experiments.

We had previously used 100ng/ml EGF because it was known to induce macropinocytosis (198) but we wanted to see if changing the concentration of EGF used would increase the amount of cells showing endosomal release. I tested a series of EGF concentrations in the HRP release assay up to a maximum of 400ng/ml EGF, 4X as much as normal. Increasing concentrations of EGF had no significant effect on the percentage of cells showing endosomal release.

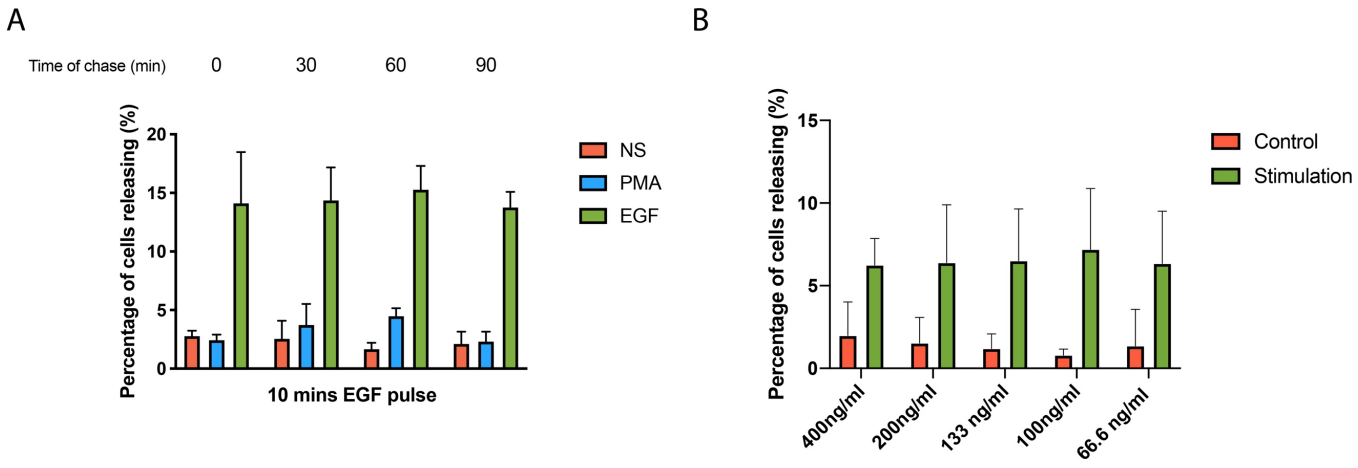

*Figure3.24: **Chase time or EGF stimulation has a limited effect on release.** A431 cells were seeded into a 384 well plate 3 days prior to the experiment. The seeding density was 1000 cells/well. Media was exchanged to serum-free media for at least 2 hours prior to performing the experiment. A) The cells were treated with 10mg/ml HRP plus a stimulation for 10 minutes followed by a chase with serum-free for the variable time shown above the graph. The No stimulation control was treated with a DMSO carrier control, PMA samples were treated with 1uM PMA and EGF samples were treated with 100ng/ml EGF. After incubation at 37°C, cells were placed on ice and washed to remove external HRP. Cells were stained with Draq5 . Dab staining was performed using 0.5mg/ml DAB with 0.003% hydrogen peroxide for 10 minutes. Images were acquired using an automated plate microscope. Release was measured using the MetaXpress high throughput imaging software using a custom module. Data shown is Mean + SD from 1 independent experiments. Experimental replicates = 4 for all conditions. A two-way ANOVA with Tukey's multiple comparison test was performed with ****p≤0.0001, *** p≤0.001, ** p≤0.01 , * p≤0.05, 'NS' p >0.05.*
*B) The cells were treated with 10mg/ml HRP plus a stimulation for 10 minutes followed by a chase with serum-free for the variable time shown above the graph. The No stimulation control was treated with nothing and EGF samples were treated with variable EGF concentrations shown. After incubation at 37°C, cells were placed on ice and washed to remove external HRP. Cells were stained with Draq5 . Dab staining was performed using 0.5mg/ml DAB with 0.003% hydrogen peroxide for 10 minutes. Images were acquired using an automated plate microscope. Release was measured using the MetaXpress high throughput imaging software using a custom module. Data shown is Mean + SD from 4 independent experiments. Experimental replicates = 16 for all conditions. A two-way ANOVA with Tukey's multiple comparison test was performed with ****p≤0.0001, *** p≤0.001, ** p≤0.01 , * p≤0.05, 'NS' p >0.05.*

3.4.6 Different Erbb pathway ligands can stimulate release

The stimulation of cells with EGF increased the delivery of endocytosed HRP to the cytosol. We investigated whether alternative ligands of the Erbb pathway could elicit a similar response to EGF stimulation. The ErbB pathway has many ligands and 4 different receptors can heterodimerise in response to activation and therefore there are many combinations of activation. The EGF ligand is a high affinity ligand of the EGF receptor (erbb1) and therefore leads to strong activation of the pathway. The other identified ligands of the ErbB pathway are usually lower affinity and can have preferences to one of the other ErbB receptors. We tested if the ErbB ligands Beta-cellulin, Heparin binding epidermal growth factor and amphiregulin could increase the delivery of HRP. As the ligands were lower affinity than EGF, we tested two concentrations for each ligand. The concentration of 100ng/ml was used for all ligands as this was the concentration of EGF used previously to allow a comparison between the ligands. Additionally, we selected concentrations form the literature for the other ligands that are known to activate the ErbB pathway. All of the ligands tested had an effect on HRP release at one of the concentrations tested (Figure3.25). The HB-EGF had the strongest effect with an increase seen at both concentrations. Amphiregulin had the weakest response with a slight increase in HRP release observed but only with a 5x higher concentration than EGF.

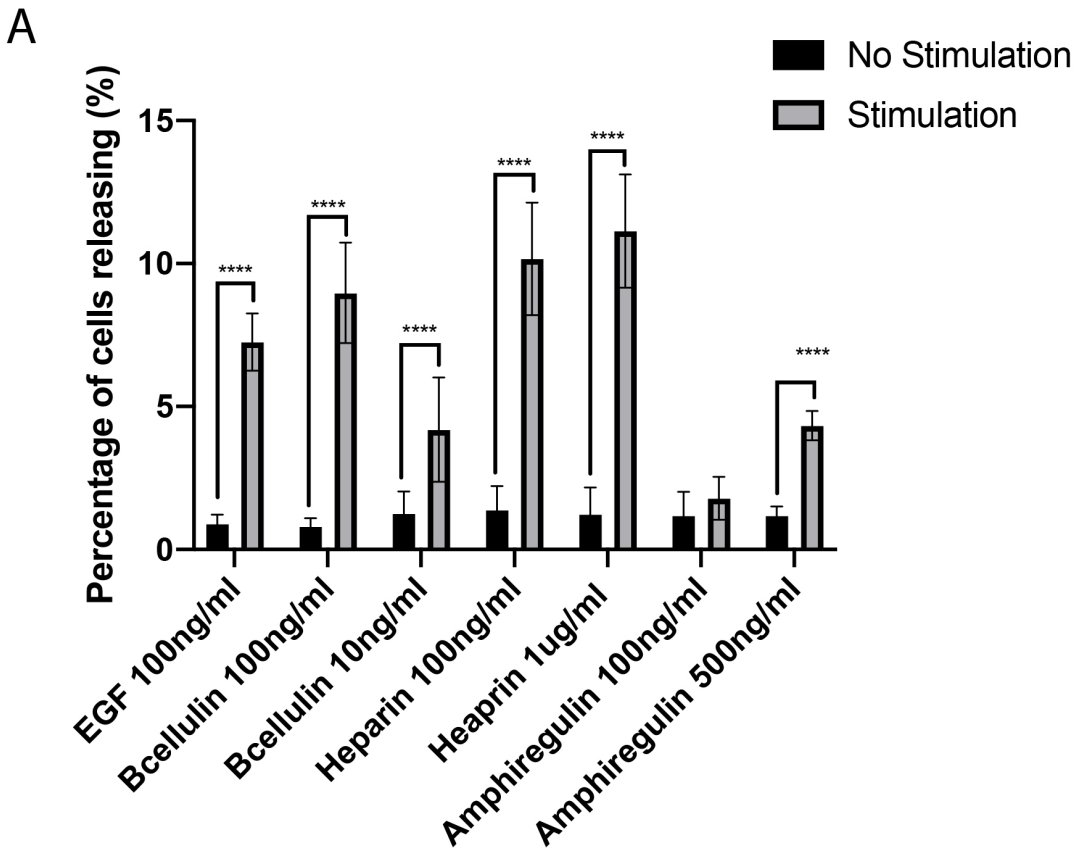

*Figure3.25**: Multiple ligands of the ERBb family of receptors can stimulate endosomal release in A431 cells.** The A431 cells were seeded and incubated at 37 ℃ for 3 days. The cells were serum starved for at least 2 hours prior to performing a HRP uptake experiment. The cells were stimulated with one of the ERBb family ligands at the concentrations shown in the graph for 10 minutes. The cells were washed with serum-free media-BSA0.2% and incubated for 90 minutes at 37 ℃. The cells were placed on ice and washed with ice-cold serum-free media-BSA 0.2% and ice-cold PBS before fixation with 4% PFA for exactly 10 minutes. A DAB solution was used to stain for the cellular location of HRP and the number of cells showing endosomal release was calculated as a percentage of total cells. Data shown is mean + SD from 2 independent biological repeats with 8 experimental replicates. A 2-way ANOVA was performed with a Sidak's multiple comparison. ****p≤0.0001, *** p≤0.001, ** p≤0.01 , * p≤0.05.*

Chapter4: An siRNA kinome screen to identify regulators of macropinocytosis

The overall aim of the project was to identify novel regulators of endosomal release following macropinocytosis. Since up- or down-regulation of macropinocytosis could indirectly affect endosomal release we needed to perform a screen for regulators of macropinocytosis to aid identification of effectors directly involved in endosomal release rather than effectors of macropinocytosis.

To elucidate cellular components involved in the regulation of macropinocytosis we decided to perform a siRNA interference screen using the optimised 70kDa dextran uptake assay. We used PMA to stimulate macropinocytosis in A431 cells. PMA directly activates PKC which is a key signalling hub for intracellular signalling pathways (207,240). Activation of PKC is downstream of growth factor activation (118,241). We decided to perform a Kinome siRNA screen to identify the signalling proteins involved in PMA induced macropinocytosis.

4.1 Assay development for a 384 well plate format

To perform the Kinome siRNA screen we initially needed to optimise the dextran uptake assay for a high throughput format. A high throughput screen requires the use of multi-well plates such as the 384 well plate. The use of 384 well plates allow a greater number of conditions to be tested using less reagents without which a high throughput screen is not possible. To transition into the smaller plate format, it is necessary to optimize transfection protocols, assay design, image capture and image analysis.

4.1.1 Optimisation of a reverse transfection protocol

Within the screen, siRNA is used to silence protein expression in each well using a unique siRNA sequence for each target gene. In order to use different siRNA in each well, an alternate transfection protocol called reverse transfection is used routinely during siRNA screening. The siRNA is added to empty 384 well plates using robotic liquid handling, which allows transfer of different siRNA sequences to unique wells. The screening plates containing unique siRNA

can be printed from siRNA libraries such as the Kinome. During reverse transfection, the transfection reagent is added to the siRNA forming the siRNA/transfection reagent mix in the well. Cells are seeded onto the transfection mix and are incubated at 37℃ for 3 days to allow sufficient knockdown of the target genes. The reverse transfection protocol allows the printing of siRNA plates containing unique siRNA in each well without the need to add unique siRNA complex to each well after cell seeding. Reverse transfection is required for high-throughput screening. However, the effect of the reverse transfection on the dextran uptake assay was unknown and required optimisation.

Initially an experiment was performed to test the reverse transfection protocol in the A431 cells. The cells were reverse transfected with non-targeting siRNA using DharmaFECT transfection reagent. Following 3 days of incubation at 37℃, a 70KDa dextran uptake experiment was performed and imaged using an ImageXpress MicroXL automated plate microscope. The initial reverse transfection experiment showed functional detection of macropinocytosis in a 384 well plate as PMA induced an increase in the number of macropinocytosis in the control conditions when compared to unstimulated cells (Figure4.01). However, when cells were reverse transfected with a non-targeting siRNA (NT) there was increased macropinocytosis in the presence and absence of PMA. The addition of Non-targeting siRNA increased the number of macropinosomes per cell to almost the same level as seen with PMA stimulation. As non-targeting siRNA has a scrambled sequence it should not specifically interact with any RNA and therefore should not have a direct effect on the RNA levels in cells. The non-specific stimulation of macropinocytosis with non-targeting siRNA could be an off-target effect of the siRNA silencing an unknown RNA, however 4 different non-targeting siRNA, with different sequences, all had a similar result (Figure4.01C) providing evidence against an off-target effect of the siRNA. The different non-targeting siRNA had similar levels of macropinocytosis indicating the non-specific macropinocytosis was due to the transfection regent used or the reverse transfection protocol.

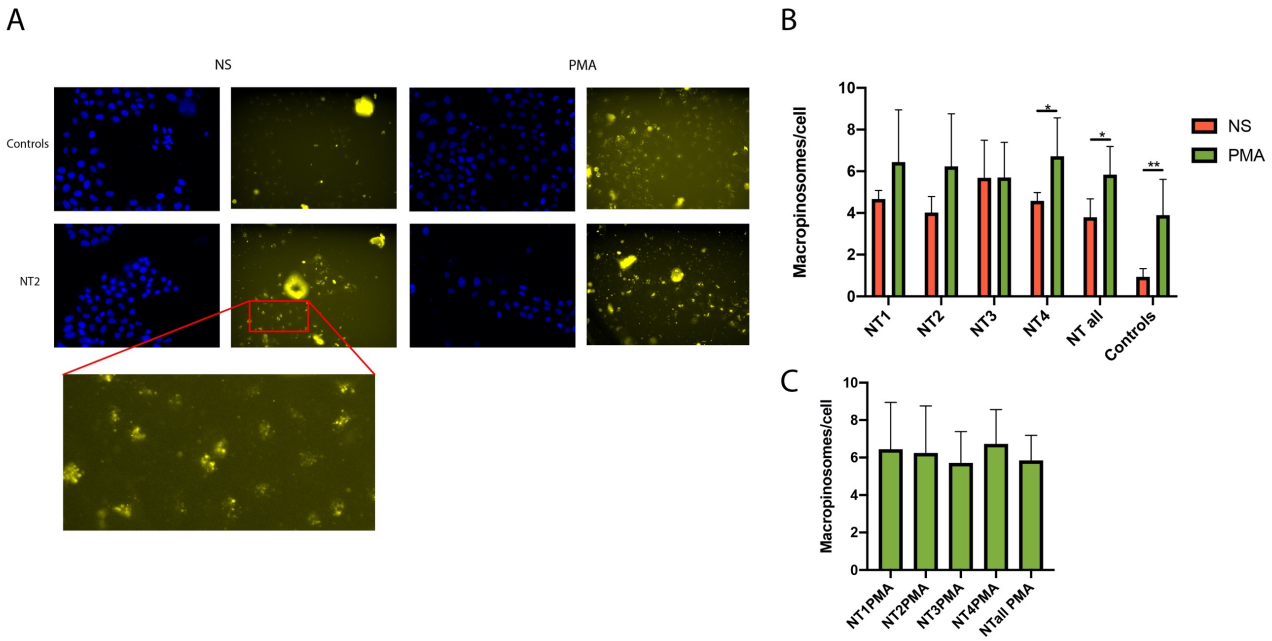

Figure4.01: ***Reverse transfection of A431 cells increases macropinocytosis independently of stimulation.*** *A431 cells were reverse transfected with non-targeting siRNA using dharmaFECT transfection reagent and incubated at 37℃ for 3 days. Control cells were not transfected. Cells were preincubated with serum free media for at least 2 hours and incubated with 0.125mg/ml TRITC dextran in the presence of either a DMSO carrier control in the no stimulation condition (NS) or with 1µM PMA in DMSO for 15 minutes. Cells were washed, fixed with 4% PFA and stained with DAPI. Images were acquired using the automated plate microscope and the number of macropinosomes detected using high-throughput automated detection as describe in the methods. B) Quantification of the number of macropinosomes per cell in unstimulated and PMA treated cells. 9 images were acquired from each well and the average value per well was averaged. Number of data points ≥ 6 with average number of cells per image ~30. A two-way ANOVA with Sidak's multiple comparison was performed with ****p≤0.0001, *** p≤0.001, ** p≤0.01 , * p≤0.05 C) The data for the non-targeting siRNA conditions comparing the number of macropinosomes under PMA stimulation. The data is from the same analysis performed in B. Data shown is mean + SD from 2 independent experiments.*

In the 384 well format, there was also an increase in large non-specific dextran staining observed that was extracellular (Figure4.01A). This background staining could affect image analysis and lead to false positive results. The increase in background staining could be a result of the washing efficiency in the 384 well plate format. An aspirating rod attached to a vacuum pump was used to remove liquid from wells during washing. When using this aspiration method, 10µl of liquid remains in order to prevent disruption of the cells. Therefore, washing is less efficient in the 384 well plate and could explain the increase in background dextran staining observed. This large background was detected during image analysis based on size and excluded during macropinocytosis detection.

Due to the non-specific macropinocytosis observed, the separation of signal between un-stimulated cells and PMA stimulated cells was minimal after reverse transfection of siRNA. During a high throughout screen the separation of signal in the assay is important to enable generation of reliable data, therefore optimisation of the assay was required to reduce the non-specific macropinocytosis.

4.1.1.1 *Removal of transfection mixture following reverse transfection did not decrease non-specific macropinocytosis*

In the initial experiments, the transfection reagent mixture was not removed from the cells following reverse transfection. We wanted to investigate if removal of the transfection mixture reduced the non-specific macropinocytosis observed previously. Following reverse transfection of A431 cells, the transfection mixture was removed and replaced with fresh media at different time points during the 3-day incubation period. The removal of the transfection mix did not decrease the non-specific macropinocytosis observed with reverse transfection at any time points (Figure4.02A).

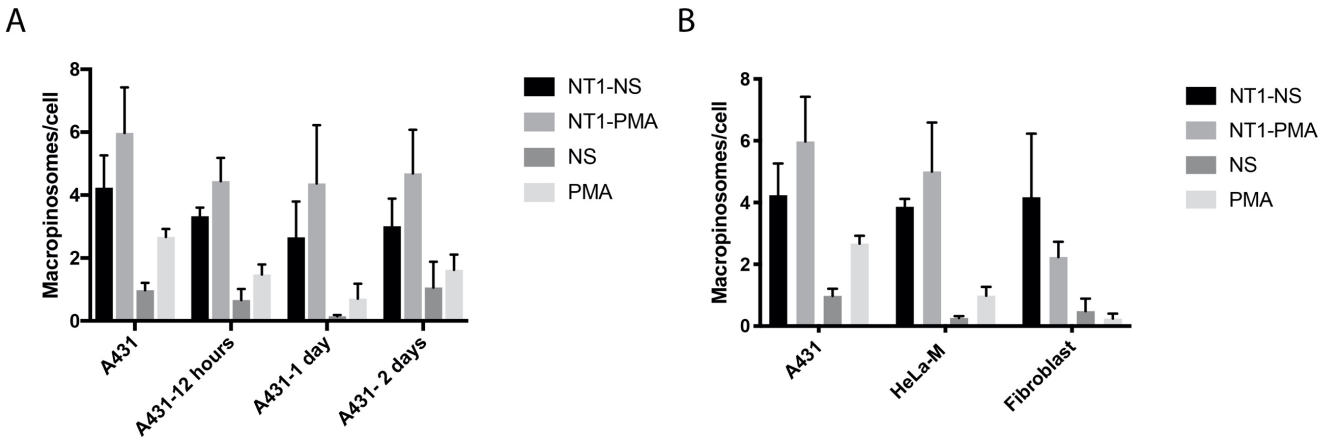

Figure4.02: ***Removal of the transfection reagent after reverse transfection or use of an alternative cell line does not reduce macropinocytosis.*** *A) A431 cells were reverse transfected with Non-targeting siRNA using dharmaFECT and incubated at 37℃for 3 days. Control cells were not transfected. The media in wells was exchanged for fresh media after the indicated times. B) A431, Hela-M or a fibroblast cell line were reverse transfected with non-targeting siRNA using dharmaFECT A+B) After 3 days, cells were preincubated with serum free media for at least 2 hours and incubated with 0.125mg/ml TRITC dextran in the presence of either a DMSO carrier control in the no stimulation condition(NS) or with 1uM PMA for 15 minutes. Cells were washed, fixed with 4% PFA and stained with DAPI. Images were acquired using the automated plate microscope and the number of macropinosomes detected using high-throughput automated detection as describe in the methods. Data shown in both A +B are Mean + SD from one experiment. The average number of macropinosomes per cell was calculated per well from 9 images acquired. Number of replicate wells= 3.*

4.1.1.2 Different cell lines showed similar non-specific macropinocytosis

To elucidate if the non-specific macropinocytosis was unique to the A431 cells, we performed reverse transfections using Hela-M and HFF-11, a fibroblast cell line. Non-specific macropinocytosis was observed in both cell-lines when reverse transfected with siRNA (Figure4.02B). The amount of non-specific macropinocytosis when reverse transfected was greater than in the un-transfected control cells stimulated with PMA in all cell lines. Thus, the non-specific macropinocytosis was not cell type specific, suggesting that the transfection mixture could be the potential cause.

4.1.1.3 DharmaFECT reverse transfection increases macropinocytosis

To investigate if DharmaFECT transfection reagent was the causative agent of non-specific macropinocytosis, we performed reverse transfection of A431 cells with non-targeting siRNA using decreasing concentrations of DharmaFECT. A macropinocytosis uptake assay was performed 3 days later. As the concentration of DharmaFECT used increased, the amount of non-specific macropinocytosis also increased (Figure4.03). This indicated the presence of the DharmaFECT was responsible for the increased macropinocytosis. However as seen previously (Figure4.02A), simply removing the transfection mix after reverse transfection was not sufficient to prevent the non-specific macropinocytosis.

As the DharmaFECT reagent increased non-specific macropinocytosis during reverse transfection we performed a standard transfection protocol in a larger plate format to determine if the reverse transfection was causative. When a standard transfection protocol was performed, where the cells are seeded and the DharmaFECT transfection mixture is added after 24 hours, non-specific macropinocytosis does not occur (Figure4.03B). Additionally, there was a good signal-to-noise ratio between the unstimulated and the PMA stimulated conditions. Included in this experiment was the use of oligofectamine as an alternative transfection reagent. The DharmaFECT transfection reagent is a lipid-based approach to deliver nucleic acid to cells. A different approach to transfection is the use of oligomers to bind to the nucleic acid to form the transfection mixture, such as the transfection reagent oligofectamine. The transfection of A431 cells with oligofectamine had no effect on

macropinocytosis when a standard transfection protocol was followed (Figure4.03B). As DharmaFECT did not increase non-specific macropinocytosis during a standard transfection protocol, we concluded that reverse transfection was the underlying cause of non-specific macropinocytosis.

In order to decrease the non-specific macropinocytosis during reverse transfection we tested a non-lipid transfection reagent, Polyfect. The Polyfect transfection regent did not increase non-specific macropinocytosis in the A431 cells after reverse transfection (Figure4.03C) and the difference between the unstimulated control and the unstimulated nontargeting siRNA transfection was minimal. Polyfect was thus used for future reverse transfections.

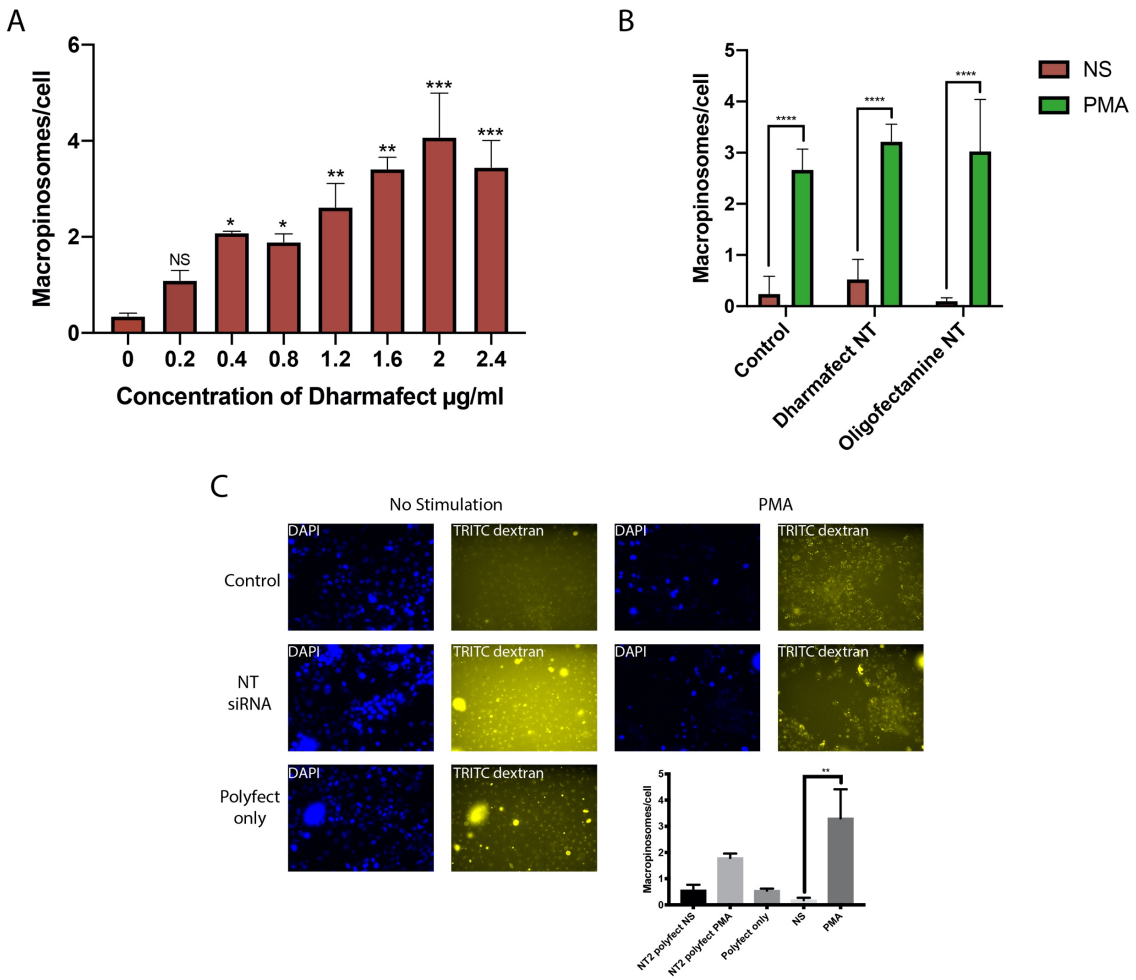

Figure4.03: ***Reverse transfection using polyfect does not result in non-specific macropinocytosis. A****) A431 cells were reverse transfected with Non-targeting siRNA using concentrations of dharmaFECT as shown. Cells were incubated at 37℃for 3 days B) A431 cells were seeded in a 12 well plate and transfected after 24 hours using a standard transfection protocol (see methods) with non-targeting siRNA (NT) using the transfection reagents shown. Cells were incubated at 37℃ for 2 days. C) A431 cells were reverse transfected with Non-targeting siRNA using polyfect transfection reagent. Cells were incubated at 37℃for 3 days. A+B+C) Cells were preincubated with serum free media for at least 2 hours and incubated with 0.125mg/ml TRITC dextran in the presence of either a DMSO carrier control (no stimulation) or with 1µM PMA in DMSO for 15 minutes. Cells were washed, fixed with 4% PFA and stained with DAPI. Images were acquired using the A +C) automated plate microscope or B) an inverted widefield system and the number of macropinosomes measured. A) Data shown is Mean + SD from one experiment. The average number of macropinosomes per cell was calculated per well from 9 images acquired. Number of replicate wells per condition = 2. A one-way ANOVA with Tukey's multiple comparison was performed with ****p≤0.0001, *** p≤0.001, ** p≤0.01 , * p≤0.05 B) Data shown are Mean + SD from one experiment. Number of experimental replicates = 4. A two-way ANOVA with Sidak's multiple comparison was performed with ****p≤0.0001, *** p≤0.001, ** p≤0.01 , * p≤0.05 C) . The average number of macropinosomes per cell was calculated per well from 9 images acquired Number of experimental replicates = 2 for Polyfect treated cells and experimental replicates = 3 for NS and PMA treated cells. A one-way ANOVA with Tukey's multiple comparison was performed with ****p≤0.0001, *** p≤0.001, ** p≤0.01 , * p≤0.05

4.1.2 Identifying control siRNA for the macropinocytosis screens

Before performing the macropinocytosis screen, identification of appropriate positive control siRNAs was required. A positive control is an siRNA that targets a gene which is known to regulate macropinocytosis and is included in the kinome screen as a control for knockdown efficiency. Additionally, these controls are used to verify the macropinocytosis assay is functional and that a difference in macropinocytosis can be detected upon PMA stimulation. To identify positive control siRNA, we investigated proteins that have been implicated in macropinocytosis from the literature. As phosphoinositides are known to be important for macropinocytosis, we selected Phosphoinositide3 kinase (PI3K) (116,118) as a potential positive control. Additionally, we selected 2 proteins that are downstream of PKC signalling, Marcks and CTBP1. To test the ability of these siRNA to reduce macropinocytosis, A431 cells were reverse transfected with the different siRNA using Polyfect transfection reagent. A macropinocytosis assay was performed and the number of macropinosomes per cell measured. The siRNA against PI3K and Marcks resulted in a significant decrease in macropinocytosis indicating they were potentially good control siRNA (Figure4.04). The CTBP1 siRNA did result in a decrease in the number of macropinosomes but this was not significantly different to the non-targeting control as less experimental replicates of CTBP1 siRNA were performed than for PI3K siRNA resulting in less statistical power. There was also greater variability in the non-target control condition which decreased significance.

As well as using the positive control siRNA identified, the cell death control siRNA PLK1 was utilised as a control. If there is sufficient knockdown of PLK1 in mammalian cells, there is an increase in cell death which can be used as a control for knockdown efficiency.

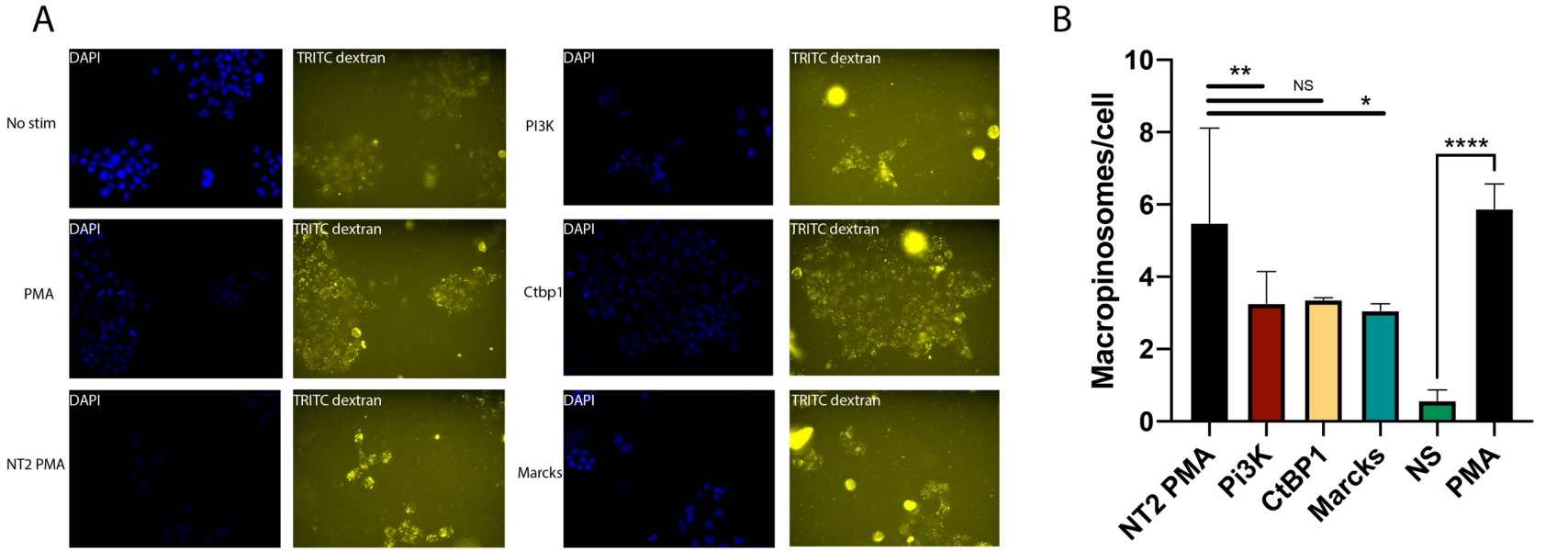

*Figure4.04: **Validation of positive control siRNA.** A431 cells were reverse transfected with different siRNAs as indicated (NT=no targeting siRNA) using Polyfect transfection reagent and incubated at 37℃ for 3 days to allow sufficient transfection. Control cells were not treated with siRNA or transfection reagent. Cells were preincubated with serum free media for at least 2 hours and incubated with 0.125mg/ml TRITC dextran in the presence of either a DMSO carrier control (NS) or with 1μM PMA in DMSO in the other conditions for 15 minutes. Cells were washed, fixed with 4% PFA and stained with DAPI.A) Images were acquired using the automated plate microscope and the number of macropinosomes detected using high-throughput automated detection as describe in the methods. B) Data shown is Mean + SEM from 3 independent experiments for PI3K and 2 independent experiments for CtBP1 and Marcks. The average number of macropinosomes per cell was calculated per well from 9 images acquired. Number of replicate wells = 4 for CtBP1 and Marcks and 9 for PI3K. A one-way ANOVA with Tukey's multiple comparison was performed with ****p≤0.0001, *** p≤0.001, ** p≤0.01 , * p≤0.05*

4.2 An siRNA kinome screen to identify regulators of PMA-induced macropinocytosis

Following the optimisation of the macropinocytosis assay using TRITC dextran in a 384 well plate format and the identification of positive control siRNA, an siRNA screen targeting the kinome was performed. Two experimental repeats of the screen were performed in quick succession to reduce cell passage between screens. It is known the passage number of cells effects reproducibility in high-throughput assays and therefore we wanted cells of similar passage for each repeat (242).

The control siRNA included in the screen were two different non-targeting siRNA (NT2, NT4), Marcks and CTBP1. Due to technical issues, during the first repeat the control siRNA could not be included in each individual plate. Instead, an additional control plate was set up containing the control siRNA. The macropinocytosis assay was performed on the control plate simultaneously with the experimental plates. Ideally the control siRNA would be distributed throughout the experimental plates to control for inter plate variations in transfection and assay efficiency. The second screen was performed with control siRNA distributed in the experimental plates.

4.2.1 Identification of trends across screening plates from the first macropinocytosis screen

The siRNA screen targeting the Kinome was performed in four 384 well plates. Each well contains a unique siRNA sequence targeting a gene. To identify trends across the screening plates, heatmaps for each plate were created representing the average number of macropinosomes per cell for each well. The heatmaps allowed identification of systematic errors by highlighting regions of consistently High- or low values. During high-throughput screening variations between conditions in individual wells can lead to systematic errors.

During high-throughput screening systematic errors can occur across the plate. For example, it is known the outer wells in a 384 well plate experience increases temperature fluctuations and increased liquid evaporation during plate incubations (243,244). Hence no test conditions are placed in the first and last columns during the screens. Production of heat maps allows identification of these systematic errors. The heat maps from the first macropinocytosis

screen showed an area of lower values towards the right-hand side of the phosphatase plate (Figure4.05). This potentially indicates a shift in focus of the microscope overtime reducing the number of macropinosomes identified as the optimal section of the cells are not imaged. Any shift in focus was of increased importance in our high-throughput assay. The macropinocytosis dextran assay in a larger format utilised Z-stacks to acquire image sections throughout the cell to enable detection of macropinosomes. For high-content imaging it was not possible to acquire Z stacks and therefore a single focus plane was captured per well. This increased the importance of correct focus position for the high-throughput assay. The heat-maps allowed identification of potential focus errors.

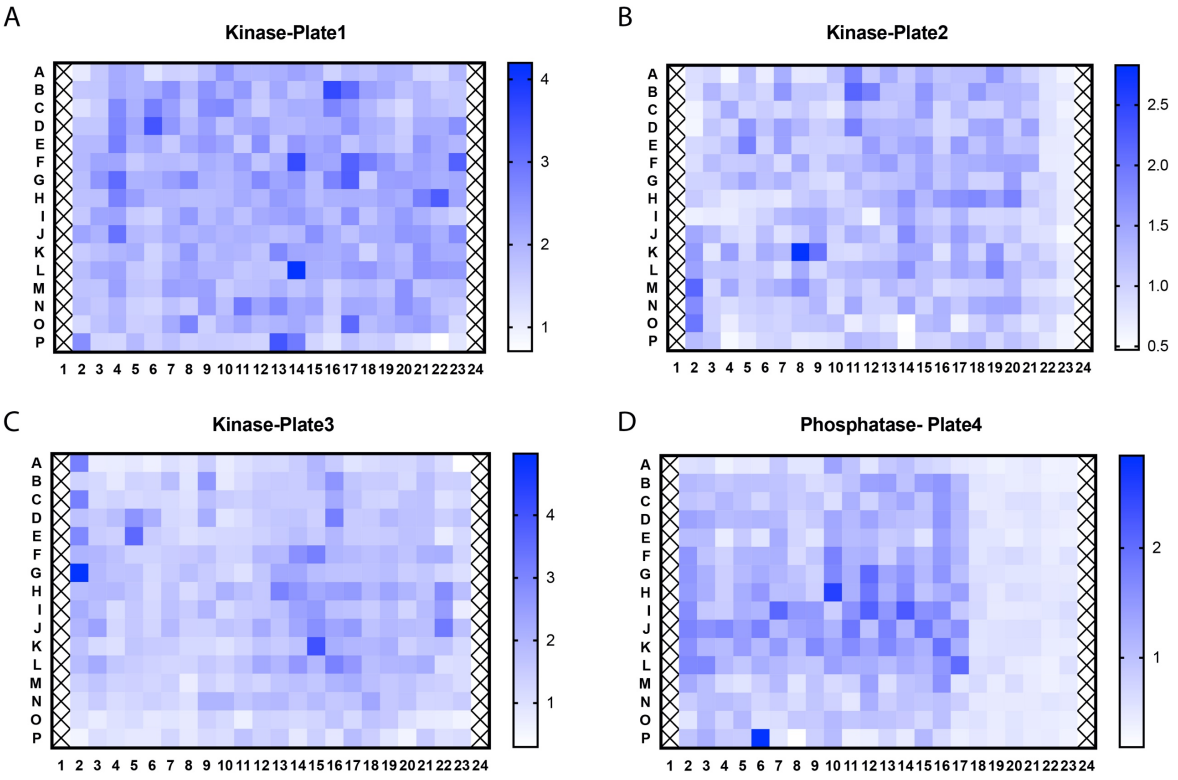

Figure4.05: ***Heatmaps from macropinocytosis screen 1****. The number of macropinosomes per cell was calculated for each image acquired from the first macropinocytosis screen. From each well, 9 images were acquired and an average number of macropinosomes per cell was calculated for each well. This averaged value of macropinosomes per cell was plotted and a heatmap was generated with a colour scale representing magnitude. A heatmap was generated for A) Kinase plate1 B) Kinase plate 2 C) Kinase plate 3 D) Phosphatase plate 4*

4.2.2 Controls from the first macropinocytosis screen

As mentioned previously, the controls for the first screen were placed in an additional plate rather than being included in each plate individually. Therefore, only one set of control data is available for the first screen rather than a set for each plate. The controls for the first screen did not show any decrease in macropinocytosis when compared to the non-targeting control (Figure4.06). This indicates the knockdown efficiency was low, however the non-targeting values were lower than expected in the control plate when compared to previous experiments which might explain the absence of an effect by the positive control siRNAs.

The cell death control, PLK1 siRNA, was included in the control plate. The PLK1 siRNA did not result in a significant decrease in the cell number in the control plate, again indicating a lack of transfection efficiency in the control plate (Figure4.07B). However, as PLK1 is a kinase it was included as an siRNA in the kinome screen. When the number of cells were compared between the non-targeting siRNA and the PLK1 siRNA in the 3rd Kinase plate, there is a significant decrease (Figure4.07A). This indicates a greater knock-down efficiency in the screening plates when compared to the control plate.

The late inclusion of the extra control plate disrupted the experimental procedure and could explain the lack of an effect from the positive controls included in the first macropinocytosis screen. The cell death control provides limited evidence for greater knockdown efficiency in the screening plates then the control plate. The positive controls used might not have as a robust effect on macropinocytosis as previously thought. For the repeat macropinocytosis screen the controls were inserted into the individual plates to monitor knockdown efficiency in each plate separately. It was decided to include alternative control siRNA as ctbp1 showed limited effect in the initial optimisation experiments and during the first macropinocytosis screen. As PMA activates PKC directly, using siRNA to silence the alpha subunit of PKC (PKCRA) was chosen as a positive control to be included in the second macropinocytosis screen.

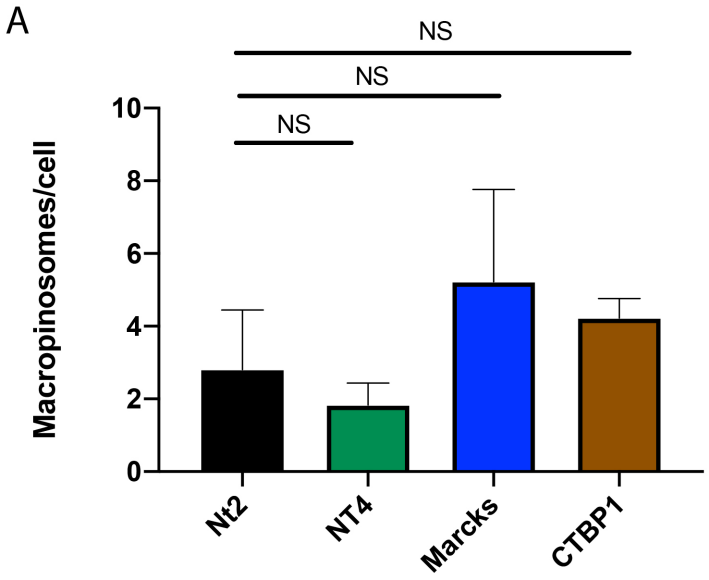

Figure4.06: ***Control results from macropinocytosis screen 1.*** *The control siRNA were manually transferred to the control plate in the first macropinocytosis screen. Two different non-targeting siRNA(NT2 and NT4) were included as well as the positive control siRNA targeting Marcks and CTBP1. A431 cells were reverse transfected with siRNA using Polyfect transfection reagent and a 70kDa macropinocytosis uptake experiment was performed at the same time as the macropinocytosis screen 1. Data shown is mean + SD from the control plate of the macropinocytosis screen 1. The average number of macropinosomes per cell was calculated per well from 9 images acquired. Number of replicate wells = 6 for each condition. A one-way ANOVA with Tukey's multiple comparison was performed with ****p≤0.0001, *** p≤0.001, ** p≤0.01 , * p≤0.05 , NS ≥ 0.05*

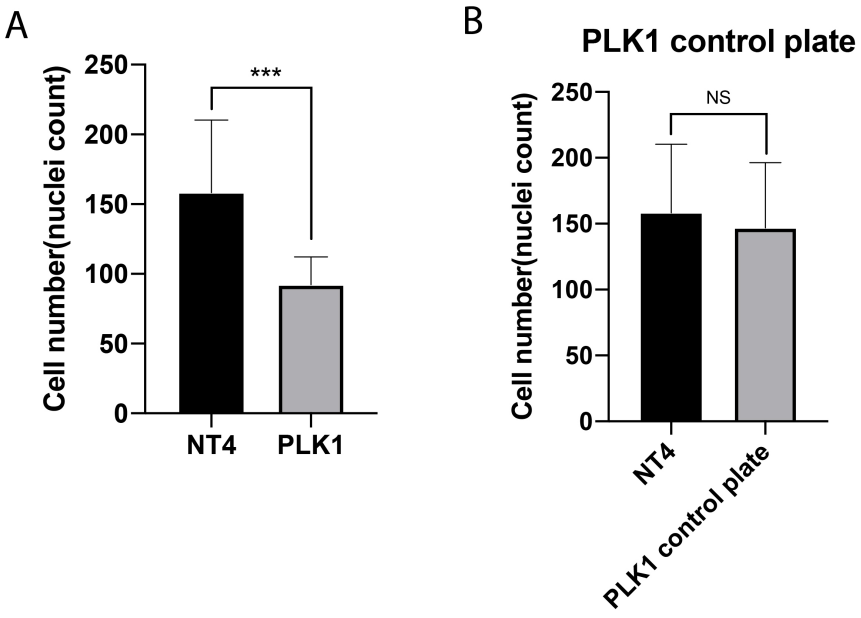

Figure4.07: ***The cell death controls from macropinocytosis screen 1****. The cell death control, PLK1 siRNA was manually transferred to the control plate in the first macropinocytosis screen. A431 cells were reverse transfected with the siRNA using Polyfect transfection reagent and a cell count was performed on the wells transfected with A) PLK1 siRNA from kinase-plate3 B) Non-targeting siRNA and PLK1 siRNA in the control plate. Cell count was performed on each image taken with 9 images taken per well. Data shown is Mean + SD from the first macropinocytosis screen with number of cells from each image plotted. A) Number of data points = 54 for NT4 and 9 for PLK1 B) Number of data points = 54 for NT4 and PLK1. An unpaired t test was performed for both data sets with ****p≤0.0001, *** p≤0.001, ** p≤0.01 , * p≤0.05*

4.2.3 Identification of trends across screening plates from the second macropinocytosis screen

As generated in the first screen, heatmaps were created from the second macropinocytosis screen for each plate (Figure4.08). The heatmaps helped identify some potential systematic errors from the second screen. There was a slight trend of decreasing values from left to right in plates 1 and 2 which could be due to a shift in focus. As the non-targeting control siRNA was distributed on both sides of the plate, the decreased values on the right of the plates will increase the variability in the non-targeting control data and so decrease the Z-scores for each siRNA hit. The phosphatase plate had a series of high well values in the start of row B that is not consistent with the previous screen result. As the addition of liquid is performed using an automated system by row, this increase could be due to a lack of liquid addition to these wells and subsequent dehydration of the cells which will increase background with the dextran assay.

To increase our confidence in the knockdown efficiency we included an additional control of a fluorescent siRNA that can be observed to determine if transfection has occurred. We included siGlow which is fluorescent in the red channel to confirm transfection. We could observe fluorescent signal from the siGlow inside the cell indicating successful transfection.

An additional control included to monitor knockdown-efficiency was the use of a fluorescent siRNA to monitor transfection. The fluorescent si-Glow siRNA was added to selected wells to monitor transfection in each plate. The si-glow siRNA is conjugated to DY-547, which has an emission wavelength in the red channel (557nm excitation) and was detected when the plates were imaged. If transfection is successful, the siRNA can be observed within cells by fluorescent microscopy. During automated image analysis the si-Glow produced punctate which were detected by the analysis software. The si-Glow siRNA was added to wells O9 and O17 which can be seen from the heatmaps to result in a high signal indicating transfection

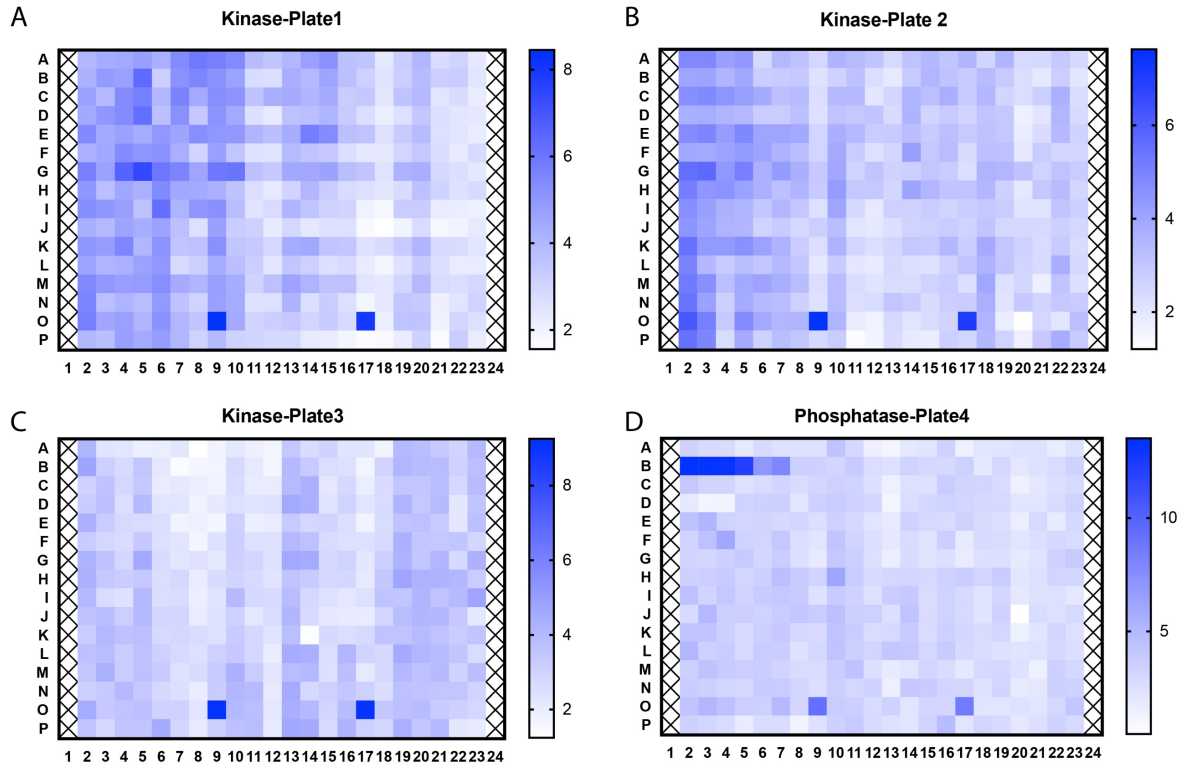

Figure4.08: ***Heatmaps from the macropinocytosis screen 2.*** *The number of macropinosomes per cell was calculated for each image acquired from the macropinocytosis screen 2. From each well 9 images were acquired and an average number of macropinosomes per cell was calculated for each well. This averaged value of macropinosomes per cell was plotted and a heatmap was generated with a colour scale representing magnitude. A heatmap was generated for A)Kinase plate1 B) Kinase plate 2 C) Kinase plate 3 D) Phosphatase plate 4*

4.2.4 Controls from the second PMA macropinocytosis screen

The positive control siRNA for the second PMA macropinocytosis screen were distributed throughout the plates to monitor transfection efficiency. The control siRNA included in the second PMA macropinocytosis screen were as follows; non-targeting siRNA (NT2), PRKCA and Marcks. After analysis of the number of macropinosomes formed per cell (Figure4.09) it can be seen that PRKCA, the alpha subunit of PKC, reduced the levels of macropinocytosis observed in plates 2,3 and 4. The knockdown of Marcks reduced macropinocytosis in plates 2 and 3 but not plates 4 and 1. The controls showed no effect in plate 1 of the second screen which indicates lower knockdown efficiency for the siRNA in the plate. The si-glow siRNA however did produce a signal indicating transfection of siRNA did occur but potential to a lower level.

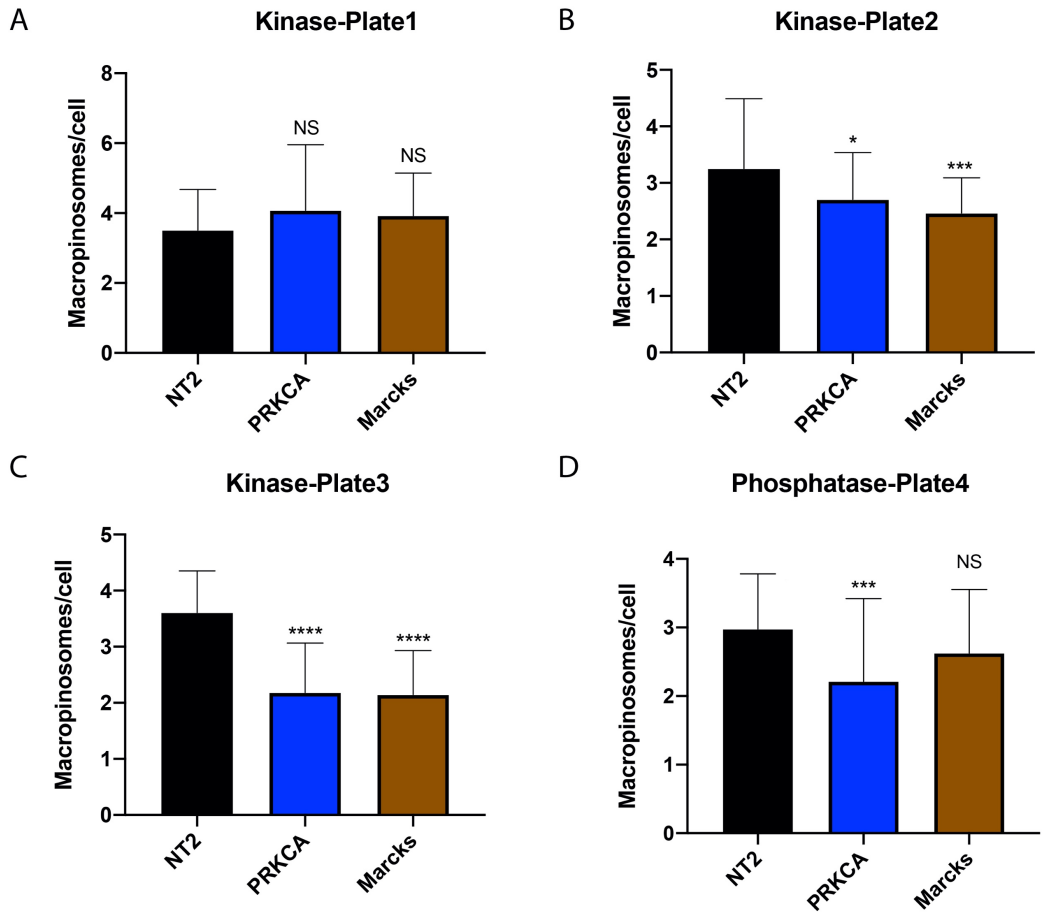

*Figure4.09: **The control siRNA from the second macropinocytosis screen.** The control siRNA was manually transferred to each of the 4 screening plates in the macropinocytosis screen 2. The control siRNA was placed in empty wells inside the screening plate as opposed to the controls in macropinocytosis screen 1 which were in a separate control plate. The siRNA included were non-targeting siRNA(NT2), Marcks and PRKCA. The Macropinocytosis screen was performed and the control wells analysed. Data shown is Mean + SD from the second macropinocytosis screen. The average number of macropinosomes per cell was calculated for each images acquired. Number of images analysed = 72 for NT2 , 36 for PRKCA and Marcks for each plate. A one-way ANOVA with Tukey's multiple comparison was performed for all data sets with ****p≤0.0001, *** p≤0.001, ** p≤0.01 , * p≤0.05*

As used in the first macropinocytosis screen, a cell death control was also included. Due to technical difficulties, the PLK1 siRNA was changed for ECT2 siRNA which is routinely used in the SRSF as a cell death control. To increase reproducibility the repeat screen was performed within a small-time frame of the first screen and it was not possible to optimise the ECT2 cell death control before the second screen was performed. The ECT2 siRNA was included in all plates. The cell count was compared between non-targeting and ECT2 siRNA transfection. The knockdown of ECT2 did decrease the number of cells in the first and fourth plates (Figure4.10).

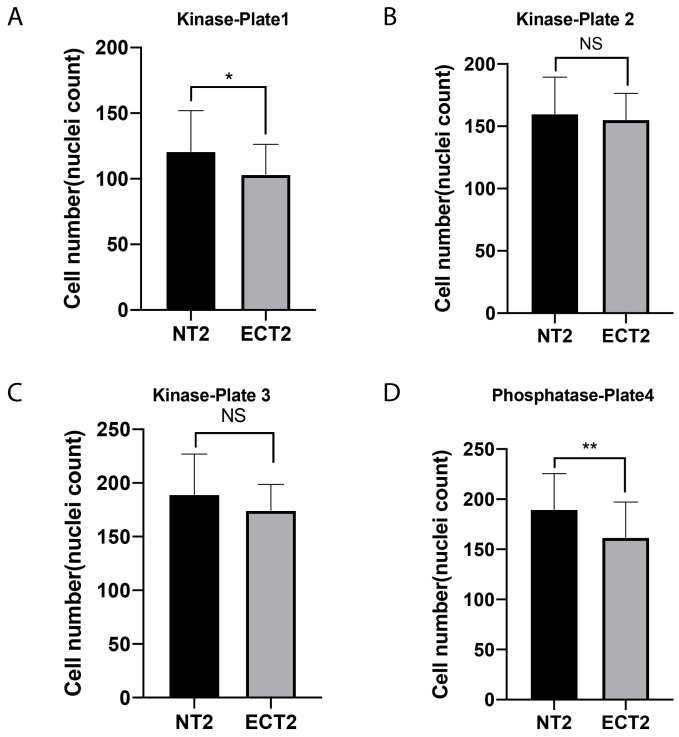

*Figure4.10**: The cell death controls from the second macropinocytosis screen.** The cell death control, ECT2 siRNA was manually transferred to each plate of the second macropinocytosis screen. A431 cells were reverse transfected with the siRNA using Polyfect transfection reagent and a cell count was performed on the wells transfected with the ECT2 siRNA and the Non-targeting siRNA for A) Kinase plate-1, B) Kinase-plate2, C)Kinase-plate3 and D) Phosphatase-plate4. Data shown is Mean + SD from the second macropinocytosis screen. A cell count was performed on each image acquired with 9 images acquired per well. Number of images NT2= 72, ECT2 = 18 . An unpaired t test was performed on all data sets with ****p≤0.0001, *** p≤0.001, ** p≤0.01 , * p≤0.05*

However, the ECT2 siRNA had no effect on cell number in plates 2 and 3 indicating lower knockdown efficiency. The effectiveness of ECT2 in A431 cells was unknown prior to the screen so as a comparison we looked at the plk1 siRNA condition that was included in plate3 of the kinome plates due to plk1 being a kinase. The cell number in the plk1 siRNA showed a significant decrease to the non-targeting control siRNA as well as being lower than the ECT2 siRNA with a decrease from an average of 174 cells with ECT2 silencing compared to 76 cells with plk1 silencing (Figure4.11). This indicates PLK1 is a more effective cell death control to use in the A431 cells.

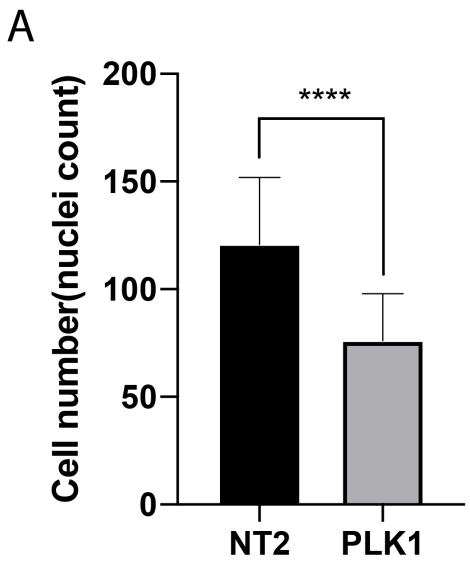

Figure4.11: ***The plk1 cell death controls from the second macropinocytosis screen****. The cell death control, plk1 siRNA was Included in the 3rd kinase plate of the second macropinocytosis screen. A431 cells were reverse transfected with the siRNA using Polyfect transfection reagent and a cell count was performed on plk1 siRNA. A cell count was performed on the non-targeting siRNA (NT2) from the 3rd kinase plate and the PLK1 siRNA from the 3rd Kinase plate. A cell count was performed on each image acquired with 9 images acquired per well. Number of images NT2= 72, PLK1 = 9. Data shown is Mean + SD and an unpaired t test was performed with ****p≤0.0001, *** p≤0.001, ** p≤0.01 , * p≤0.05*

4.2.5 Overview of the hits identified from the PMA screens

To compare the data between the two screens we performed a Z-score analysis. The Z score enables comparison between screens to account for variations in the non-targeting siRNA as well as giving an indication of the strength of the hits identified. To calculate the Z-score, the average number of macropinosomes per cell was calculated from each image set. Each well had 9 sites where images were captured, with a mean number calculated from the 9 sites. To calculate the z score for each siRNA condition, the average macropinosomes per cell of the non-targeting control was subtracted from the mean number of macropinosomes per cell of the different siRNA and divided by the standard deviation of the non-targeting control siRNA. To assess the variability between the two screens, we plotted the Z scores obtained for each plate (Figure4.12). As the data are from two replicates of the same screen, the distribution and magnitude of the Z scores should be the same. The distribution of Z score for kinase plate 1 was similar between the two repeats but the results from Screen 2 have a negative shift in the magnitude. As a larger number of macropinosomes were identified in the non-targeting control siRNA, this would explain the negative skew. Kinase-plate 2 had a similar distribution of Z scores with Screen 2 showing, overall, a higher value. This could be explained by the non-

targeting siRNA from the first screen being in a separate plate. Since Z scores for the first screen plates were calculated using the non-targeting siRNA from this control plate rather than internal plate controls, this may have affected the magnitude of Z scores identified. Kinase plate3 showed a similar distribution and magnitude between the repeats with some outlying results in the first screen having high positive Z scores. The phosphatase plate 4 shows a negative skew in magnitude in the first repeat with a distribution centred around 0 for the repeat screen.

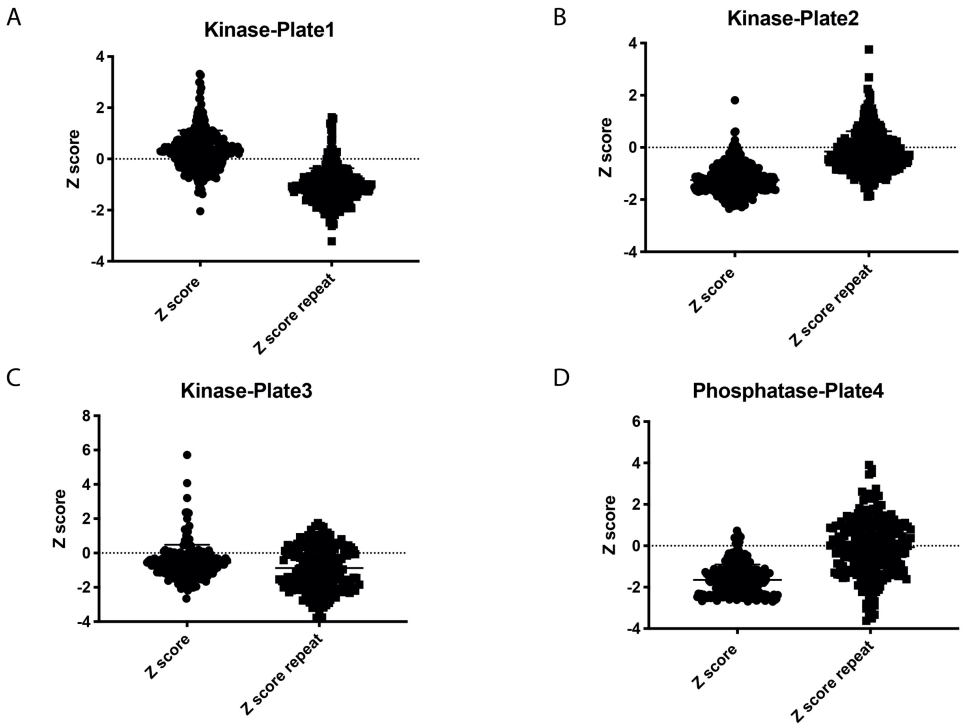

*Figure4.12: **A comparison of the distribution of Z scores from the macropinocytosis screens.** The Z scores from the two repeats of the macropinocytosis screen were plotted by plate to allow comparison. A) Kinase plate 1 B) Kinase plate 2 C) Kinase plate 3 D) Phosphatase plate 4.*

4.2.5.1 Distribution of combined Z scores

The Z scores from each screen were averaged to generate a single Z score identified for each siRNA. The Z scores were plotted by ascending order to visualise the distribution (Figure4.13). The data showed a trend with more siRNA having a negative Z score indicating more hits decreased macropinocytosis. There were some hits that increased macropinocytosis, but they were found to have more variable Z scores between the two screens. Due to membrane

availability, it is likely that there is an upper limit on the amount of macropinocytosis that can be performed in a cell. Additionally, we were observing the initial round of macropinocytosis as a short time point of 15 minutes was used. As PMA induces macropinocytosis to a high level, the ability to increase macropinocytosis beyond PMA induction is difficult which might explain the negative skew in Z scores.

Figure4.13: ***The Z score distributions from the macropinocytosis kinome screens.*** *The Z scores calculated from the first and second macropinocytosis Kinome screens were averaged for each siRNA and plotted in ascending order*

4.2.5.2 Identification of interesting hits for validation

From the initial macropinocytosis screen we needed to identify the siRNA to take forward for further validation. The siRNA to be further validated, termed hits, were selected based on the average Z score and the standard deviation between the two repeat screens (Table4.01). This enables selection based on the magnitude of the effect on macropinocytosis and on the reproducibility of the data. There were two siRNA with an average Z-score above positive 2 indicating they increased the amount of macropinocytosis. However, these hits had large variability between the two repeats as seen in the standard deviation, indicating low confidence in the effect seen and therefore were not taken forward. On the other hand, a larger number (36) hits were identified with a Z score lower than negative 2. As mentioned previously, PMA induces macropinocytosis to a high level and so increasing macropinocytosis to a greater level than PMA stimulation is less likely then identifying hits that decrease the

amount of macropinocytosis. Many of these hits had low standard deviation between screens indicating reproducibility. We did not directly observe cell viability in the screens and the different siRNA treatments will affect viability differently which may alter the amount of macropinocytosis. The cell viability analysis could be included in subsequent screens.

Routinely, a z score of ±3 is considered a significant cut off for hit selection during high throughput screening. The initial macropinocytosis screens had limitations which will have reduced the Z score achieved. There was variability in the non-targeting siRNA which directly effects the Z scores for all the siRNA. To improve future macropinocytosis screens, beyond this project, further optimisation of the assay and screening protocol would reduce the variation and improve the magnitude of the Z-scores. A source of variation in the assay was correct detection of the focus plane in the cell. Due to assay design and equipment limitations, a shift in the focus level during an experiment could result in variable data that contributed to the variability seen. Additionally, the positive control siRNA provided limited confirmation of successful knockdown of the targeted proteins. From the first macropinocytosis screen the inclusion of the positive control siRNA in a separate control plate limited our ability to detect knockdown efficiency in the individual plates. The cell death siRNA again showed limited knockdown efficiency in both macropinocytosis screens. The control data from the screens indicate that partial knockdown was achieved but the degree of silencing of target genes could be greater which would likely increase the effect on macropinocytosis observed. A selection of hits were taken forward for validation based on the Z-scores and standard deviation. As well as identifying hits for further validation based on the Z-score and standard deviation, manual selection of interesting siRNA occurred with selection of hits from interesting protein families.

Macropinocytosis Kinome screens -Decrease					Macropinocytosis Kinome screens -Increase				
Gene	Z score Screen 1	Z score Screen 2	Average	Standard deviation	Gene	Z score Screen 1	Z score Screen 2	Average	Standard deviation
FBXO42	-1.7867438	-3.7790484	-2.7828961	1.4087721	UHMK1	0.87738711	1.26275881	1.07007296	0.27249894
NT5M	-1.6882586	-3.6241763	-2.6562174	1.36890052	MAPK7	1.5148716	0.63510798	1.07498979	0.62208682
DUSP22	-2.2592114	-3.0300934	-2.6446524	0.54509587	ITPKC	1.80867892	0.36093141	1.08480517	1.02371208
NT5C	-2.3583071	-2.8825482	-2.6204277	0.37069439	DLG1	-0.3931907	2.6096854	1.10824735	2.12335405
KIAA0310	-2.5170804	-2.6774589	-2.5972696	0.11340476	PDGFRL	1.01685118	1.21874551	1.11779834	0.14276085
PON2	-2.2337162	-2.9374052	-2.5855607	0.49758325	EYA2	0.42863644	1.80958325	1.11910985	0.97647685
PPAP2B	-2.6966585	-2.3774827	-2.5370706	0.22569137	PDK2	0.32857352	1.9525902	1.14058186	1.1483532
FBXW10	-2.1861275	-2.7259699	-2.4560487	0.38172618	DUSP14	-1.4047946	3.70706008	1.15113274	3.61462711
PPP1CB	-1.3814369	-3.5020821	-2.4417595	1.49952261	EPHB4	0.80559822	1.56540586	1.18550204	0.53726513
PTPLB	-2.5659028	-2.2271941	-2.3965484	0.23950318	NT5C1B	0.72592532	1.67442183	1.20017358	0.67068831
MTMR4	-1.8949686	-2.8829278	-2.3889482	0.69859261	RPS6KL1	0.58424671	1.83910201	1.21167436	0.88731669
PTPNS1	-1.4101942	-3.2625165	-2.3363554	1.30978968	BUB1	1.11763077	1.34777206	1.23270142	0.16273447
INPP5D	-1.8518241	-2.7918092	-2.3218167	0.66466979	EPHB6	1.70250589	0.77172681	1.23711635	0.6581602
SOCS3	-1.2912545	-3.1557669	-2.2235107	1.3184093	TYRO3	2.99888115	-0.5193689	1.23975612	2.48777848
PPP2R3A	-2.2305054	-2.1843507	-2.207428	0.03263634	ALPL	-1.4082496	3.90062208	1.24618624	3.75393917
DUSP10	-2.4156764	-1.9820069	-2.1988417	0.30665064	LATS2	0.24387945	2.25404083	1.24896014	1.42139875
ASB13	-1.9897516	-2.3735992	-2.1816754	0.27142127	DGKG	1.20864639	1.30119416	1.25492028	0.06544116
NUDT12	-2.4479522	-1.9087827	-2.1783674	0.38125041	STK22D	0.87739865	1.6504951	1.26394687	0.54666174
PON1	-1.0140523	-3.3280617	-2.171057	1.63625178	PAPSS1	0.88759673	1.65107498	1.26933585	0.53986065
SPSB1	-1.1314345	-3.1939589	-2.1626967	1.45842503	LRRK2	0.90783156	1.64235489	1.27509322	0.51938643
FBP2	-2.3526922	-1.9622812	-2.1574867	0.2760623	P101-PI3K	1.27591493	1.302417	1.28916597	0.0187398
FBXO17	-1.5063941	-2.7822657	-2.1443299	0.90217745	IRAK1	1.12601498	1.49188841	1.3089517	0.25871158
FBXO40	-1.5592673	-2.7214719	-2.1403696	0.82180281	PAPSS2	1.83072644	0.92801195	1.37936919	0.63831554
INPP1	-2.3518203	-1.8996027	-2.1257115	0.31976612	FLJ32685	1.51038254	1.44540123	1.47789188	0.04594873
EYA3	-2.5539425	-1.69308	-2.1235113	0.60872168	KIAA2002	0.28559065	2.69227322	1.48893193	1.70178157
NUDT2	-2.4759874	-1.7514108	-2.1136991	0.51235302	MAST4	2.13720192	0.86054386	1.49887289	0.90273357
LL0XNC01-23	-1.9549169	-2.2693406	-2.1121288	0.22233117	PTPLA	-0.5130628	3.52000399	1.50347057	2.85180891
FBXL15	-2.0191365	-2.1946184	-2.1068774	0.12408443	CDKN2C	1.59246451	1.44317224	1.51781838	0.10556558
DUSP23	-2.6117059	-1.5381993	-2.0749526	0.75908379	PRKDC	2.00848179	1.0380029	1.52324234	0.6862322
PTPN23	-2.5083291	-1.611588	-2.0599586	0.63409167	MAP2K3	2.97006366	0.13991817	1.55499092	2.00121507
CILP	-2.4994813	-1.5650057	-2.0322435	0.66077408	RP6-213H19	2.3648116	0.80383986	1.58432573	1.1037737
MAP4K3	-1.0093264	-3.0338957	-2.021611	1.43158669	CDC2L2	3.26845513	0.02685732	1.64765622	2.2921558
PPP2R5B	-1.7838002	-2.2330075	-2.0084038	0.31763754	PIM2	0.31481773	3.07424955	1.69453364	1.95121295
FBXO5	-0.2621909	-3.7515673	-2.0068791	2.46736175	STK35	3.3226589	0.14890939	1.73578415	2.2441798
PTPN13	-2.1877066	-1.822755	-2.0052308	0.25805975	MST1R	4.07577568	0.61976133	2.3477685	2.44377118
FBXO43	-1.8907896	-2.1156576	-2.0032236	0.15900569	PRKCB1	5.71646187	0.92913887	3.32280037	3.38514856

Table4.01: ***The siRNA Z scores from the macropinocytosis kinome screens****. The Z scores calculated from the first and second macropinocytosis Kinome screens were averaged for each siRNA and the Z scores with the lowest values (Left) and the highest values (Right) were displayed in the table.*

4.2.6 Validation of identified hits using siGenome siRNA

To validate the hits identified as effectors of macropinocytosis, a secondary validation screen was performed using an alternative siRNA collection. The siGenome siRNA uses alternative sequences and is an unmodified siRNA, whereas the OTP siRNA uses a "dual-strand-modification pattern to decrease off-target effects(245). The use of a secondary siRNA sequence increases confidence the decrease in macropinocytosis is due to a decrease in the target protein levels and not in an off-target effect of the siRNA. As fewer siRNA were being tested in the validation screens, 4 experimental replicates for each siRNA were included in the validation screens with two biological replicates being performed. The validation screens were performed using the same experimental method as the initial screens to allow a direct comparison.

4.2.6.1 Macropinocytosis validation plate trends

As with the Kinome screens, heatmaps for the two validation screens were created to observe trends in the plates (Figure4.14). There are no obvious trends across the plate with an even spread of values observed. There were some wells showing high values that were not consistent between the repeats indicating they are false positive results, potential due to high background staining.

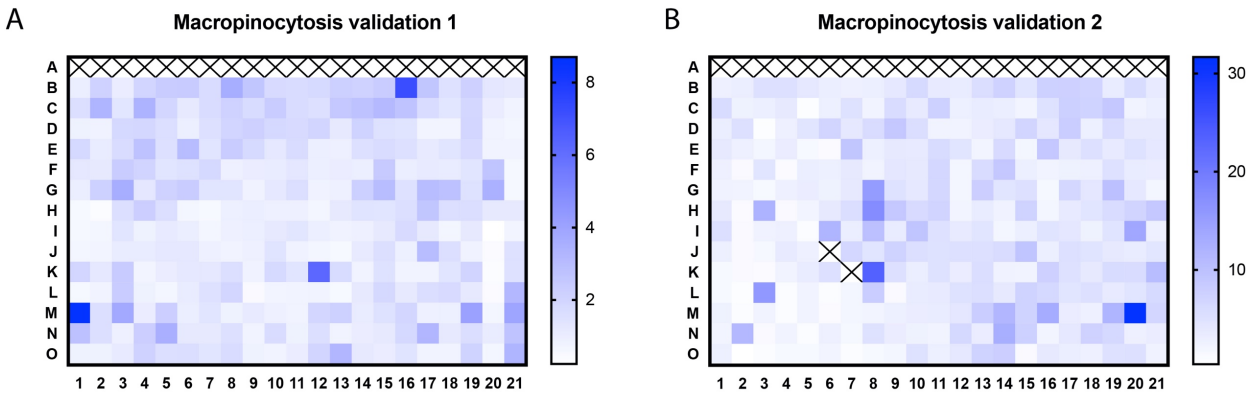

Figure4.14: Heatmaps from the validation macropinocytosis screens. *The number of macropinosomes per cell was calculated for each image acquired from the two validation macropinocytosis screens. From each well 9 images were acquired and an average number of macropinosomes per cell was calculated for each well. This averaged value of macropinosomes per cell was plotted and a heatmap was generated with a colour scale representing magnitude. A heatmap was generated for A) the First validation screen B) the Second validation screen*

4.2.6.2 Macropinocytosis validation controls

To verify the transfection efficiency in the macropinocytosis validation screen, positive control siRNA was included. In order to be comparable to the initial screen Marcks and ctbp1 siRNA were included as controls. Limited transfection efficiency was seen in the first validation screen with either Marcks or ctbp1 siRNA and only knockdown of Marcks showed reduction in the second validation screen (Figure4.15). These controls indicated that a low level of transfection efficiency was achieved during the validation screens. However, as previously discussed it is unknown how effective Marcks and Ctbp1 were as positive control siRNA.

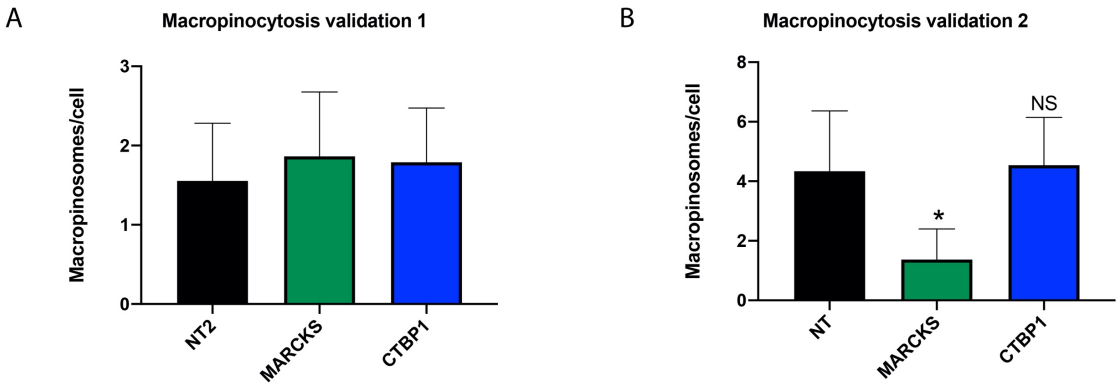

Figure4.15: ***The control siRNA from the validation macropinocytosis screen.*** *The Z-scores for the control siRNA from the validation macropinocytosis screens were calculated. A) The first validation screen B) The second validation screen*

4.2.6.3 The distribution of Z scores in the validation screen

The overall distribution of Z scores from the validation screens were lower than the original screen. The transfection protocol was not altered between the kinome screen and the validation screen. It is possible the siGenome siRNA had a lower transfection efficiency in the A431 cells than the OTP siRNA. A lower transfection efficiency would result in a decreased observed effect on macropinocytosis. Later experiments did show the siGenome siRNA to be less effective in the A431 cells than the On-Target plus siRNA (Chapter5, Figure5.10). The distribution of Z scores showed a greater number of siRNA with Z scores below zero as seen in the Kinome screens.

4.3 Identification of hits from the overall screen data

The macropinocytosis screens were performed to identify effectors of macropinocytosis after PMA stimulation. The screen would also act as a control for the endosomal release screen performed. Any effectors of endosomal release could be acting indirectly by affecting macropinocytosis and therefore, the macropinocytosis screens would allow identification of direct effectors of endosomal release.

The data from the initial macropinocytosis screen of the Kinome screen and the validation screens were collated. Due to technical difficulties when performing the screens, the Z scores achieved were not as strong as expected. However, we did observe hits that decreased macropinocytosis in all of the screens performed. To confirm the effects observed, further validation of the selected hits in a larger assay format is required to be confident in their ability to affect macropinocytosis. In order to identify the most effective hits, the average Z score from the 4 screens performed so far were averaged and sorted in ascending order (Table4.2). The top hits showed consistent reduction in macropinocytosis indicating a reproducible effect. The screen was performed as a control for the endosomal release however, we identified interesting proteins that have unknown function in macropinocytosis. Further validation and experimentation would identify if and how they are regulating macropinocytosis.

Macropinocytosis Kinome screens -Overall							Macropinocytosis Kinome screens -Overall						
Gene	Z score Screen 1	Z score Screen 2	Z score Validation 1	Z score Validation 2	Average	Standard deviation	Gene	Z score Screen 1	Z score Screen 2	Z score Validation 1	Z score Validation 2	Average	Standard deviation
FBXO42	-1.7867438	-3.7790484	-1.2749064	-0.1857986	-1.4052994	1.30294395	SPHK2	-0.8767406	-1.1421056	-1.1058534	-0.4273034	-0.7104006	0.28477969
KIAA0310	-2.5170804	-2.6774589	-1.0818742	-0.5047885	-1.3562404	0.92649447	FBXL15	-2.0191365	-2.1946184	0.5605126	0.26524156	-0.6776001	1.26571643
PON2	-2.2337162	-2.9374052	-1.1107303	-0.1442872	-1.2852278	1.06636799	PTPN23	-2.5083291	-1.611588	-0.3818835	1.29731966	-0.6408962	1.42746536
FBXO40	-1.5592673	-2.7214719	-1.4125	-0.7283637	-1.2843206	0.71661493	SSH2	-1.9419696	-0.9869103	-0.3986368	0.20802471	-0.6238984	0.792877
SOCS3	-1.2912545	-3.1557669	-1.4871611	-0.4249691	-1.2718303	0.9885276	AKT1	-0.4003101	0.24693267	-1.8164231	-1.0835368	-0.6106674	0.76875736
PPP1CB	-1.3814369	-3.5020821	-0.6194012	-0.6874394	-1.2380719	1.16715894	PON1	-1.0140523	-3.3280617	-0.3205414	1.65059468	-0.6024122	1.77928209
MTMR4	-1.8949686	-2.8829278	-0.642421	-0.5943552	-1.2029345	0.9518495	PIK3CB	-0.5800127	-0.2885812	-0.5219415	-1.4403087	-0.5661688	0.43680269
PTPNS1	-1.4101942	-3.2625165	-0.7021903	-0.6121798	-1.1974162	1.06527144	PIK3C2B	-0.9115822	0.27666541	-1.1411144	-0.9811786	-0.551442	0.56387674
SMG1	-1.5202461	-2.9014052	-0.9208661	-0.4734356	-1.1631906	0.91448193	CSNK2A1	-1.0293095	-1.857213	-0.0213215	0.21236565	-0.5390957	0.82732567
INPP5D	-1.8518241	-2.7918092	-0.4922616	-0.4177261	-1.1107242	0.99115982	PIK3R3	0.18327032	-0.7220154	-0.3023809	-1.7893612	-0.5260974	0.72771498
DUSP19	-2.5250832	-1.3978947	-1.2060792	-0.3331393	-1.0924393	0.78052326	SGPP2	-2.5779781	-2.520053	2.78323984	-0.1555496	-0.4940682	2.19326309
DUSP23	-2.6117059	-1.5381993	-0.4429075	-0.6533749	-1.0492375	0.8557905	EIF2AK3	-0.9065333	-1.3037479	-1.1387062	0.87920231	-0.493957	0.87553557
PTPN13	-2.1877066	-1.822755	-0.5519802	-0.5999146	-1.0324713	0.7263943	FGFR2	-1.1824256	-1.2379575	-0.6307535	0.58768403	-0.4926905	0.73429251
FBXO17	-1.5063941	-2.7822657	-0.4679755	-0.3803667	-1.0274004	0.97168774	SSH1	-1.3466211	1.03937397	-1.0496391	-0.9614409	-0.4636654	0.94553388
SPSB1	-1.1314345	-3.1939589	-0.629235	-0.1556042	-1.0220465	1.15899175	PIP5K1A	-0.9604734	-0.9145853	0.63207457	-0.9318118	-0.4349592	0.67903104
MAP2K4	-1.0325647	-1.377226	-0.8179325	-1.7428567	-0.994116	0.35101222	PIP5K2B	-1.1205866	-1.0651917	0.40033169	-0.1110442	-0.3792982	0.64493692
INPP1	-2.3518203	-1.8996027	-0.2066064	-0.2006555	-0.931737	0.97425119	IRAK3	-1.0434281	-1.1799927	-1.5202246	1.91663638	-0.3654018	1.38123245
PIK3R4	-1.6669235	-1.5566276	0.20793348	-1.6250503	-0.9281336	0.79085374	PIK3C3	-0.2695314	-0.9655426	-0.1888517	-0.3355385	-0.3518928	0.30791322
FBXW10	-2.1861275	-2.7259699	-1.0444772	1.3354885	-0.9242172	1.56092266	RAF1	-0.8857857	-0.8513324	-0.0731764	0.1868504	-0.3246888	0.47189998
PIK3C2A	-1.1362107	-0.6130724	-1.4117962	-1.1833899	-0.8688938	0.29232241	PIK3CD	-1.0523445	0.51309097	-0.310301	-0.6649326	-0.3028974	0.57786147
MAP4K2	-1.5263185	-1.3638783	-0.6044896	-0.8173224	-0.8624018	0.37910447	PAK1	0.21700597	0.45166883	-0.7169566	-1.4451304	-0.2986824	0.75762044
PPP2R5B	-1.7838002	-2.2330075	0.2474467	-0.5309529	-0.8600628	0.98592995	PIK3CA	0.51630651	0.74826943	-0.9379668	-1.6756504	-0.2698082	1.00735884
PIK3R1	-1.9797088	-0.8619578	-1.0245083	-0.2430706	-0.8218491	0.62238333	PIK3C2G	0.42321638	-0.7199218	0.67910412	-1.3251321	-0.1885467	0.82042222
PTPRO	-2.2243043	-1.667181	-0.7574025	0.79782721	-0.7702121	1.14340959	ASB13	-1.9897516	-2.3735992	-0.3443235	3.79203051	-0.1831288	2.44343702
MTMR3	-1.1875377	-1.9331132	-0.8989458	0.2036879	-0.7631818	0.76754067	AKT3	0.54210051	-0.2377151	-0.4287992	-0.2605225	-0.0769873	0.37585842
PPP2R3A	-2.2305054	-2.1843507	0.83169685	-0.1112443	-0.7388807	1.32650696	AKT2	0.09230987	0.66945778	-0.4390881	-0.4530023	-0.0260646	0.46110147
SSH3	-2.3677426	-0.5032218	0.21473252	-1.0217027	-0.7355869	0.94440762	KCNH2	-0.5866824	-1.1363978	-0.7885635	2.4136676	-0.0195952	1.42133918
PAK2	-1.4153217	-1.4698608	-0.8271557	0.04808198	-0.7328512	0.61103013	PIK3R2	0.07792585	0.18461149	0.23296895	-0.0711857	0.08486412	0.11670881
ARAF1	-2.0389846	-0.598154	0.01650201	-1.0421383	-0.732555	0.74959839	PIK3CG	-0.4773078	1.28874245	1.46650846	-1.8393647	0.08771569	1.35780167
DUSP4	-1.7492878	-2.1185661	0.58966161	-0.2812479	-0.7118881	1.09632658	DLG3	-1.4912967	-1.8849016	-0.886338	5.6188039	0.27125352	3.06893739

*Table 4-02: **Overall siRNA Z scores from the macropinocytosis screens (Sorted-Zscore)** A single average Z score and standard deviation was calculated for each siRNA from the macropinocytosis kinome screens and the validation screens. The Z-scores were sorted in ascending order of Z scores*

Macropinocytosis Kinome screens -Overall 1st							Macropinocytosis Kinome screens -Overall 2nd						
Gene	Z score Screen 1	Z score Screen 2	Z score Validation 1	Z score Validation 2	Average	Standard deviation	Gene	Z score Screen 1	Z score Screen 2	Z score Validation 1	Z score Validation 2	Average	Standard deviation
AKT1	-0.4003101	0.24693267	-1.8164231	-1.0835368	-0.6106674	0.76875736	PIK3C2G	0.42321638	-0.7199218	0.67910412	-1.3251321	-0.1885467	0.82042222
AKT2	0.09230987	0.66945778	-0.4390881	-0.4530023	-0.0260646	0.46110147	PIK3C3	-0.2695314	-0.9655426	-0.1888517	-0.3355385	-0.3518928	0.30791322
AKT3	0.54210051	-0.2377151	-0.4287992	-0.2605225	-0.0769873	0.37585842	PIK3CA	0.51630651	0.74826943	-0.9379668	-1.6756504	-0.2698082	1.00735884
ARAF1	-2.0389846	-0.598154	0.01650201	-1.0421383	-0.732555	0.74959839	PIK3CB	-0.5800127	-0.2885812	-0.5219415	-1.4403087	-0.5661688	0.43680269
ASB13	-1.9897516	-2.3735992	-0.3443235	3.79203051	-0.1831288	2.44343702	PIK3CD	-1.0523445	0.51309097	-0.310301	-0.6649326	-0.3028974	0.57786147
CSNK2A1	-1.0293095	-1.857213	-0.0213215	0.21236565	-0.5390957	0.82732567	PIK3CG	-0.4773078	1.28874245	1.46650846	-1.8393647	0.08771569	1.35780167
DLG3	-1.4912967	-1.8849016	-0.886338	5.6188039	0.27125352	3.06893739	PIK3R1	-1.9797088	-0.8619578	-1.0245083	-0.2430706	-0.8218491	0.62238333
DUSP19	-2.5250832	-1.3978947	-1.2060792	-0.3331393	-1.0924393	0.78052326	PIK3R2	0.07792585	0.18461149	0.23296895	-0.0711857	0.08486412	0.11670881
DUSP23	-2.6117059	-1.5381993	-0.4429075	-0.6533749	-1.0492375	0.8557905	PIK3R3	0.18327032	-0.7220154	-0.3023809	-1.7893612	-0.5260974	0.72771498
DUSP4	-1.7492878	-2.1185661	0.58966161	-0.2812479	-0.7118881	1.09632658	PIK3R4	-1.6669235	-1.5566276	0.20793348	-1.6250503	-0.9281336	0.79085374
EIF2AK3	-0.9065333	-1.3037479	-1.1387062	0.87920231	-0.493957	0.87553557	PIP5K1A	-0.9604734	-0.9145853	0.63207457	-0.9318118	-0.4349592	0.67903104
FBXL15	-2.0191365	-2.1946184	0.5605126	0.26524156	-0.6776001	1.26571643	PIP5K2B	-1.1205866	-1.0651917	0.40033169	-0.1110442	-0.3792982	0.64493692
FBXO17	-1.5063941	-2.7822657	-0.4679755	-0.3803667	-1.0274004	0.97168774	PON1	-1.0140523	-3.3280617	-0.3205414	1.65059468	-0.6024122	1.77928209
FBXO40	-1.5592673	-2.7214719	-1.4125	-0.7283637	-1.2843206	0.71661493	PON2	-2.2337162	-2.9374052	-1.1107303	-0.1442872	-1.2852278	1.06636799
FBXO42	-1.7867438	-3.7790484	-1.2749064	-0.1857986	-1.4052994	1.30294395	PPP1CB	-1.3814369	-3.5020821	-0.6194012	-0.6874394	-1.2380719	1.16715894
FBXW10	-2.1861275	-2.7259699	-1.0444772	1.3354885	-0.9242172	1.56092266	PPP2R3A	-2.2305054	-2.1843507	0.83169685	-0.1112443	-0.7388807	1.32650696
FGFR2	-1.1824256	-1.2379575	-0.6307535	0.58768403	-0.4926905	0.73429251	PPP2R5B	-1.7838002	-2.2330075	0.2474467	-0.5309529	-0.8600628	0.98592995
INPP1	-2.3518203	-1.8996027	-0.2066064	-0.2006555	-0.931737	0.97425119	PTPN13	-2.1877066	-1.822755	-0.5519802	-0.5999146	-1.0324713	0.7263943
INPP5D	-1.8518241	-2.7918092	-0.4922616	-0.4177261	-1.1107242	0.99115982	PTPN23	-2.5083291	-1.611588	-0.3818835	1.29731966	-0.6408962	1.42746536
IRAK3	-1.0434281	-1.1799927	-1.5202246	1.91663638	-0.3654018	1.38123245	PTPNS1	-1.4101942	-3.2625165	-0.7021903	-0.6121798	-1.1974162	1.06527144
KCNH2	-0.5866824	-1.1363978	-0.7885635	2.4136676	-0.0195952	1.42133918	PTPRO	-2.2243043	-1.667181	-0.7574025	0.79782721	-0.7702121	1.14340959
KIAA0310	-2.5170804	-2.6774589	-1.0818742	-0.5047885	-1.3562404	0.92649447	RAF1	-0.8857857	-0.8513324	-0.0731764	0.1868504	-0.3246888	0.47189998
MAP2K4	-1.0325647	-1.377226	-0.8179325	-1.7428567	-0.994116	0.35101222	SOCS3	-1.2912545	-3.1557669	-1.4871611	-0.4249691	-1.2718303	0.9885276
MAP4K2	-1.5263185	-1.3638783	-0.6044896	-0.8173224	-0.8624018	0.37910447	SPHK2	-0.8767406	-1.1421056	-1.1058534	-0.4273034	-0.7104006	0.28477969
MTMR3	-1.1875377	-1.9331132	-0.8989458	0.2036879	-0.7631818	0.76754067	SPSB1	-1.1314345	-3.1939589	-0.629235	-0.1556042	-1.0220465	1.15899175
MTMR4	-1.8949686	-2.8829278	-0.642421	-0.5943552	-1.2029345	0.9518495	SSH1	-1.3466211	1.03937397	-1.0496391	-0.9614409	-0.4636654	0.94553388
PAK1	0.21700597	0.45166883	-0.7169566	-1.4451304	-0.2986824	0.75762044	SSH2	-1.9419696	-0.9869103	-0.3986368	0.20802471	-0.6238984	0.792877
PAK2	-1.4153217	-1.4698608	-0.8271557	0.04808198	-0.7328512	0.61103013	SSH3	-2.3677426	-0.5032218	0.21473252	-1.0217027	-0.7355869	0.94440762
PIK3C2A	-1.1362107	-0.6130724	-1.4117962	-1.1833899	-0.8688938	0.29232241	SMG1	-1.5202461	-2.9014052	-0.9208661	-0.4734356	-1.1631906	0.91448193
PIK3C2B	-0.9115822	0.27666541	-1.1411144	-0.9811786	-0.551442	0.56387674	SGPP2	-2.5779781	-2.520053	2.78323984	-0.1555496	-0.4940682	2.19326309

*Table 4-3: **Overall siRNA Z scores from the macropinocytosis screens (Sorted-Alphabetical)** A single average Z score and standard deviation was calculated for each siRNA from the macropinocytosis kinome screens and the validation screens. The Z-scores were sorted in alphabetical order of the siRNA*

4.3.1 String network interaction of top hits identified

To aid identification of pathways involved in macropinocytosis, a String network interaction analysis was performed on the top 30 hits from the collated data (Figure4.16). The String analysis compares a list of proteins to a database of known protein-protein interactions. Based on interaction criteria, using experimental data or theoretical interaction, proteins are clustered to highlight interactions and therefore potential pathways. From the string interaction, both MTMR3 and MTMR4 were highlighted as they are from a known family involved in macropinocytosis (116), indicating known effectors of macropinocytosis were identified during our macropinocytosis screen. A collection of proteins that interact were identified from the F-box protein family (FBXO40, FBXO17, FBXO42). The FBXO family are E3 ubiquitin ligases and were included in the original kinome screen due to extra space in the plates and because ubiquitination is an important post-translational modification in cells. We were interested in this group of interacting proteins for further validation as their function in macropinocytosis was unknown.

Using the String network statistical analysis, we calculated the PPI enrichment p value. The PPI enrichment value, a statistical test, is used to determine whether a list of proteins has been statistically enriched, or the number of interactions is expected from a group of proteins. With the top 30 proteins we achieved a p value of 0.0543 and was not a significant enrichment. However, the top 20 proteins had a p value of 0.0471 indicating a significant enrichment. The p values show our positive hits are on the border of statistical enrichment, but this value is only calculated from known interactions. As many of our top hits have limited information in the literature the p value is likely to be more significant as they have other unknown interactions.

The macropinocytosis screen did identify some interesting proteins that could be involved in the regulation of macropinocytosis. There are some limitations on the reliability of the data produced during the screens, due to errors made during the screening. However, the screens main function was to help identify interesting hits for further validation as well as acting as a control screen for the endosomal release screen to aid identification of direct effectors of endosomal release.

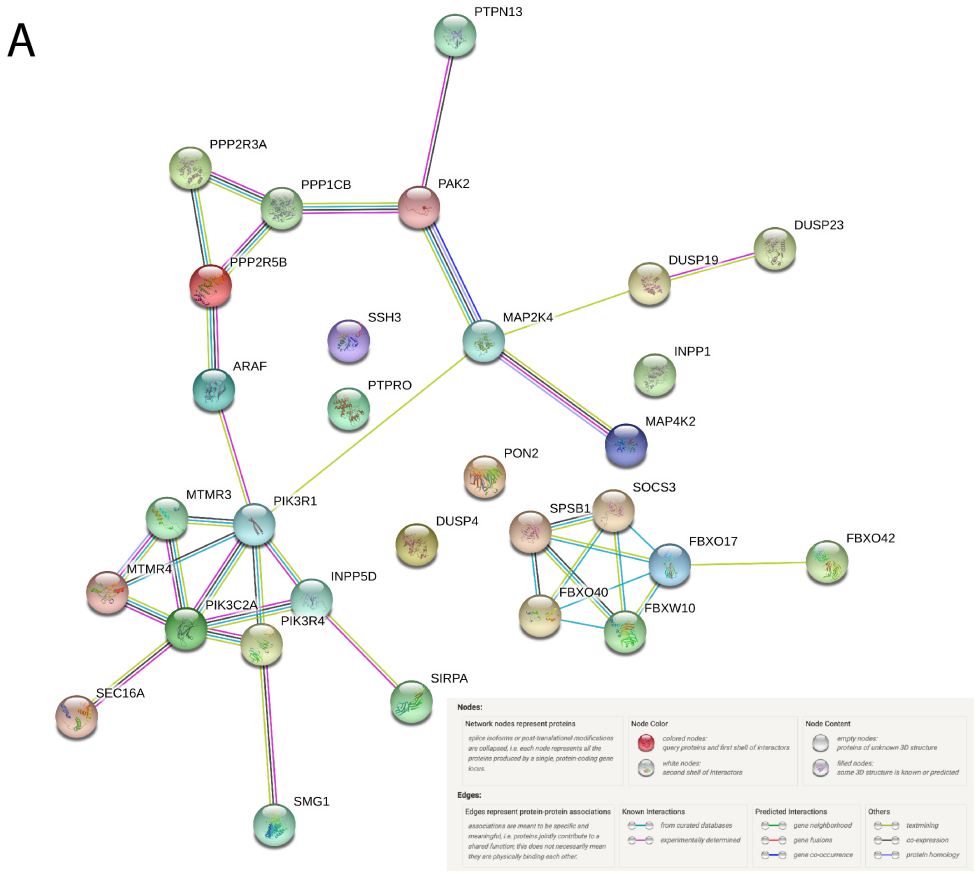

Figure4.16: ***A string network interaction diagram for the top 30 hits that decrease macropinocytosis.*** *The top 30 hits that decrease macropinocytosis, based on the average Z score from the macropinocytosis kinome screens and validation screens, were used to create a String network diagram using the String database (See methods)*

Chapter5: EGF induced endosomal release screen

The next step was to perform a Kinome siRNA interference screen using the previously optimised HRP release assay to identify regulators of endosomal release. Our previous data showed EGF stimulation of A431 cells resulted in endosomal release (Figure3.20). The EGF ligand effects multiple cellular pathways including cell growth, proliferation and cell survival. The binding of the EGF ligand to its cell surface receptors triggers a cascade of signalling throughout the cell via a series of complex signalling pathways. We wanted to identify the signalling proteins involved in the EGF signalling responsible for increasing the cytosolic release of HRP and therefore endosomal permeability.

5.1 Optimisation of the HRP release assay for high-throughput screening

The HRP assay required optimisation for a high-throughput format. The HRP-release assay was developed in a larger plate format and required further optimisation to ensure optimal conditions for the high-content Kinome screen.

5.1.1 EGFR knockdown decreases EGF dependent endosomal release

We initially identified a positive control siRNA to use in the endosomal release kinome screen. The positive control siRNA monitors the transfection efficiency in each plate to confirm successful knockdown occurred. A prominent cell surface receptor of the EGF pathway is the epidermal growth factor receptor (EGFR). We investigated whether silencing of EGFR using siRNA decreased the number of cells with endosomal release after EGF stimulation. A431 cells were reverse transfected with EGFR siRNA using Polyfect transfection reagent. After 3 days to allow sufficient silencing, a HRP release assay was performed with EGF stimulation. The number of cells showing cytosolic staining were identified. The knockdown of the EGFR

reduced the percentage of cells showing cytosolic release (Figure5.01). Hence EGFR siRNA was used as a positive control siRNA during the EGF dependent endosomal release screens.

5.1.2 High-throughput image acquisition and analysis of DAB staining

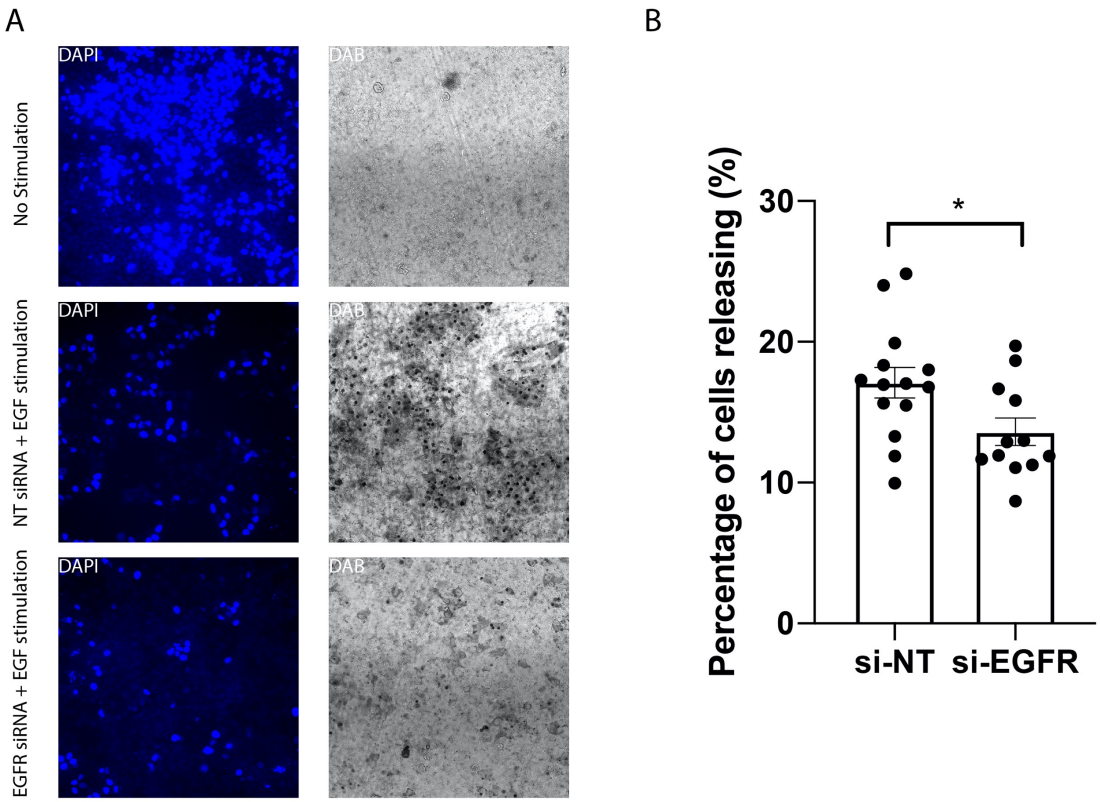

*Figure5.01: **Identification of EGFR siRNA as a positive control for EGF stimulated HRP release.** A431 cells were reverse transfected with EGFR siRNA or Non-targeting(NT) siRNA in a 384 well plate using Polyfect transfection reagent for 3 days. Cells, serum starved for at least 2 hours, were stimulated with EGF (100ng/ml) in the presence of 10mg/ml HRP for 10 minutes. Cells were washed and incubated in fresh serum-free media for 90 minutes. Cells were washed and fixed in PFA before DAB staining to locate intracellular HRP. B) The number of cells showing cytosolic staining was quantitated by automated image analysis. Data shown is mean + SEM from 3 independent repeats. An unpaired two-tailed T test was performed, with ****p≤0.0001, *** p≤0.001, ** p≤0.01, * p≤0.05*

Endosomal release is detected in the HRP uptake screens by using the HRP substrate DAB which is converted into an insoluble brown precipitate by HRP. HRP that has escaped from the endosomal system produces DAB staining that is cytosolic whereas endosomal HRP results in DAB puncta. The two staining types can be distinguished using brightfield microscopy and image analysis. As brightfield images were required to observe DAB staining, an alternative high-content automated plate microscope was required to acquire brightfield images. An Incell analyser 2000 was utilized to acquire brightfield images of the DAB stain and images were analysed using the ImageXpress MetaXpress image analysis software.

The high-throughput image analysis had to be optimised extensively to positively identify the cells showing cytosolic release. The full custom module used for analysis is located in the

appendix (Section8.1) but briefly, nuclei were detected using a nuclei stain (initially DAPI for some pre-screen experiments but Draq5 was used after optimisation of nuclei detection (Figure3.23). After the nuclei were detected, a cell mask was created and the DAB signal for each cell measured. Cells showing endosomal release had a greater DAB staining area increasing the DAB signal detected. The cells were filtered based on the DAB signal detected in the cell mask to identify endosomal releasing cells. Using the filtered cells, a percentage of cells showing endosomal release could be calculated.

5.1.3 Observations about the HRP release assay in a screening format

The HRP release assay had not previously been performed in a high-throughput format. From the initial experiments performed there were some observations made about the HRP assay in a 384 well plate.

Stronger DAB staining was observed towards the periphery of the wells in the 384 well plate. It was unknown if peripheral cells had an increased uptake of HRP or the DAB staining reaction was more efficient. However, nine images were acquired from fixed sites across each well to reduce the impact on analysis and allow valid comparison between wells.

The quality of DAB staining between experiments had variation due to the use of different DAB preparations for each independent experiment. The DAB solution was freshly prepared before each experiment due to the low stability of DAB in solution. To control for the variability between DAB preparations, the same DAB solution was used during a screen to stain all plates simultaneously. However, it was also noted the quality of the DAB stain decreased overtime after staining with an accumulation of background staining. Therefore, imaging had to occur as soon as possible post DAB staining. As the Kinome is composed of four 384 well plates the last plate to be imaged had the longest time since staining and therefore the highest background. During the first Kinome screen using the HRP release assay the plates were stained simultaneously to enable the use of a single DAB preparation to reduce variability. However, upon completion of the initial screen, we decided to perform the repeat Kinome screen separated over two days with 2 plates performed on each day. This decreased the complexity of the screening assay and enabled fast acquisition of images from both plates after staining to aid the reduction of the background observed.

5.2 The Kinome endosomal release screen

The kinome screens were performed using the HRP uptake assay. The siRNA was reverse transfected using Polyfect transfection reagent. The transfection agent Polyfect was selected as it had previously been used in the macropinocytosis kinome screens. A431 cells were reverse transfected and incubated at 37°C for 3 days to allow sufficient time for knockdown to occur. A HRP uptake assay was performed with EGF stimulation on all conditions apart from the non-stimulation control cells that were un-transfected and unstimulated with EGF to monitor non-specific DAB staining. The plates were imaged and analysed to calculate the number of cells with cytosolic HRP staining for each siRNA condition.

5.2.1 Control siRNA from the first endosomal release screen

The control siRNA included in the first endosomal release screen were EGFR and PI3K siRNA. The knockdown of EGFR was shown earlier to decrease the number of cells with endosomal release (Figure5.01). The PI3K siRNA was additionally included as a control as a decrease in macropinocytosis was thought to decrease the amount of endosomal release. The kinase plate 1 showed a significant reduction with both si-EGFR and si-PI3K (Figure5.02). The phosphatase plate did show reductions with the si-EGFR and si-PI3K but due to a high variation in the non-targeting controls they were not significantly different. The positive controls did not have an effect in the kinase plate 2 and kinase plate 3 indicating lower transfection efficiency.

There was a good separation of signal between unstimulated (NS) and EGF stimulated un-transfected control cells in all of the plates apart from kinase 3 indicating the assay was functional and a separation of signal could be detected. The controls indicate kinase plate 1 and the phosphatase plates have the most reliable knockdown followed by Kinase plate 2. The kinase plate-3 controls indicate less successful transfection and the separation between the unstimulated (NS) and EGF stimulated un-transfected control cells indicate the assay was less successful. This could have been due to the degradation of the DAB signal overtime as

kinase-plate3 was imaged later than kinase-1 and kinase-2 and so a larger amount of time occurred between imaging and staining.

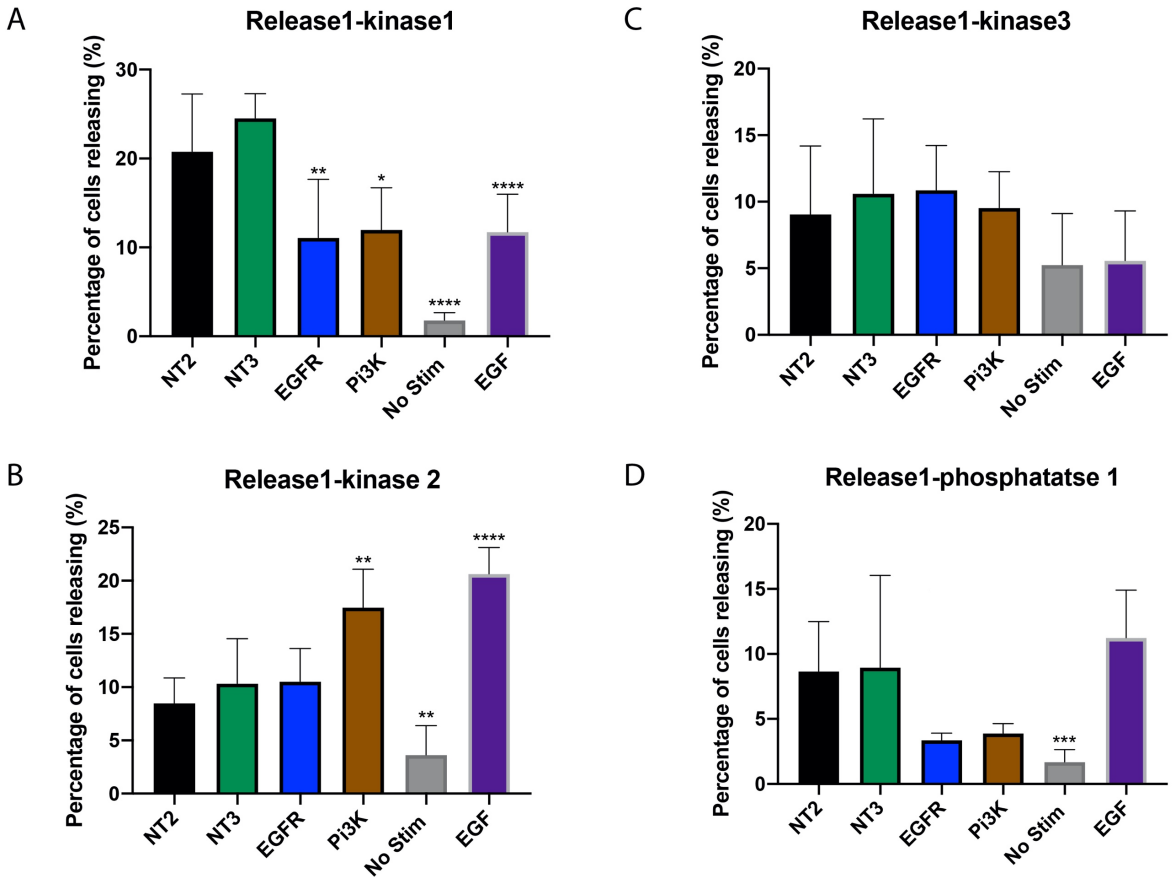

*Figure5.02: **Release screen 1 control siRNA**. Control siRNA that was previously observed to decrease the delivery of HRP to the cytosol was included in each plate of the HRP release screen. See material and methods (release screen 1) for details on performing the screen. The average percentage of cells releasing for each well was calculated and the data for the controls were compared. The control siRNA included in the release screen-1 were two different non-targeting siRNA (NT2 and 3), siRNA for EGFR and siRNA for PI3K. Data for NT2,NT3, EGFR and PI3K siRNA are with 100ng/ml EGF stimulation. A No stimulation control without transfection were included (No stim) in the comparison. A) Controls from the first kinase plate B) Controls form the second kinase plate C) Controls from the third kinase plate D) Controls from the first phosphatase plate. All data shown is mean + SD. A One-way ANOVA with Tukey's multiple comparisons test was performed, *'s above bars indicate significance to NT2 from the respective plate. ****p≤0.0001, *** p≤0.001, ** p≤0.01, * p≤0.05*

5.2.2 Trends identified from the first endosomal release screen

Heatmaps were generated from the first endosomal release screen to identify intraplate trends(Figure5.03). The average percentage of cells releasing was calculated for each well and plotted with a colour scale. Plate areas of high or low signal could indicate high background staining or poor DAB staining respectively. Kinase plate 1 showed mostly consistent staining apart from column 5 which showed a trend of lower values which could indicate less effective

staining. Kinase 3 also had a column with low values (column 16) indicating less effective staining.

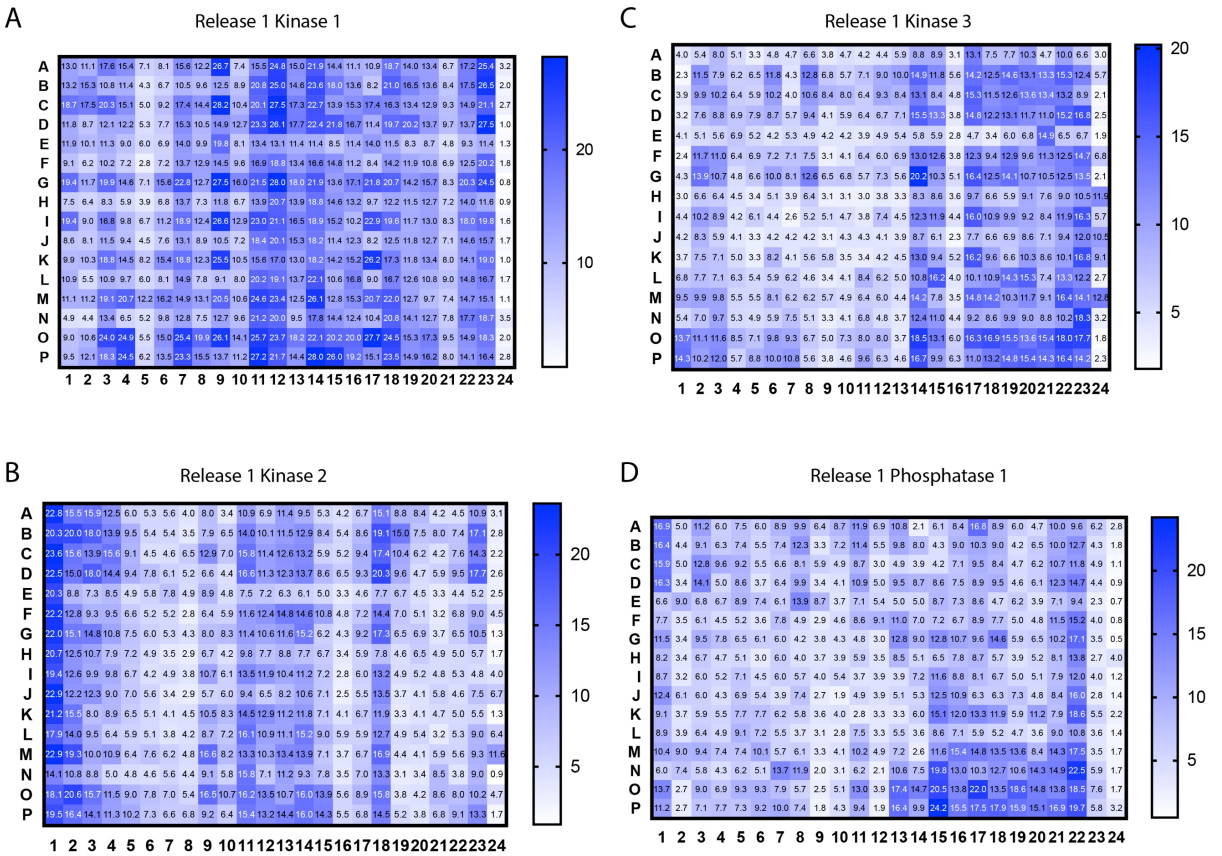

Figure5.03: ***The first HRP Release screen heat maps.*** *The average percentage of cells releasing for each image was calculated from the first release screen. The percentage of cells releasing from each field of view were averaged to get a single value per well and plotted on to a 384 well plate map. A colour scale was mapped to the values to identify any trends in the plates. Each colour scale is unique to each plate heatmap with individual keys located to the right of the heat maps.*

5.2.3 The distribution of Z scores from the first endosomal release screen

To enable comparison between the plates a Z score was calculated for each well from the average percentage of cells releasing (Figure5.04). From each well, nine images were acquired and the percentage of cells releasing was calculated for each image. The mean and standard deviation was calculated from the non-targeting siRNA conditions in each plate and the Z score was calculated as the number of non-targeting siRNA standard deviations away from the mean of the non-targeting siRNA. The Z scores were sorted in ascending order and plotted to see the distribution (Table5.01). A similar number of siRNA had a Z score greater than zero as less than zero. However, the positive Z scores were of higher magnitude with the highest being over 5 indicating a stronger effect on release.

A

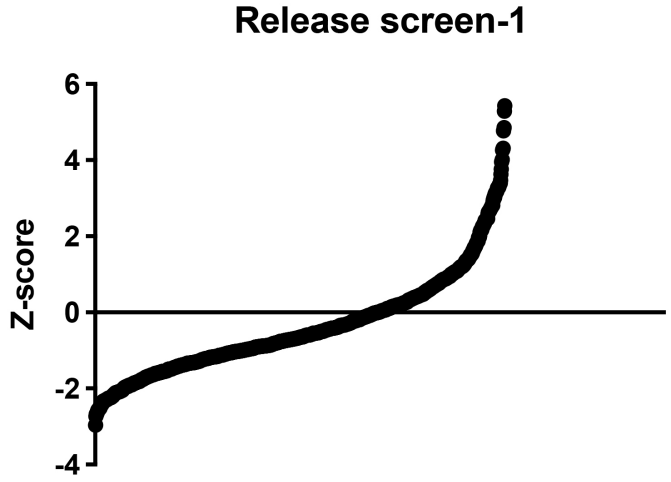

Figure5.04: ***The first HRP Release screen distribution of z-scores****. The Z-score was calculated for each hit (see material and methods for Z score calculation) and the Z scores from all 4 plates were collated. The z scores for each siRNA plotted in ascending order to observe the distribution of hits identified from the HRP release screen-1*

A431- HRP release screen 1 increase			A431- HRP release screen 1 decrease		
Gene	Percentage of cells releasing-HRP %	Non targeting 2 Z score	Gene	Percentage of cells releasing-HRP %	Non targeting 2 Z score
DGKI	15.10569478	2.969583693	RELA	2.817581743	-2.965365211
PIK3C3	15.21350027	3.017909448	LATS2	4.257416924	-2.727636472
ARK5	15.22223538	3.021825119	PDK4	2.501971356	-2.680262861
PTEN	19.76844194	3.091951905	PIP5K2A	4.54688653	-2.679842638
CSNK2A1	15.38756165	3.095935605	CKB	4.807762766	-2.636769806
CRK7	15.48192506	3.138235705	LYN	5.01728036	-2.602176713
GRK4	15.49625731	3.144660395	STK22C	5.170474639	-2.576883066
LRRK1	15.5550648	3.171021914	MAK	2.76137277	-2.563981495
MAPKAPK3	15.58748229	3.185553638	MPP2	5.290719409	-2.557029656
NUCKS	15.6626403	3.219244575	GRK7	2.808763338	-2.542737817
SGKL	15.75488897	3.260596704	STK32A	2.862489264	-2.518654201
ACVR2B	15.79753455	3.279713356	PIP5KL1	5.532345517	-2.51713518
CDK9	15.80347794	3.282377591	PAK7	2.873698345	-2.513629528
NUDT3	20.4829923	3.290728018	EPHB6	5.851901647	-2.464373811
MAP3K11	15.89675355	3.324190064	CARKL	5.971845613	-2.444570067
GCK	15.95822789	3.351747049	EFNA4	6.048230612	-2.431958269
MARK4	15.98658078	3.364456744	STK32C	3.056413652	-2.431724093
IRAK3	16.06257659	3.398523236	AKT2	6.20698418	-2.405746738
OSR1	16.22013952	3.469153664	SLK	3.161093467	-2.384799476
MAPK13	16.57535485	3.62838535	PRKCD	3.167330441	-2.38200364
FGFRL1	16.86555975	3.758474934	DCK	3.262982805	-2.339125741
DGUOK	17.29634236	3.951581015	CAMK2B	6.662817717	-2.330484838
CSNK1A1L	17.43050329	4.011721075	AKT3	6.663425803	-2.330384438
MAP2K6	17.99581142	4.265130647	PCTK1	3.291215926	-2.326469735
ALK	18.04194734	4.285811908	PINK1	6.699260108	-2.324467896
PPP4R1	24.16204087	4.314178601	GRK5	6.730465979	-2.319315548
BMPR1A	19.12458571	4.771124101	PRKY	3.332402594	-2.308007068
RPS6KL1	19.31076731	4.854583363	MARK1	6.801656084	-2.307561471
CLK4	20.27264796	5.285763729	PNCK	3.353337024	-2.298622831
KIAA2002	20.58708527	5.426715929	CDC42BPB	6.895773753	-2.292021863

Table5.01: ***The first siRNA HRP release screen data.*** *The values for percentage of cells releasing and the z-scores from the first siRNA HRP release screen with gene identifiers plotted in a table. The table shows the top hits identified that increased or decreased the Z scores.*

5.2.4 Controls from the second endosomal release screen

The endosomal release screen was repeated to generate a second data set. The control siRNA, PI3K was included in all the plates. The EGFR control siRNA was not available for the repeat screen. The PI3K siRNA reduced the percentage of cells releasing in Kinase plate 3 slightly and to a greater degree in the phosphatase plate, however these were not significant to the non-targeting control (Figure5.05). Additionally, the separation of the unstimulated and EGF control cells was less pronounced in the repeat screen which indicates less effective DAB staining when compared to the initial release screen. The overall values measured in the repeat screen were lower than the previous repeat, again indicating less effective staining. The control siRNA from the second endosomal release screen suggests the assay did not function as effectively during this screen. Potentially the staining was not as effective, but the control siRNA was not consistent which lowers our confidence in the repeat data. However, the effectiveness of the PI3K siRNA as a positive control was not validated fully and so it is hard to draw conclusions from the control siRNA.

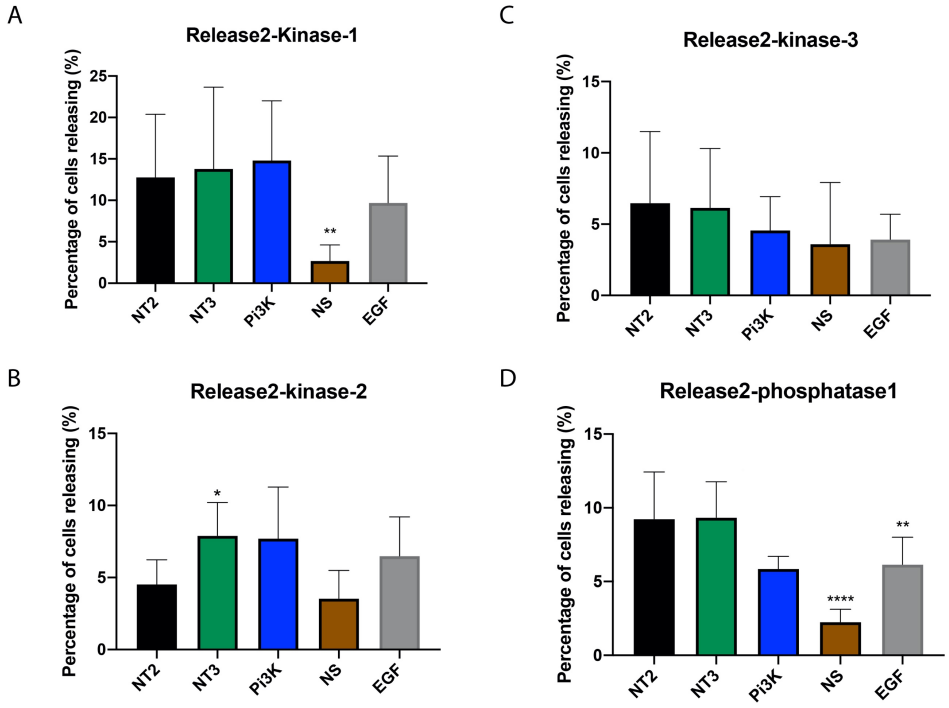

*Figure5.05: **Release screen 2 control siRNA**. Control siRNA that was previously observed to decrease the delivery of HRP to the cytosol was included in each plate of the HRP release screen. See material and methods (release screen) for details on performing the screen. The average percentage of cells releasing for each well was calculated and the data for the controls were compared. The control siRNA included in the release screen-1 were two different non-targeting siRNA (NT2 and 3),and siRNA for PI3K. Data for NT2,NT3 and PI3K siRNA are with 100ng/ml EGF stimulation. A No stimulation control without transfection were included (No stim) in the comparison. A) Controls from the first kinase plate B) Controls form the second kinase plate C) Controls from the third kinase plate D) Controls from the first phosphatase plate. All data shown is mean + SD. A One-way ANOVA with Tukey's multiple comparisons test was performed, *'s above bars indicate significance to NT2 from the respective plate. ****p≤0.0001, *** p≤0.001, ** p≤0.01, * p≤0.05*

5.2.5 Trends identified from the second endosomal release screen

Heat maps were generated for the second endosomal release screen (Figure5.06). The average percentage of cells releasing for each well was calculated and plotted with a colour scale. From the heat maps there were no obvious trends in the data to indicate systematic errors or areas of ineffective DAB staining. Potentially row L from the kinase plate-1 had low values which might indicate ineffective liquid transfer at a point during the screen.

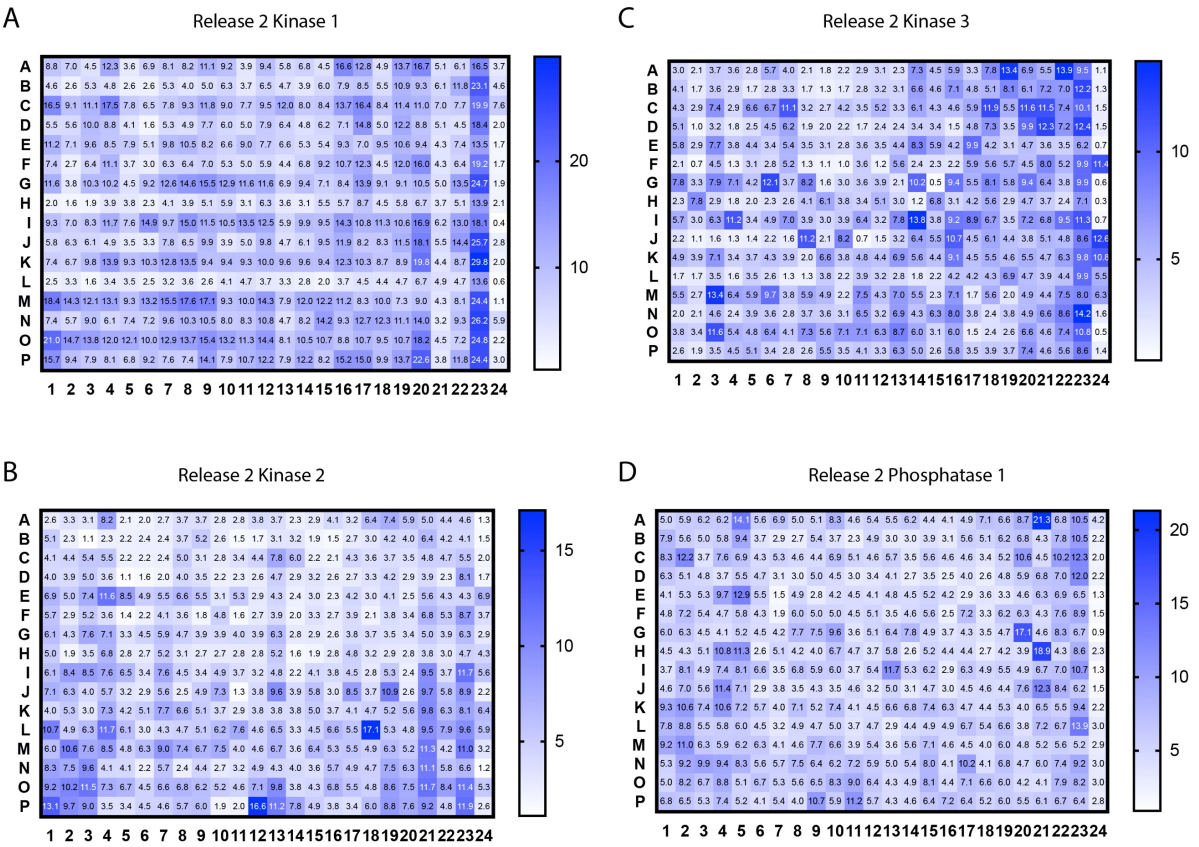

Figure5.06: ***The second HRP Release screen plate maps.*** *The average percentage of cells releasing for each image was calculated from the second release screen. The percentage of cells releasing from each field of view were averaged to get a single value per well and plotted on to a 384 well plate map. A colour scale was mapped to the values to identify any trends in the plates. Each colour scale is unique to each plate heatmap with individual keys located to the right of the heat maps.*

5.2.6 The distribution of Z scores from the second endosomal release screen

The Z scores from the second endosomal release screen were plotted in ascending order to visualise the distribution (Figure5.07). The distribution was similar to the first endosomal release screen with a similar number of siRNA conditions with positive Z scores and negative Z scores. Additionally, the magnitude of the positive Z scores were greater than the negative Z scores as seen previously. The overall magnitude of Z scores in the centre were lower resulting in a lower initial gradient indicating some of the less effective hits had a lower observable in the repeat screen. However, the siRNA with higher Z-score magnitude had similar values to the first repeat (Table5.03).

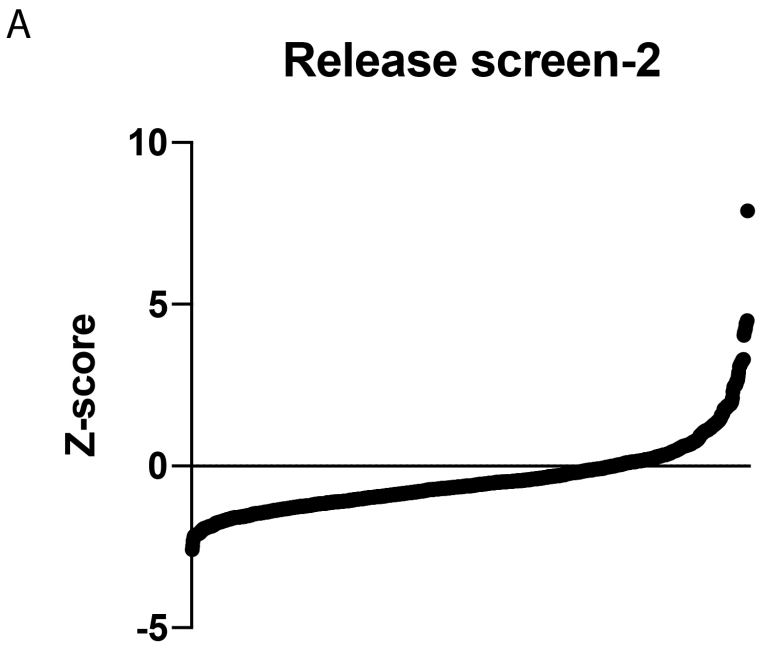

*Figure5.07**: The second HRP Release screen distribution of z-scores**. The Z-score was calculated for each hit (see material and methods for Z score calculation) and the Z scores from all 4 plates were collated**.** The z scores for each siRNA plotted in ascending order to observe the distribution of hits identified from the second HRP release screen*

A431- HRP release screen 3 increase			A431- HRP release screen 3 decrease		
Gene	Percentage of cells releasing-HRP %	Non targeting 2 Z score	Gene	Percentage of cells releasing-HRP %	Non targeting 2 Z score
CLK3	7.890217882	2.106721412	EYA4	1.540141686	-2.584715138
FLJ13052	8.186781277	2.292773298	PPAP2A	1.879697703	-2.470787882
RET	8.418476787	2.438129694	NS	2.254198111	-2.345136143
ERBB4	8.452171108	2.459268149	DUSP2	2.322648211	-2.322169883
EPHA2	8.454341207	2.460629582	PTPRF	2.685128005	-2.20055128
TRIB3	8.510297406	2.495734239	SPEG	1.083269681	-2.163682711
CDK5R1	8.520623311	2.502212294	DUSP5	2.818736725	-2.15572311
MAP2K4	8.576511	2.537273971	MAP2K6	1.121576649	-2.139650469
FBP2	17.09623752	2.634639628	PSPH	2.891468607	-2.131320233
PDK1	8.815859351	2.68743145	SYNJ2	2.893571978	-2.130614513
PTK7	8.978715886	2.789601057	PTPN12	2.921765953	-2.121154919
IPMK	9.150233233	2.897204106	PPP1R12A	2.926377522	-2.119607653
ASK	9.477996766	3.102829697	PPP1R3D	2.987017027	-2.09926199
SLK	9.493343835	3.112457828	SYNJ1	2.990401121	-2.098126564
CDKN1C	9.56581364	3.157922454	PPP1R12C	3.000813519	-2.094633014
TESK1	9.647503383	3.209171296	PPEF2	3.042740724	-2.08056567
PTPRZ1	18.85592351	3.225046472	PPP2R2D	3.093593182	-2.06350374
PKMYT1	9.700838396	3.242631527	NUDT11	3.130307205	-2.051185513
RAGE	9.765045311	3.28291235	PALD	3.241316262	-2.013939944
MAP3K1	9.793793721	3.30094794	CDC25C	3.250972763	-2.010700011
PFKFB4	10.94424772	4.022696274	SPHK2	1.346963381	-1.998251944
ALPPL2	21.27658932	4.03722414	TENS1	3.400663318	-1.960476091
PRKD2	11.10273659	4.122125782	NTRK2	1.416531575	-1.954607672
SRMS	11.23003889	4.2019901	MTMR3	3.457721418	-1.941332054
CERK	11.33905538	4.270382638	PPP2R1B	3.488795794	-1.930906033
NUCKS	11.54103004	4.397093374	PIP5K3	1.456253237	-1.929687907
TEX14	11.55002796	4.402738304	EYA2	3.493287609	-1.929398947
PIM3	11.6877721	4.489153409	DUSP8	3.515830207	-1.921835493
PFKFB2	16.59978214	7.570749936	KIAA0377	3.536916673	-1.914760597
PIK3C2B	17.11013874	7.890927034	PPP1R1A	3.557750918	-1.907770327

*Table5.02**: The second siRNA HRP release screen data.** The values for percentage of cells releasing and the z-scores from the second siRNA HRP release screen with gene identifiers plotted in a table. The table shows the top hits identified that increased or decreased the Z-score.*

5.2.7 Identification of hits for further validation

After performing the endosomal release screen, we identified the siRNA to validate further. We decided to focus on the hits that increased endosomal permeability as the aim of the project was to identify the mechanisms of endosomal release as a route to enhancing cytosolic delivery of endocytosed therapeutics. Therefore, it was decided the hits that increased the endosomal release would be validated first. We selected hits based on the Z scores as well as reproducibility between the screens. To aid selection we looked for families of proteins and potential signalling pathways. For example, we noticed many proteins were associated with immunity and so other immune related proteins were included for further validation.

A431- HRP Kinome screen combined -increase			A431- HRP Kinome screen combined - decrease		
Gene	Non targeting 2 Z score	Standard deviation	Gene	Non targeting 2 Z score	Standard deviation
DGUOK	1.700239705	2.251341309	RELA	-2.121310716	0.844054495
CSNK1A1L	1.70533338	2.306387694	LATS2	-2.076524488	0.651111985
SGKL	1.714882899	1.545713805	PIP5K2A	-1.991959758	0.68788288
CRK7	1.735292542	1.402943163	PSPH	-1.945145698	0.186174535
OSR1	1.756263774	1.71288989	CKB	-1.912476537	0.724293269
SRPK1	1.759503328	0.426166514	MPP2	-1.891880376	0.66514928
PIM3	1.788033985	2.701119424	MARK1	-1.889987296	0.417574175
CDK5R1	1.793379952	0.708832343	STK32A	-1.885621603	0.633032597
MAGI-3	1.826880558	0.877004118	AKT3	-1.879584118	0.450800319
LRRK1	1.888340633	1.282681282	EFNA4	-1.87103798	0.56092029
BMPR1A	1.915282011	2.85584209	MAP2K3	-1.867084582	0.297353009
PIK3R4	1.920269021	0.316045952	EPHB6	-1.858013873	0.606359938
FGFRL1	2.001844435	1.756630499	PCTK1	-1.85731695	0.469152785
FLJ13052	2.056225092	0.236548206	PDK4	-1.822567997	0.857694864
PRKD2	2.062049794	2.060075987	MARK3	-1.806347206	0.432857307
MAP2K5	2.063417447	0.89631552	JAK3	-1.793766444	0.268559021
RAGE	2.139835216	1.143077134	SYK	-1.77407382	0.478827239
PFKFB2	2.150733475	0.921962815	CDK5R2	-1.769331983	0.317021348
TEX14	2.195621117	2.207117187	CKMT2	-1.750146793	0.42372802
ALPPL2	2.204947772	1.832276368	PAK6	-1.746913288	0.402143748
CLK4	2.269675943	3.016087786	ACVR2	-1.743666254	0.491929402
ALK	2.286861285	1.998950624	CDC42BPB	-1.741437248	0.550584615
MGC16169	2.359407049	0.455219751	PRKAR2A	-1.73621372	0.492280851
IRAK3	2.648101477	0.750421759	LOC91461	-1.712505388	0.428680959
MARK4	2.70701241	0.657444334	PIM2	-1.7082471	0.549900578
RPS6KL1	3.09174798	1.762835383	CAMK2B	-1.703515691	0.626969146
KIAA2002(PEAK1)	3.239063082	2.187652846	GRK1	-1.697408493	0.503169226
SRMS	3.433490704	0.768499396	PNCK	-1.694269483	0.604353349
NUCKS	3.808168975	0.5889244	PAK7	-1.691327913	0.822301615
PIK3C2B	4.886667328	3.004259706	CDADC1	-1.686114251	0.428486641

*Table5.03: **siRNA HRP release screen combined data.** The values for the z-scores from the siRNA HRP release screens with gene identifiers plotted in a table. The table shows the top hits identified that increased or decreased the combined Z score calculated form the first and second kinome release screens.*

5.2.8 Endosomal release validation screen

To validate the hits identified that increased endosomal permeability we performed a secondary screen using an alternative siRNA. The siGenome siRNA was used in the validation screens and would validate the hits identified and confirm the effect seen on endosomal release were not off-target effects of the OTP siRNA used in the initial screens. A validation screen, using the HRP uptake assay, was performed with the selected siRNA identified from the kinome screens. To increase confidence, 4 experimental replicates of each siRNA were included in the validation screens and 3 biological replicates were performed.

5.2.9 Validation screen controls

The control siRNA used in the validation screens were PI3K and EGFR siRNA. The control siRNA used was from the siGenome library of siRNA. Both of the control siRNA, PI3K and EGFR, did not result in a significant decrease in any of the validation screens (Figure5.08) . There was strong separation of signal between unstimulated and EGF stimulated cells in all of the validation screens indicating the HRP release assay was successful. Heatmaps were generated from the 3 validation repeat screens performed in order to compare the data (Figure5.09). There were not any obvious systematic errors observed in the heatmaps generated for the validation screens.

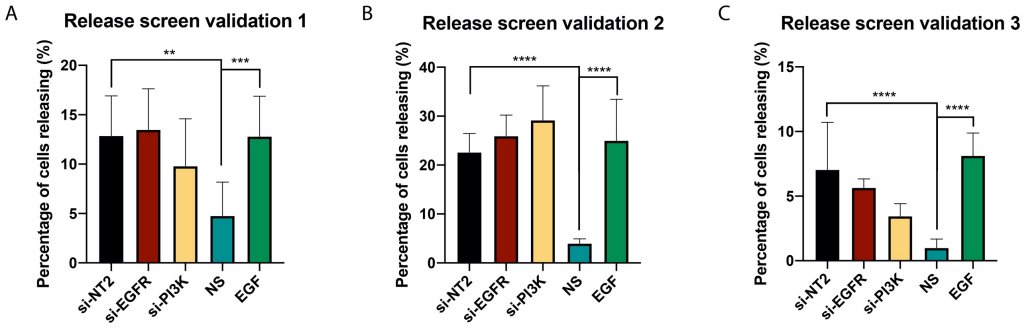

*Figure5.08: **The control siRNA from the release validation screens.** The hits that were selected from the HRP release screens that increased HRP release, were validated using a different type of siRNA. A431 cells were reverse transfected with control siGenome siRNA and hit siRNA using Polyfect transfection reagent for 3 days. A HRP release assay was performed with cells stimulated with EGF(100ng/ml) in the presence of 10mg/ml HRP. Non transfected controls were included that were either stimulated with 100ng/ml EGF or unstimulated (NS and EGF). The percentage of release for each control siRNA was calculated for the 3 biological replicate validation screens performed. All data shown is mean + SD. A One-way ANOVA with Tukey's multiple comparisons test was performed with ****p≤0.0001, *** p≤0.001, ** p≤0.01, * p≤0.05*

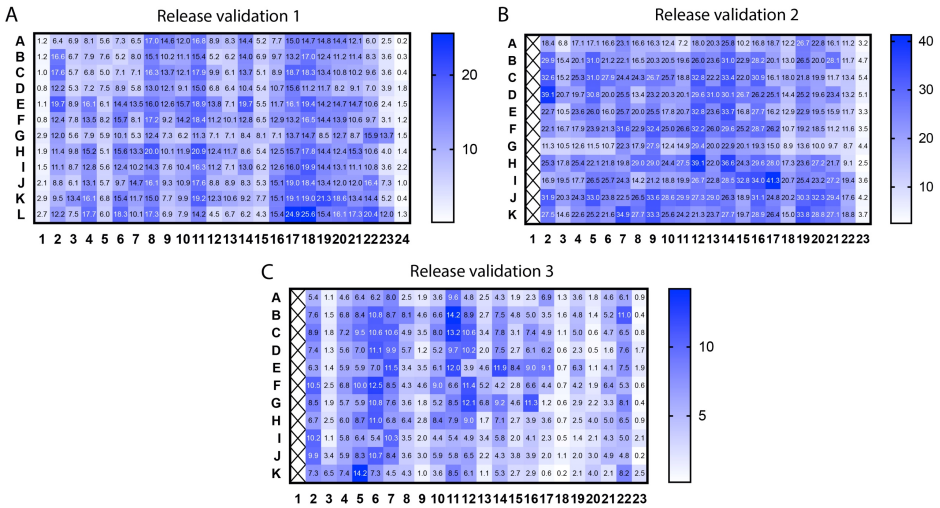

*Figure5.09: **The validation Release screen plate maps.** The average percentage of cells releasing for each image was calculated from the validation release screens. The percentage of cells releasing from each field of view were averaged to get a single value per well and plotted on to a 384 well plate map. A colour scale was mapped to the values to identify any trends in the plates. Each colour scale is unique to each plate heatmap with individual keys located to the right of the heat maps.*

5.2.10 Validation screen conclusions

The validation screen positive control siRNA showed no significant difference compared to the non-targeting control. Additionally, the Z scores observed for each siRNA hit were low in magnitude when compared to the kinome siRNA endosomal release screens (Table5.04). These results indicate that successful knockdown was not achieved in the control conditions and the evidence from the magnitude of the Z scores indicate low knockdown efficiency for the test siRNA. The same transfection procedure used in the kinome endosomal release screen was used in the validation screens without optimisation for the siGenome siRNA due to time constraints. Optimisation of the transfection procedure of the siGenome siRNA could increase the magnitude of the Z-scores observed and increase the effect seen with the control siRNA.

It was speculated the siGenome siRNA is harder to successfully transfect into the A431 cells. As the EGFR siRNA had no effect in the first two validation screen, we included the OTP EGFR siRNA in the third validation screen as this had previously been used as a positive control in the kinome screen. The data showed si-Genome EGFR siRNA was less effective as a positive control for the HRP release assay than OTP- EGFR siRNA when transfected with Polyfect transfection reagent (Figure5.10). This experiment indicates the siGenome is harder to transfect when using Polyfect transfection reagent. We performed the validation screen 3 times before deciding an alternative approach was required for validation. In order to validate the hits identified in the Kinome endosomal release screen we wanted to use an alternative assay to verify the siRNA identified had an effect on endosomal release.

HRP release validation - A431 cells								
Validation-1			Validation-2			Validation-3		
Gene	Release percentage	Z score	Gene	Release percentage	Z score	Gene	Release percentage	Z score
ALPPL2	9.55	-0.88	ALPPL2	11.34	0.67	ALPPL2	3.83	-0.94
BMP2K	6.43	-1.71	BMP2K	10.96	0.50	BMP2K	7.96	0.27
BMPR1A	11.04	-0.49	BMPR1A	11.73	0.85	BMPR1A	2.11	-1.45
CDKN1B	9.14	-0.99	CDKN1B	16.20	2.88	CDKN1B	5.15	-0.55
CLTC	18.34	1.45	CLTC	11.28	0.65	CLTC	1.47	-1.63
CTBP1	9.31	-0.95	CTBP1	11.99	0.97	CTBP1	3.92	-0.91
DUSP10	8.96	-1.04	DUSP10	10.02	0.07	DUSP10	6.19	-0.25
DUSP19	12.93	0.01	DUSP19	13.86	1.82	DUSP19	9.36	0.68
DUSP7	8.28	-1.22	DUSP7	10.22	0.16	DUSP7	5.63	-0.42
EGF only	12.80	-0.02	EGF only	11.97	0.96	EGF only	8.13	0.32
EGFR	13.49	0.16	EGFR	12.54	1.22	EGFR	5.65	-0.41
EPHA4	15.56	0.71	EPHA4	14.65	2.18	EPHA4	8.47	0.42
FBP2	10.21	-0.71	FBP2	7.95	-0.87	FBP2	4.07	-0.87
FBXL13	9.64	-0.86	FBXL13	7.12	-1.25	FBXL13	4.02	-0.89
FBXL22	12.94	0.02	FBXL22	12.05	0.99	FBXL22	5.80	-0.37
FBXO22	11.38	-0.40	FBXO22	4.30	-2.53	FBXO22	5.81	-0.36
FBXO3	13.69	0.22	FBXO3	11.56	0.77	FBXO3	6.94	-0.03
FBXO41	9.18	-0.98	FBXO41	7.29	-1.17	FBXO41	9.09	0.60
FGFRL1	15.94	0.81	FGFRL1	8.46	-0.64	FGFRL1	3.20	-1.13
HIPK3	10.75	-0.56	HIPK3	13.23	1.53	HIPK3	4.23	-0.83
IRAK3	11.75	-0.30	IRAK3	13.06	1.45	IRAK3	4.46	-0.76
KHK	14.31	0.38	KHK	9.93	0.03	KHK	3.35	-1.08
LRRK1	11.59	-0.34	LRRK1	7.14	-1.24	LRRK1	4.13	-0.85
MAP2K5	7.51	-1.42	MAP2K5	13.68	1.74	MAP2K5	4.82	-0.65
MARK4	12.37	-0.13	MARK4	12.67	1.28	MARK4	10.94	1.14
NEK5	11.57	-0.35	NEK5	9.11	-0.34	NEK5	9.35	0.67
NEK7	11.09	-0.47	NEK7	9.98	0.05	NEK7	8.87	0.53
NLRC5	16.30	0.91	NLRC5	6.96	-1.32	NLRC5	3.71	-0.98
No stim	4.77	-2.15	No stim	0.97	-4.04	No stim	1.00	-1.77
NT2	12.88	0.00	NT2	9.86	0.00	NT2	7.05	0.00
NT2-O	13.15	0.07	NT2-O	12.62	1.25	NT2-O	2.47	-1.34
NTRK1	9.14	-0.99	NTRK1	11.81	0.89	NTRK1	6.67	-0.11
NUCKS1	9.46	-0.91	NUCKS1	7.85	-0.91	NUCKS1	6.74	-0.09
NUDT3	12.63	-0.07	NUDT3	4.47	-2.45	NUDT3	5.73	-0.38
PAK1	10.55	-0.62	PAK1	11.19	0.61	PAK1	7.79	0.22
PEAK1	13.19	0.08	PEAK1	13.38	1.60	PEAK1	2.90	-1.21
PFKFB2	6.22	-1.77	PFKFB2	9.72	-0.06	PFKFB2	3.96	-0.90
PIK3C2A	9.80	-0.82	PIK3C2A	13.48	1.65	PIK3C2A	3.44	-1.06
PIK3C2B	7.11	-1.53	PIK3C2B	15.50	2.56	PIK3C2B	9.54	0.73
PPP1R16B	15.48	0.69	PPP1R16B	7.23	-1.20	PPP1R16B	1.50	-1.62
PPP4R1	8.36	-1.20	PPP4R1	12.79	1.33	PPP4R1	7.72	0.20
PPP6C	8.86	-1.07	PPP6C	10.88	0.46	PPP6C	4.56	-0.73
PTEN	12.00	-0.23	PTEN	8.53	-0.61	PTEN	2.89	-1.22
PTK2	7.40	-1.45	PTK2	6.14	-1.69	PTK2	3.51	-1.03
PTPRR	12.74	-0.04	PTPRR	9.01	-0.39	PTPRR	6.11	-0.27
PTPRZ1	13.84	0.25	PTPRZ1	9.08	-0.36	PTPRZ1	6.45	-0.17
RFK	11.96	-0.24	RFK	8.25	-0.73	RFK	4.16	-0.84
RPS6KL1	14.98	0.56	RPS6KL1	7.17	-1.22	RPS6KL1	3.32	-1.09
SRMS	7.36	-1.46	SRMS	9.62	-0.11	SRMS	3.49	-1.04
TAOK1	11.64	-0.33	TAOK1	9.38	-0.22	TAOK1	6.83	-0.06
TBCK	8.98	-1.03	TBCK	6.54	-1.51	TBCK	5.10	-0.57
TULP4	12.44	-0.12	TULP4	13.87	1.82	TULP4	6.48	-0.17

Table5.04: ***The release validation siRNA HRP release screen data.*** *The values for percentage of cells releasing and the z-scores from the validation siRNA HRP release screens with gene identifiers plotted in a table. The table shows all hits included in the validation screen ordered alphabetically by gene. NT (Non-targeting), No stim = No transfection control with no stimulation, EGF only = No transfection control with EGF stimulation.*

A

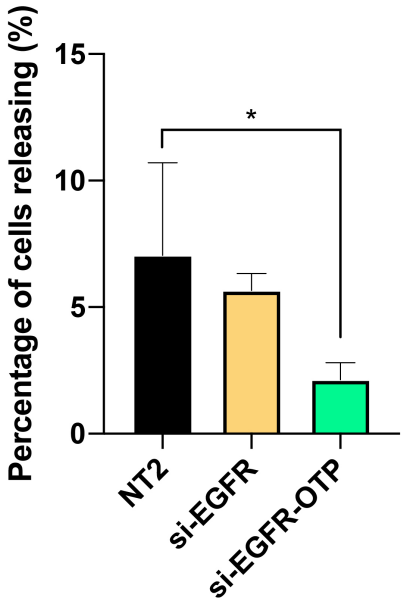

Figure5.10: ***The effect of siGenome siRNA and on-Target siRNA on EGFR knockdown and the effect on EGF stimulated HRP release.*** *Data shown was taken from the third release screen validation experiment. The siRNA against EGFR from the On-target plus library and si-Genome library were included in the experiment as a comparison. A431 cells were reverse transfected with the siRNA using Polyfect transfection reagent for 3 days. A HRP release assay was performed with cells stimulated with EGF(100ng/ml) in the presence of 10mg/ml HRP.). The percentage of release for each control siRNA was calculated for the 3 biological replicate validation screens performed. All data shown is mean + SD. A One-way ANOVA with Tukey's multiple comparisons test was performed with ****p≤0.0001, *** p≤0.001, ** p≤0.01, * p≤0.05*

5.3 Lipid nanoparticle assay to measure functional delivery of mRNA

In order to validate the hits identified in the HRP delivery screen, an established assay at AstraZeneca was utilized. The assay functions by detecting the delivery of mCherry mRNA and subsequent translation to produce fluorescent protein. The mCherry mRNA was inserted into a MC3-Lipid nanoparticle (MC3-LNP) to aid delivery and prevent degradation. The nanoparticles were manufactured by an internal team at AstraZeneca, where each batch underwent quality control for encapsulation of mRNA and concentration determination. Manipulation of protein levels by either using siRNA to reduce protein levels or overexpression by transient addition of mRNA is an attractive therapeutic option (246,247). The internalisation of LNPs do occur under basal conditions in cells indicating a mechanism of uptake which probably occurs via fusion with endosomes after being endocytosed. LNPs have been shown to be taken up via macropinocytosis (247,248) which could indicate an effective route for increasing intracellular delivery of LNPs.

The advantages of the assay for detecting intracellular delivery of cargo include, the mRNA being delivered acts as a proxy for therapeutic molecules. In principle it could be replaced with an alternative mRNA, meaning that any increase in delivery could enable an increase in therapeutic output of potential therapeutics. Additionally, the assay produces a signal only with functional delivery, as the mRNA must escape the endosomal system to produce the fluorescent mCherry protein. This reduces the background fluorescence as the LNP does not produce a fluorescent signal directly and so no signal is observed from endosomal LNP or extracellular LNP unlike with other delivery assays.

In the previous siRNA kinome screen performed using the HRP delivery assay, a list of potential siRNA hits that increased cytosolic delivery of HRP were identified. The delivery of HRP to the cytosol was stimulated with EGF (100ng/ml) and no basal delivery of HRP was observed. The detection of HRP in the cytosol was sensitive to the macropinocytosis inhibitor, EIPA (Figure 3.20). This indicates the uptake of HRP via macropinocytosis is required for the subsequent release step. As it has been shown LNPs can be taken up via macropinocytosis, the hits identified in the HRP release screen might also have a positive effect on the delivery of LNPs to the cytosol after uptake. An increase of LNP delivery would validate the findings of the HRP release screen as the release can be shown using two distinct mechanisms. The siRNA

from the HRP screen that showed increased cytosolic delivery were selected to be validated using the LNP-mCherry delivery assay.

In order to perform the LNP uptake assay, cells are reverse transfected with siRNA for 3 days and then treated with mCherry-LNP for 24 hours plus and minus EGF stimulation. After 24 hours treatment cells were fixed using 4% PFA, washed and imaged using an automated plate microscope. After imaging, analysis was performed using an automated script. Briefly, cell nuclei were identified using Hoechst staining. The mean mCherry value per cell in a field of view was calculated with 9 fields of view taken per well. This mean mCherry value was normalised to a cell number titration curve (Figure5.13).

5.3.1 The effect of buffer volume on H358 cells

The LNP delivery assay had previously been used at AstraZeneca for a siRNA trafficome screen for effectors of LNP uptake in H358 cells. Due to this previous screen, we knew delivery of mRNA and subsequent expression of fluorescent protein in the cytosol could occur in the H358 cell line. Additionally, the optimum conditions for the assay had been previously observed and so an initial screen could be performed without optimising for a new cell line. As the LNP uptake assay had been performed before in the H358 cell line, siRNA that were known to have an effect on LNP delivery could be utilized as controls for our subsequent screens. It was therefore decided to perform an initial LNP uptake screen in the H358 cells using the siRNA hits that increased delivery of HRP in our previous kinome screen.

The siRNA used previously with the H358 cells had been delivered using an Echo liquid handling system which can transfer nanolitre volumes. This allows a negligible volume of siRNA buffer to be transferred into each well. Due to the experimental setup and the siRNA that we had available, the use of the echo to transfer the test siRNA was not possible and so a larger volume was transferred using an automated multichannel pipette. Before the validation LNP screen could be performed, an optimisation experiment was required to observe the effects of siRNA buffer on the H358 cells. Due to the addition of siRNA via an automated multichannel pipette, a larger volume of siRNA buffer was added to the cells. The effect of this larger volume of siRNA buffer on knockdown efficiency and cell growth was not known for the H358 cells. To assess their ability to tolerate the extra siRNA buffer H358 cells were transfected with different control siRNA: Non-targeting siRNA, PLK1 siRNA and

Transferrin receptor siRNA (Figure5.11). Non-targeting RISC free control was used as the negative control as it does not engage the RISC complex and so should not result in any gene silencing. PLK1 siRNA was used as a knockdown control as loss of PLK1 results in cell death(249). Transferrin receptor knockdown results in a decrease in transferrin uptake in the cells and can give an indication of the degree of gene silencing when combined with a fluorescent transferrin uptake assay. The siRNA was transferred to wells using the echo liquid handling system and then different volumes of siRNA buffer was added. To observe the effect on cell growth, the cells were imaged using an IncuCyte® cell imager over 3 days. The images can be analysed to give a percentage confluency value for each buffer condition. The higher volumes of buffer did have a negative effect on cell growth (Figure5.11A) in the RISC-free control, with a lower confluency of 41% observed when 10µl of buffer was added compared to 56% for the 0µl control after 3 days. The confluency increase ratio was calculated by dividing the confluency detected after 3 days with the initial confluency. The same number of cells were seeded per well, but the initial confluency might be different depending on clustering of the cells. The effect of different buffer volumes on confluency with RISC-free siRNA seems to be amplified when compared to no siRNA being added (Figure5.11B). This indicates that the transfection reagent is required for the buffer volume to effect confluency. Additionally, the buffer volume has no effect on the PLK1 cell death control indicating no effect on knockdown efficiency. The same degree of cell death was observed under all conditions.

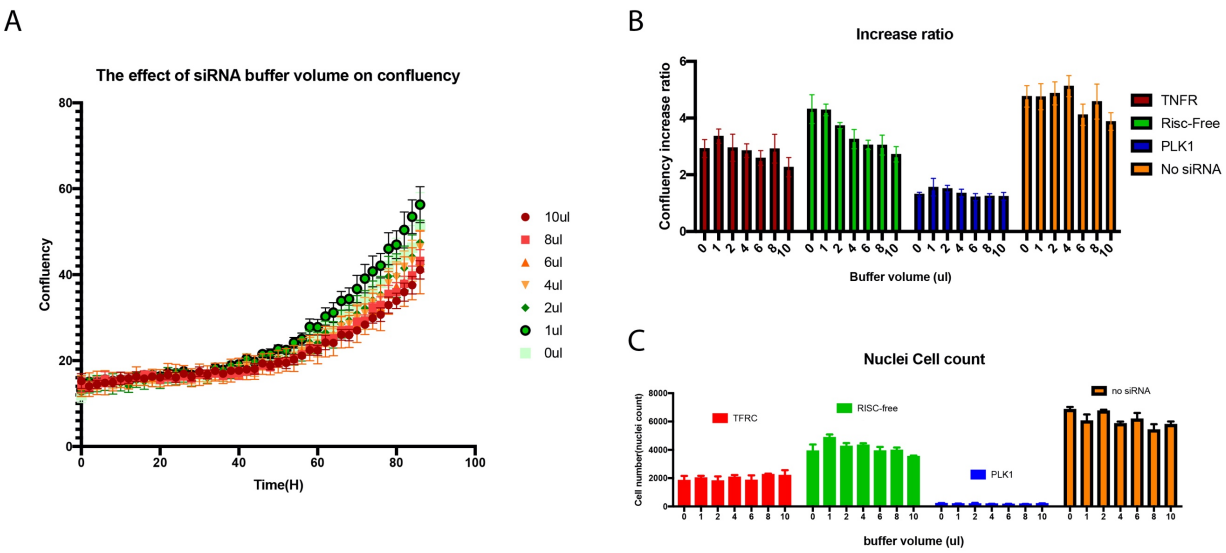

*Figure5.11: **The effect of siRNA buffer on cell growth.** A) H358 cells were reverse transfected with RISC-free siRNA using RNAi Max reagent followed by addition of variable volumes of siRNA buffer. Cell growth was observed using an incucyte incubator microscope and confluency calculated by detecting the percentage of covered surface. B+C) Reverse transfection with additional buffer added for siRNA targeting the transferrin receptor (TNFR), Risc-free control, PLK1 cell death control or no siRNA added. The effect of the buffer and siRNA on the B) ratio of confluency increase or the C) DAPI nuclei count can be seen. Data is Mean + SD from 4 replicate wells from 1 independent experiment.*

In addition to observing PLK1 cell death, a transferrin uptake assay was utilised to assess the level of silencing of the transferrin receptor with different buffer volumes. Transferrin conjugated to alexa-fluor-647 was feed to cells that had been transfected with either transferrin receptor siRNA or a RISC-free siRNA (Figure5.12). The level of transferrin internalisation could be calculated by fluorescent microscopy. There was some variability in the assay, with buffer volumes of 2µl and 4µl not showing any transferrin uptake in the RISC-free control with TFN-647. This likely indicates an error where no transferrin was transferred to these wells when compared to the other results as Buffer volume 0 µl and 10µl had similar transferrin uptake. Importantly siRNA knockdown of the transferrin receptor reduced the signal to the same level as no TFN-647 indicating complete knock down of the transferrin receptor in 0µl and 10µl buffer conditions.

A nuclei count was performed using Hoechst staining and automated nuclei counting (Figure5.11 C). This method differs from the confluency detection as individual nuclei are counted giving a more accurate cell number but could only be performed on day 3. The buffer volume has less effect on nuclei count then observed with the confluency which might indicate an effect of the buffer on cell size or clustering but the PLK1 siRNA still indicates high levels of knockdown across all buffer volumes. These experiments show that the H358 cells can tolerate moderate siRNA buffer volumes and the efficiency of siRNA knockdown is not

affected. In order to ensure enough siRNA was added to each well, 5µl of siRNA was selected as a volume sufficient for effective knockdown without a large effect on cell viability.

A

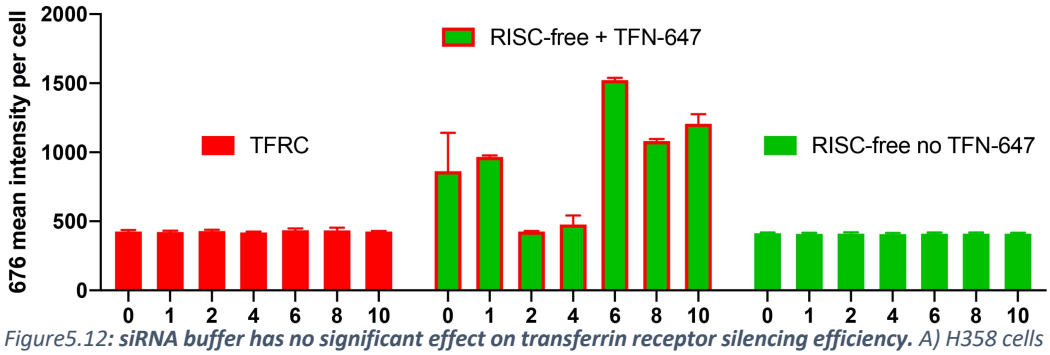

*Figure5.12: **siRNA buffer has no significant effect on transferrin receptor silencing efficiency.** A) H358 cells were reverse transfected using RNAiMax with siRNA targeting either the Transferrin receptor (TFRC) or RISC-Free siRNA. Additional siRNA buffer was added to each well as shown. After 3 days incubation at 37℃ to allow for sufficient gene silencing, a transferrin uptake assay was performed using fluorescent 676-transferrin. The mean intensity of transferrin per cell was calculated and averaged per well. Data is Mean + SD from 4 replicates for TFRC and 2 replicates for RISC-free +- TFN-647 from one independent experiment*

5.4 LNP uptake screen +/- EGF stimulation in H358 cells

To validate the hits identified from the HRP release screen that increased endosomal release, an initial LNP-mCherry delivery screen was performed in the H358 cell line. Cells were reverse transfected with the siRNA library containing the genes identified to result in increased HRP delivery. After 3 days, LNP containing mCherry was added for 24hours either in the presence or absence of EGF. The cells were fixed and imaged with automated analysis detecting the mean mCherry fluorescence value per cell for each image. The screen was performed with and without EGF stimulation to compare the EGF dependence of the siRNA library to increase delivery. The previous HRP screens were performed with EGF stimulation as there was no delivery of HRP to the cytosol under basal conditions and required the EGF stimulation to promote release. This differs from the LNP assay as there is basal release of LNP and a signal observed under no stimulation. Therefore, it was decided to perform the LNP uptake assay to perform the LNP uptake assay with both EGF stimulation and without EGF stimulation.

5.4.1 Cell number titration curve

From the previous LNP experiments performed at AstraZeneca it was known that cell number affects the amount of LNP uptake and so the mean mCherry value. Fewer cells results in an increase in mCherry signal indicating increased delivery. Fewer cells result in increased available LNPs per cell and so a greater amount of uptake is observed per cell over the 24-hour LNP uptake. The process of siRNA transfection and knockdown of target genes will have an effect on cell number and viability which would result in different final number of cells per well for each condition. In order to correct for this, a calibration curve was performed alongside each screen to normalise the mCherry value to the value expected for a given number of cells. This prevents false positive values that have an effect on cell number rather than delivery. Different cell numbers were seeded into an additional plate and the effect of cell number on LNP delivery observed. A non-linear regression analysis was performed, and an equation calculated that could be used to normalise the data acquired from the screens (Figure5.13). This value indicates the amount of mCherry signal following normalisation of cell number.

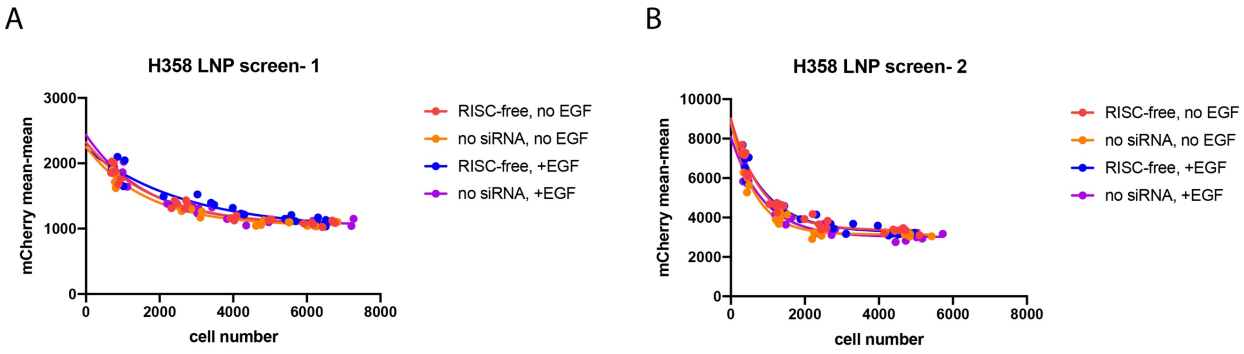

*Figure5.13: **H358 LNP screen cell number calibration curve.** During the LNP screen an additional plate was set up to generate the cell number calibration curve. Different numbers of cells were seeded to generate a calibration curve with different siRNA transfections using RNAi Max. After 3 days at 37℃ the cells were treated with 20ng LNP + and – EGF for 24 hours. The mean mCherry signal per cell was calculated and the cell number was acquired by automated DAPI counting. Data is mean mCherry per cell plotted against mean nuclei count from 9 images taken across each well. A) 1st repeat for LNP uptake screen in H358 cells, B) 2nd repeat for LNP uptake screen in H358 cells*

5.4.2 The effect of doubling LNP-mCherry concentration on productive delivery

In order to assess the ability of the assay to detect variable levels of LNP delivery, double the mass of LNP was added to control RISC-free wells. The mass of LNP used per well was

previously optimised to be 20ng as this results in a detectable amount of mCherry signal under basal conditions. The addition of double the mass of LNP should result in a theoretical doubling in the amount of delivery under basal conditions as there is an increase in the amount of available LNP per cell and so a greater amount will be taken up and delivered. From figure 5.14, addition of 40ng LNP resulted in an increase of the mean normalised mCherry fluorescence to 1.3-fold change with EGF stimulation and a 1.26-fold change without EGF stimulation when normalised to the cell number calibration curve. This result showed an increase in mCherry signal that is proportional to twice as much LNP being delivered. Any hits can be compared directly to this figure to assess their ability to increase delivery. The siRNA that result in greater release than the 40ng LNP control shows an increase in the delivery of LNP to the same degree as addition of twice the amount of LNP. This increase was used as a positive control for the delivery of LNP but additionally suggests that under the conditions of the assay the LNP uptake and delivery is not saturated and increased LNP delivery can be detected.

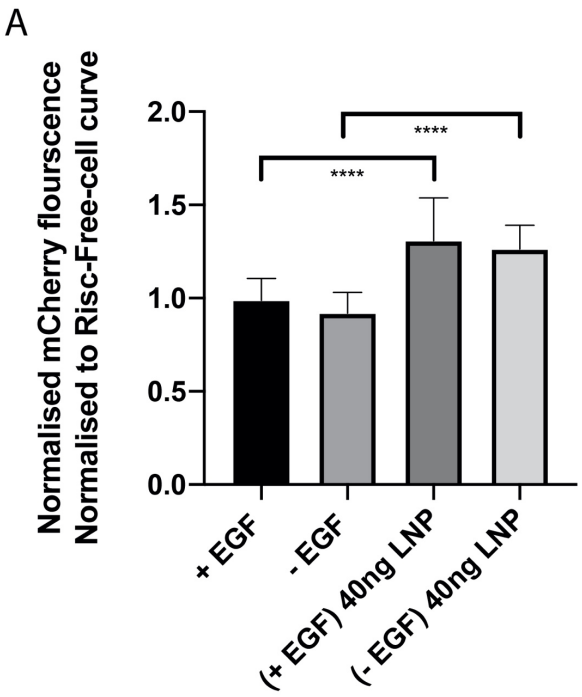

Figure 5.14: Addition of 40ng LNP results in an increase in mCherry signal. *The addition of twice the concentration of LNP to wells as a control in the H358 LNP uptake screen. H358 cells were reverse transfected for 3 days followed by incubation with mCherry-LNP for 24 hours. EGF to a final concentration of 100ng/ml was used to stimulate cells at the same time as LNP addition. Here, cells treated with RISC-Free siRNA were incubated with either 20ng LNP or 40ng LNP plus and minus EGF. The mean mCherry signal per cell was calculated and a cell average per well was calculated. Data shows Mean + SD from two independent repeats with n≥20. A One-way ANOVA with Tukey's multiple comparisons test was performed, with ****p≤0.0001*

5.4.3 Positive control siRNA identified from previous LNP uptake screens

Previous studies at AstraZeneca had used the trafficome to identify regulators of LNP release. Two top hits that positively affected LNP delivery and release were identified and are called A and B for confidentiality, while C was identified to negatively affect LNP release. We used the siRNA previously identified (A,B and C) as positive control siRNA in the H358 LNP uptake screens as they were known to effect LNP delivery. The control siRNA, A and B resulted in an increase delivery in both of our H358 LNP screens indicating they are robust controls (Figure5.15). C resulted in variable effects on uptake in the first screen but the expected inhibition was observed in the second screen. This indicates that there might have been insufficient knock down of target genes in the first screen. This is additionally highlighted by looking at the PLK1 cell death control. PLK1 knockdown influences cell viability and can be utilised to control for knockdown efficiency. The screens were performed in two 384 well plates and so a comparison of PLK1 mediated cell death in each plate can identify potential lack of knockdown. The PLK1 cell death control resulted in complete loss of viability in plate one from the first screen but did not in the second plate (Figure 5.16A). This indicates that there might have been insufficient knockdown in the second plate of the first screen. To observe potential differences, the plates were compared to look for variability between plate 1 and 2 which indicated that there is some variability, but most repeat values are similar between the two plates (Figure5.16 C, D). This indicates that the problem might be with PLK1 siRNA transfer as the other plate2 values are similar to plate 1 and both positive controls showed increased delivery in both plates indicating successful knockdown. The second screen showed cell death in all PLK1 knockdown and so complete knockdown was achieved.

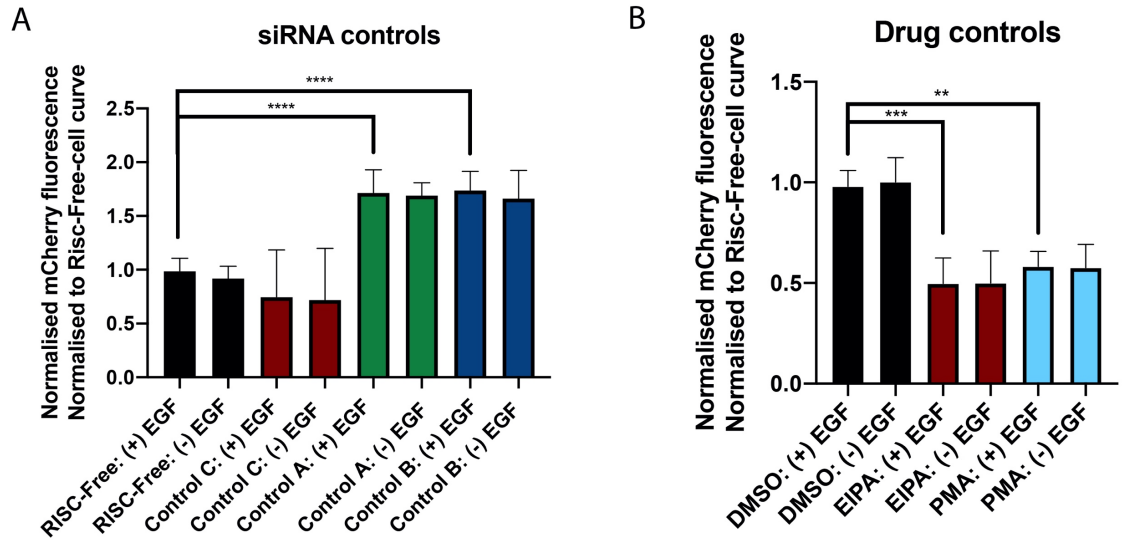

Figure5.15: ***Control siRNA and drug controls from the H358 LNP screen.*** *Control siRNA and drug controls were dispersed throughout the screening plates to control for siRNA transfection and liquid handling. A) Control siRNA reverse transfection followed by addition of LNP for 24 hours B) Risc-Free control siRNA reverse transfection for 3 days followed by addition of LNP and drug controls for 24 hours. Data shows Mean + SD from 2 independent experiments. A One-way ANOVA with Tukey's multiple comparisons test was performed, with ****p≤0.0001, *** p≤0.001, ** p≤0.01, * p≤0.05*

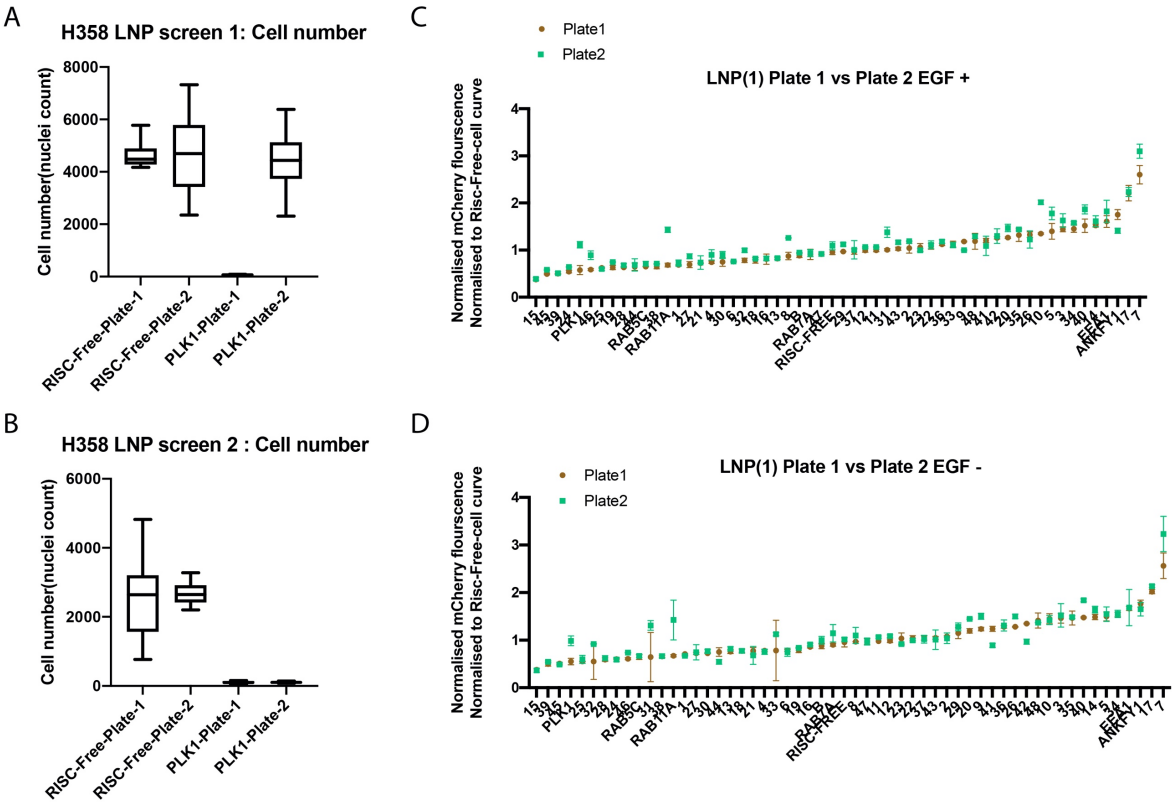

Figure5.16: ***Knockdown of PLK1 results in cell death.*** *As a control for knockdown in the H358 LNP uptake screen, PLK1 siRNA was used. PLK1 siRNA was reverse transfected using RNAiMax reagent. Cell death in the PLK1 control indicates successful knock down. A + B) Knockdown of PLK1 in the duplicate plates from the first and second H358 LNP screens respectively. Nuclei were counted after 3-day knockdown and 24-hour LNP uptake, using Hoechst staining. C + D) Comparison of mCherry signal for each siRNA in each replicate plate in the first H358 LNP screen. C) Plate 1 vs plate 2 with EGF stimulation D) Plate 1 vs plate 2 without EGF stimulation*

5.4.4 Inclusion of pharmaceutical inhibitors to observe the effect on LNP release

Pharmacological inhibitors were included in the LNP uptake assay to validate the assay and observe their effect on the LNP release. The drug EIPA is an inhibitor of macropinocytosis (131) and was included in the LNP uptake screen. The inhibition of macropinocytosis via EIPA should affect LNP delivery, if macropinocytosis is an uptake route for the LNP. It was shown previously that HRP uptake in A431 cells was sensitive to inhibition of macropinocytosis by EIPA. We also included a set of cells treated with PMA because although PMA stimulates macropinocytosis (118,207) it did not result in increased HRP delivery (Figure3.20). It was found that both EIPA and PMA treatment resulted in decreased mean mCherry signal per cell (Figure 5.15 B). Both resulted in ~50% reduction in signal observed and had the same result independent of EGF stimulation. The result for EIPA was expected as a decrease in macropinocytosis should result in decreased delivery, if the LNPs are taken up by macropinocytosis, and it validates the uptake of these LNPs can occur via macropinocytosis. PMA results in increased macropinocytosis and so it was unknown what the effect of PMA would have on LNP delivery. The PMA treatment resulted in decreased mCherry signal indicating reduced delivery. Due to experimental set-up the drug treatment occurred at the same time as the LNP dose which had to be maintained for 24 hours in order to observe a strong mCherry signal. PMA was used previously for a short period of up to 25 mins to stimulate macropinocytosis but it is known to have other effects during longer treatments, such as cell differentiation (127). Potentially the longer treatment of PMA has an effect on protein translation or other cellular processes which could affect the mCherry production and so result in decreased signal observed. On the other hand, the stimulation by PMA could actively decrease delivery by changing the signalling activation and potentially the type of macropinosomes formed which could reduce LNP delivery. Additional experiments would have to be performed to elucidate the exact mechanism of LNP entry and if PMA does have a negative effect on uptake or if the observation is an artefact of long drug treatment.

5.4.5 The effect of EGF stimulation on LNP delivery

As previously mentioned, the LNP uptake screen was perform in the presence and absence of EGF. In the HRP release assay in A431 cells, EGF showed an increased in cytosolic delivery. We tested whether EGF evoked a similar release in H358 cells and found to our surprise that EGF stimulation had no significant effect on the amount of LNP delivery. This can be seen by comparing plus and minus EGF stimulation for each siRNA condition and observing the limited variation between the two results (Figure5.16). Additionally, from the cell number titration curve (Figure5.13) there is no difference between the curves for EGF stimulation and without EGF stimulation indicating no effect on LNP delivery. This indicates that the delivery of LNPs does not require EGF stimulation and can occur under basal conditions. This could be an effect of the LNP uptake mechanism which is likely to occur by fusion of the LNP with the endosomal lipid membrane. The H358 cell line might have activated signalling pathways which differ from A431 cells. H358 cells might respond differently to EGF stimulation, which is supported by the ras mutation that they have acquired. H358 cells have constitutively active K-Ras mutation, G12C (250), which results in continuous growth factor pathway activation. We found previously in N-RAS HT1080 cells (237) HRP delivery to the cytosol can occur in unstimulated cells, with both PMA and EGF resulting in a greater proportion of cells releasing (Figure3.21). This could indicate that RAS signalling is important for intracellular delivery.

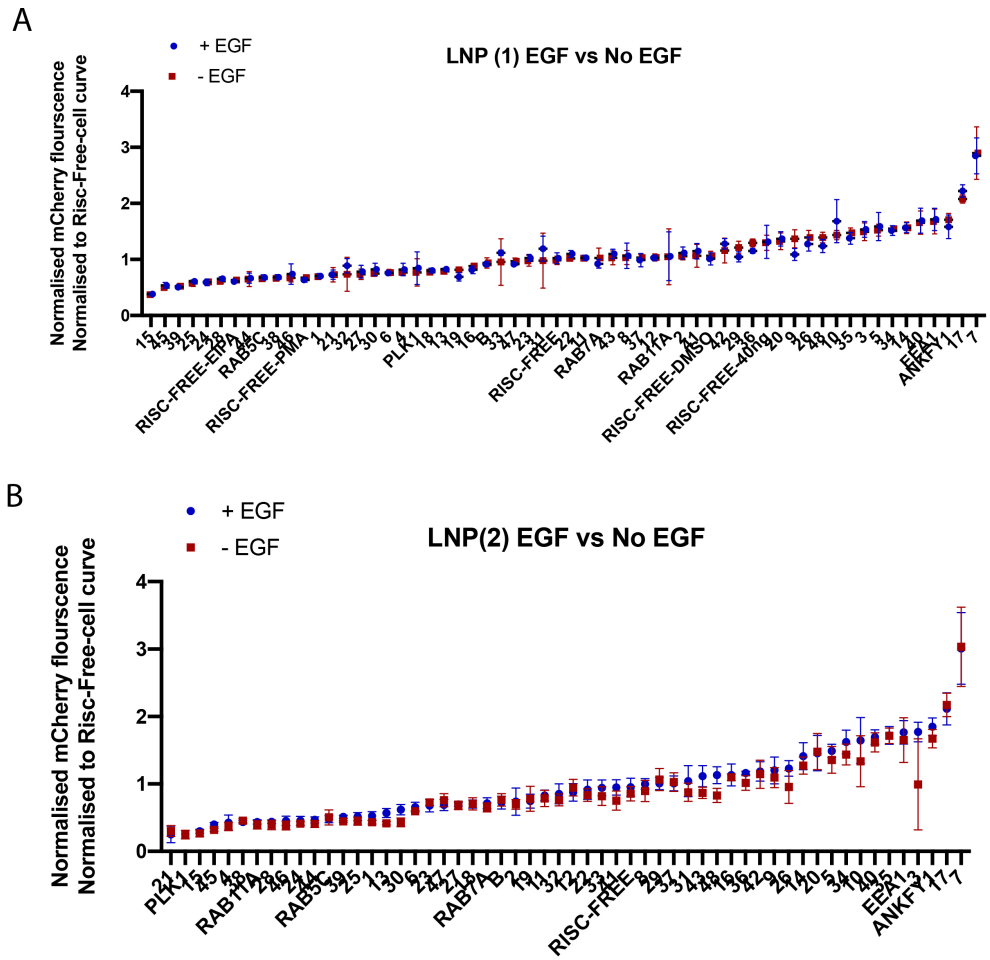

*Figure5.17: **The effect of EGF on the uptake of LNP with each siRNA.** A comparison between the mCherry signal from LNP delivery for each siRNA with EGF stimulation and without stimulation A) from the first H358 screen B) from the second H358 screen. Test siRNA on the x-axis was blinded and represented by numbers whereas control siRNA is marked by standard designation. Data shows Mean + SD for each independent repeat screen. Each hit siRNA was performed in quadruplicate for each condition per screen.*

5.4.6 Identification of hits that improve productive LNP delivery

The HRP assay is dependent on the quality of stain produced and is sensitive to changing conditions which results in a degree of variability. As the LNP-mCherry uptake assay has been optimized extensively and developed for high-throughput screening, with the aid of sophisticated automated liquid handling, the variability between repeats is low. This enables increased confidence in hits identified in both release screens. We identified several siRNA conditions that resulted in increased LNP delivery (Figure5.18) that was greater than the double LNP concentration control. This indicates that these hits result in more delivery than addition of double the LNP concentration.

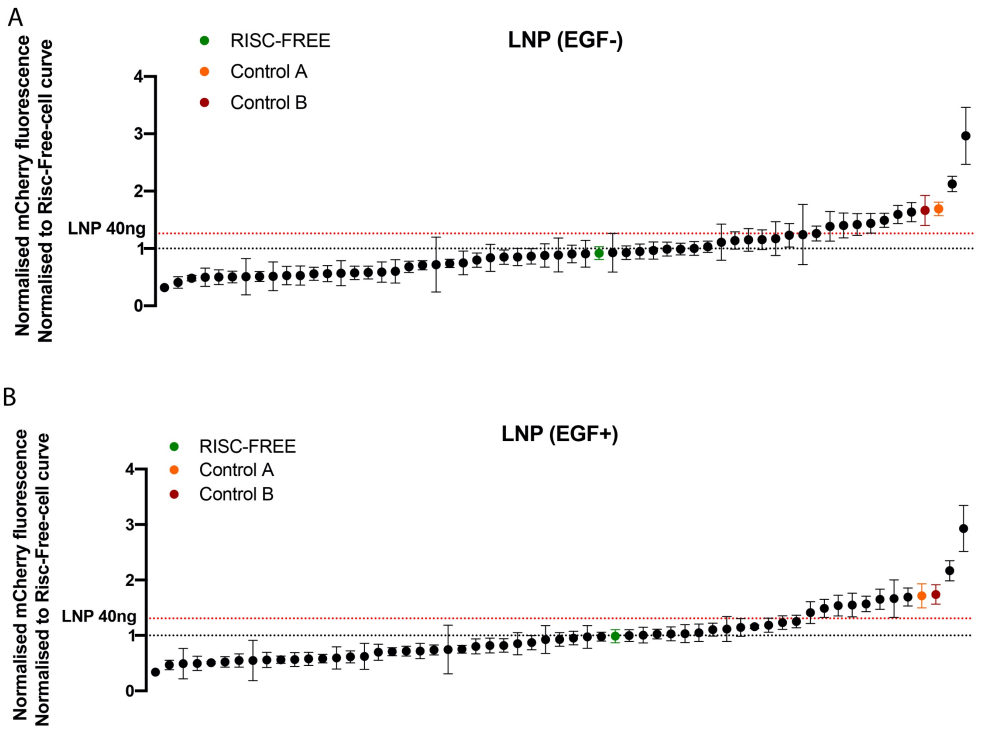

*Figure5.18: **Overview of hits identified compared to 40ng LNP control and positive control siRNA.** The mean normalized mCherry signal for each siRNA was ordered in increasing value for the H358 LNP uptake screen. The mCherry signal was normalized to the cell titration curve and plotted with the value for the 40ngLNP control as well as the control siRNA in order to compare the effect on LNP delivery of the top hits. Data shown is Mean + SD from the two independent screens. Each siRNA N = 8*

There was no noticeable difference of EGF stimulation on the LNP delivery to the cytosol and had limited effect on normalised mCherry value observed for each siRNA condition, with the hits resulting in the greatest release being similar in EGF+ and EGF- conditions. When compared to the HRP release screen, there are some siRNA conditions that are positive release regulators in both but also some that are only positive in one screen or the other (Table 5.03, Table 5.06). This could be due to the difference in cell type or the uptake mechanism of the LNP and HRP molecules. SRMS siRNA resulted in the greatest increase in LNP delivery to the cytosol and increased the m-Cherry signal from the LNP by 198% when compared to the RISC-free siRNA. This is compared to the 32.5% increase by the 40ng control indicating a large increase in LNP delivery.

To allow a direct comparison between LNP uptake and HRP delivery the LNP delivery assay was then repeated in A431 cells.

H358- LNP release screen (+) EGF				Continued			
Gene	Average normalised LNP delivery	STD	N	Gene	Average normalised LNP delivery	STD	N
ALPPL2	0.5659647	0.12458063	8	NEK5	1.53829664	0.1853098	8
BMP2K	0.92595094	0.25129347	8	NEK7	1.00611714	0.14068237	8
BMPR1A	0.71675166	0.08860288	8	NLRC5	0.54724576	0.11945574	8
CDKN1B	0.97351418	0.20574506	8	NTRK1	0.73761438	0.08922931	8
CLTC	1.18548236	0.12628998	8	NUCKS1	1.66364618	0.33718509	8
CTBP1	0.5954591	0.19998388	8	NUDT3	1.69286842	0.16193182	8
DUSP10	1.15702685	0.03284562	8	PAK1	0.69682496	0.14420488	8
DUSP19	1.54866958	0.21357254	8	PEAK1	1.14512917	0.15885082	8
DUSP7	0.9980058	0.1067194	8	PFKFB2	0.92792991	0.12370572	8
EGFR	0.46671902	0.08475089	8	PIK3C2A	0.8022031	0.13454812	8
EPHA4	0.56253888	0.06467561	8	PIK3C2B	0.95220125	0.12157162	8
FBP2	1.04839575	0.15826746	8	PPP1R16B	0.55822863	0.13579312	8
FBXL13	1.11663624	0.22447179	8	PPP4R1	1.23152726	0.12321344	8
FBXL22	0.52289787	0.09378237	8	PPP6C	1.56807393	0.14040618	8
FBXO22	0.71964084	0.13942567	8	PTEN	0.50792134	0.02057781	8
FBXO3	0.85212502	0.19997507	8	PTK2	0.61397587	0.10790394	8
FBXO41	0.87032762	0.12951919	8	PTPRR	1.02970164	0.12465988	8
FGFRL1	0.75167966	0.07109177	8	PTPRZ1	1.10650355	0.1168016	8
HIPK3	0.70671129	0.07168687	8	RFK	0.62315568	0.23447338	8
IRAK3	1.48895652	0.16434608	8	RPS6KL1	1.03271633	0.16124484	8
KHK	1.02538076	0.08681478	8	SRMS	2.92914193	0.4150003	8
LRRK1	0.4907337	0.27288494	8	TAOK1	1.65314939	0.18231378	8
MAP2K5	2.16789036	0.18123641	8	TBCK	1.41128232	0.19605403	8
MARK4	0.33948761	0.05078133	8	TULP4	1.25177015	0.11381533	8

Table 5.05: ***Overall data from the H358 LNP release screen with EGF stimulation.*** *The average normalized LNP delivery for each siRNA in the H358 LNP release screen sorted alphabetically. Average normalized LNP delivery is the average mCherry value normalized to the cell number control curve from the corresponding screen.*

H358- LNP release screen (+) EGF				Continued			
Gene	Average normalised LNP delivery	STD	N	Gene	Average normalised LNP delivery	STD	N
MARK4	0.33948761	0.05078133	8	CDKN1B	0.97351418	0.20574506	8
EGFR	0.46671902	0.08475089	8	DUSP7	0.9980058	0.1067194	8
LRRK1	0.4907337	0.27288494	8	NEK7	1.00611714	0.14068237	8
PTEN	0.50792134	0.02057781	8	KHK	1.02538076	0.08681478	8
FBXL22	0.52289787	0.09378237	8	PTPRR	1.02970164	0.12465988	8
NLRC5	0.54724576	0.11945574	8	RPS6KL1	1.03271633	0.16124484	8
PPP1R16B	0.55822863	0.13579312	8	FBP2	1.04839575	0.15826746	8
EPHA4	0.56253888	0.06467561	8	PTPRZ1	1.10650355	0.1168016	8
ALPPL2	0.5659647	0.12458063	8	FBXL13	1.11663624	0.22447179	8
CTBP1	0.5954591	0.19998388	8	PEAK1	1.14512917	0.15885082	8
PTK2	0.61397587	0.10790394	8	DUSP10	1.15702685	0.03284562	8
RFK	0.62315568	0.23447338	8	CLTC	1.18548236	0.12628998	8
PAK1	0.69682496	0.14420488	8	PPP4R1	1.23152726	0.12321344	8
HIPK3	0.70671129	0.07168687	8	TULP4	1.25177015	0.11381533	8
BMPR1A	0.71675166	0.08860288	8	TBCK	1.41128232	0.19605403	8
FBXO22	0.71964084	0.13942567	8	IRAK3	1.48895652	0.16434608	8
NTRK1	0.73761438	0.08922931	8	NEK5	1.53829664	0.1853098	8
FGFRL1	0.75167966	0.07109177	8	DUSP19	1.54866958	0.21357254	8
PIK3C2A	0.8022031	0.13454812	8	PPP6C	1.56807393	0.14040618	8
FBXO3	0.85212502	0.19997507	8	TAOK1	1.65314939	0.18231378	8
FBXO41	0.87032762	0.12951919	8	NUCKS1	1.66364618	0.33718509	8
BMP2K	0.92595094	0.25129347	8	NUDT3	1.69286842	0.16193182	8
PFKFB2	0.92792991	0.12370572	8	MAP2K5	2.16789036	0.18123641	8
PIK3C2B	0.95220125	0.12157162	8	SRMS	2.92914193	0.4150003	8

Table5.06: ***Overall data from the H358 LNP release screen with EGF stimulation sorted by average release.*** *The average normalized LNP delivery for each siRNA in the H358 LNP release screen sorted alphabetically. Average normalized LNP delivery is the average mCherry value normalized to the cell number control curve from the corresponding screen.*

H358- LNP release screen (-) EGF				Continued			
Gene	Average normalised LNP delivery	STD	N	Gene	Average normalised LNP delivery	STD	N
ALPPL2	0.5277337	0.1207073	8	NEK5	1.43954575	0.08317926	8
BMP2K	0.87853429	0.18114734	8	NEK7	0.92747097	0.09123022	8
BMPR1A	0.79676509	0.01774349	8	NLRC5	0.50003157	0.10795889	8
CDKN1B	0.98985207	0.10734318	8	NTRK1	0.70885135	0.02616739	8
CLTC	1.10973316	0.28098601	8	NUCKS1	1.38628802	0.04980385	8
CTBP1	0.52834341	0.14493615	8	NUDT3	1.63624507	0.02027996	8
DUSP10	1.15406425	0.14048108	8	PAK1	0.60201434	0.18612958	8
DUSP19	1.5946245	0.1194606	8	PEAK1	1.23086883	0.13653494	8
DUSP7	1.03029244	0.00281313	8	PFKFB2	0.90402841	0.11845464	8
EGFR	0.40858848	0.09059661	8	PIK3C2A	0.86371756	0.10571166	8
EPHA4	0.51121803	0.06355137	8	PIK3C2B	0.98999804	0.04488504	8
FBP2	0.90876375	0.15544862	8	PPP1R16B	0.55869791	0.10235336	8
FBXL13	0.92693369	0.05027976	8	PPP4R1	1.15090893	0.00682721	8
FBXL22	0.50422052	0.09270382	8	PPP6C	1.49169001	0.05544544	8
FBXO22	0.58817278	0.15861679	8	PTEN	0.48314389	0.038723	8
FBXO3	0.85104176	0.12494024	8	PTK2	0.56067463	0.12975767	8
FBXO41	0.7487899	0.01393696	8	PTPRR	0.88663587	0.06689844	8
FGFRL1	0.73946878	0.03376093	8	PTPRZ1	0.94845941	0.08020777	8
HIPK3	0.68024134	0.08552813	8	RFK	0.56850651	0.19948566	8
IRAK3	1.4181559	0.14597005	8	RPS6KL1	0.96407093	0.06895224	8
KHK	1.13843324	0.07405164	8	SRMS	2.96508322	0.06833802	8
LRRK1	0.51473853	0.21339818	8	TAOK1	1.24269244	0.24970323	8
MAP2K5	2.12441745	0.04706794	8	TBCK	1.40119019	0.07824866	8
MARK4	0.31753576	0.05286446	8	TULP4	1.17289578	0.21730387	8

Table5.07: ***Overall data from the H358 LNP release screen under no stimulation sorted alphabetically.*** *The average normalized LNP delivery for each siRNA in the H358 LNP release screen sorted alphabetically. Average normalized LNP delivery is the average mCherry value normalized to the cell number control curve from the corresponding screen.*

H358- LNP release screen (-) EGF				Continued			
Gene	Average normalised LNP delivery	STD	N	Gene	Average normalised LNP delivery	STD	N
MARK4	0.31753576	0.05286446	8	FBP2	0.90876375	0.15544862	8
EGFR	0.40858848	0.09059661	8	FBXL13	0.92693369	0.05027976	8
PTEN	0.48314389	0.038723	8	NEK7	0.92747097	0.09123022	8
NLRC5	0.50003157	0.10795889	8	PTPRZ1	0.94845941	0.08020777	8
FBXL22	0.50422052	0.09270382	8	RPS6KL1	0.96407093	0.06895224	8
EPHA4	0.51121803	0.06355137	8	CDKN1B	0.98985207	0.10734318	8
LRRK1	0.51473853	0.21339818	8	PIK3C2B	0.98999804	0.04488504	8
ALPPL2	0.5277337	0.1207073	8	DUSP7	1.03029244	0.00281313	8
CTBP1	0.52834341	0.14493615	8	CLTC	1.10973316	0.28098601	8
PPP1R16B	0.55869791	0.10235336	8	KHK	1.13843324	0.07405164	8
PTK2	0.56067463	0.12975767	8	PPP4R1	1.15090893	0.00682721	8
RFK	0.56850651	0.19948566	8	DUSP10	1.15406425	0.14048108	8
FBXO22	0.58817278	0.15861679	8	TULP4	1.17289578	0.21730387	8
PAK1	0.60201434	0.18612958	8	PEAK1	1.23086883	0.13653494	8
HIPK3	0.68024134	0.08552813	8	TAOK1	1.24269244	0.24970323	8
NTRK1	0.70885135	0.02616739	8	NUCKS1	1.38628802	0.04980385	8
FGFRL1	0.73946878	0.03376093	8	TBCK	1.40119019	0.07824866	8
FBXO41	0.7487899	0.01393696	8	IRAK3	1.4181559	0.14597005	8
BMPR1A	0.79676509	0.01774349	8	NEK5	1.43954575	0.08317926	8
FBXO3	0.85104176	0.12494024	8	PPP6C	1.49169001	0.05544544	8
PIK3C2A	0.86371756	0.10571166	8	DUSP19	1.5946245	0.1194606	8
BMP2K	0.87853429	0.18114734	8	NUDT3	1.63624507	0.02027996	8
PTPRR	0.88663587	0.06689844	8	MAP2K5	2.12441745	0.04706794	8
PFKFB2	0.90402841	0.11845464	8	SRMS	2.96508322	0.06833802	8

Table5.08: ***Overall data from the H358 LNP release screen under no stimulation sorted by average release.*** *The average normalized LNP delivery for each siRNA in the H358 LNP release screen sorted alphabetically. Average normalized LNP delivery is the average mCherry value normalized to the cell number control curve from the corresponding screen.*

5.5 LNP uptake screen +/- EGF stimulation in A431 cells

As the LNP uptake assay had not been optimised for the A431 cells, initially some optimisation experiments had to be performed to determine if the LNP uptake assay would function as expected in the A431 cell line. Due to circumstances, the A431 cells used for these experiments were not the same as used in the previous HRP delivery experiments. To distinguish the difference cell lines, the second type of A431 cells used will be referred to as A431-M cells with the screen referred to as the A431-M LNP screens. These cell lines were initially from the same patient sample and so will have similar characteristics. However due to separation and time, there might be differences between the two cell lines. Anecdotally, there is variations in A431 cells used in Sheffield with some having a ruffling phenotype which indicates their ability to perform macropinocytosis while others have a lower ability to perform macropinocytosis. Previous experiments had been performed using the ruffling A431 cells but as these cells could not be used for the LNP assay it was important to test the characteristics of the A431-M cells before performing an LNP uptake screen.

5.5.1 A431-M cell line validation

5.5.1.1 Growth rate and seeding density of A431-M cells

In order to use the A431-M cells in a 384 well plate, the seeding density had to be optimised to result in the optimum cell number for imaging. As the A431 cells require cell-to-cell contacts they grow in clusters which can make imaging difficult. Proper optimisation of seeding density is required for automated imaging to ensure each field of view acquired during microscopy contains a similar number of cells. Different concentrations of cells per well were seeded and incubated for 3 days (Figure5.19). Representative images were acquired and 6000 cells per well was selected as an optimum number of cells per field of view. This experiment highlighted a difference between the two A431 cells, with the A431-M cells having a slower growth characteristic as more cells per well were required for optimum density.

A

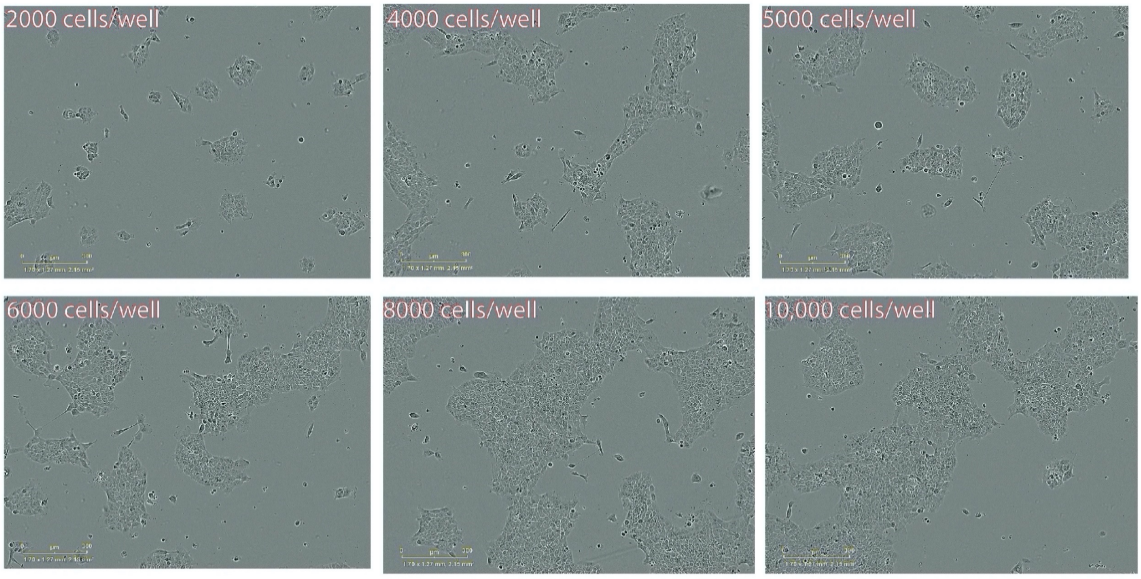

Figure5.19 ***: A431-M cells growth characteristics at different seeding densities.*** *A431-M cells were seeded at different cell densities in a 384 well plate. The cell density was monitored using an Incucyte microscope and brightfield images were acquired periodically over 3 days. A) Brightfield images acquired for each seeding density on day 3 after seeding. Figure shows representative images from 24 wells for each seeding density from 1 independent experiment*

5.5.1.2 The effect of EGF on dextran uptake

To verify the A431-M cells had similar responses to EGF, a dextran uptake assay was performed to observe macropinocytosis. A431-M cells were plated into a 384 well plate and incubated with 70 kDa dextran for different times in the absence or presence of EGF (100ng/ml) and then fixed with 4% PFA. The total fluorescence per cell was calculated using automated analysis on automated microscopy images. There was an EGF dependent increase in dextran uptake for the A431-M cells (Figure5.20) which is the same as the A431 cells used previously. The A431-M cells showed very little basal macropinocytosis in the absence of EGF (compare –EGF with 0 time point). This is a difference compared to the original A431 cell line as those cells displayed a higher basal macropinocytosis rate.

Previously the experiments involving stimulation with EGF were performed after serum starvation for 2 hours in order to reduce basal signalling from growth factors found in serum. For the LNP uptake experiments, a serum starvation step was not possible due to an inability to wash plates in a sterile environment. Due to this, it was required to test whether serum starvation was necessary for EGF dependent macropinocytosis in A431M cells and this was achieved using a 70kD dextran uptake assay. At multiple time points, the effect of serum starvation on the degree of macropinocytosis induced by EGF was not significant, indicating

that serum starvation was not vital in order to see a an EGF dependent response (Figure 5.20B). This validated that the LNP uptake screen could be performed without serum starvation in the A431-M cell line.

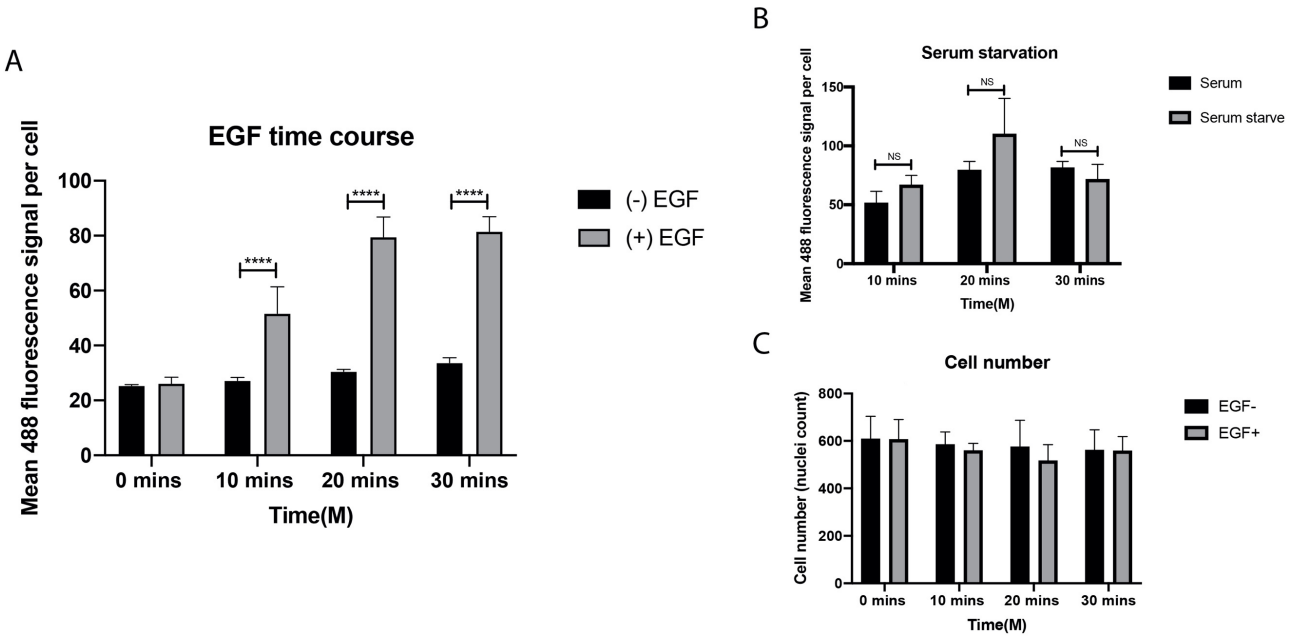

*Figure5.20**: Assessing the macropinocytosis ability of A431-M cell line using a dextran uptake assay.** A431-M cells were seeded in a 384 well plate on day 0 and incubated at 37℃ for 2 days. After the two days, some of the cells were serum starved for 2 hours prior to the experiment. Oregon green (70kDa) dextran addition was performed either under no stimulation or alongside EGF stimulation at 100ng/ml EGF. The dextran uptake was performed for different time points and cells were fixed by addition of 8% PFA (4% after dilution in the well). Cells were stained with Hoechst nuclei stain and images acquired using a Yokogowa Cell Voyager CV8000 plate format microscope. After image acquisition, Nuclei and cellular cytosol was detected by Hoechst signal thresholding. The mean signal from the 488 channel images was calculated per cell. A) The mean dextran signal was acquired for each time point for either (-) EGF or (+) EGF. B) The mean dextran signal for the different uptake time points under (+) EGF stimulation for both serum starved cells and without serum starvation to observe the effect of serum starvation. C) The nuclei count using the Hoechst staining as a control for the effect of (+) EGF stimulation on cell number. Data represents Mean + SD from one independent experiment, N=4 for each condition. A Two-way ANOVA was performed for both A) and B) with a Sidak's multiple comparison test, with ****p≤0.0001, *** p≤0.001, ** p≤0.01, * p≤0.05*

5.5.1.3 A431-M transfection optimisation

As the cells responded to EGF, the next optimisation step was the siRNA knockdown conditions. Two different transfection agents were tested, Polyfect and RNAi-MAX, at multiple concentrations (Figure5.21). PLK1 siRNA was used to monitor knockdown efficiency by observing cell death. RNAi-Max resulted in PLK1 induced cell death at all concentrations indicating siRNA transfection, whereas polyfect only resulted in PLK1 cell death at high concentrations (1 in 10 and 1 in 20). Additionally, high concentrations of polyfect were not tolerated by the RISC-free control siRNA wells resulting in cell death. Polyfect also had a

negative effect on the LNP-mCherry signal, resulting in a decreased signal when compared to RNAi-MAX. RNAi MAX was chosen for the A431 LNP uptake screen due to these reasons.

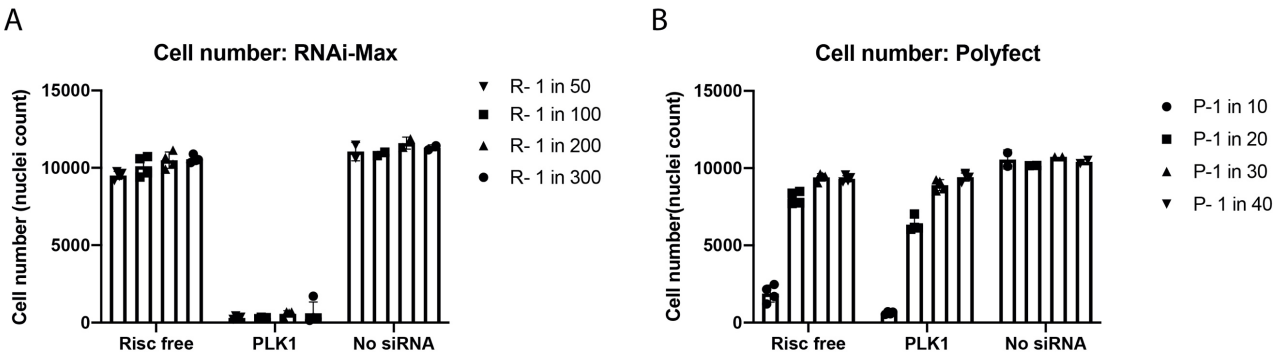

Figure5.21: ***Testing the Knockdown efficiency in A431-M cells using RNAi-Max and Polyfect.*** *A431-M cells were reverse transfected with Risc-Free siRNA, PLK1 siRNA or No siRNA. Different concentrations of transfection reagent were used for the reverse transfection and after 3 days the cells were fixed, Hoechst stained, and the cell count was performed using automated nuclei detection. PLK1 knockdown results in cell death and so the cell number is an indication of knockdown efficiency. The toxicity of the transfection reagent can also be assessed in in the cell count of the RISC-free condition. A) Reverse transfection using RNAi-Max transfection reagent. B) Reverse transfection using Polyfect transfection reagent. Data shows Mean + SD, N=4 for RISC-Free and PLK1 N=2 for No siRNA*

5.5.1.4 A431 LNP uptake optimisation

The dynamics of LNP uptake had to be optimised in the A431 cells to be sure an increase or decrease in delivery could be observed and that the signal was not saturated. Different concentrations of LNP were used for uptake and the mCherry value per cell calculated (Figure5.22). There was an increase in signal observed with increasing concentrations of LNP indicating that the assay signal was not at saturation and that increases in delivery would be detectable in the screen if 20ng of LNP was added per well. The same trend was seen with and without EGF stimulation but interestingly stimulation with EGF resulted in a decrease in m-Cherry per cell indicating less delivery. The increased amount of LNP did result in a decrease in cell number indicating increased toxicity as higher concentrations of LNPs were used (Figure5.22 B). As the cell number effects the mCherry signal observed per cell the value was normalised to cell number to confirm the increase in signal observed was due to the increase in LNP concentration and not the increased toxicity and therefore cell death. The

normalised values still increase as the concentration of LNP increases indicating that the trend is not due to cell death caused by increased toxicity. (Figure5.22 C)

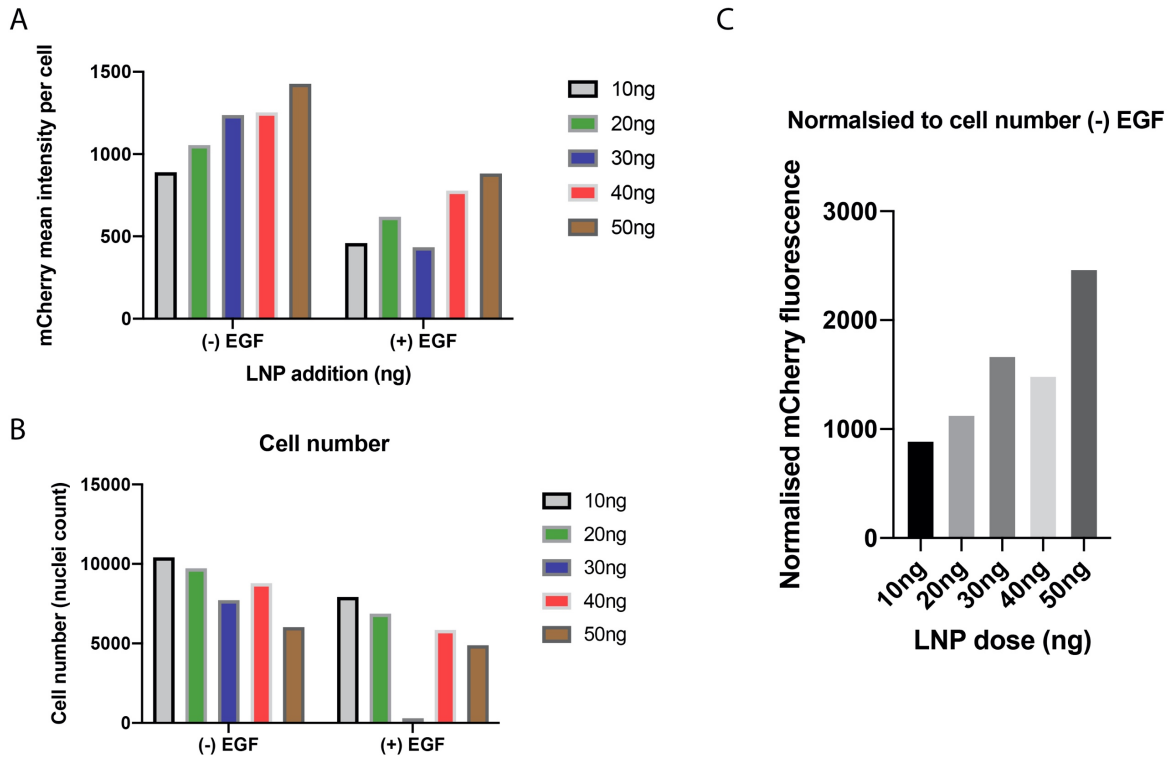

*Figure5.22: **Measuring the sensitivity of the LNP uptake assay in A431-M cells.** A431-M cells were reverse transfected with Risc-Free siRNA using RNAi-Max transfection reagent. After 3 days the cells were treated with mCherry LNP for 24 hours with and without EGF stimulation. Different amounts of LNP were added to observe the dynamic range of the assay in these cells. A) The effect of LNP concentration on the mean mCherry value observed in each cell. B) The effect of different LNP concentration on cell number. C) The normalized values of mean mCherry to cell number. Data shows Mean, N=1 for each LNP concentration*

5.5.2 LNP uptake screen in A431-M cells

The previous optimization studies showed that A431-M cells were a valid experimental system to use for an LNP uptake screen. In the next series of experiments, the same experimental setup was used as for the H358 LNP screen using the same siRNA library that included the hits identified from the HRP uptake screen. As this assay had not been performed previously, no positive control siRNA was known that effect LNP uptake in this cell line. It was decided to include the same control siRNA that were previously used in the H358 cell line (A, B and C) to allow comparison between the two LNP uptake screens and to observe if these control siRNA would have a similar effect in the A431-M cell line.

5.5.2.1 Cell number titration curve

As performed previously for the H358 LNP screen, a cell number normalisation curve was created for the A431-M cell line. Due to this being the first screen performed in these cells using this assay, the effect of cell number on LNP uptake and delivery was unknown. However, there was no reason to believe the A431 cells would have a different response to cell number and so a normalisation curve was performed. The mean mCherry values from the screen were normalised to the curve in order to correct for the siRNA effect on cell number. The curves previously generated in the H358 cell line were from a non-linear regression analysis. This was the case for the second A431-M repeat but the best fit for the normalisation curve in the first A431 repeat was a linear regression (Figure5.23). This might have had an effect on normalisation of the first repeat which might explain some differences between the repeats and the increased variability when compared to the H358 screens.

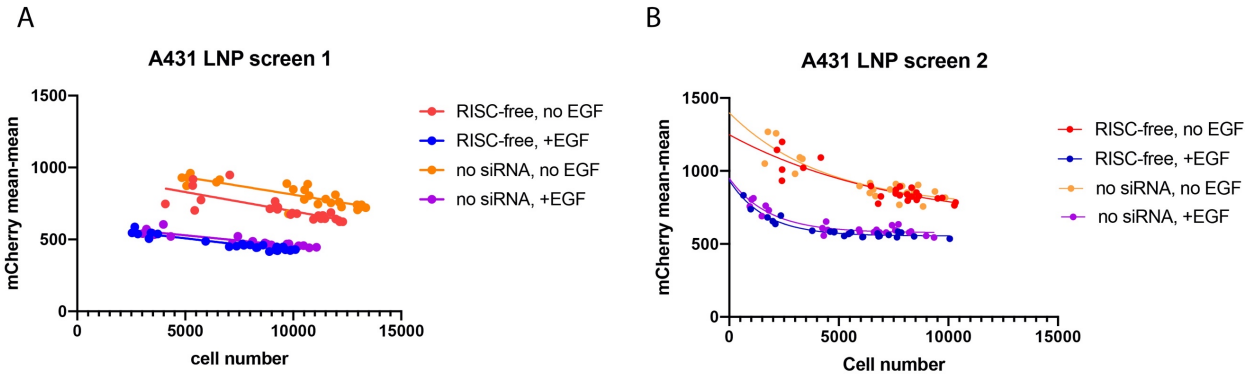

*Figure5.23: **A431 LNP screen cell number calibration curve.** During the LNP screen an additional plate was set up to generate the cell number calibration curve. Different numbers of cells were seeded to generate a calibration curve with different siRNA transfections using RNAi Max. After 3 days at 37°C the cells were treated with 20ng LNP + and – EGF for 24 hours. The mean mCherry signal per cell was calculated and the cell number was acquired by automated DAPI counting. Data is mean mCherry per cell plotted against mean nuclei count from 9 images taken across each well. A) 1st repeat for LNP uptake screen in A431-M cells, B) 2nd repeat for LNP uptake screen in A431-M cells*

5.5.2.2 The effect of 40ng LNP on uptake in A431-M cells

The addition of 40ng LNP per well compared to 20ng LNP was used as a control for uptake. Double the amount of LNP should result in an increase in productive delivery. This was the case with A431 cells that were not stimulated with EGF (Figure5.24) and resulted in an increase in the mean mCherry value per cell. When cells were stimulated with 100ng/ml EGF, 40ng LNP had no effect on the mean mCherry fluorescence. This suggests that EGF stimulation

in this assay effects the signal observed and might indicate that the mCherry value is no longer representative of LNP delivery.

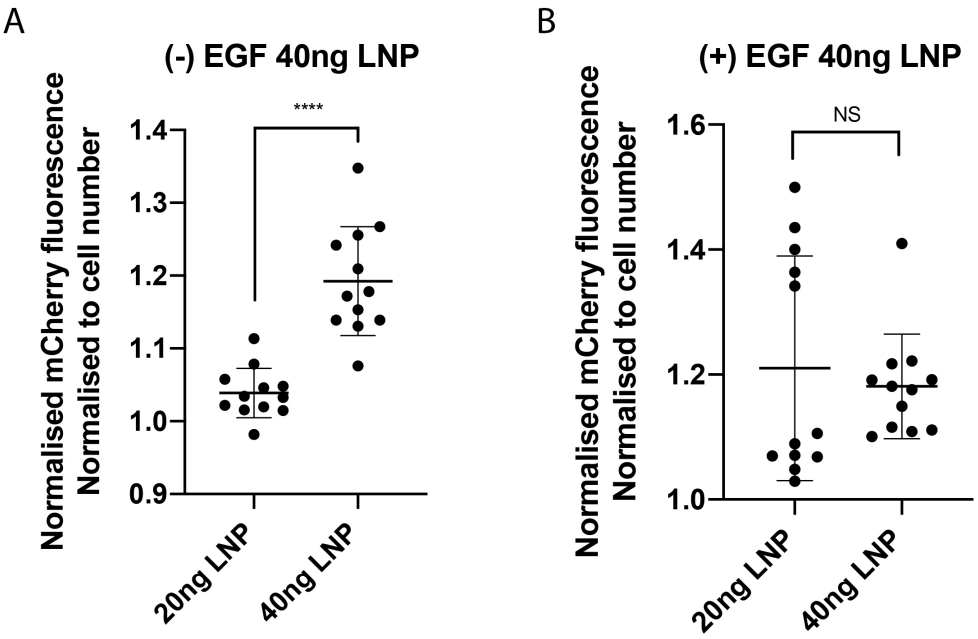

*Figure5.24: **Addition of 40ng LNP results in an increase in mCherry signal.** The addition of twice the concentration of LNP to wells as a control in the A431-M LNP uptake screen. A431-M cells were reverse transfected for 3 days followed by incubation with mCherry-LNP for 24 hours. EGF to a final concentration of 100ng/ml was used to stimulate cells at the same time as LNP addition. Here, cells treated with RISC-Free siRNA were incubated with either 20ng LNP or 40ng LNP plus and minus EGF. The mean mCherry signal per cell was calculated and a cell average per well was calculated. Data shows Mean + SD from two independent repeats with n≥20. An unpaired t test was performed, with ****p≤0.0001*

5.5.2.3 Control siRNA

The same control siRNA (A, B and C), were used for the A431 LNP uptake screen as with the H358 cells. It was unknown if these siRNA had the same effect as in the H358 cells, but they were included to allow direct comparison between the two screens. RISC-free siRNA was used as a neutral control that should not affect the assay as the siRNA does not engage with the RISC complex.

There was no statistical difference between the RISC-free siRNA treated cells when comparing to the siRNA used as positive controls in the H358 cells. There is a slight decrease in mCherry signal observed with Control C knockdown without EGF stimulation but is not statistically significant (Figure5.25). Additionally, the control siRNA B knockdown slightly increases the mCherry signal observed without EGF stimulation but not to the same extent as seen in the H358 LNP uptake screen. Control siRNA A did not have any noticeable change. The lack of

effect of the controls seen with these siRNA between the two LNP uptake screens could be due to differences in the dependency of the cell type on the protein being knocked down or different expression levels and degree of knockdown achieved in the two cell lines. We could not validate that the control siRNA A, B or C had an effect in A431 cells prior to the screen due to time and so we did not know if they would function the same as in H358 cells. Alternatively, the increased variability in the A431-M LNP uptake screen could account for the loss of significance of the control siRNA. The differences in the cell number titration curve could have resulted in changes to the normalised values, especially at lower cell numbers as the titration curve for the first A431 LNP uptake screen is linear (Figure5.23A). When comparing these two cell number titration curves, the cell numbers in the A431 LNP screen 1 are higher and the lowest cell number values are higher. The same number of cells were seeded for both cell titration curves but differences in cell conditions might have resulted in different growth amounts and cell number. These differences could explain the higher variability observed between the LNP screens in the two cell lines.

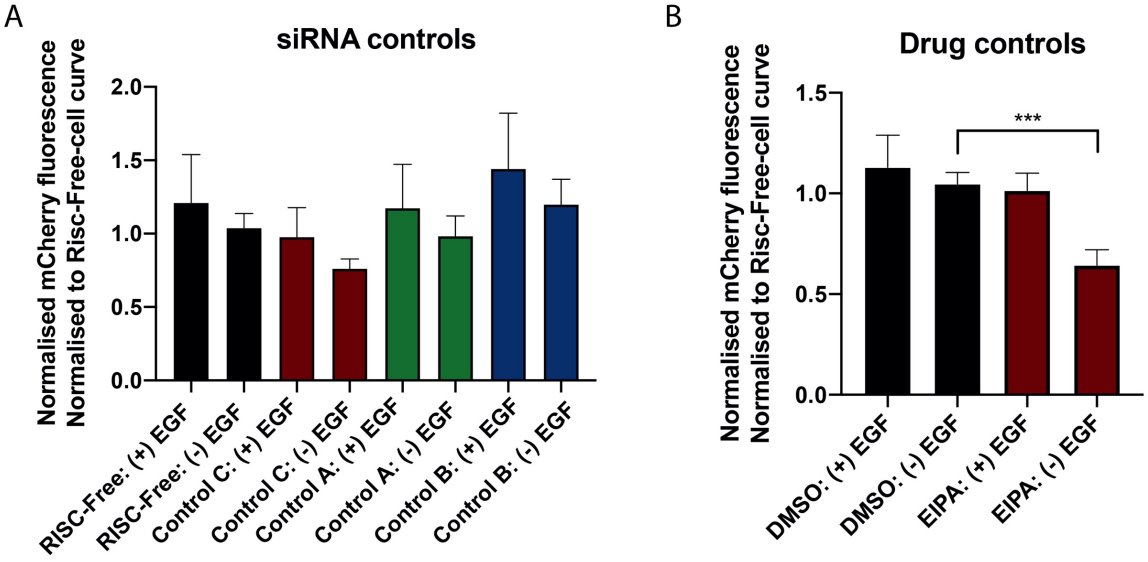

*Figure5.25: **Control siRNA and drug controls from the A431-M LNP screen.** Control siRNA and drug controls were dispersed throughout the screening plates to control for siRNA transfection and liquid handling. A) Control siRNA reverse transfection followed by addition of LNP for 24 hours B) Risc-Free control siRNA reverse transfection for 3 days followed by addition of LNP and drug controls for 24 hours. Data shows Mean + SD from 2 independent experiments. A One-way ANOVA with Tukey's multiple comparisons test was performed, with ****p≤0.0001, *** p≤0.001, ** p≤0.01, * p≤0.05*

5.5.2.4 PLK1 silencing effects cell number

The silencing of PLK1 results in reduction of cell viability and so can be used as a control for knockdown efficiency. The PLK1 silencing resulted in complete loss of cell viability indicating that sufficient knockdown was achieved in both A431 LNP screens performed (Figure5.26). The use of the PLK1 control allows confidence that proper knockdown was achieved in the experimental conditions and there was not an error during liquid handling using automated machinery. The distribution of PLK1 across the plate layout allows identification of any errors in liquid handling.

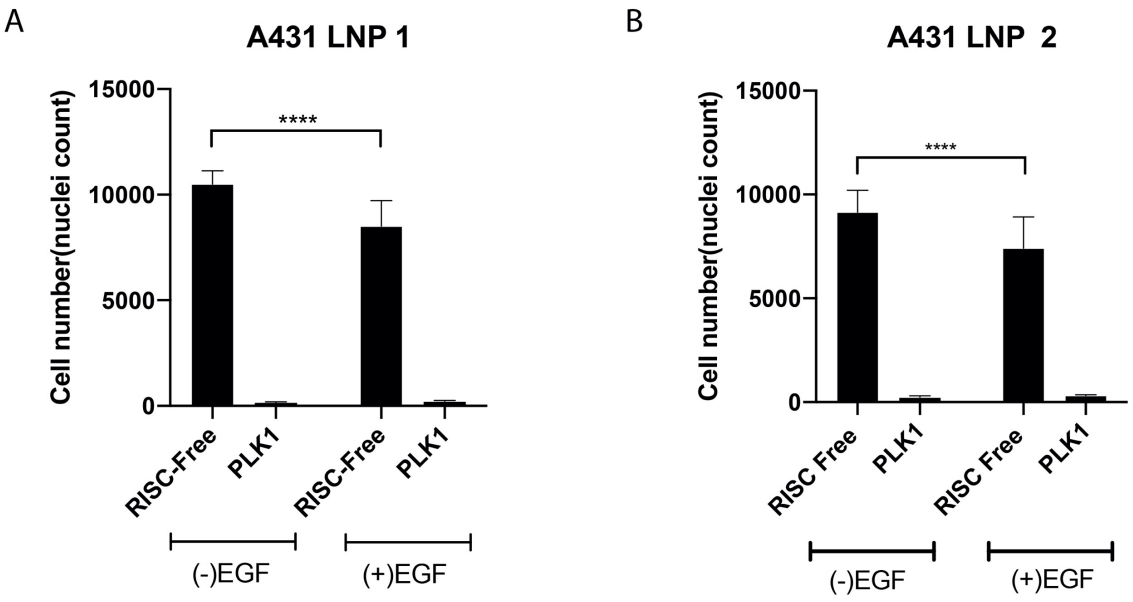

Figure 5.26: ***Knockdown of PLK1 results in cell death.*** *As a control for knockdown in the H358 LNP uptake screen, PLK1 siRNA was used. PLK1 siRNA was reverse transfected using RNAiMax reagent. Cell death in the PLK1 control indicates successful knock down. A + B) Knockdown of PLK1 from the first and second A431-M LNP screens, respectively. Nuclei were counted after 3-day knockdown and 24-hour LNP uptake, using Hoechst staining. Automated analysis was utilized to detect nuclei using the Hoechst staining and automated thresholding. Data shows Mean + SD from two independent experiments, N=12. A Two-way ANOVA with Sidak's multiple comparisons test was performed, with ****p≤0.0001, *** p≤0.001, ** p≤0.01, * p≤0.05*

5.5.2.5 The effect of Pharmacological inhibitors on LNP delivery in A431-M cells

Similar to the H358 LNP screen, pharmacological inhibitors were included in the A431-LNP screen. EIPA, an inhibitor of macropinocytosis was included. Inhibition of macropinocytosis with EIPA resulted in a significant decrease of LNP delivery without EGF stimulation which is the same effect observed in the H358 cells (Figure5.25B). Therefore, macropinocytosis

appears to be a major uptake mechanism for the LNP particles in both cell lines. Interestingly EIPA had no effect on cells that were treated with EGF. A carrier control, in which the same volume of DMSO was added, had no effect on delivery when compared to the RISC-free control.

5.5.2.6 EGF stimulation decreases LNP uptake in A431-M cells

It was discovered that EGF stimulation did not have an effect on the delivery of LNP particles in the H358 cells but in the A431-M cells, 24 hour treatment with EGF decreased the amount of mCherry signal observed per cell. This can be seen in the cell number calibration curve for the A431 LNP-screen (Figure5.23) which shows the EGF treatment reduces the mCherry signal observed. As the values are normalised to this curve this effect is not seen the in the normalised data (Figure5.27) but can be seen when comparing the raw values. This decrease in signal indicates that either EGF is inhibiting LNP delivery but more probably, the long EGF stimulation of 24hours is having an effect on cellular process which result in a decrease in mCherry signal observed.

A

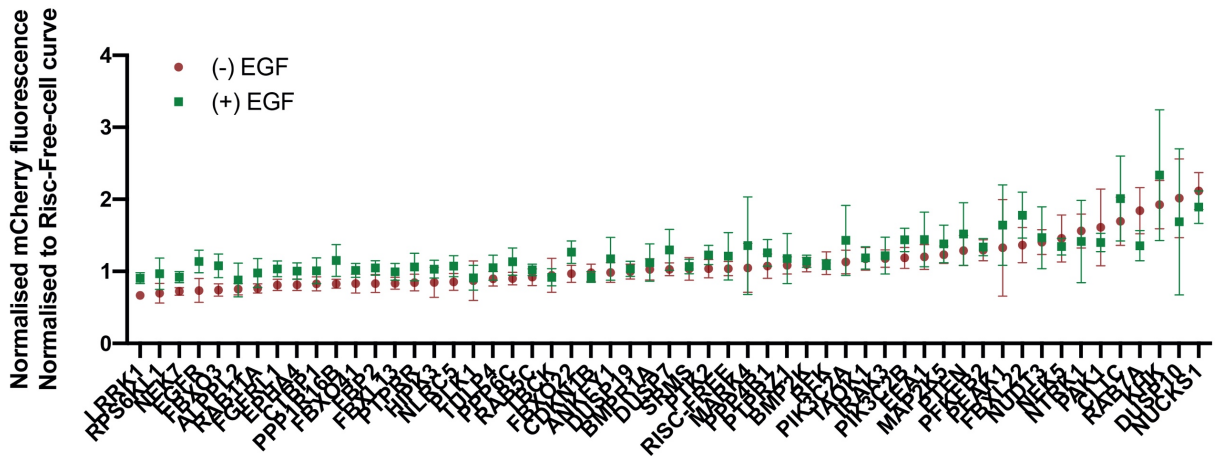

Figure 5.27: ***The effect of EGF on the uptake of LNP with each siRNA.*** *A comparison between the mCherry signal from LNP delivery for each siRNA with EGF stimulation and without stimulation. Data shown is a combined value of the two repeat screens and data with and without EGF stimulation is plotted superimposed. Data shows Mean + SD from two repeat screen N=8 for each siRNA.*

5.5.2.7 Stimulation of cells with EGF decreases surface EGFR in A431-M cells

To observe the effect of 24-hour EGF stimulation has on the cell, an antibody against EGFR was utilized. Cells from the LNP uptake screens were stained with an anti-EGFR antibody to assay the level of EGFR after 24-hour treatment. Risc-free siRNA cells which were treated with

and without EGF from both screens, H358 and A431-M, were stained. A431-M cells not treated with EGF have an EGFR staining pattern on the cell membrane. After EGF treatment for 24 hours, there is no EGFR staining on the cell membrane with limited intracellular staining. This indicates that after 24-hour EGF treatment there is a large reduction of cell surface EGFR which could be due to over activation and degradation (Figure5.28). Interestingly there is little change in the EGFR staining in the H358 cells after 24-hour. There is overall less staining in the H358 cells compared to the A431-M cells as A431 cells are known to have a large amounts of EGFR expression. The difference in response to EGFR could explain the effect seen in the screen with EGF treatment. In the H358 cells, EGF treatment had very little effect on the delivery and expression of mCherry LNP whereas in the A431-M screen the treatment with EGF resulted in a decrease in mCherry signal observed. The effect on EGFR surface levels in the A431-M cells could explain this result as the long treatment with EGF might affect subsequent mCherry processing after delivery.

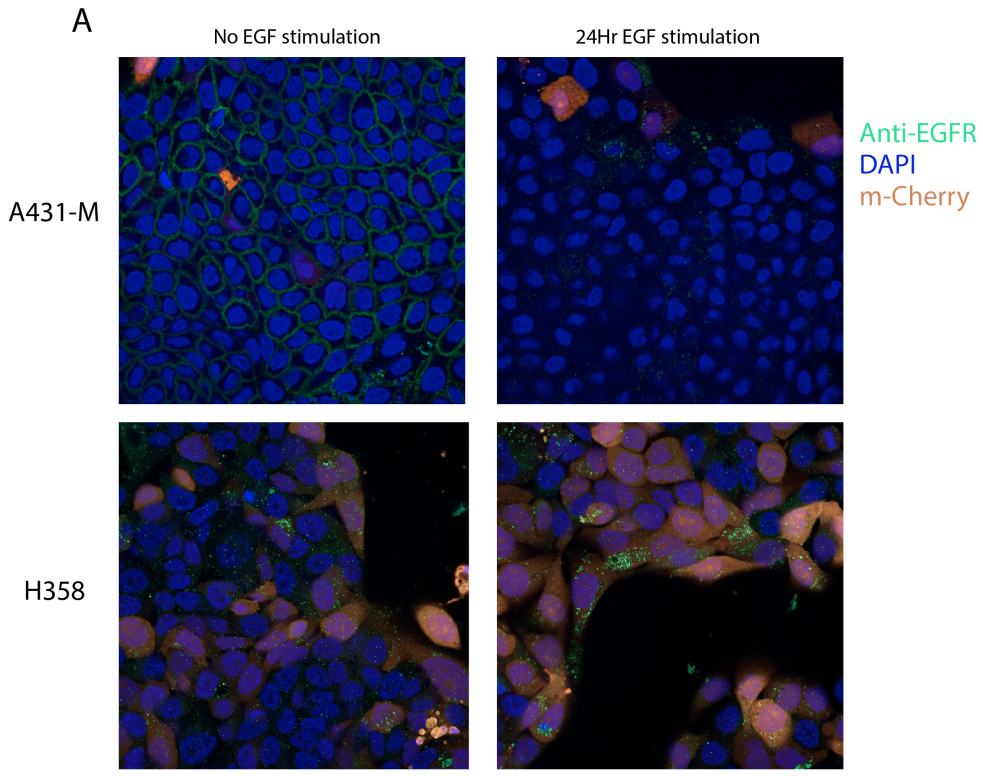

Figure 5.28: ***Anti EGFR staining to observe the effect of EGF stimulation on the two cell types, A431-M and H358.*** *Control RISC-free siRNA from both screens were stained using an anti-EGFR antibody. The LNP screens using H358 cells and A431-M cells were re stained using an immunofluorescence protocol after the cells were fixed during the initial screens. In the original screen, cells were reverse transfected with RISC-free siRNA using RNAiMax transfection reagent. After 3 days, cells were treated with LNP + and – EGF treatment. After 24 hours, the cells were fixed using 4% PFA and imaged using an automated confocal microscope. After initial imaging and analysis, plates were stained using Anti-EGFR antibody and re-imaged.*

5.5.2.8 EGFR knockdown does not reduce mCherry expression with EGF stimulation in A431-M cells

An additional control siRNA was included in the pool of siRNA chosen to be used in the LNP screen validation. Knockdown of EGFR was used in the HRP release screen as a control as it reduced the EGF dependent release of HRP. Interestingly the knockdown of EGFR reduced the mCherry expression, and so the delivery of LNP, in the H358 LNP uptake screen (Figure 5.29). This effect was observed plus and minus EGF stimulation indicating that EGFR is important for the delivery of LNP or that loss of EGFR reduces the capacity of the cells to take up LNP's. However, in A431-M cells the knockdown of EGFR only decreases the mCherry signal in the absence of EGF. In cells stimulated with EGF for 24 hours, no difference was seen between RISC-free and EGFR siRNA. This result could be supported by the EGFR localisation immunostaining as EGF treatment in the A431-M cells seemed to result in degradation of EGFR. The Knock down of EGFR using siRNA reduced mCherry expression in all conditions apart from in A431-M cells treated with EGF for 24 hours and from the immunostaining, the levels of EGFR are depleted in these cells by the EGF treatment and so the knockdown of EGFR by the siRNA does not have an additive effect and so could explain why no effect on LNP delivery was seen.

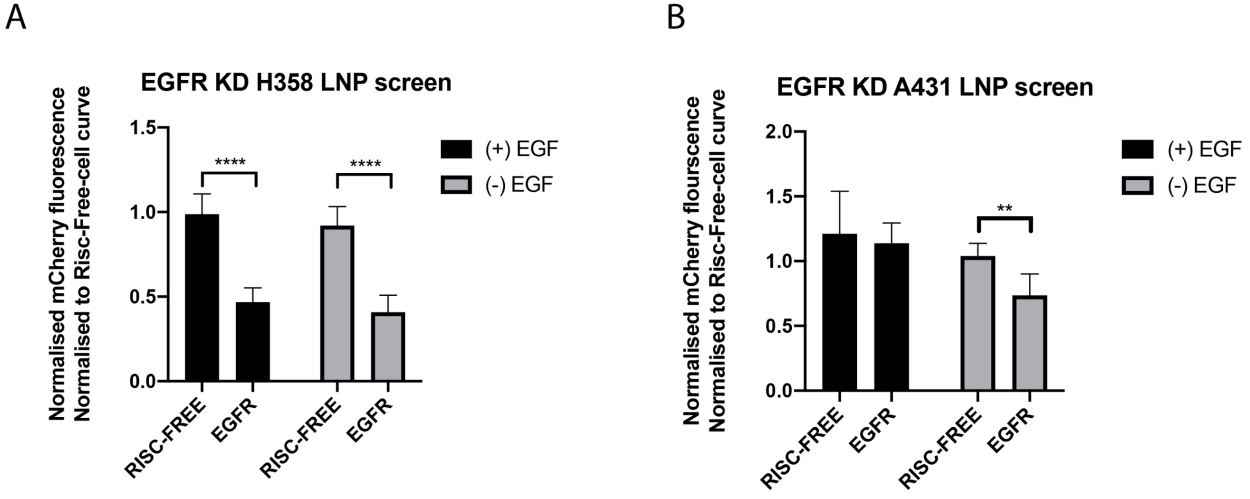

*Figure5.29: **The effect of EGFR knockdown on mCherry expression.** EGFR siRNA was included in the pool of siRNA used for screening. The data shown is from the mCherry-LNP uptake screen in A) H358 cells and B) A431 cells. Cells were reverse transfected onto siRNA using RNAi-MAX reagent and incubated at 37℃ for 3 days. After 3 days, cells were treated with 20ng LNP-mCherry with or without the addition of EGF. After 24 hours at 37℃ cells were fixed and imaged using an automated plate microscope. Automated analysis calculated the mCherry fluorescence per cell and this was normalised to the cell titration curve from the screen. RISC-free siRNA was used as a negative control as the siRNA does not engage the RISC complex. Data shows mean + SD with N=24 for RISC-free and N=8 for EGFR. A Two-way ANOVA with Sidak's multiple comparisons test was performed, with ****p≤0.0001, *** p≤0.001, ** p≤0.01, * p≤0.05*

5.5.2.9 *Identification of hits from the A431-M screen*

The siRNA that resulted in an increase in LNP delivery and so mCherry signal above that of the 40ng LNP controls were designated as positive hits (Figure5.30). These hits were compared to the LNP uptake screen in the H358 cell line as well as to the HRP uptake screen performed in the A431 ruffling cells. As the two assays were performed under different conditions and the entry mechanism of HRP and the LNP likely to be different, the identification of 4 hits that were positive regulators of release in all forms of the screens was encouraging. The 4 hits identified in all of the screens were IRAK3, MAP2K5, NUCKS1 and PEAK1. These 4 hits were then taken forward to further validation.

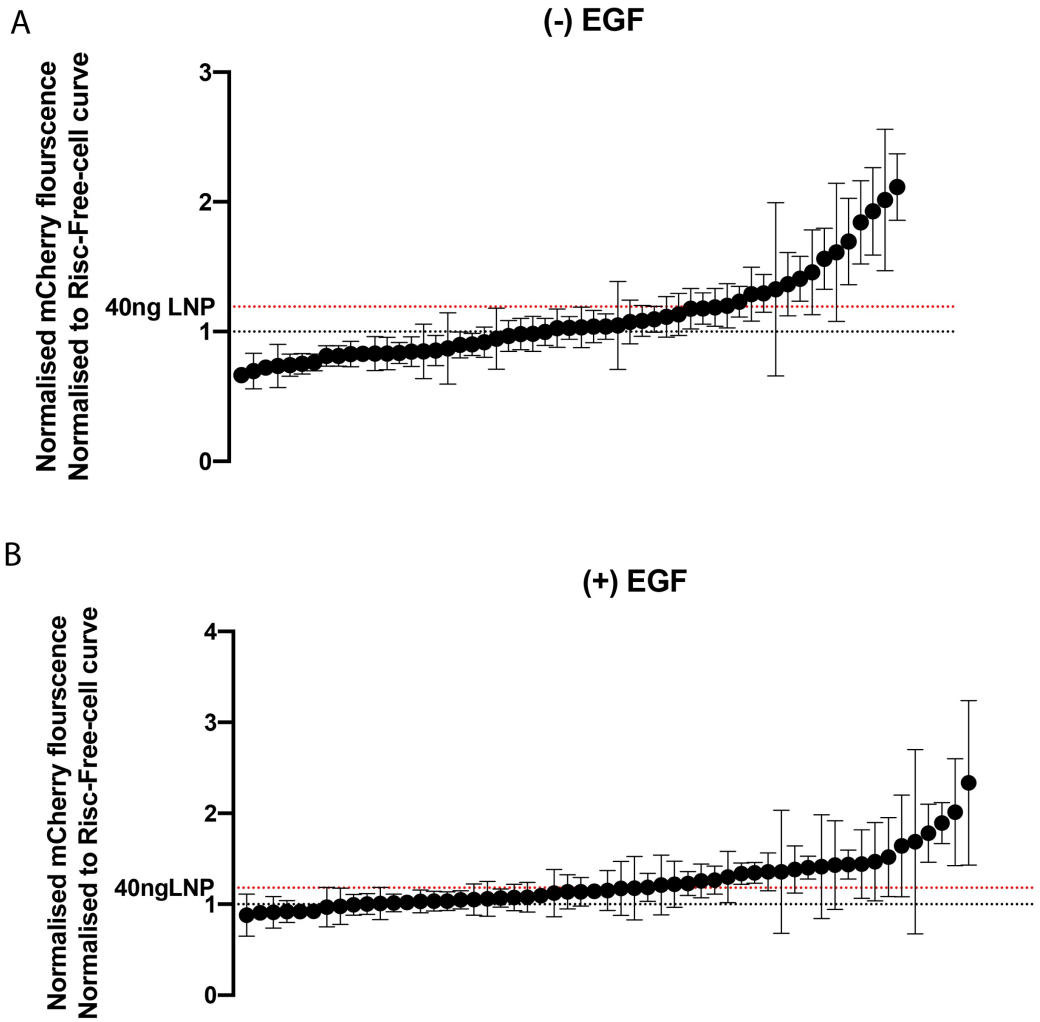

*Figure5.30: **Overview of hits identified compared to 40ng LNP control.** The mean normalized mCherry signal for each siRNA was ordered in increasing value for the A431-M LNP uptake screens. The mCherry signal was normalized to the cell titration curve and plotted with the value for the 40ngLNP control plotted as a red line on the Y axis to compare the effect on LNP delivery of the top hits. Data shown is Mean + SD from the two independent screens. Each siRNA N = 8*

A431- LNP release screen (+) EGF				Continued			
Gene	Average normalised LNP delivery	STD	N	Gene	Average normalised LNP delivery	STD	N
ALPPL2	0.8807507	0.23254065	8	NEK5	1.34446156	0.11489961	8
ANKFY1	1.17458849	0.2984404	8	NEK7	0.91982949	0.07635147	8
BMP2K	1.14159139	0.08372473	8	NLRC5	1.07351268	0.14485849	8
BMPR1A	1.1224842	0.25973499	8	NTRK1	1.41491108	0.57106522	8
CDKN1B	0.92174703	0.07621345	8	NUCKS1	1.89161952	0.22686287	8
CLTC	2.01164841	0.58849598	8	NUDT3	1.46733165	0.43000469	7
CTBP1	1.00874066	0.17762952	8	PAK1	1.40142159	0.12665599	8
DUSP10	1.68841047	1.01452973	8	PEAK1	1.64270874	0.55854575	8
DUSP19	1.03552186	0.1048488	8	PFKFB2	1.33754998	0.11887531	8
DUSP7	1.29884437	0.28361695	8	PIK3C2A	1.43026652	0.48768904	8
EEA1	1.44277805	0.37858162	7	PIK3C2B	1.43763721	0.16212638	8
EGFR	1.13739967	0.15713352	8	PPP1R16B	1.15102519	0.21920682	8
EPHA4	1.00379868	0.11483236	8	PPP4R1	1.25719669	0.18483791	8
FBP2	1.04743334	0.09979247	8	PPP6C	1.13605619	0.18867078	8
FBXL13	0.99341987	0.11616541	8	PTEN	1.52022936	0.43438047	8
FBXL22	1.78105959	0.31976756	8	PTK2	1.2271349	0.13318988	8
FBXO22	1.26663718	0.15533396	8	PTPRR	1.05981447	0.19056854	8
FBXO3	1.07751838	0.16267517	8	PTPRZ1	1.17723872	0.34807454	8
FBXO41	1.01327105	0.09662804	8	RAB11A	0.97767975	0.1990945	8
FGFRL1	1.03541306	0.10863119	8	RAB5C	1.0207107	0.08048366	8
HIPK3	1.03086369	0.12505678	8	RFK	1.09480059	0.06774322	8
IRAK3	1.21879048	0.25512143	8	RPS6KL1	0.96826881	0.21753521	8
KHK	2.33597833	0.9061615	8	SRMS	1.06835463	0.10074159	8
LRRK1	0.90505796	0.07436812	8	TAOK1	1.18638949	0.15565896	8
MAP2K5	1.38169095	0.26146459	8	TBCK	0.9187657	0.11983261	8
MARK4	1.35687004	0.67610017	8	TULP4	1.04994073	0.1736056	8

*Table5.09**: Overall data from the A431 LNP release screen with EGF stimulation.** The average normalized LNP delivery for each siRNA in the A431 LNP release screen sorted alphabetically. Average normalized LNP delivery is the average mCherry value normalized to the cell number control curve from the corresponding screen.*

A431- LNP release screen (-) EGF				Continued			
Gene	Average normalised LNP delivery	STD	N	Gene	Average normalised LNP delivery	STD	N
ALPPL2	0.75199063	0.07956478	8	NEK5	1.45700275	0.32695056	8
ANKFY1	0.9839512	0.13712399	8	NEK7	0.72250684	0.05135328	8
BMP2K	1.09448775	0.10011598	8	NLRC5	0.85471114	0.11718334	8
BMPR1A	1.02754555	0.14863376	8	NTRK1	1.56080815	0.23620536	8
CDKN1B	0.9805653	0.12060748	8	NUCKS1	2.11539949	0.25694476	8
CLTC	1.69538638	0.33307952	8	NUDT3	1.40660522	0.1733181	8
CTBP1	0.82732699	0.09751759	8	PAK1	1.61098175	0.53335664	8
DUSP10	2.01553094	0.5459024	8	PEAK1	1.32665461	0.66882551	8
DUSP19	0.99749984	0.10306815	8	PFKFB2	1.29411272	0.14580327	8
DUSP7	1.02881276	0.08814549	8	PIK3C2A	1.13227581	0.16328442	8
EEA1	1.19979627	0.17133222	8	PIK3C2B	1.18645969	0.14538371	8
EGFR	0.73503759	0.16647143	8	PPP1R16B	0.82818925	0.06195064	8
EPHA4	0.81308182	0.08057867	8	PPP4R1	1.07395897	0.16890267	8
FBP2	0.83133367	0.12526398	8	PPP6C	0.90157903	0.08645696	8
FBXL13	0.83526731	0.08097535	8	PTEN	1.2897538	0.20897801	8
FBXL22	1.36559291	0.24353145	8	PTK2	1.03838656	0.12642357	8
FBXO22	0.96591629	0.11891879	8	PTPRR	0.84478652	0.11536212	8
FBXO3	0.74182112	0.0852003	8	PTPRZ1	1.0832846	0.11904844	8
FBXO41	0.83091996	0.13106695	8	RAB11A	0.76270065	0.06420873	8
FGFRL1	0.81193133	0.07953354	8	RAB5C	0.91916904	0.11658459	8
HIPK3	0.84794345	0.2095584	8	RFK	1.11384649	0.15657219	8
IRAK3	1.17830824	0.12086613	8	RPS6KL1	0.69647624	0.13736949	8
KHK	1.92745495	0.33665983	8	SRMS	1.03339425	0.1569152	8
LRRK1	0.66510014	0.05452017	8	TAOK1	1.17571821	0.15747434	8
MAP2K5	1.22999158	0.12009558	8	TBCK	0.94512301	0.23612951	8
MARK4	1.04829419	0.33895578	8	TULP4	0.89828469	0.10063724	8

*Table5.10: **Overall data from the A431 LNP release screen without EGF stimulation.** The average normalized LNP delivery for each siRNA in the A431 LNP release screen sorted alphabetically. Average normalized LNP delivery is the average mCherry value normalized to the cell number control curve from the corresponding screen.*

A431- LNP release screen (+) EGF				Continued			
Gene	Average normalised LNP delivery	STD	N	Gene	Average normalised LNP delivery	STD	N
ALPPL2	0.8807507	0.23254065	8	PPP1R16B	1.15102519	0.21920682	8
LRRK1	0.90505796	0.07436812	8	ANKFY1	1.17458849	0.2984404	8
TBCK	0.9187657	0.11983261	8	PTPRZ1	1.17723872	0.34807454	8
NEK7	0.91982949	0.07635147	8	TAOK1	1.18638949	0.15565896	8
CDKN1B	0.92174703	0.07621345	8	IRAK3	1.21879048	0.25512143	8
RPS6KL1	0.96826881	0.21753521	8	PTK2	1.2271349	0.13318988	8
RAB11A	0.97767975	0.1990945	8	PPP4R1	1.25719669	0.18483791	8
FBXL13	0.99341987	0.11616541	8	FBXO22	1.26663718	0.15533396	8
EPHA4	1.00379868	0.11483236	8	DUSP7	1.29884437	0.28361695	8
CTBP1	1.00874066	0.17762952	8	PFKFB2	1.33754998	0.11887531	8
FBXO41	1.01327105	0.09662804	8	NEK5	1.34446156	0.11489961	8
RAB5C	1.0207107	0.08048366	8	MARK4	1.35687004	0.67610017	8
HIPK3	1.03086369	0.12505678	8	MAP2K5	1.38169095	0.26146459	8
FGFRL1	1.03541306	0.10863119	8	PAK1	1.40142159	0.12665599	8
DUSP19	1.03552186	0.1048488	8	NTRK1	1.41491108	0.57106522	8
FBP2	1.04743334	0.09979247	8	PIK3C2A	1.43026652	0.48768904	8
TULP4	1.04994073	0.1736056	8	PIK3C2B	1.43763721	0.16212638	8
PTPRR	1.05981447	0.19056854	8	EEA1	1.44277805	0.37858162	7
SRMS	1.06835463	0.10074159	8	NUDT3	1.46733165	0.43000469	7
NLRC5	1.07351268	0.14485849	8	PTEN	1.52022936	0.43438047	8
FBXO3	1.07751838	0.16267517	8	PEAK1	1.64270874	0.55854575	8
RFK	1.09480059	0.06774322	8	DUSP10	1.68841047	1.01452973	8
BMPR1A	1.1224842	0.25973499	8	FBXL22	1.78105959	0.31976756	8
PPP6C	1.13605619	0.18867078	8	NUCKS1	1.89161952	0.22686287	8
EGFR	1.13739967	0.15713352	8	CLTC	2.01164841	0.58849598	8
BMP2K	1.14159139	0.08372473	8	KHK	2.33597833	0.9061615	8

Table5.11: ***Overall data from the A431 LNP release screen with EGF stimulation.*** *The average normalized LNP delivery for each siRNA in the A431 LNP release screen sorted by ascending LNP delivery. Average normalized LNP delivery is the average mCherry value normalized to the cell number control curve from the corresponding screen.*

A431- LNP release screen (-) EGF				Continued			
Gene	Average normalised LNP delivery	STD	N	Gene	Average normalised LNP delivery	STD	N
LRRK1	0.66510014	0.05452017	8	DUSP7	1.02881276	0.08814549	8
RPS6KL1	0.69647624	0.13736949	8	SRMS	1.03339425	0.1569152	8
NEK7	0.72250684	0.05135328	8	PTK2	1.03838656	0.12642357	8
EGFR	0.73503759	0.16647143	8	MARK4	1.04829419	0.33895578	8
FBXO3	0.74182112	0.0852003	8	PPP4R1	1.07395897	0.16890267	8
ALPPL2	0.75199063	0.07956478	8	PTPRZ1	1.0832846	0.11904844	8
RAB11A	0.76270065	0.06420873	8	BMP2K	1.09448775	0.10011598	8
FGFRL1	0.81193133	0.07953354	8	RFK	1.11384649	0.15657219	8
EPHA4	0.81308182	0.08057867	8	PIK3C2A	1.13227581	0.16328442	8
CTBP1	0.82732699	0.09751759	8	TAOK1	1.17571821	0.15747434	8
PPP1R16B	0.82818925	0.06195064	8	IRAK3	1.17830824	0.12086613	8
FBXO41	0.83091996	0.13106695	8	PIK3C2B	1.18645969	0.14538371	8
FBP2	0.83133367	0.12526398	8	EEA1	1.19979627	0.17133222	8
FBXL13	0.83526731	0.08097535	8	MAP2K5	1.22999158	0.12009558	8
PTPRR	0.84478652	0.11536212	8	PTEN	1.2897538	0.20897801	8
HIPK3	0.84794345	0.2095584	8	PFKFB2	1.29411272	0.14580327	8
NLRC5	0.85471114	0.11718334	8	PEAK1	1.32665461	0.66882551	8
TULP4	0.89828469	0.10063724	8	FBXL22	1.36559291	0.24353145	8
PPP6C	0.90157903	0.08645696	8	NUDT3	1.40660522	0.1733181	8
RAB5C	0.91916904	0.11658459	8	NEK5	1.45700275	0.32695056	8
TBCK	0.94512301	0.23612951	8	NTRK1	1.56080815	0.23620536	8
FBXO22	0.96591629	0.11891879	8	PAK1	1.61098175	0.53335664	8
CDKN1B	0.9805653	0.12060748	8	CLTC	1.69538638	0.33307952	8
ANKFY1	0.9839512	0.13712399	8	KHK	1.92745495	0.33665983	8
DUSP19	0.99749984	0.10306815	8	DUSP10	2.01553094	0.5459024	8
BMPR1A	1.02754555	0.14863376	8	NUCKS1	2.11539949	0.25694476	8

Table5.12 ***Overall data from the A431 LNP release screen without EGF stimulation.*** *The average normalized LNP delivery for each siRNA in the A431 LNP release screen sorted by ascending LNP delivery. Average normalized LNP delivery is the average mCherry value normalized to the cell number control curve from the corresponding screen.*

Chapter6: Validation of selected hits regulating endosomal release.

6.1 Validation of the identified release hits

We had successfully identified several genes that appeared to be promising candidates to regulate endosomal release. The hits selected for further validation were Irak-M(Irak-3), Peak1 and MAP2K5. The selected hits had been shown to increase endosomal release in all the screens performed: the HRP release assay in A431 cells and the LNP uptake assay in both the A431 and H358 cell lines (Chapter5). Because siRNA targeting these proteins promoted release in all the screening formats our confidence was increased that these genes should be for further study, both to validate them as having a role in endosomal release and to elucidate their mechanism of action in promoting endosomal permeability.

6.1.1 Optimization of transfection efficiency in A431 cells

The LNP assay used to validate the hits from the HRP release screens was optimised by researchers in AstraZeneca (Morag-Rose Hunter and Arpan Desai) using the RNAiMax transfection reagent. This transfection reagent is routinely used for high-throughput screening assays using siRNA due to its high transfection efficiency. We decided to test if RNAiMax was effective in the A431 cell line used for the HRP uptake screens, as a way to increase the transfection efficiency, since we had previously observed a lower transfection efficiency than the On-targetPlus siRNA compared to siGenome. To test efficiency of siRNA-mediated knockdown, A431 cells were reverse transfected with siRNA targeting PLK1 and the transferrin receptor using either Polyfect or RNAiMax at two different concentrations of siRNA. The silencing of PLK1 increases cell death and was used as a marker for transfection efficiency. After 3 days, the cells were stained with DAPI and nuclei were counted to obtain cell number for each condition. The higher concentration of Polyfect transfection reagent did result in a significant decrease in the cell count in the PLK1 siRNA condition when compared to the Non-targeting control however the RNAiMax transfection reagent had a greater effect

and resulted in the loss of nearly all cells indicating a very high level of gene silencing (Figure6.01A). To further confirm knockdown efficiency, we utilised a transferrin uptake experiment where cells were transfected with siRNA targeting the transferrin receptor. The cells were incubated with fluorescent transferrin and internalisation of the fluorescent transferrin was measured. The higher concentration of Polyfect and RNAiMax using siRNA targeting the transferrin receptor both decreased the internalised transferrin signal, indicating successful knockdown efficiency (Figure6.01B). The higher concentration of Polyfect had a greater level of signal in the non-targeting condition and greater variability. Due to the high knockdown efficiency observed in the PLK1 and transferrin assays we were able to confirm RNAi-MAX resulted in greater knockdown efficiency than Polyfect and therefore RNAiMax was used in further experiments.

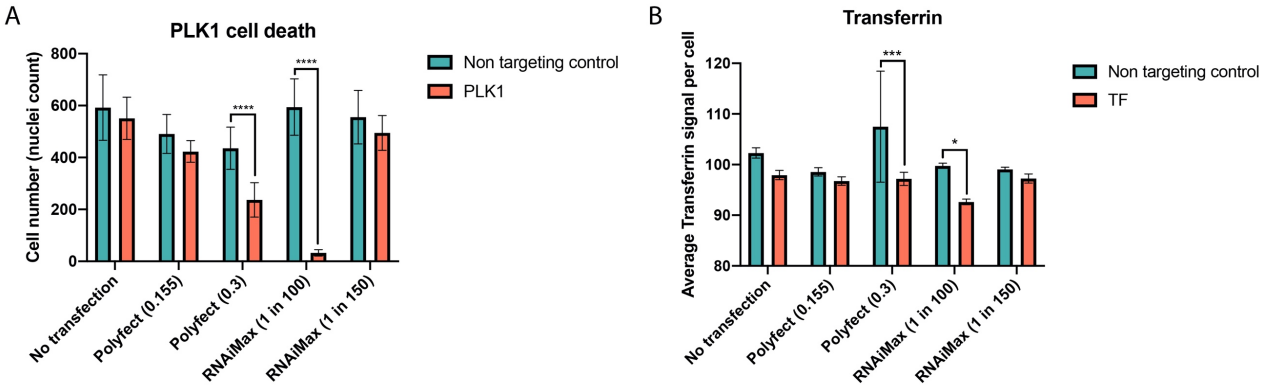

*Figure6.01: **RNAiMAX transfection reagent has greater transfection efficiency in A431 cells than Polyfect transfection reagent.** A) A431 cells were reverse transfected with PLK1 siGenome siRNA using Polyfect transfection reagent or RNAiMAX transfection reagent in variable combinations. Following incubation for 3 days at 37℃. the cells were washed, fixed with 4% PFA and stained with DAPI to mark nuclei. The number of surviving cells was determined using a high-throughput microscope and DAPI analysis. B) A431 cells were reverse transfected with siGenome siRNA targeting the transferrin receptor using either Polyfect transfection reagent or RNAiMAX transfection reagent at two different concentrations. Following incubation for 3 days at 37℃, the cells were serum starved for 2 hours prior to incubation with alexafluor647transferrin- (8.33ug/ml) for 10 minutes. The cells were washed, fixed and imaged using a high-throughput microscope. The average transferrin signal per well was detected. From each well 9 images were acquired, and the values averaged. The data showed mean + SD with 4 experimental replicates for each condition from one biological repeat. A 2-way ANOVA with a Sidak's multiple comparison test was performed on the data with ****p≤0.0001, *** p≤0.001, ** p≤0.01 , * p≤0.05*

6.1.2 Validating successful knockdown of identified hits

When performing an siRNA screen, it is not possible to confirm the successful knockdown of every target gene for each siRNA before or during the screen. The inclusion of appropriate positive and transfection controls confirms successful transfection during the screen but the knockdown efficiency for each gene will vary and therefore after identification of positive hits we needed to verify their successful knockdown and the degree of silencing achieved using

the siRNA. The next series of experiments aimed to validate the level of knockdown as well as confirming the effect on endosomal release.

The level of mRNA expression of IRAK-M, Map2K5 and Peak1 in A431 cells following knockdown was determined using quantitative PCR. A431 cells were transfected with either Non-targeting siRNA or siRNA targeting the identified hits. After 3 days, mRNA was extracted from cells and reverse transcribed to create cDNA. Using primer pairs complementary to the genes of interest and a control protein, GAPDH, quantitative-PCR was performed to determine the relative mRNA levels of the genes of interest in the Non-targeting siRNA condition and the corresponding siRNA-treated cells to confirm the level of knockdown. We were able to show a reduction in the RNA expression levels after knockdown with siRNA targeting MAP2K5 and PEAK1 indicating the siRNA was targeting the correct gene (Figure6.02). The Irak-M showed limited decrease after si-RNA treatment, however the qPCR reaction had high CT values using the IRAK-M primers. This indicated the reaction was less effective which could have been due to low abundance of Irak-M mRNA or the primer pair used was not effective. Further optimisation of the qPCR reaction is required to confirm knockdown by the IRAK-M siRNA.

A

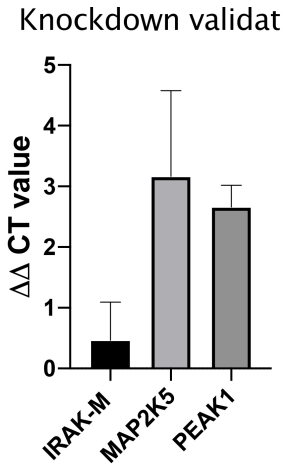

Figure6.02: ***Confirmation of knock-down using on-target plus siRNA in A431 cells:*** *To confirm the knockdown efficiency of our hits using On-target plus (OTP) siRNA we performed qPCR analysis to assess the mRNA levels of our proteins of interest. A431 cells were seeded into 6 well plates on day 0 and were transfected with OTP siRNA using RNAiMAX transfection reagent on day 1. Following 3 days of knockdown the RNA was extracted from the cells and reverse transcribed to form cDNA. A qPCR reaction was performed using appropriate primers to amplify the genes of interest in the cDNA. A CT value was calculated and the expression levels between the Non-targeting control siRNA and the different siRNA were compared to assess the degree of knockdown. Data shown is mean + SEM from 3 independent repeats with 6 experimental replicates per condition.*

6.1.3 Silencing of the identified hits using an alternative siRNA increases endosomal release

We previously performed a smaller re-screen of promising hits identified from the initial HRP release screen using an alternative siRNA(siGenome) to validate the effects observed on endosomal release was due to the direct action of the siRNA on targeted genes. However, the screening controls were not consistent, and the calculated Z-scores did not show a significant effect. We hypothesised that the decreased response in the validation screen using siGenome siRNA was due to a lower transfection efficiency achieved with siGenome then with OnTarget Plus siRNA. To overcome this issue, we repeated the siGenome knockdown using the RNAiMax transfection reagent which we had demonstrated had increased transfection efficiency. We performed the HRP uptake experiment following silencing using the si-Genome siRNA and were able to show an increase in endosomal release for all of the identified hits, IRAK-M, MAP2K5 and PEAK1(Figure6.03). Observing effects with two different siRNAs of different chemistries increased our confidence that the effects on endosomal release were due to direct inhibition of the expression level of our specific candidates rather than off-target effects of the siRNA.

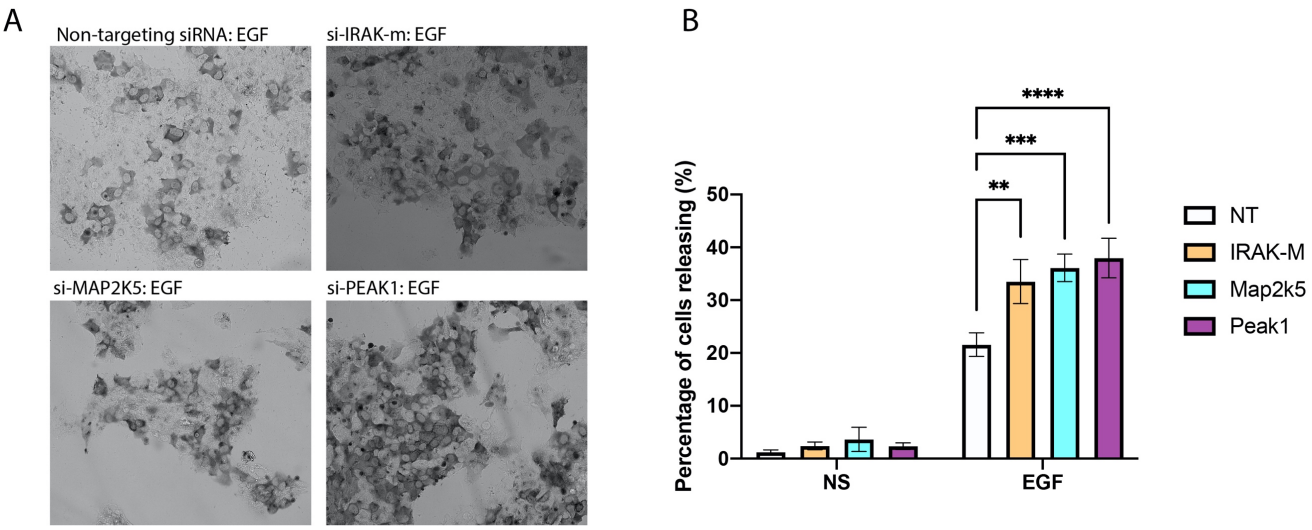

Figure6.03: ***Knockdown using si-Genome siRNA increases endosomal release with EGF stimulation.*** *A431 cells were transfected with siGenome siRNA targeting the identified hits shown using RNAiMAX transfection reagent. A non-targeting siRNA was included as a negative control. Following 3 days of knockdown the cells were serum starved for at least 2 hours prior to stimulation with EGF for 10 minutes at 37℃ in the presence of HRP(10mg/ml). The HRP solution was removed and the cells were washed and incubated for 90 mins in serum-free media-BSA(0.2%). The cells were placed on ice and washed with serum-free media-BSA(0.2%) and PBS to remove external HRP. The cells were fixed with 4% PFA for 10 minutes. The cells were stained using DAB to localise the internalised HRP. The images were analysed to detect cells showing endosomal release and the percentage of cells releasing calculated. Data shown is mean + SEM from 3 biological repeats, with 30 images analysed for each siRNA. A 2 way-ANOVA with a Sidak's multiple comparison was performed with ****p≤0.0001, *** p≤0.001, ** p≤0.01 , * p≤0.05*

6.1.4 EGF stimulated macropinocytosis is unaffected by reduced levels of IRAK-M, MAP5K and Peak1.

To further confirm the specificity of our selected hits on endosomal release, we tested whether they affected the uptake of material by macropinocytosis which we had shown was essential for endosomal release. In an endosomal release assay, any increase in the endocytosis of the signal molecule could indirectly contribute to increased endosomal release, and therefore we needed to control for increased uptake by endocytosis. The identified hits may be increasing endosomal release by increasing the amount of macropinocytosis. We therefore wanted to investigate if the knockdown of the identified hits increases macropinocytosis.

We previously performed the Kinome screen for effectors of macropinocytosis, and the identified hits had limited effect on macropinocytosis from the screen (Average Z-score from macropinocytosis screens: IRAK-M=-1.11, MAP2K5=-0.90 and peak1=1.49). However, as the macropinocytosis screen was performed with PMA stimulation (Chapter4) we wanted to confirm that the identified hits were not affecting EGF stimulated macropinocytosis. We thus measure EGF-dependent dextran uptake assay following knockdown of the identified hits. The siRNA targeting the EGF receptor was included as a positive control and was seen to decrease EGF stimulated macropinocytosis as expected. The identified hits either had no effect on macropinocytosis or had a significant decrease in macropinocytosis compared to the non-targeting control (Figure6.04). Therefore, the effect of these hits on delivery was not due to an increase in uptake via macropinocytosis.

A

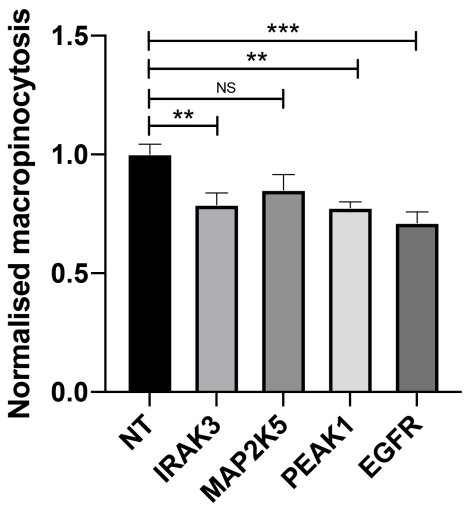

*Figure6.04:**The effects of the identified hits on macropinocytosis:** A431 cells were reverse transfected in a 384 well plate using RNAiMAX transfection reagent with different OnTargetPlus siRNA, including a control Non-targeting (NT) siRNA. Following incubation for 3 days at 37°C, cells were serum starved for at least 2 hours prior to incubation with 70kDa TRITC-dextran (0.25mg/ml) and EGF(100ng/ml) for 10 minutes. The cells were washed and fixed with 4% PFA and imaged using a high-throughput imaging system. Image analysis was performed to identify macropinosomes and the number of macropinosomes per cell was quantified as described in the methods. Data shown is Mean + SEM from 3 independent biological replicates. The data is pooled from the biological repeats, with 12 experimental replicates for each condition. A one-way ANOVA was performed with a Dunnett's multiple comparison with ****p≤0.0001, *** p≤0.001, ** p≤0.01 , * p≤0.05*

6.2 Understanding the mechanism of action of IRAK-M, MAP2K5 and Peak1 in endosomal release

After validating that knockdown of the identified proteins was having an effect on the delivery of material, we wanted to identify the mechanism of action for each hit to gain an increased understanding of how they are affecting endosomal release.

6.2.1 The identified hits do not increase recruitment of Galectin

A potential explanation for an increase in endosomal release could be through direct damage to the endosomal membranes resulting in material being released. To investigate if the endosomal membranes were damaged by knockdown of the selected hits, we utilized a galectin puncta assay. Upon membrane disruption the glycolipids that are usually found on the outer plasma membrane or the inner membrane of the endosomal system are exposed to the cytosol. This enables cytosolic galectins to bind to the glycolipids which results in accumulation of galectin to sites of endosomal damage (251,252). The cellular localisation of the galectin can be determined by immunofluorescence using a galectin-3 antibody. Cells were transfected with the relevant siRNAs, Non-targeting siRNA or EGFR siRNA. For this initial experiment we included some additional identified siRNA, SRMS and NUCKS1 to observe if they had an effect of galectin recruitment. The cells were incubated for 3 days and treated with EGF for 10 minutes before the galectin-3 antibody was used to identify the intracellular localisation of galectin. None of the hits identified increased the accumulation of galectin into punctate structures compared to the non-targeting control (Figure6.05). As a positive control, cells were treated with the compound LL-OME, a lysosomal disruption agent that is known to increase galectin puncta (251). Treatment of cells with LL-OMe resulted in galectin puncta verifying the assay is functional for detecting endosomal damage. These results indicate the mechanism of action of the identified hits is unlikely to be direct membrane disruption which would result in recruitment of galectin. However, LLOMe causes large membrane disruption and the sensitivity of the assay was not determined and therefore the identified hits may have been affecting membrane stability to a lesser degree than LLOMe, which might not necessarily be detected by our assay. It is possible the damage caused by knockdown of the

hits is compensated by cellular membrane repair mechanisms and therefore is not detectable by the galectin recruitment assay. The endosomal release may be performed by a non-membrane damaging process such as a proteinaceous pore which would not result in recruitment of galectin. From the literature, the galectin assay has been shown to produce punctata when cells are infected with the enveloped Adenovirus but galectin punctate were not seen upon infection with the non-enveloped reovirus(253). Therefore, the type of endosomal permeability dictates whether a positive result is obtained from the galectin assay and our hits are unlikely to lead to direct membrane damage.

A

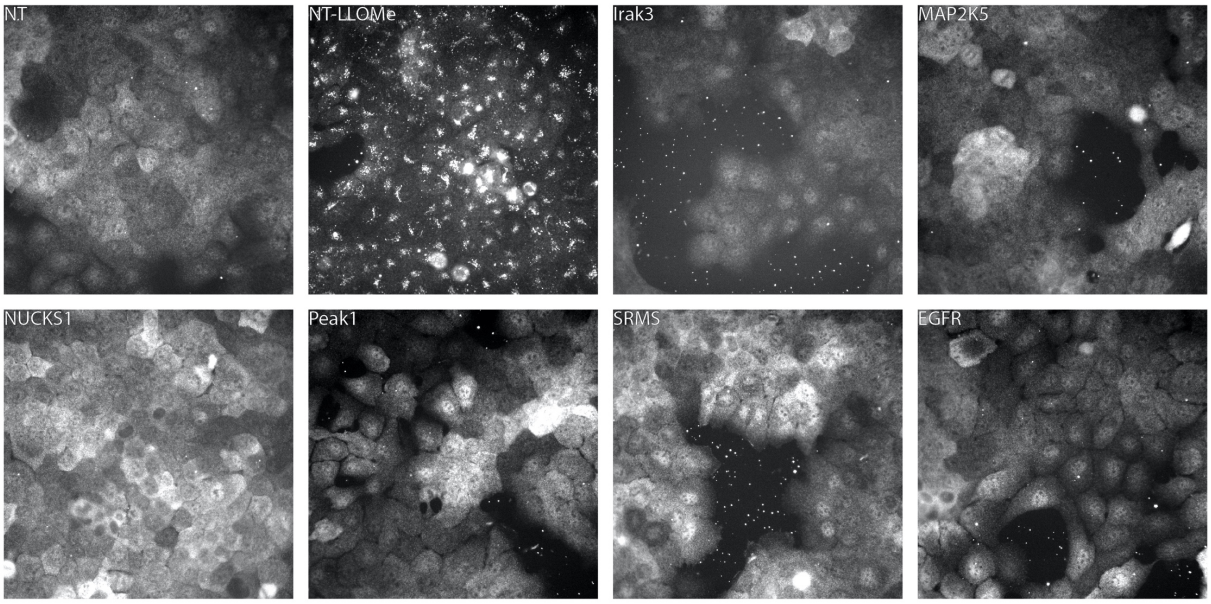

*Figure6.05: **Knockdown of selected hits does not recruit galectin to endosomal membranes.** A431 cells were reverse transfected with OnTargetPlus siRNA targeting the identified hits shown using RNAiMAX transfection reagent. A non-targeting siRNA(NT) and si-EGFR were included as a negative controls. Following 3 days of knockdown the cells were serum starved for at least 2 hours prior to stimulation with EGF for 10 minutes at 37℃ and a 90-minute chase period in serum-free DMEM. As a positive control, cells were pre-treated, before EGF stimulation, with LLOME(2mM) for 1 hour to induce endosomal release **(NT-LLOMe).** The cells were washed and then fixed in 4% PFA and processed for immunofluroesence using anti-galactin3 antibodies. The cells were imaged using an IncellAnalyzer high-content microscope. The images shown are representative images from 4 experimental replicates (4 wells), with 9 images acquired per well. The images were acquired from one biological replicate.*

6.2.2 Investigating Pharmacological inhibitors for the identified hits

As an alternative to reducing the function of the selected genes using siRNA, we asked whether pharmacological inhibitors targeting the hits affected endosomal release. We tested each inhibitor at 1 hour pre-treatment and 4-hour pre-treatment.

From the literature we identified a direct inhibitor for MAP2K5 protein, Bix-02189 (254). At 1-hour pre-treatment the MAP2k5 inhibitor, BIX-02189 decreased the endosomal release

observed (Figure6.06). At 4-hour pre-treatment there was a slight increase in endosomal release however it was not significant (Figure6.07).

The proteins IRAK-M and Peak-1 are pseudo-kinases and do not have active kinase domains. As there is no active site for a small molecule to bind there are less pharmacological inhibitors targeting pseudo-kinases. Previous research (unpublished data from Stefan Knapp) showed that two pharmacological compounds, Tak901 and BX912, were able to bind to IRAK-M and therefore potentially act as inhibitors, however their efficacy and/or specificity for IRAK-M was not known. We tested these pharmacological inhibitors using the HRP release assay. While incubation for 1 hour with these drugs showed minimal effect on EGF-dependent endosomal release (Figure6.06), incubation for 4 hours prior to the HRP release experiment resulted in a significant increase in release for BX912 (Figure6.07).

As well as observing the effect of inhibitors against the identified hits, we included an additional pharmacological inhibitor BX795 that inhibits the NF-kB pathway as the hits identified had connections to this pathway. Inhibition of the pathway using BX795 at both 1 (Figure6.06) and 4 hours of inhibition (Figure6.07) resulted in an increase in the release observed indicating inhibition of NF-kB signalling has an effect on endosomal release. The inhibition of the identified hits could be affecting NF-kB signalling which is therefore increasing the endosomal release observed.

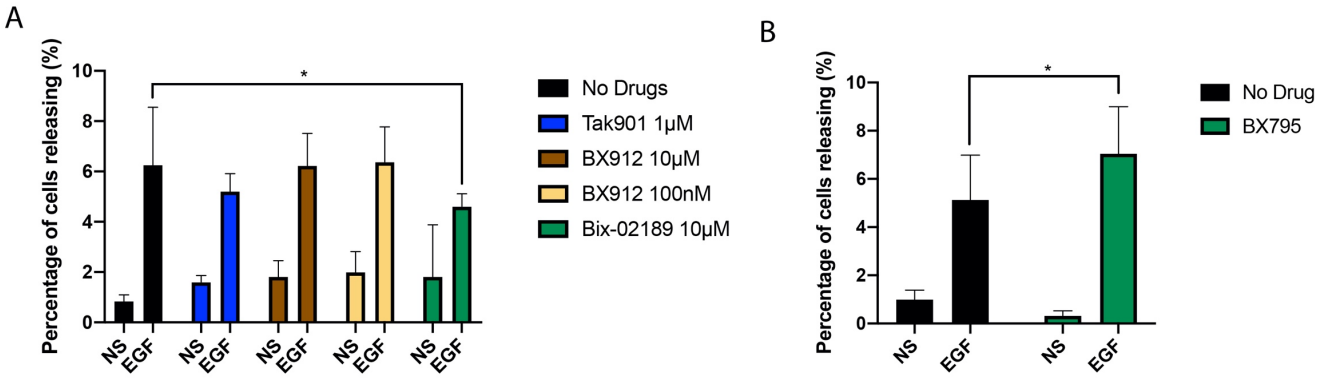

*Figure6.06: **Inhibition of the identified hits with pharmacological inhibitors** A) A431 cells were serum starved for at least 2 hours, followed by treatment with different pharmacological inhibitors for 1 hour prior to performing a HRP endosomal release experiment. The pharmacological inhibitors were dissolved in DMSO and DMSO was added to the control condition(No Drugs. The cells were incubated with HRP(10mg/ml) in the absence (NS) or presence of EGF(100ng/ml) for 10 minutes. The HRP solution was removed and the cells were washed and incubated for 90 mins in serum-free media-BSA(0.2%). Following washing, the cells were fixed with 4% PFA for 10 minutes. The cells were stained using DAB to localise the internalised HRPand imaged using an Incell Analyzer high-content microscope using brightfield imaging to detect the DAB stain. The images were analysed to detect cells showing endosomal release and the percentage of cells releasing calculated. A) Data shown is mean + SD from 2 independent experiments for BX912 and BIX-02189 with 8 experimental replicates in total. The TAK-901 data is from one-biological replicate with 4 experimental replicates. A 2 way-ANOVA with a Dunnetts's multiple comparison was performed B) Data shown is mean + SD from 2 independent experiments with 8 experimental repeats in total. A 2-way ANOVA with a sidak's multiple comparison test was performed. ****p≤0.0001, *** p≤0.001, ** p≤0.01 , * p≤0.05*

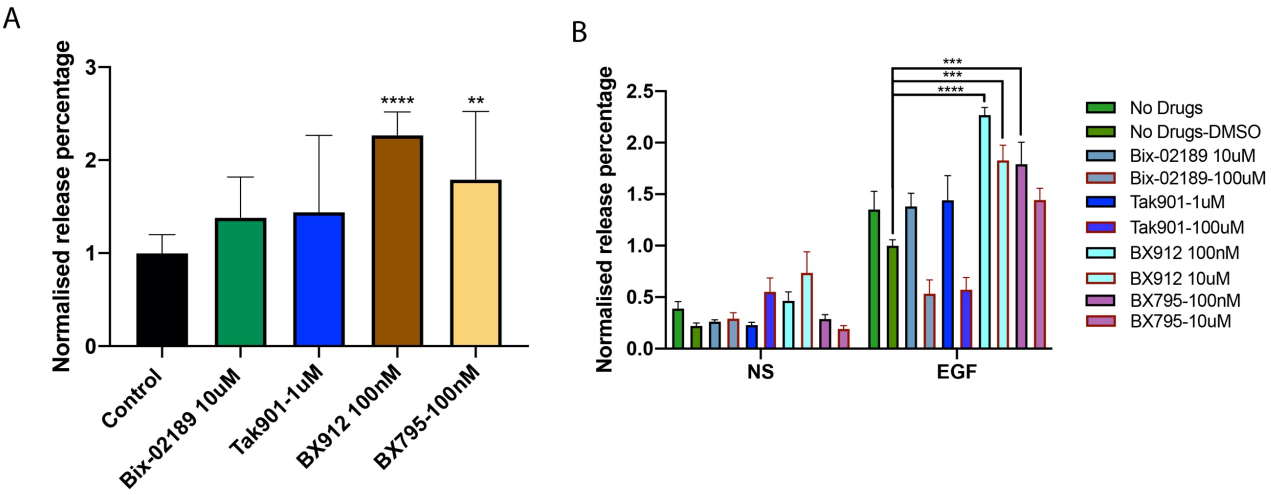

*Figure6.07: **Inhibition of the identified hits with pharmacological inhibitors-4-hour treatment***
*A) A431 cells were were serum starved for at least 2 hours prior to performing the experiment. The cells were treated with the different pharmacological inhibitors for 4 hours prior to performing a HRP endosomal release experiment. As the pharmacological inhibitors were dissolved in DMSO, a carrier control was included (Control). The cells were incubated with HRP(10mg/ml) with either EGF(100ng/ml) or unstimulated(NS). The HRP solution was removed, the cells were washed and incubated for 90 mins in serum-free media. After washing. the cells were fixed with 4% PFA for 10. The cells were stained using DAB to localise the internalised HRP. The stained cells were imaged and analysed to detect cells showing endosomal release and the percentage of cells releasing calculated. A) Shows the EGF stimulated conditions with selected concentrations of the pre-treated pharmacological inhibitors. The data is normalised to the control condition. Data shown is mean + SD from 3 biological repeats with 12 experimental replicates. A one-way ANOVA was performed with a Dunnett's multiple comparison. B) Data shows the full experiment analysis including unstimulated and EGF stimulated conditions and the various pharmacological inhibitor concentrations tested. The data is normalised to the No Drug-DMSO condition in each biological replicate. The Data shown is Mean + SEM from 3 biological replicates with 12 experimental repeats. A 2-way ANOVA with a sidak's multiple comparison test was performed. ****p≤0.0001, *** p≤0.001, ** p≤0.01 , * p≤0.05*

6.3 Investigating a role for NF-kB signalling in endosomal release

6.3.1 Treatment of A431 cells with EGF increases the nuclear translocation of NF-kB

The proteins IRAK-M, MEK5 have both been implicated in the NF kappa b signalling pathway and our pharmacological data also implied a potential role for this signalling pathway. To explore this further in the context of our endosomal release assay, we asked whether treating cells with EGF caused activation of the NF kappa b pathway in our cell model. The NF-kB signalling pathway can be activated by mitogen signalling such as growth factors. It is known EGF stimulation can trigger activation and nuclear accumulation of *NF-kB* (213,255). Activation of the pathway can be measured by accumulation of NF kappa B in the nucleus (256). A431 cells were stimulated with 100ng/ml EGF for different time points and using an antibody that recognised the RelA NF-kB subunit, its cellular localisation was determined by immunofluorescence. The percentage of cells with nuclear NF-kB localisation was determined for each time point. Control cells (NS) which were not treated with EGF had low NF-kB nuclear accumulation (Figure6.08). There was a significant increase in nuclear accumulation of rel-A after 20 minutes of EGF stimulation, increasing with increasing incubation times to 40% after 60 minutes. During the HRP release experiments, only a subset of cells shows cytosolic release, and we considered the possibility that cells that activate NF-kB are those that show endosomal release. In order to verify the cells with NF-kB activity are the cells showing cytosolic delivery, the HRP assay would need to be performed simultaneously with the NF-kB immunofluorescence. Unfortunately, the DAB staining is not compatible with the immunofluorescent protocol and this experiment would need to be performed either with a different release assay or using a transient expression of a fluorescent NF-kB. My results do confirm that A431 cells show NF-kB activation upon treatment with EGF under the same conditions that increase endosomal release.

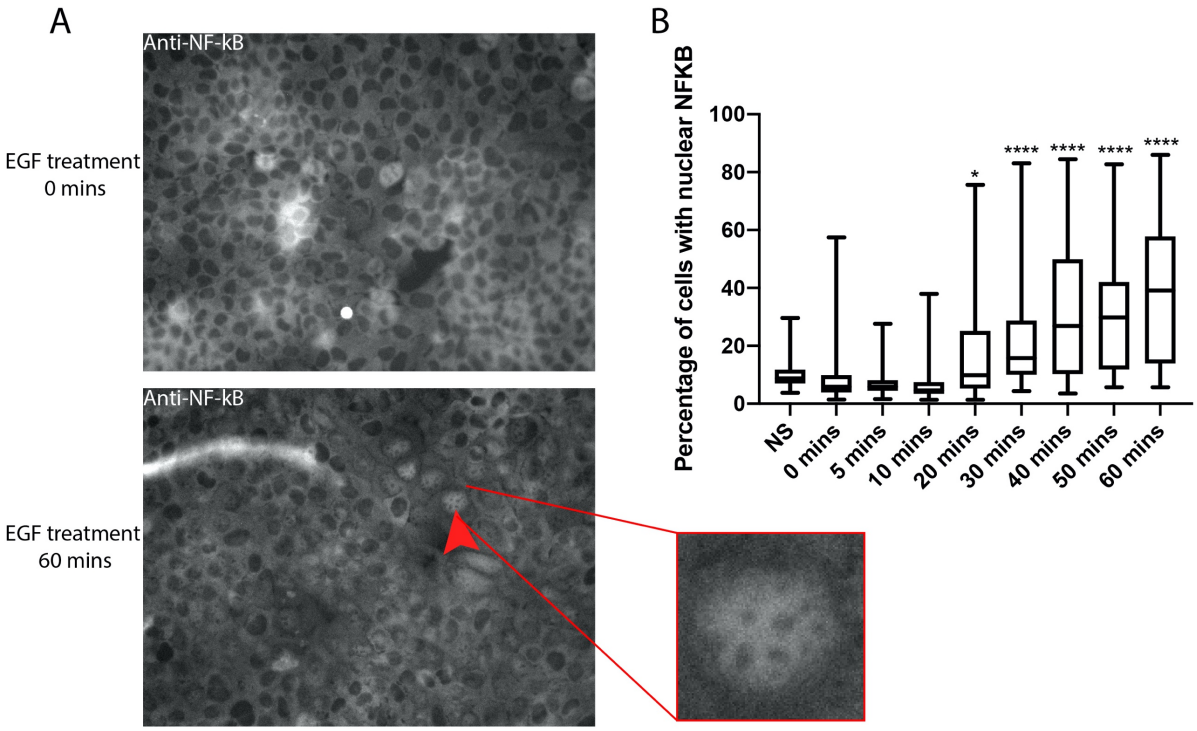

Figure6.08: ***Stimulation of A431 cells with EGF increases nuclear localisation of NF-kB:*** *A431 cells were serum starved for at least 2 hours prior to stimulation with EGF (100ng/ml) EGF for different time points before cells were fixed with PFA(4%). The samples were stained with an Anti-RelA(NF-kB subunit) antibody and images were captured using an Incell analyser high content imaging microscope. The images were analysed to detect cells showing nuclear accumulation of NFKB. The red arrow highlights a cell with positive NF-kB nuclear translocation. Data shown is mean + SD from 2 biological repeats. A One-way ANOVA was performed with Tukey's multiple comparison with ****p≤0.0001, *** p≤0.001, ** p≤0.01 , * p≤0.05*

6.3.2 Pharmacological inhibitors of canonical NF-kB inhibit endosomal release

We had shown the pharmacological inhibitor of NF-kB, BX795, had an effect on endosomal release therefore we looked to see if additional pharmacological inhibitors of NF-kB had an effect on endosomal release. We tested two inhibitors of NF-kB, Amlexanox and IKK-16. Amlexanox inhibits IKKepsilon and TBK1 proteins which are both involved in the non-canonical NF-kB pathway, whereas IKK-16 inhibits the IKK complex which can be involved in both canonical and non-canonical signalling. We tested the inhibition for 4 hours and were able to see an effect with the IKK-16 inhibitor (Figure6.09), with a complete loss of endosomal release observed. The Amlexanox treatment had no observable effect on release potentially indicating the non-canonical NF-kB pathway is less important for endosomal release.

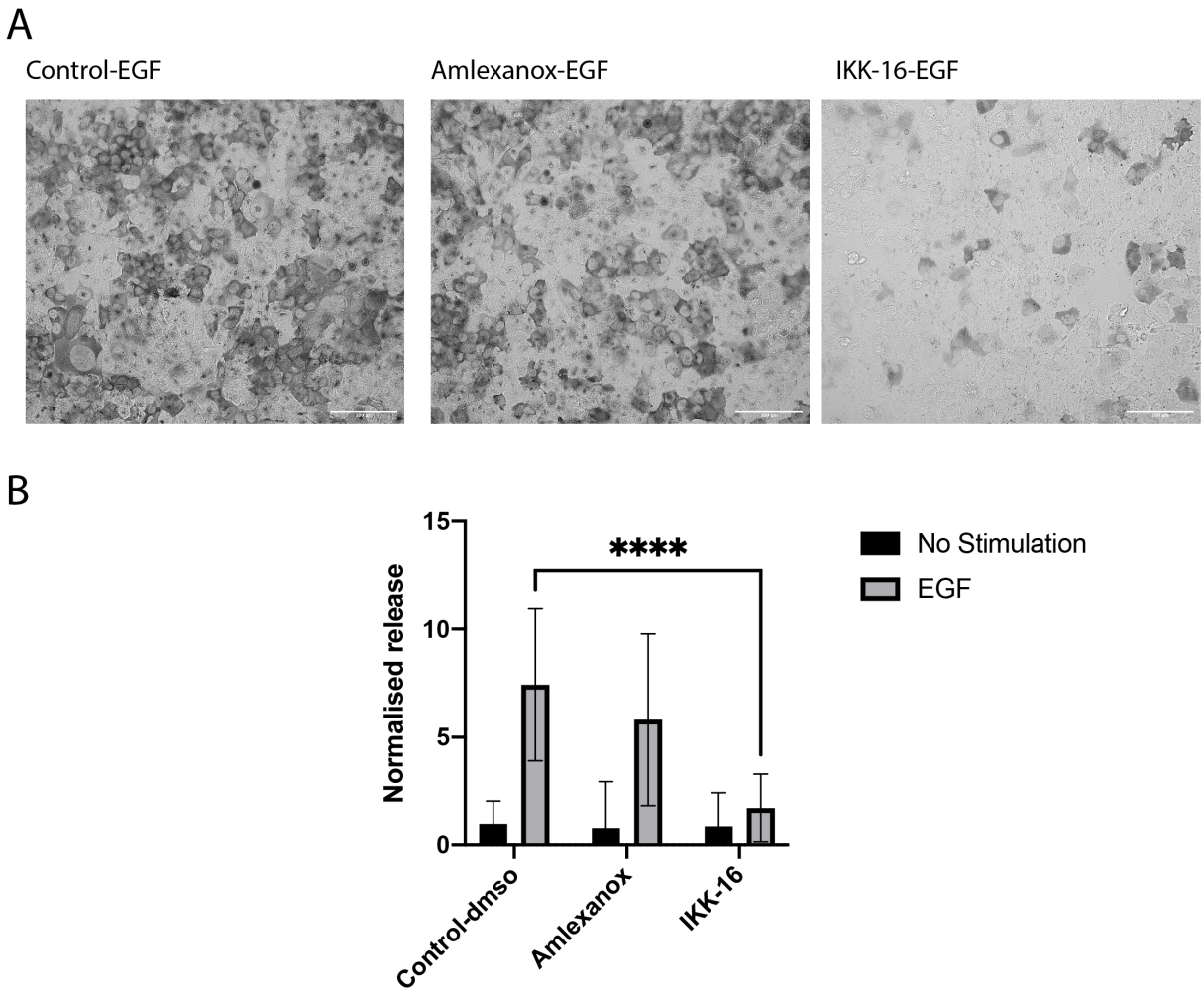

*Figure6.09: **The effect of 4-hour NF-kB inhibitor treatment on endosomal release.** A) A431 cells were seeded 3 days prior to performing a HRP uptake experiment. The cells were serum starved for at least 2 hours prior to performing the experiment. The cells were treated with the NF-kB inhibitors Amlexanox(10μM) or IKK-16(10μM) for 4 hour prior to performing a HRP uptake experiment. As the pharmacological inhibitors were dissolved in DMSO, a carrier control was included. The cells were incubated with HRP(10mg/ml) with either EGF(100ng/ml) or unstimulated(NS). The HRP solution was removed, the cells were washed and incubated for 90 mins. The cells were placed on ice and washed with serum-free media-BSA(0.2%) and PBS. The cells were fixed with 4% PFA for 10 minutes and quenched with ammonium chloride. The cells were stained using DAB to localise the internalised HRP. The stained cells were imaged using an Incell Analyzer high-content microscope using brightfield imaging to detect the DAB stain. The images were analysed to detect cells showing endosomal release and the percentage of cells releasing calculated.*

6.3.3 Pre-treatment with interferon-Y increases EGF-dependent endosomal release

As NF-kB is a signalling pathway involved in the immune response and regulation of inflammation we wanted to see if cytokines had an effect on the EGF release. We pre-treated the A431 with interferon-Y for 16 hours prior to an HRP endosomal release experiment where cells were stimulated with either EGF or PMA to stimulate release. Cells treated with EGF had significantly increased endosomal release when compared to PMA treatment (figure6.10). The cells treated with IFN-Y for 16 hours showed a large increase in endosomal release when treated with EGF when compared to EGF stimulation alone. Interesting the IFN-Y did

significantly increase the PMA stimulated release however this may be due to some outlying data points that increased the mean value. The pre-treatment of Ifn-Y had the greatest effect on the EGF stimulated release indicating that Ifn-y activation may promote the endosomal release observed. The activation of Nf-kB signalling by Ifn-Y may explain the results observed.

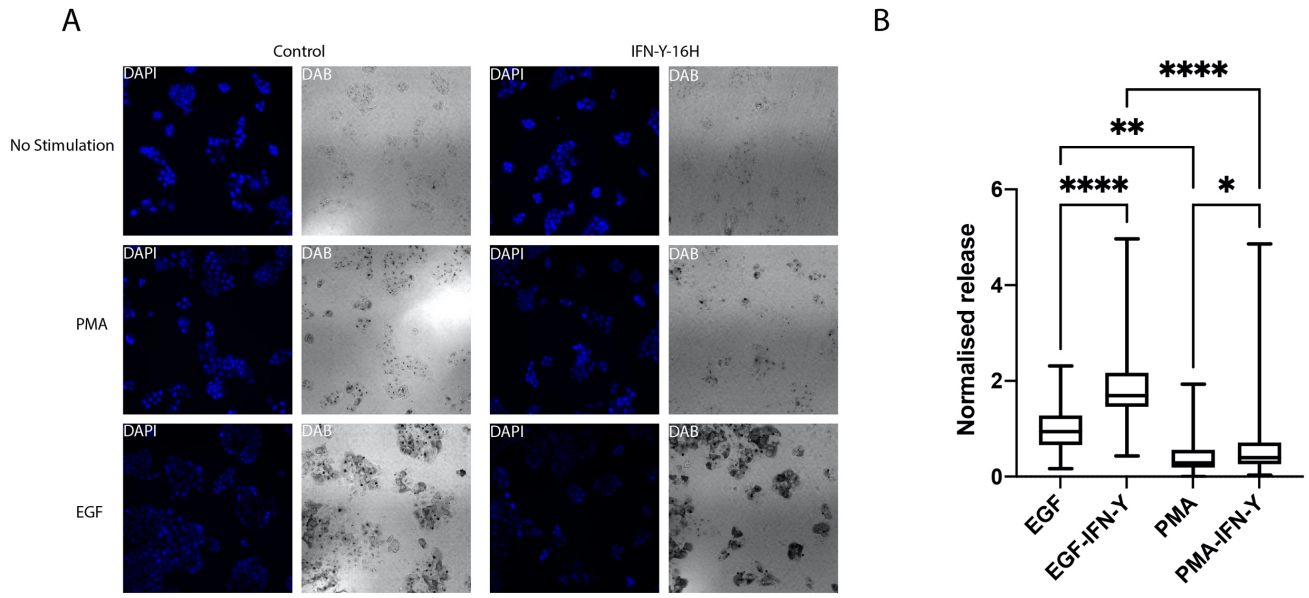

*Figure6.10: **The preincubation of cells with IFN-y increases EGF stimulated release in A431 cells:** A431 cells were seeded and incubated at 37 ℃. The cells were stimulated with IFN-Y for 16 hours prior to performing a HRP uptake assay. The cells were stimulated with either PMA, EGF or left unstimulated for 10 minutes in the presence of 10mg/ml HRP. The cells were washed with serum-free media-BSA0.2% and incubated for 90 minutes. The cells were placed on ice and washed with ice-cold serum-free media-BSA 0.2% and ice-cold PBS before fixation with 4% PFA for exactly 10 minutes. A DAB solution was used to stain for the cellular location of HRP and the number of cells showing endosomal release was calculated as a percentage of total cells. B) The Data were normalised to mean percentage of cells releasing from the EGF control and compared to the IFN-Y treated cells. Data shown is Mean + SD from 2 independent biological replicates with 6 experimental replicates. The data is normalised to the EGF condition and shows 44 data points for each condition from multiple images acquired per replicate. A unpaired two-tailed T-test was performed with ****p≤0.0001, *** p≤0.001, ** p≤0.01 , * p≤0.05*

6.3.4 EGF stimulation increases phosphorylation of NF-kB and the degradation of IkB

The nuclear translocation of NF-kB is a late stage temporally in the NF-kB pathway. To test whether EGF stimulation affected earlier stages of the NF-kB pathway, which would equate with the time course of endosomal release, we measured the phosphorylation of NF-kB which occurs in the cytosol before nuclear translocation and the degradation of the IkB protein using Western blotting. Figure 6.11 shows a Western blot of *the phosphorylation of NF-kB(p65)* and figure 6.12 shows IkB degradation in response to 10-minute EGF treatment, followed by chase for various times. We could observe in the A431 cells that EGF stimulation results in rapid phosphorylation of NF-kB (Figure6.11). Treatment with EGF is sufficient to activate p65

phosphorylation to the same level as ionomycin, a known activator of NF kappa B signalling. Phosphorylation of p65 is sustained through a 60-minute chase, again consistent with the conditions of endosomal release (Figure3.24, chapter3). I also probed the lysates for levels of IkB and demonstrated increased degradation of the IkB protein with increasing chase time further indicating sustained activation of the NF-kB pathway (Figure6.12). This result reinforced the activation of NF-kB could occur in a short time frame and that activation of EGF with 60 minutes chase had a similar level of activation to 60 minutes Ionomycin treatment, indicating strong activation of the pathway. The kinetics of IkB degradation are slightly delayed when compared to NF-kB phosphorylation as the IkB protein needs to be degraded before the effect is visible and therefore a decrease in IKB levels is observed after 10 minutes chase.

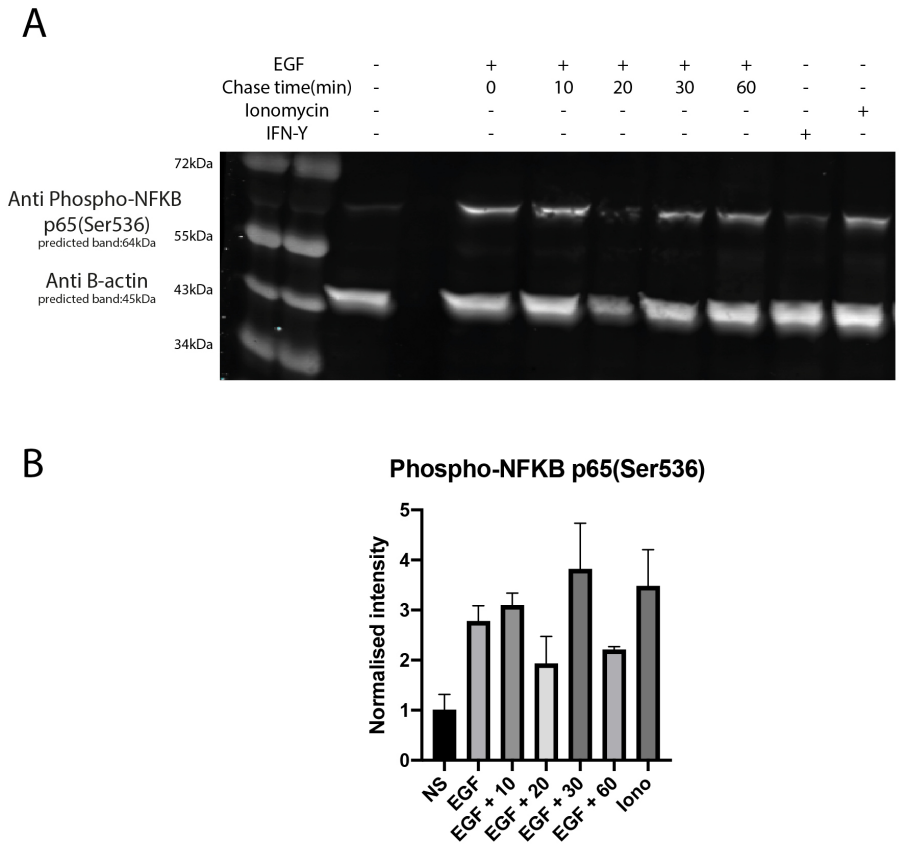

Figure6.11: ***Stimulation of A431 cell with EGF increases the phosphorylation of NF-kB(p65):*** *A431 cells were serum starved for at least 2 hours. The cells were stimulated with EGF(100ng/ml) for 10 minutes followed by variable times of serum-free DMEM chase as shown in the figure. Negative control cells were left unstimulated and positive controls of 60 minutes Ionomycin/PMA and 60-minute IFN-Y treatment were included. The cells were placed on ice and washed with ice-cold PBS prior to cell lysate and collection of the lysates. Equal protein volumes were loaded onto a SDS-page gel followed by western blot analysis using an Anti-Phospho-NF-kB p65(Ser536) antibody and an Anti-B-actin antibody as a loading control. The fluorescent intensity was detected and the values for each band was normalised to the loading control. The histogram shows is mean + SD from 3 lysates for each condition collected from 3 independent biological replicates.*

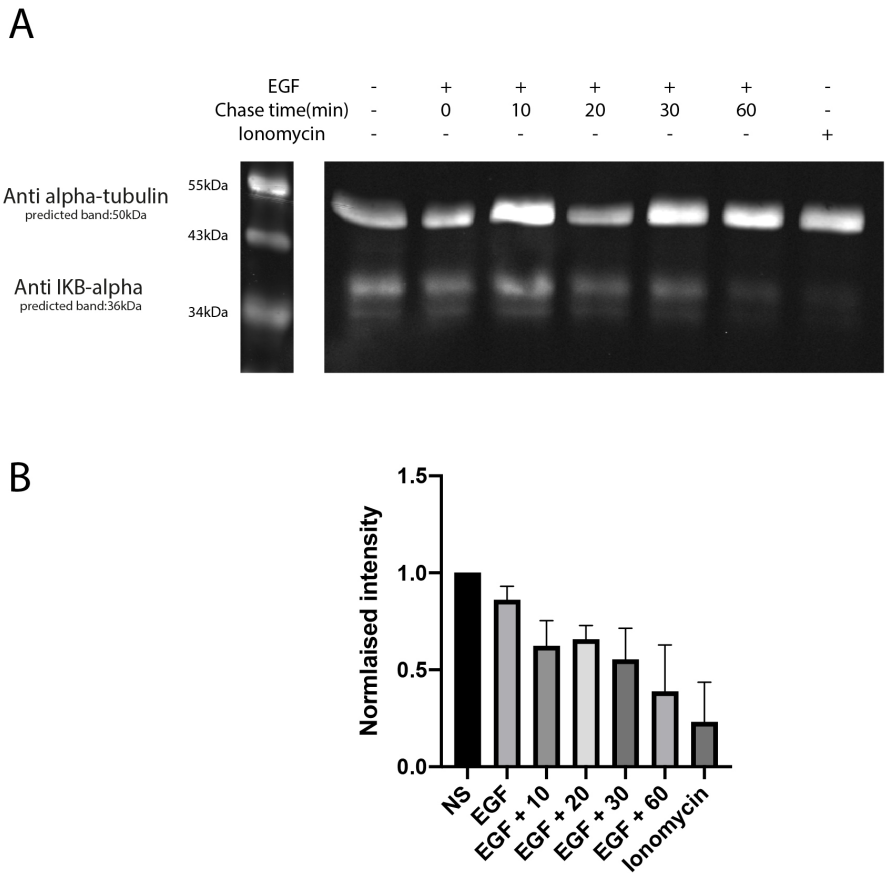

Figure6.12: ***Stimulation of A431 cell with EGF increases the degradation of the IkB protein:*** *A431 cells were serum starved for at least 2 hours. The cells were stimulated with EGF(100ng/ml) for 10 minutes followed by variable times of serum-free DMEM chase as shown in the figure. Negative control cells were left unstimulated and a positive control of 60 minutes Ionomycin/PMA was included. The cells were placed on ice and washed with ice-cold PBS prior to cell lysate and collection of the lysates. Equal protein volumes were loaded onto an SDS-page gel followed by western blot analysis using an Anti I-kB antibody and an Anti-alpha-tubulin antibody as a loading control. The fluorescent intensity was detected and the values for each band was normalised to the loading control. The data for each condition was normalised to the unstimulated (NS) condition. The data shown is mean + SD from 3 lysates for each condition collected from 3 independent biological replicates.*

6.3.5 Knockdown of IRAK-M, MEK5 and Peak 1 reduce NF-kB signalling

We next investigated whether si-RNA mediated knockdown of our selected hits affected NF kappa B signalling. A431 cells were treated for three days with siRNAs targeting Irak-M, Map2K5 or PEAK1 as well as a control with non-targeting siRNA. Cells were then either unstimulated, stimulated for 10 minutes with EGF or stimulated with EGF for 10 minutes followed by a 30-minute chase in serum-free media. The levels of phospho NF-kB and IkB were measured by Western blotting to observe any differences in NF-kB activation when cells are depleted of the identified hits by siRNA interference.

We analysed the quantity of phospho-NF-kB for each siRNA condition and normalised the values to the non-targeting siRNA, unstimulated condition. The IRAK-M condition had similar phosphorylation of NF-kB to the non-targeting control, there was only a very slight increase in the unstimulated condition indicating a slight increase in basal signalling (Figure6.13). The si-MAP2K5 condition showed a similar level of initial phospho-NFkB after 10 minutes EGF stimulation however after the 30-minute chase the levels were lower than the non-targeting control, indicating the NF-kB pathway activation was sustained for a shorter time in si-MAP2K5 condition or possibly that the activation of NF-kB occurred faster and therefore less phospho-NFkB was seen at the later time point. The same response was observed in si-PEAK1 treated cells but a greater decrease in phospho-NF-kB was seen after 30-minute chase indicating a bigger effect on NF-kB signalling. The unstimulated condition in both si-PEAK1 and si-MAP2K5 showed increased signal than the non-targeting control.

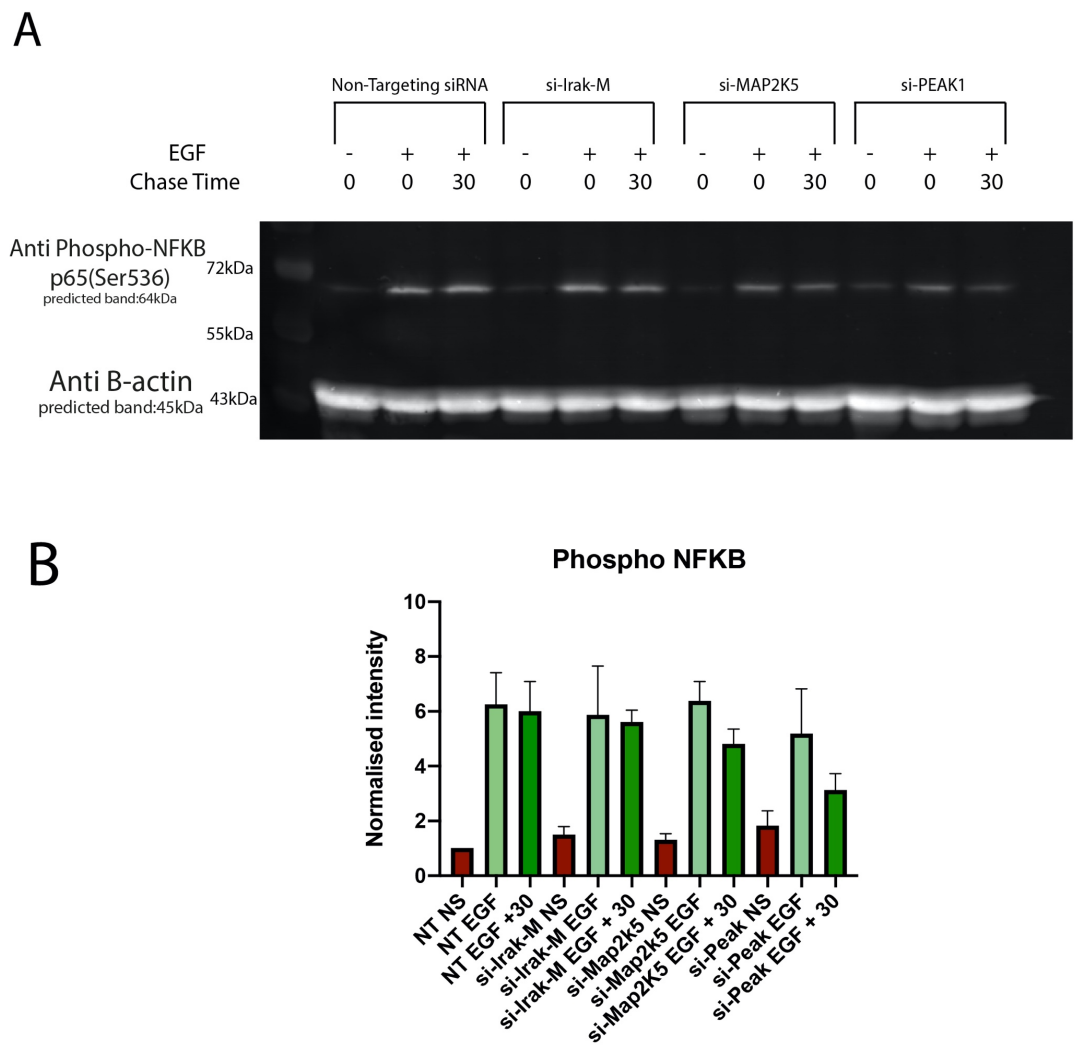

Figure6.13: ***The siRNA silencing of the identified protein hits effect NF-kB phosphorylation in A431 cells:*** *A431 cells transfected with non-targeting siRNA (NT) or one of the identified hit siRNA (IRAK-M,MAP2K5 and PEAK1) and incubated at 37 °C for 3 days. The cells were serum starved for at least 2 hours prior to the experiment. The cells were stimulated with EGF(100ng/ml) for 10 minutes followed by variable times of serum-free DMEM chase as shown in the figure. Negative control cells were left unstimulated (NS). The cells were placed on ice and washed with ice-cold PBS prior to cell lysate and collection of the lysates. Equal protein volumes were loaded onto an SDS-page gel followed by western blot analysis using an Anti-Phospho-NF-kB p65(Ser536) antibody and an Anti-B-actin antibody as a loading control. The fluorescent intensity was detected and the values for each band was normalised to the loading control. The data is shown in two ways B) shows the data normalised to the non-targeting siRNA unstimulated condition (NT NS), C) shows the data normalised to the unstimulated (NS) condition for each siRNA separately. The data shown is mean + SEM from 3 lysates for each condition collected from 3 independent biological replicates.*

We also analysed the degradation of IkB (Figure6.14) following knockdown of the selected hits. Figure 6.14 shows that degradation of IkB was faster in cells treated with siRNA targeting the selected hits compared to the non-targeting control. IRAK-M knockdown resulted in an increase in the degradation of IkB initially as the level was lower after 10 minutes, however the level of IkB was greater than the non-targeting in the 30-minute chase condition indicating a lower activation of NF-kB in the longer time point. However, it is possible the activation of NF-kB is slowed down in the Irak-M cells which would prevent degradation of IkB and may be the cause of increased endosomal release. The MAP2K5 condition had similar kinetics to the non-targeting control with degradation of IkB. The initial levels of IkB may have been greater in this condition but the data is not clear due to variability. The Peak1 condition had lower initial levels of IkB then the non-targeting control which is consistent with the effect seen in the phospho-NFKB experiment where a greater amount of Phospho-NF-kB was observed in the unstimulated PEAK1 condition. These results indicate the silencing of PEAK1 has increased basal NF-kB signalling.

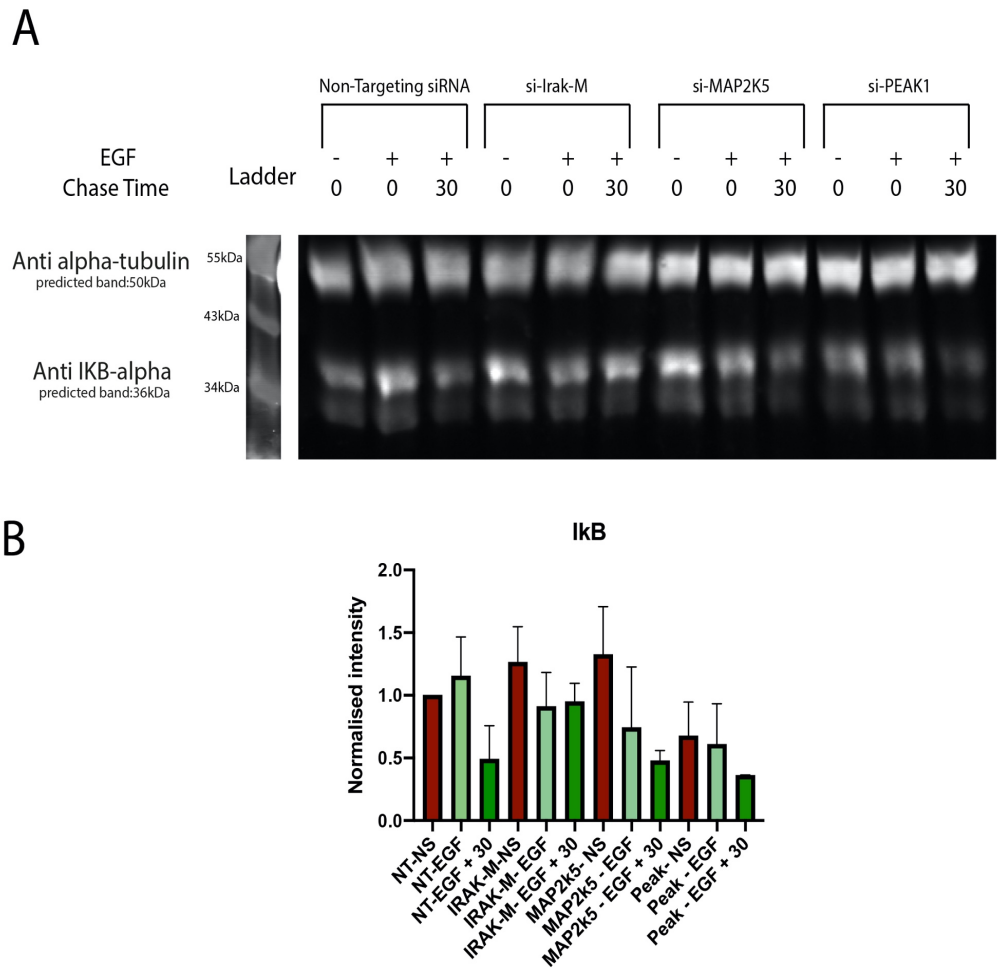

Figure6.14: ***The siRNA silencing of the identified protein hits effect IkB degradation in A431 cells :*** *A431 cells were transfected with non-targeting siRNA (NT) or one of the identified hit siRNA (IRAK-M,MAP2K5 and PEAK1) and incubated at 37 ℃ for 3 days to allow sufficient time for knockdown to occur. The cells were serum starved for at least 2 hours prior to the experiment. The cells were stimulated with EGF(100ng/ml) for 10 minutes followed by variable times of serum-free DMEM chase as shown in the figure. Negative control cells were left unstimulated(NS). The cells were placed on ice and washed with ice-cold PBS prior to cell lysate and collection of the lysates. Equal protein volumes were loaded onto an SDS-page gel followed by western blot analysis using an Anti I-kB antibody and an Anti-alpha-tubulin antibody as a loading control. The fluorescent intensity was detected and the values for each band was normalised to the loading control. The data is shown in two ways B) shows the data normalised to the non-targeting siRNA unstimulated condition (NT NS), C) shows the data normalised to the unstimulated (NS) condition for each siRNA separately. The data shown is Mean + SEM from 3 lysates for each condition collected from 3 independent biological replicates.*

6.3.6 Ionomycin abolishes EGF dependent release in A431 cells.

As the treatment of A431 cells with EGF increased both cytosolic delivery and NF-kB activation we wanted to test if activation of NF-kB via a different method had the same effect on release. It is known that treatment of cells with ionomycin and PMA can activate NF-kB signalling. Ionomycin is a calcium ionophore that can transport calcium ions from the ER into the cytosol and so increases intracellular calcium levels. PMA activates Protein kinase C (PKC) which as well as the increased calcium levels leads to activation of the NF-kB pathway. Previously we used (1µM) PMA to stimulate macropinocytosis but stimulation of NF-kB activation only requires 30 nM. We therefore pre-treated A431 cells with Ionomycin (100µM) + PMA (30nM)

for 30 minutes before performing an HRP endosomal release assay. To our surprise the cells treated with Ionomycin and PMA lost the EGF-dependent endosomal release (figure6.15A). This result was not expected as we hypothesized that stimulation of the NF-kB pathway would increase endosomal delivery. We had incubated the cells with ionomycin for 30 minutes prior to the experiment. This raised the possibility that the pre-treatment was affecting the temporal activation of NF-KB preventing it from promoting endosomal permeability. Therefore, we compared ionomycin pre-treatment with adding ionomycin at the same time as EGF(Figure6.15B). As observed before, ionomycin pre-treatment inhibited the delivery seen with EGF but addition of ionomycin at the same time as EGF recovered the release seen with EGF. This release was not greater than in the control EGF condition so there was no additive effect of the ionomycin. This could be due to not sufficient time to cause an effect or the NF-kB activation is already saturated by EGF alone. However, no increase in delivery is observed with the ionomycin treatment without EGF treatment indicating ionomycin alone does not increase delivery. As well as pre-treating with ionomycin we decided to pre-treat with EGF and PMA (Figure6.15B). The pre-treatment with EGF and PMA both prevented the increase in release seen with EGF treatment, a similar effect to ionomycin. We hypothesis the pre-treatment with EGF and PMA result in endocytosis of cell surface receptors, thus decreasing the signalling for the HRP uptake experiment. The activation of NF-kB might be regulated to only result in endosomal release of newly formed macropinosomes and therefore pre-treatment activates the NF-kB pathway too early to increase release of HRP.

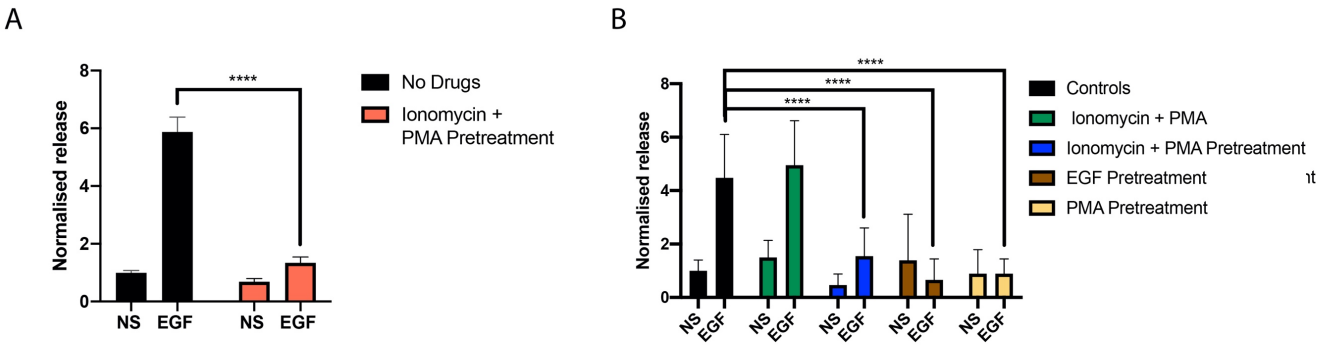

Figure6.15: ***The pre-treatment of A431 cells effects endosomal release:*** *A431 cells cells were pre-treated with either Ionomycin/PMA, EGF(100ng/ml) or PMA for 1 hour prior to performing a HRP uptake experiment. The cells were stimulated with either EGF or left unstimulated for 10 minutes in the presence of 10mg/ml HRP. The cells were washed with serum-free media-BSA-0.2% and incubated for 90 minutes at 37 ℃. The cells were placed on ice and washed with ice-cold serum-free media-BSA 0.2% and ice-cold PBS before fixation with 4% PFA for exactly 10 minutes. A DAB solution was used to stain for the cellular location of HRP and the number of cells showing endosomal release was calculated as a percentage of total cells. A) Data shown is mean + SEM from 4 independent biological replicates with 16 experimental replicate data points. A 2-way ANOVA was performed with a Sidak's multiple comparison. B) Data shown is mean + SD from 2 independent biological replicates with 8 experimental replicate data points. A 2-way ANOVA was performed with a Dunnet's multiple comparison. ****p≤0.0001, *** p≤0.001, ** p≤0.01 , * p≤0.05.*

6.3.7 Temporal activation by EGF is important for delivery

To further investigate the importance of temporal activation of endosomal release by EGF we performed experiments to see if altering the time of EGF pre-treatment has an effect on delivery. We performed a time course of different length pre-incubation with EGF prior to an HRP endosomal release assay (Figure6.16A). The stimulation of cells with EGF prior to the HRP uptake assay prevented delivery of HRP to the cytosol for all time-points. The result indicated that the activation by EGF is required at the same time as the cargo in order to see delivery. This potential is due to internalisation of the EGF receptors after pre-treatment preventing activation during the HRP release assay. We additionally wanted to see if the cells could recover their ability to stimulate release after incubation with EGF. A431 cells were treated with EGF for 10 minutes, washed and placed in fresh media at multiple time points prior to an HRP release assay. Cells pre-stimulated with EGF 11 hours before the HRP assay showed the EGF dependent release of HRP to the cytosol (figure6.16B). The release observed after 11-hour pre-treatment was greater than with the control cells without any pre-treatment indicating a greater response. The ability to recover the delivery of HRP highlights the A431 cells after EGF treatment are viable and the release stimulated does not have detrimental effects on the cells.

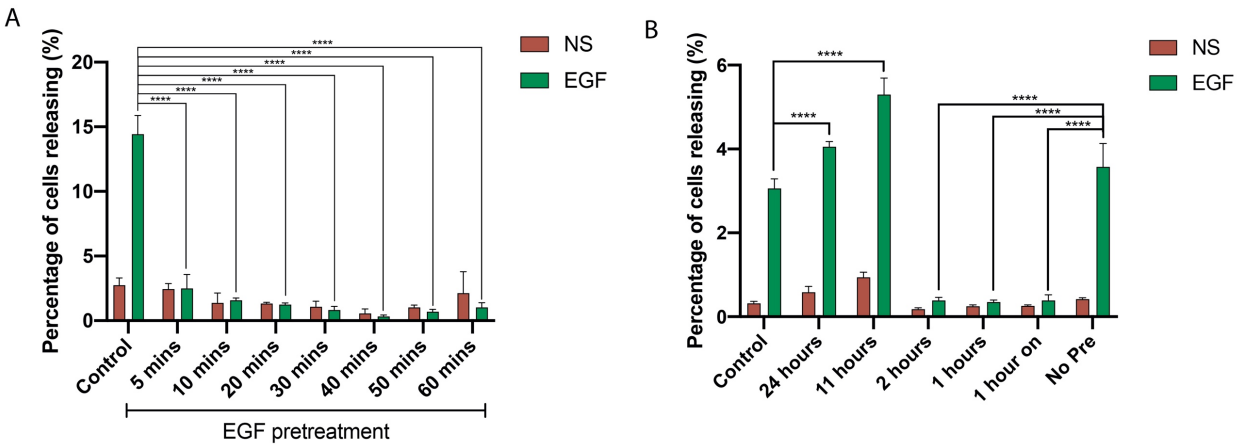

*Figure6.16: **The time-course of EGF pre-treatment in A431 cells:** A431 cells were seeded and incubated at 37 ℃ for 2-3 days. A) The cells were serum starved for 2 hours prior to the experiment. Cells were pre-treated with 100ng/ml EGF for variable time points as shown and then a HRP uptake assay was performed. B) The cells were treated with EGF (100ng/ml) for 10 minutes and then washed in serum-free media and left to recover for the time shown on the graph. The 1 hour on condition was EGF pre-stimulation for 1 hour prior to the HRP uptake. The control condition underwent the same protocol as the 24 hour condition without EGF added whereas the no pre-treatment (No-pre) had no media removed before the HRP uptake experiment. A+B) The HRP experiment was performed the same for both experiments. The cells were stimulated with either EGF or left unstimulated for 10 minutes in the presence of 10mg/ml HRP. The cells were washed with serum-free media-BSA0.2% and incubated for 90 minutes at 37 ℃. The cells were fixated with 4% PFA for exactly 10 minutes. A DAB solution was used to stain for the cellular location of HRP and the number of cells showing endosomal release was calculated as a percentage of total cells. Data shown is mean + SD from one biological repeat. A) Data is from 4 experimental replicates with a Two-way ANOVA and Tukey's multiple comparison. B) Data is from 3 experimental replicates with a Two-way ANOVA and Tukey's multiple comparison. ****p≤0.0001, *** p≤0.001, ** p≤0.01 , * p≤0.05.*

6.3.8 The proteasome inhibitor MG132 prevents endosomal release

The process of NF-kB activation requires the degradation of IkB, which we were able to show earlier via western blotting for IkB after EGF stimulation. The IkB protein is degraded by the proteasome and so we tested if MG132 inhibition had an effect on endosomal release. We observed nearly complete prevention of endosomal release with MG132 indicating that degradation of proteins is important in endosomal release (Figure6.17). This may be due to preventing degradation of IkB but many processes require degrading proteins in the proteasome.

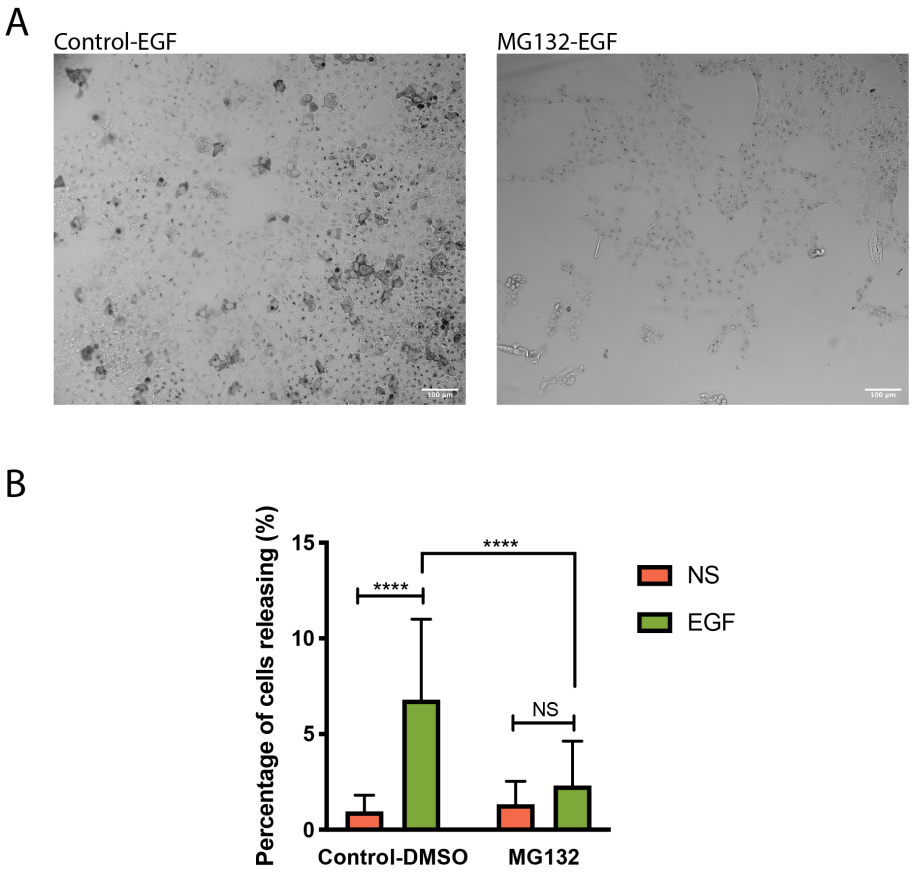

*Figure6.17: **The effect of the inhibitor MG-132 treatment on endosomal release.** A) A431 were serum starved for at least 2 hours prior to performing the experiment. The cells were treated with the inhibitor MG132(20μM) for 1 hour prior to performing a HRP uptake experiment. As the pharmacological inhibitors were dissolved in DMSO, a carrier control was included. The cells were incubated with HRP(10mg/ml) with either EGF(100ng/ml) or unstimulated(NS). The HRP solution was removed, the cells were washed and incubated for 90 mins. After washing, cells were fixed with 4% PFA for 10 minutes and quenched with ammonium chloride. The cells were stained using DAB to localise the internalised HRP. The images were analysed to detect cells showing endosomal release and the percentage of cells releasing calculated. Data shown is mean + SD from two independent biological repeats. A 2-way ANOVA was performed with a Sidak's multiple comparison. ****p≤0.0001, *** p≤0.001, ** p≤0.01 , * p≤0.05.*

6.3.9 HSP90 is not involved in refolding released proteins

Having implicated NF-kB pathway in endosomal release, we next wanted to try to understand the mechanism of action of the release. As NF-kB is involved in the immune responses we were interested in the process of antigen cross presentation as a biological mechanism for releasing endosomal content. Antigen cross presentation is the process where endocytosed antigens are released to the cytosol to allow presentation onto the MHC1 pathway. The mechanism of how proteins escape from the endosomal system in antigen cross presentation is not known. However there have been studies on proteins that effect the successful cross presentation of endocytosed proteins. It has been theorized that if antigens are transported across the membrane via a pore protein and the antigen requires unfolding to cross, then the chaperone HSP90 would be important for refolding in the cytosol. It has been shown that HSP90 can be required for successful cross presentation. We therefore used the HSP90 inhibitor, radicicol to observe any effect on the endosomal release. We did not observe any effect on endosomal release using radicicol (Figure6.18).

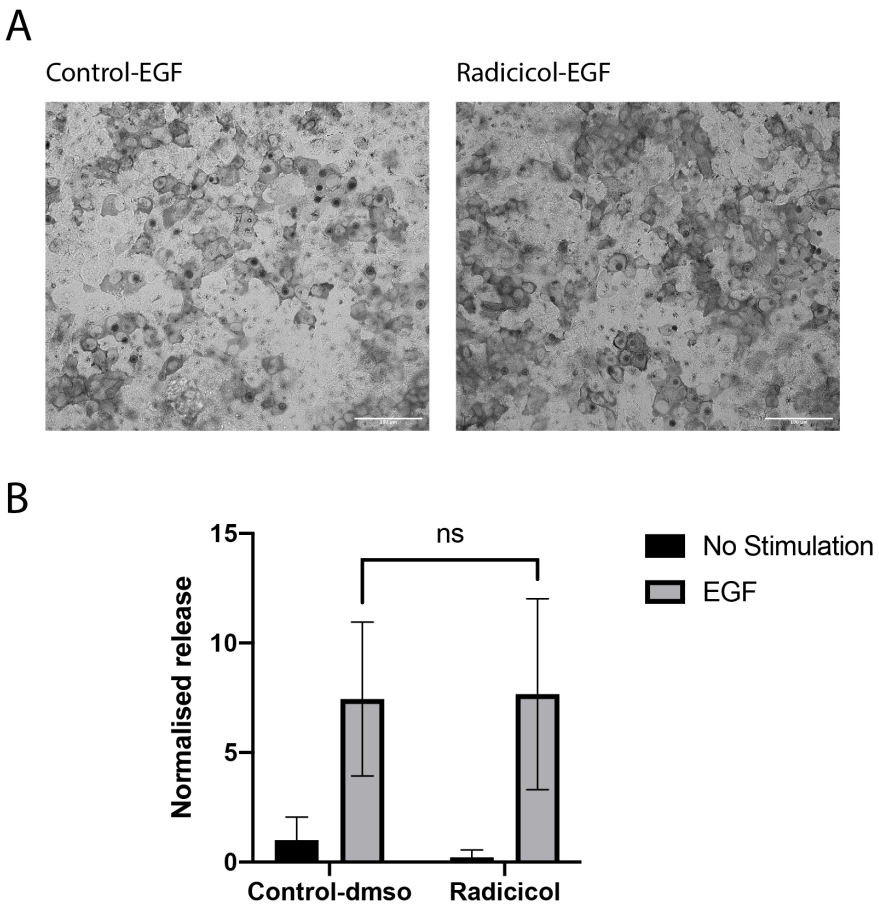

*Figure6.18**: The effect of the HSP90 inhibitor radicicol treatment on endosomal release.** A) A431 cells were serum starved for at least 2 hours prior to performing the experiment. The cells were treated with the inhibitor Radicicol(500nM) for 4 hour prior to performing a HRP uptake experiment. As the pharmacological inhibitors were dissolved in DMSO, a carrier control was included. The cells were incubated with HRP(10mg/ml) with either EGF(100ng/ml) or unstimulated(NS). The HRP solution was removed, the cells were washed and incubated for 90 mins. After washing the cells were fixed with 4% PFA for 10 minutes. The cells were stained using DAB to localise the internalised HRP. The images were analysed to detect cells showing endosomal release and the percentage of cells releasing calculated. Data shown is mean + SD from two independent biological repeats. A 2-way ANOVA was performed with a Sidak's multiple comparison. ****p≤0.0001, *** p≤0.001, ** p≤0.01 , * p≤0.05.*

6.3.10 We could not directly observe antigen cross presentation in the A431 cells

We were interested in antigen-cross presentation as the potential mechanism involved in release and therefore, we performed an experiment to directly detect processing of endocytosed antigens. We utilised a protocol used to detect antigen cross presentation in dendritic cells. A peptide of the Ova-albumin, SIINFEKL, is fed to the cells and following endocytosis the antigen is cross-presented to the cell surface by the MHC-1 pathway. We used an antibody that directly recognises the MHC-1-SIINFEKL complex and not SIINFEKL alone, allowing direct detection of antigen cross presentation. We performed the SIINFEKL uptake experiment under basal conditions (NS) and with EGF stimulation for 2 hours to allow sufficient time for cross presentation to occur. The cells were dissociated and collected by

centrifugation to allow staining of MHC-1-SIINFEKL on the surface by flow cytometry staining protocol. The cells were analysed by flow cytometry, but we could not observe any difference between unstimulated and the EGF condition (Figure6.19A). We also included a condition without SIINFEKl added as a negative control which showed the same pattern indicating no MHC-1-SIINFEKl could be detected on the cell surface. We performed a flow cytometry experiment using a pan-MHC-1 antibody that recognises any MHC-1 complex and were able to observe signal validating our staining protocol and that the cells had a functional MHC-1 pathway (Figure6.19).

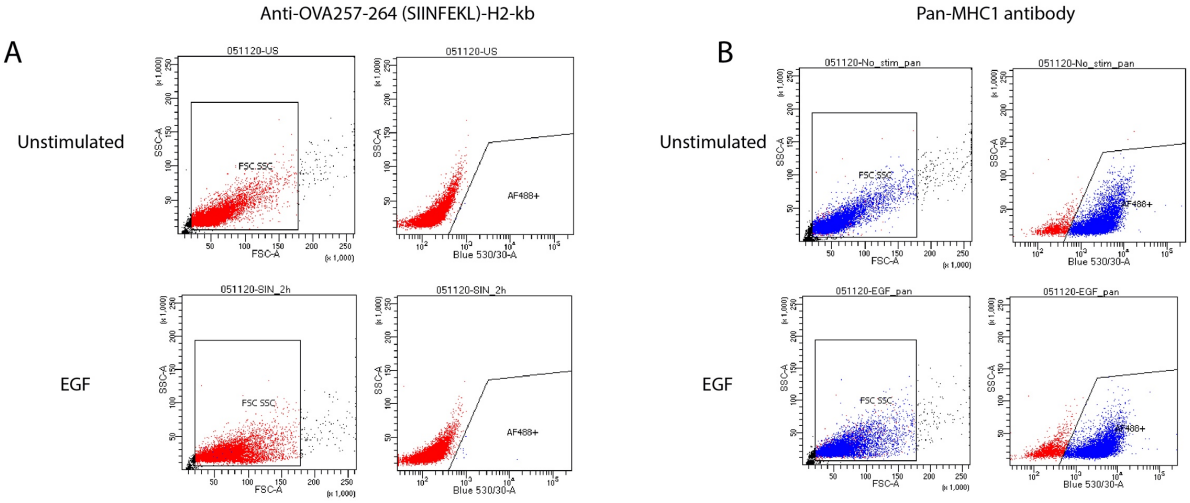

Figure6.19: ***Analysis of antigen cross presentation in A431 cells:*** *The A431 cells were seeded 2 days prior to the experiment. The cells were serum starved for 2 hours. The cells were incubated with a SIINFEKL peptide for the time indicated with and without EGF stimulation. The cells were washed with serum-free media and the cells were dissociated using an enzyme free dissociation buffer. This enabled the collection of a cell pellet by centrifugation and the subsequent processing for flow cytometry. The samples were stained with a A) Anti-SIINFEKL-MHC1 specific antibody or B) A Pan-MHC-1 antibody. The samples were analysed, and a graph produced that shows forward scatter vs side scatter as well as a second graph to show the fluorescent intensity associated with the cell. For each sample 10,000 particles were detected.*

Chapter 7. Discussion

6.4 Summary of results identified

During this project we wanted to identify proteins involved in endosomal permeability that could be manipulated to increase the release of material from the endosomal system to the cytosol. The ability to increase endosomal permeability could increase the therapeutic output of current molecules as well as enabling the use of alternative therapeutics that could not previously be delivered into the cell by conventional routes. Additionally, the results identified will increase our knowledge of proteins and signalling pathways that are involved in endosomal permeability.

During the project I set up and optimises a HRP based endosomal release assay that can successfully detect endosomal release. Using this assay we reproduced the effect observed by Norbury et al (173) that EGF stimulation induces the endosomal release of content to the cytosol in A431 cells. We utilised this HRP release assay, as well as a dextran uptake assay to perform a kinome siRNA screen to identify effectors of endosomal release and macropinocytosis respectively. We identified some promising leads from the macropinocytosis screen that can be investigated further in future work.

We identified several effectors of endosomal release, IRAK-M, PEAK1 and MAP2K5. We are able to show the reduction in the levels of these proteins increases the delivery of endocytosed material to the cytosol. The identified hits were able to increase the delivery of HRP as well as a LNP-mCherry cargo in two distinct release assays. The targets were validated using two different siRNAs as well as by using pharmacological inhibitors to validate the inhibition of the target proteins was responsible for the effect on endosomal release. After identification of the hits, we were able to implicate the NF-kB signalling pathway as a likely pathway involved in the EGF stimulated endosomal release. We additionally started to try to elucidate the mechanisms of action of the endosomal release by exploring the process of antigen-cross presentation.

6.5 Adenovirus signalling in A431 cells

At the beginning of the project, we required a method to increase the release of endosomal content to the cytosol, to study the mechanisms involved in endosomal permeability. Initially the project was focused on the use of the Adenovirus to increase the amount of endosomal release as a result of the infectious process of the virus during cell invasion. During infection, adenovirus is endocytosed and enters the endosomal system(148). In order to deliver the adenovirus DNA to the nucleus for replication, the virus particle needs to be released from the endosome to the cytosol. The exact mechanism of release has not been elucidated completely but there is evidence for an adenovirus protein VI which is membrane lytic and disrupts the endosomal membrane to allow release of content (257). However research into adenovirus escape highlighted a potential signalling component activated by virus binding to the host cell surface that increases escape of virus particles from the endosomal system (232). The paper from the Greber group showed adenovirus stimulates macropinocytosis and clathrin mediated endocytosis, the canonical route of adenovirus uptake. Using a fluorescent FITC-BSA molecule with a nuclear localisation sequence attached, they were able to show that adenovirus could stimulate the release of content from macropinosomes. Further analysis revealed that macropinosomes could release content even when the number of virus particles on the macropinosome membrane was too low to cause rupture by a lytic mechanism, indicating an additional process is required. The use of a dominant negative Dynamin^{K44A} mutant of the dynamin protein prevented the uptake of adenovirus via clathrin mediated endocytosis but had no effect on macropinocytosis. The K44A mutant did not decrease the amount of endosomal release observed which suggested that cell surface binding of adenovirus was sufficient to cause endosomal release without the need for adenovirus endocytosis. Together these results suggested an additional mechanism(s), likely a signalling pathway, caused endosomal release which did not require endocytosis of the virus. We initially wanted to identify and understand the signalling pathway and proteins involved in this adenovirus triggered endosomal release.

6.5.1 The incubation of Adenovirus did not increase endosomal release in A431 cells

To enable experimentation into adenovirus stimulated endosomal release, a fluorescent GFP-NLS was cloned, expressed and purified prior to the start of the project. Initially we wanted to reproduce the detection of macropinosomal release after incubation of cells with adenovirus using our GFP-NLS protein. We produced adenovirus using the AdEasy adenovirus system and successfully determined the viral titre using an immuno-titre assay, which indicated we were able to generate biologically active adenovirus. However, we could not show nuclear accumulation of GFP after co-incubation of GFP-NLS and adenovirus indicating we had not detected endosomal release as previously demonstrated by Meier et al (232). The fluorescent signal strength detected from the GFP-NLS after endocytosis was weak, with only a slight increase in fluorescent signal when compared to the background signal observed around the cells. A high concentration of 40mg/ml FITC-BSA-NLS was used previously (24) and the low signal in our release assay could be due to a lower concentration (0.15mg/ml) of endocytosed marker being used. In order to use the GFP-NLS at 40mg/ml, increased protein production would have been required and we encountered aggregation of the GFP-NLS at concentration greater than 1.5 mg/ml. We were also concerned about the efficiency of nuclear delivery of the GFP-NLS. We attempted to test this using an anti-GFP antibody to amplify any GFP signal in the cell but could not detect nuclear localisation of GFP indicating there could be a potential problem with the GFP-NLS protein produced. Potentially, a greater concentration of GFP-NLS protein was required to observe nuclear translocation as only a small fraction of endocytosed material is released and the lower concentration was not sufficient for detection, even when enhanced by the GFP-antibody. As an alternative, we tested a second marker for endosomal release utilised by Norbury et al (173) which used horse radish peroxidase (HRP) enzyme in the fluid phase as a marker for endosomal escape following stimulation of A431 cells with EGF. Using this HRP based endosomal release assay we could observe very limited adenovirus stimulated release, however the release observed was variable, both within samples with release being observed in cell clusters, rather than a uniform release across all cells in the sample. There was also considerable variability between experiments, with release observed in some experiments but not in others. We hypothesised this could have been due to the adenovirus preparations we produced and the stability of the adenovirus in storage. Immunofluorescence with an anti-adenovirus antibody supported

endosomal release of HRP in cells where the virus was bound. However overall, the stimulation of endosomal release using adenovirus was limited in our A431 cells and we did not have an effective positive control for endosomal release in order to validate our release assay.

We therefore tested a J774.2 cell line that had previously been shown to release endosomal content in the absence of stimulation. This J774.2 cell line was shown to be sensitive to the ribosome-inactivating drug, saporin without requiring a transfection reagent for delivery (193). As this cell line had been shown to be semi-permeable to exogenous material, we wanted to test whether our assay could detect release in these cells and to determine the sensitivity of the assay by observing the number of cells staining positive for endosomal release. Using this cell line, we could show effective detection of endosomal release using our HRP based assay and a large number of cells were showing release indicating high-efficiency in detecting endosomal release. Additionally, we observed an increase in adenovirus triggered endosomal release using J774.2 cells that was more effective than in A431 cells. Adenovirus can utilise multiple different secondary receptors for triggering internalisation and intergrin alphaV can be utilised as a secondary receptor to trigger adenovirus endocytosis (258). We showed that J774.2 cells had low expression levels of this receptor, compared to A431 cells. This integrin was also shown to be important for adenovirus stimulated macropinocytosis in the study by Meier et al (232). The lower levels of intergrin alpha-V in the J774.2 cells could suggest an alternative secondary receptor for the adenovirus was being utilised. This alternative receptor might have a more potent effect on endosomal permeability and adenovirus escape, explaining why a greater effect on endosomal release was observed in the J774.2 cells with adenovirus.

In order to identify signalling components involved in endosomal release, we required a robust assay with a significant signal to noise ratio in order to perform key experiments such as a siRNA based high-throughput screen for effectors of endosomal release. High-throughput screens require robust assays that have high-reproducibility and low variability. We therefore concluded adenovirus did not stimulate endosomal release robustly enough to be used as an effective assay to study endosomal release. We therefore required an alternative mechanism to stimulate endosomal release that would be compatible with HRP release which we could

clearly detect. We reproduced the effect observed by Norbury et al (173) in which EGF stimulation of A431 cells increased the release of endosomal content to the cytosol using the HRP uptake assay.

To study the effectors of endosomal permeability we required robust models where content is released from the endosome to the cytosol. We had validated two independent systems where we could detect endosomal release of HRP, the J774.2 cells and EGF-stimulated A431 cells. We chose EGF stimulation for further experiments as it offered us several advantages over the J774.2 system. There was no prior knowledge of why this strain of J774.2 cells was more permeable to proteins as the previous studies involving the cells focussed on what could be delivered rather than underlying mechanisms of release. Additionally, J774.2 cells are a routinely used cell line which show no increased endosomal permeability indicating that the increased endosomal permeability observed in the strain of J774.2 cells we used is likely due to genetic mutations that could act on many processes to cause the phenotype observed in these cells. By contrast, EGF stimulation allowed us to consider the well-studied EGF signalling pathway, and suggested candidate signalling components involved in increasing release. The endosomal release was able to be stimulated using EGF, with low basal endosomal release observed in unstimulated cells. This would allow us to trigger endosomal release and we know the endosomal release was directly related to the effects of EGF stimulation, aiding identification of effectors. Additionally, an inducible system of endosomal release is more appealing for therapeutic delivery as less damage to the cell occurs if release can be transiently triggered. The EGF stimulated release could be specifically inhibited using the macropinocytosis inhibitor EIPA indicating the endosomal release was dependent on endocytosis via macropinocytosis. EIPA had limited effects on the release observed in the J774.2 cells suggesting that the release may occur more generally through the endosomal network. The J774.2 cells are also smaller making it more difficult to distinguish between releasing and non-releasing cells. However, due to the larger morphology and flatter appearance in A431 cells, the distinction was greater and therefore easier to analyse.

6.6 Macropinocytosis screen

Before performing an siRNA screen to identify effectors of endosomal release, we first needed to perform a control screen for effectors of macropinocytosis. From our preliminary experiments we had discovered the endosomal release in A431 cells was sensitive to inhibition with EIPA, a macropinocytosis inhibitor. Therefore, it was likely that macropinocytosis plays an important role in uptake of the fluid-phase marker HRP prior to endosomal escape. Furthermore EGF stimulates macropinocytosis in A431 cells, further linking the processes of uptake and release (107,122). Based on our previous findings with EIPA, any siRNA that has an effect on macropinocytosis in A431 cells would indirectly prevent endosomal release and therefore could be identified as an effector of endosomal release in any release screens. To eliminate regulators of macropinocytosis which might also affect release, we aimed to perform a screen for regulators of macropinocytosis. To stimulate macropinocytosis we utilised the phorbol ester PMA. We had optimised the macropinocytosis dextran uptake assay using PMA and we had achieved a large separation of signal which is required for successfully identifying effectors in a high-throughput screen. We therefore performed the macropinocytosis screen using PMA stimulation instead of EGF stimulation, however we later validated the identified effectors of endosomal release did not affect EGF stimulated macropinocytosis directly.

6.6.1 Reverse transfection using DharmaFECT resulted in non-specific macropinocytosis

Before performing the macropinocytosis high throughput kinome screen, we optimised the 70kDa dextran uptake experiment for use in a 384 multi-well plate format. During the initial optimisation experiments performed in 384 well plates we observed non-specific macropinocytosis in wells treated transfected with siRNA. The macropinocytosis was non-specific as cells that were unstimulated had equivalent numbers of macropinosomes per cell when compared to PMA stimulation. We could not perform the macropinocytosis screen with the non-specific staining and therefore investigated the cause of the non-specific macropinocytosis. We were able to identify the DharmaFECT transfection reagent as the cause of the non-specific macropinocytosis but only when reverse transfection was used. This effect was not observed with non-lipid-based transfection reagent Polyfect, which was

therefore used in the macropinocytosis screen. The non-specific macropinocytosis was observed in multiple cell lines and not confined to our A431 cells. The identification of non-specific macropinocytosis with lipid-based reverse-transfection is important for future high-throughput screens as induction of macropinocytosis may alter results from other screening assays.

6.6.2 Limitations of the dextran uptake assay for high-content screening

Upon completing the siRNA screens for macropinocytosis some challenges were identified in the screening approach and the assay selected. In a large-scale format, the dextran uptake assay was effective at detecting macropinosomes in the A431 cells, however in order to detect all the macropinosomes formed, a Z-stack was taken to acquire images at multiple z-locations. The image analysis to detect the number of macropinosomes was subsequently performed on max projections of the Z-stack. The high-content plate-microscope used to image the macropinocytosis screen could only acquire a single Z-slice for each imaging site. During the small-scale optimisation experiments we manually selected the focus plane to detect the most macropinosomes, however the assay did lose sensitivity as macropinosomes could form outside this focus plane and remain undetected. We concluded from the optimisation experiments the dextran assay was sensitive enough to perform the screen with only acquiring one z-slice per site. During image acquisition of the macropinocytosis screens a fault in the high-content microscope's auto focus was detected, which occasionally caused a focus-shift over time. Before imaging a screen plate, we manually set the focus offset in a control condition to image at the correct Z-plane in order to detect the greatest number of macropinosomes. The microscope-autofocus uses a laser to automatically detect the bottom of the plate and then is offset by the focus offset provided. This should result in the same section of the cell being imaged in each condition; however, we noticed the focus-shift overtime which affected our image quality during the macropinocytosis screens. The focus shift could be due to incorrect detection of the plate bottom during auto-focusing that occurs during prolonged imaging with the microscope. An alternative hypothesis is prolonged imaging was sensitive to changes in the ambient temperature of the microscope which could have affected the focus offset and caused the shift in focus observed over the plate. This error was not noticed during the preliminary experiments as a smaller number of wells were

imaged and the shift of focus occurred after when imaging large number of wells. This error in imaging occurred sporadically and to overcome this error the images were visually inspected post-acquisition, and the plate was reimaged if a shift in focus was observed. We additionally used heat maps from the plates to look for any negative trends in the number of macropinosomes detected across the plate which would be expected if the focus had shifted during imaging.

As our assay relied on focusing on a particular focus plane to capture the macropinosomes, it was particularly sensitive to the systematic error of the auto-focus. For future screens using the dextran assay to detect macropinocytosis, a more advanced imaging system would be required to acquire Z-stack images to alleviate the challenges of correct focus. This would itself have drawbacks as acquiring a Z-stack increases acquisition times, increases image set memory and can complicate image analysis. I believe a more effective approach would be to use a flow-cytometry based assay to detect the fluorescent levels after dextran uptake. This approach would remove the need for correct focusing on the macropinosomes, increase sensitivity of the assay as individual cell data can be acquired and provide detailed information on the level of dextran uptake with low background staining.

As our dextran uptake assay was based on detecting large endosomal vesicles it is possible any hits identified may not be effecting macropinocytosis but altering the endosomal structure, such as inhibition of a negative regulator of endosomal fusion may result in increased large structures that are positive in our assay. Therefore, any hits will need to be validated as being directly involved in macropinocytosis.

6.6.3 The limitations of the macropinocytosis screen positive control siRNA

Our degree of confidence in the data acquired from the macropinocytosis screen is modulated by our confidence in the positive controls. Due to an experimental error during the first macropinocytosis screen, the control siRNA was placed in a separate control plate rather than being distributed in the screening plates. This reduces our confidence due to the lack of controls to monitor for transfection efficiency in each plate. This is confounded by the control siRNA (Marcks, CTBP1) data from the control plate not showing a significant decrease

in macropinocytosis as expected. Additionally, siRNA targeting plk1 showed no cell death in the control plate indicating low transfection efficiency. However, the plk1 siRNA located in one of the screening plates showed a significant reduction in cell death indicating effective knockdown. There potentially was an issue with delivering of transfection reagent to the control well. Analysis of the Z-scores identified potential siRNA hits that decreased the number of macropinosomes per cells and indicated the siRNA were having an effect rather than being clustered around the non-targeting control. During the second screen we were able to include siRNA controls in each plate and the control included showed limited reductions in some of the screening plates. Due to availability of siRNA we had to include alternative positive controls, however these should have been validated more extensively before use as positive controls and therefore the effectiveness was not fully determined.

6.6.4 Identification of effectors of macropinocytosis in A431 cells

From the macropinocytosis screens we were able to identify siRNA that resulted in a reduction in the levels of macropinocytosis in PMA stimulated A431 cells. In total we performed 2 full kinome siRNA screens, followed by 2 validation screens using an alternative siRNA. The positive hits were selected from siRNA that consistently decreased macropinocytosis across the four screening experiments. The decrease in macropinocytosis observed for the hits in 4 independent experiments gave us confidence the effect observed was due to the siRNA interference as a consistent result was seen. However, the challenges identified with the screening assay and controls means further validation is required to ascertain the potential of the hits as effectors of macropinocytosis. The macropinocytosis screen was performed as a control for the release screen and we were able to successfully identify siRNA that affected the levels of macropinocytosis in the A431 cells and therefore could use the hits identified to later aid selection of hits from the endosomal release screen. A secondary use of the screen is to guide further study into effectors of macropinocytosis in A431 cells and we were able to identify some promising strong candidates for involvement in the formation of macropinosomes that can be followed up in future work.

6.6.5 Identified hits from the macropinocytosis screen

From the macropinocytosis screen we were able to identify a list of hits that were potential effectors of macropinocytosis. An encouraging find were effectors that were already known to be involved in macropinocytosis. We identified PAK2, a key signalling component that is known to be involved in macropinocytosis signalling(259). The PAK proteins have been found to be activated by the EGFR signalling pathway to activate macropinocytosis in response to amino acid starvation (123). As well as identifying PAK, some top hit were members of the myotubularin family, MTMR3 and MTMR4. This family of proteins are phosphoinositide phosphatases and are thought to be important for the manipulation of phosphoinositide levels on the forming macropinosomes and throughout maturation (133),(260,261). The identification of these known effectors of macropinocytosis gives confidence in the ability of our screen to identify effectors of macropinocytosis.

We generated a string interaction diagram from the top hits of the macropinocytosis screen to aid identification of interesting proteins. The string interaction analysis groups proteins that are known or predicated interactors. From the string diagram generated using our macropinocytosis hits we identified a cluster of interactions. The five hits that clustered together were FBXO40, FBXO17, FBXW10, SPSB1 and SOCS3. Three of the hits, FBXO40, FBXO17, FBXW10, are members of the F-box family of proteins. This family of proteins are important components involved in targeting proteins for degradation. The F-box proteins are named after a 40 amino-acid sequence that allows interaction with a protein called SKP1 (262). The F-box proteins were originally identified during analysis of cell-cycle mutants in budding yeast and a protein complex was subsequently identified that was able to ubiquitinate proteins, targeting them for degradation. This complex is formed by 3 components, the SKP1 protein, the Cullin protein and a member of the F-box proteins and so the complex was named the SCF. The SCF complex is a functional E3 ubiquitin ligase and provides the substrate specificity for the ubiquitination complex. Different SCF complexes can form depending on the F-box protein incorporated, with the F-box protein providing the specificity for the target protein. The system allows the complex to target a variety of proteins for degradation and the F-box proteins are known to affect a variety of different processes in the cell. Ubiquitination not only targets proteins for degradation but can have wide ranging

effects on the protein. We identified three f-box containing proteins FBXO40, FBXO17, FBXW10 that resulted in decreased macropinocytosis and are predicted to be involved in formation of a SCF complex to function as a E3 ubiquitin ligases. We were interested in this group of interacting proteins as the hits identified had not previously been associated with macropinocytosis and therefore offers the potential to be novel regulators. An important component of the ubiquitin system is the ubiquitin binding domains (UBD) that allow proteins to interact and recognise ubiquitin. The ubiquitin-binding associated protein-2 (UBAP2) contains a ubiquitin binding domain and was found to regulate the activity of kRAS signalling in cancerous cells (263). Additionally UBAP2 was pulled down along with a nano-carrier that was endocytosed by the macropinocytosis pathway indicating the protein was localised to macropinosomes (263). Silencing of the UBPA2 protein significantly decreased dextran-uptake indicating a reduction in macropinocytosis. The F-box containing proteins we identified from our macropinocytosis screen may be involved in a similar pathway in A431 cells and act upstream of the ubiquitin-binding proteins to ubiquitinylate target-proteins to help regulate RAS signalling to promote macropinocytosis. It is well known RAS mutations are prevalent mutations in cancer and additionally it is becoming apparent macropinocytosis is an important endocytic mechanism for nutrient uptake in cancerous cells. It is also well known E3-ubiquitin ligases are important regulators that becomes dysregulated in many cancers to promote cell survival, interrupt the cell stress response, promote cell growth and a multitude of other functions (87,264,265). The F-box proteins identified could play a role in macropinocytosis regulated by ubiquitination in cancer cells and therefore could be an interesting drug target to limit cancer cells performing macropinocytosis to exploit nutrient uptake. An alternative hypothesis is the F-box proteins identified are involved indirectly in regulating macropinocytosis uptake. The SCF complex was initially discovered as a component of the cell cycle checkpoint and functioned to degrade proteins to allow progression, similar to the anaphase promoting complex, APC. It is possible the f-box proteins identified are involved in regulating the cell cycle and their silencing is causing a non-specific effect on macropinocytosis by interrupting the cell cycle progression. Stalling of the cell in a particular cell cycle may have an effect on endocytosis and therefore change the amount of macropinocytosis that can occur. During the macropinocytosis screen the cells were not synchronised and therefore a subsection of cells would be in each cell cycle stage. Effecting

the degree of cells in a stage of the cell cycle may change the amount of macropinocytosis observed.

The non f-box containing proteins, SPSB1 and SOCS3, that were identified in the screen are also thought to be involved in ubiquitination of proteins. They are thought to be the substrate recognition proteins of a protein complex similar to the SCF called an ECS(Elongin BC- Cullin-SOCS-box protein). These proteins both contain SOCS-domains which allow them to engage with the complex. The SPSB1 protein has been implemented in the degradation of the inducible nitric oxide synthase(iNOS) in macrophage cell lines. The SPSB1 was able to ubiquitinate the iNOS protein and target it for degradation. Nitric oxide produced by iNOS is important for the destruction of bacterium engulfed by macrophages, however if the levels of NO are too high this can cause damage to the macrophage, including cell death by apoptosis. The SPSB1 functions to reduce the levels of iNOS to prevent damage to the macrophage. A potential hypothesis is the SPSB1 protein reduces macropinocytosis alongside decreasing iNOS activity to prevent the uptake of additional material that requires inactivation by NO until the macrophage has recovered from damage and prevent the need to produce a toxic level of nitrous oxide. It would be interesting to perform experiments using macrophages to see if SPSB1 has a similar effect on macropinocytosis as well as iNOS activity. We could perform dextran uptake experiments in macrophages to observe if SPSB1 knockdown is able to perturb macropinocytosis and if iNOS is degraded. Additionally, we could study if inhibition of macropinocytosis using EIPA has an effect on NO production and toxicity in the cells to observe If regulation of macropinocytosis may be important in the system.

The suppressor of cytokine signalling-3 (SOCS3) is named after its function to supress the signalling of cytokines, predominantly through the JAK-stat signalling pathway. The release of cytokines allows the transduction of signals to cells to coordinate the immune response to infection. An important aspect of the immune system is inflammation however the homeostasis of inflammation is vital to the correct function of the immune system. Un-controlled inflammation can cause significant damage to the body and excess inflammation is associated with many medical conditions. The SOCS-3 protein has been found to mediate the downregulation of cytokine signalling through the JAK-STAT pathway by inhibiting the

Janus kinase directly as well as being able to inhibit cytokine receptors through physical interaction. The SOCS-3 protein does contain a SOCS-box that allows it to bind to the E3-ubquitin ligase machinery, however it was found SOCS-3 has a lower affinity SOCS-box than other SOCS proteins and the inhibition of JAK-STAT signalling was found to be via direct binding to the receptors and preventing recruitment of receptor substrates. It is possible the SOCS3 protein utilises the E3 ubiquitin ligase machinery for an alternative function. The SOCS3 protein could be involved in modulating macropinocytosis by degradation or changing the function of an effector through its E3 ubiquitin ligase activity to effect macropinocytosis in order to internalise receptors to downregulate the cytokine signalling pathway.

As the macropinocytosis screen was performed as a preliminary screen to the endosomal release screen, there was no time to follow the hits up from the macropinocytosis screen. The hits would need to be validated initially to confirm the effect on macropinocytosis, but the screen has identified some promising candidates to follow up in subsequent projects that focus on macropinocytosis directly.

6.7 Endosomal release screen

We used the endosomal release of HRP to carry out a high throughput screen of the kinome as this was likely to implicate key signalling pathways. The HRP assay had not been utilised previously as a high-content assay and therefore initially the assay needed optimisation to function correctly in the high-content format

6.7.1 Optimisation of the HRP release assay

As for the screen for regulators of macropinocytosis, the high content assay for endosomal release needed to be optimized. A major challenge in detecting endosomal release is that the assay needs to be sufficiently sensitive to detect the signal after release into the cytosol, which has a massive volume of fluid when compared to the endosomal compartments. The dilution of signal makes detection of release challenging but has been overcome successfully, for example the GFP-NLS used in the original adenovirus infection study (24), by allowing the

relocation and concentration of GFP in the nucleus where it can be detected more easily. Our HRP release assay overcomes the problem of cytosolic detection as the production of observable signal is an enzymatic reaction where HRP converts the DAB substrate into the product continuously until the product has built up to levels that become self-inhibitory to the HRP enzyme. This essentially means the HRP enzyme will continue producing signal to fill the available space, so cytosolic HRP show total cell staining rather than endosomal punctate. This means that the assay is sensitive enough to detect endosomal release. However, as the signal is amplified, a small amount of HRP can produce a large amount of product and therefore the signal observed is not proportional to the amount of HRP delivered to the cytosol, so the amount of release cannot be directly determined. Therefore, the HRP assay produces a binary response and we cannot compare the total amount of HRP delivered.

The amplification of signal by the HRP also produced some of the most challenging aspects of using the assay for high-content screening. The high sensitivity meant the assay was sensitive to background signalling caused by un-washed HRP that was not internalised by the cell. When staining the samples, any extracellular HRP molecules could produce a large amount of signal causing non-specific staining in the well. The wash steps in a high-content format are less effective and therefore the background staining was initially higher in the 384 well plates.

The analysis programme had to be optimised for the high-content image analysis of the HRP release assay. The cells releasing endosomal content needed to be identified from the DAB stain. However as bright-field imaging was required for detection of DAB stain this made the analysis harder due to uneven illumination and variations in DAB intensity meant appropriate thresholding of the stain was difficult. We utilised a module that thresholded the brightfield image to identify regions of dark staining in the local pixel environment which was able to successfully locate releasing cells where the cytosolic stain created a region of low intensity pixels that were darker than the immediate surroundings. The module alleviated any problems with uneven illumination and allowed detection of releasing cells.

The quality of the DAB stain was an important factor to consider when using the HRP release assay. The DAB substrate needs to be made fresh for each experiment, and variations in the stain produced different staining qualities observed in different experiments. The DAB

substrate is unstable in solution and slowly degrades overtime and therefore we decided to stain all samples using the same DAB solution at the same time to maintain the same quality of stain across the samples. However, we noticed the background staining increased overtime post staining and therefore we imaged all the plates as soon as possible post-staining to minimise this effect. However, as the kinome requires four 384 well plates, during the screen the incubation time after staining was increased due to image acquisition times being longer when performing the screen which increased the background observed and increased variability in the data. The quality of the stain also affected the sensitivity of the assay and increased variability between repeats as different quality of staining increased variability. We were able to significantly improve the quality and consistency of the DAB stain by optimising the buffer used during staining to a phosphate buffer and optimisation of the fixation procedure using PFA also increased the quality of stain. In the endosomal release screens using the HRP assay there was high variability observed in some conditions and this could be due to the quality of the DAB stain produced.

The HRP-release assay functioned most consistently in the larger format compared to the high-content screens. However even with the lower quality of the high throughput format, we were able to identify hits that increased release that could be taken forward to be validated using an alternative assay.

6.7.2 The endosomal release screens

Endosomal release was dependent on EGF and we confirmed that this was mediated by EGFR by targeting the receptor with siRNA. This was a useful control for the endosomal release assay. We also used PI3K siRNA as a control when the EGFR siRNA was unavailable. Knockdown of PI3K decreased macropinocytosis, and we had shown that endosomal release was dependent on macropinocytosis, using EIPA to inhibit macropinocytosis. The positive control siRNA for the endosomal release screen would ideally have been optimised more before performing the screen to generate more reliable results as the PI3K siRNA was less effective than the EGFR inhibition. Ideally multiple positive controls would have been utilised to increase our confidence in the data.

6.7.3 Identification of hits from the endosomal release screen

The endosomal release screen identified promising hits that both increased and decreased endosomal release in A431 cells. As an aim of the project was to increase endosomal delivery of endocytosed therapeutics, we decided to focus on those hits that increased endosomal release. The data set of siRNAs that decreased endosomal release was useful to compare with pathways that increased release. We took the top hits promoting release and looked for similarities in function and pathways. From our initial analysis we noticed a large number of the hits were involved in the regulation of the immune system. We generated a list of hits to take forward for validation based on the Z-scores generated from the HRP endosomal release screen as well as including siRNA that were had increased endosomal release but were involved in interesting pathways, such as immunity. We validated these top hits using an alternative library, the siGENOME, to control for off target effects of the siRNA. The siGenome library utilises different sequences and RNA modification and therefore if a similar effect on endosomal release is observed using an alternative siRNA, our confidence in the validity of the hit increases. As well as using an alternative siRNA we wanted to use an alternative assay to the HRP assay. The HRP assay allowed identification of hits that increased endosomal release, however due to the binary nature of the assay we could not directly ascertain the amount of release in the cells, just the total number of cells showing release. We therefore validated the assay using an LNP-uptake assay used by AstraZeneca in high-content screens to increase the delivery of LNP therapeutics to the cell.

6.7.4 LNP-uptake screen

The LNP uptake assay performed at AstraZeneca allowed validation of the endosomal release screen hits that increased endosomal release. The assay used a lipid-nanoparticle which contained an mRNA encoding the fluorescent protein, mCherry. Upon endosomal release the mCherry mRNA would be processed by the cellular machinery to produce the fluorescent protein. Importantly the quantity of mCherry produced is proportional to the amount of LNP delivered to the cytosol. The assay enables quantification of the amount of endosomal delivery of mCherry mRNA and is very sensitive to release as mRNA is transcribed multiple times, resulting in an amplification of the signal. The LNP assay had been designed for high-

content screening and therefore was highly optimised with low variability in the controls. The LNP-assay had low background as the LNPs were not themselves fluorescent.

The readout from the LNP release assay differed slightly to those from the HRP assay. The LNP assay produced the total amount of endosomal release occurring across all the cells observed. This is in contrast to the HRP screen in which the total number of cells that had detectable endosomal release occurring. These two assays have slightly different outputs that give us additional information into the release observed and the effect our hits are having on the release. A caveat to using the LNP release screen is the difference in the type of endosomal release being observed in the assay. The LNPs are formulated to act as a carrier for cargo to enable delivery of the cargo into the cytosol. Thus, LNPs themselves stimulate endocytosis and endosomal release. There is a moderate degree of release observed under basal conditions when using the LNP release assay. When performing the LNP assay using our hits we wanted to see if the siRNA that increased endosomal release in the HRP release screen had a similar effect on the LNP release screen.

The LNP release assay had been optimised for use in H358 cells and therefore we initially tested the effect of knocking down our identified hits in this cell line.
The experimental procedure used for an LNP uptake experiment requires a longer incubation time (24 hours) to allow translation of the mRNA to produce the fluorescent signal observed. It is likely EGF stimulation for this length of time would have vastly different effects, including transcriptional changes, compared to the much shorter incubation time used in the HRP release assay. As the LNPs promote their own endosomal release, we performed the assays both with without EGF stimulation to see whether EGF might enhance release in the H358 cells. EGF did not stimulate release in the LNP release assay. H358 cells are RAS activated and therefore have overactive RAS signalling without external activation. Since RAS is activated by EGF signalling under regular conditions, the constitutive RAS activation in the H358 could explain why EGF did not have an effect in the LNP assay.

The LNP uptake assay worked very effectively in the H358 cells and we were able to identify the siRNAs that increased the delivery of LNP to the cytosol. As a positive control in the LNP screen I included a sample with twice the usual amount 2x(20ng) of LNP which is expected to

increase the amount of fluorescent protein translated. Any siRNA that increased delivery to a greater extent than the 40ng control was concluded as a positive hit because it would represent a significant improvement for delivery of therapeutic molecules as lower doses are required to generate the same effect.

We repeated the LNP assay in the A431 cell line to generate results from both assays in the same cell line. The LNP assay had greater variability between repeats in A431 cells. The LNP assay had not previously been used in the A431 cells and limited optimisation could be performed prior to performing the screen due to time constraints. Importantly, however, there were several hits identified that increased LNP delivery to a greater extent than the 40ng LNP control. We identified hits that were able to consistently promote release to the same level of release as the 40ng control.

The stimulation of A431 cells with EGF decreased the intensity of LNP signal indicating a decrease in delivery. EGF stimulation of LNP release was insensitive to EIPA, indicating that the uptake of LNP is not dependent on macropinocytosis when cells have been treated with EGF for a long period of time. *The decrease in LNP signal in cells treated with EGF could be due to decreased macropinocytosis in these cells, which would explain why EIPA has no effect. In* A431 cells treated with EGF the signal observed could be LNP delivered through a non-macropinosomal uptake pathway and is therefore no longer affected by EIPA. The 24 hour treatment of cells with a high concentration of EGF could affect cellular trafficking pathways such as macropinocytosis. To explain the differences observed in the H358 cells and A431 cells, we used immunofluorescent staining to examine the effect of the longer EGF stimulation on the EGFR in the two cell types. Regardless of the presence of EGF, H358 cells showed intracellular staining of the receptor indicating a high turnover from the cell surface. This is likely due to the activated RAS affecting the EGFR localisation. In A431 cells the EGFR was located at the cell surface under basal conditions but when cells were treated with EGF for 24 hours there was, as expected, a large decrease in the amount of EGFR present indicating degradation, and the remaining EGFR was endosomal. This data showed the longer time with EGF had dramatic effects on the A431 cell receptor localisation and signalling and therefore it is unsurprising this had an effect on the signal observed (266). Interestingly, in the LNP assay in A431 cells, siRNA targeting the EGFR had no effect in the EGF condition but

caused a reduction in delivery in unstimulated cells. If EGF stimulation results in degradation of the EGFR over the 24-hour period, then our result that EGFR knockdown has no effect is explained as receptor is degraded anyway and therefore silencing it has no effect. It is interesting that EGFR silencing decreased LNP delivery when cells were unstimulated and therefore without EGF. This could be due to background EGF signalling from molecules present in the serum used. Due to the experimental design, we could not serum starve the cells and prevent this background signalling.

We selected siRNA that increased LNP delivery to a greater extent than the 40ng LNP control from the A431 LNP release screen and compared them to the previous screens, the H358 LNP screen and the A431 HRP screen. From the combined screens, we were able to identify four siRNA that increased endosomal delivery in all of the screens performed and therefore were selected as promising candidates for further study. The hits identified were IRAK-M, PEAK1, MAP2K5 and NUCKS1. These 4 siRNA had been identified to increase endosomal release in two distinct assays and in two different cell types. We had completed our aim of identifying promising hits to take forward for further validation and analysis.

6.7.5 Validation of the hits

After identification of the hits, we performed a literature search to acquire information that was known about the proteins and possible mechanisms they might be affecting endosomal release. The protein IRAK-M is a component of the innate immune system. The protein is a negative regulator of TLR signalling which can be induced by recognition of pathogenic patterns or via cytokine activity. It plays an important role in the regulation of the inflammatory response by preventing overactivated inflammation that can result in damage to the body.

The peak1 protein is a pseudo-kinase thought to be involved in EGFR signalling. Pseudo-kinases are a sub-group of kinases that are predicted to lack functional catalytic domains based on sequence analysis and therefore are not thought to be involved in direct phosphorylation of target proteins. The pseudo-kinases regularly function as scaffolding proteins and peak1 is believed to function as a scaffolding protein involved in EGFR signalling.

The MAP2K5 protein is a member of the MEK/ERK signalling pathway which is involved in cell growth and proliferation. The MEK-ERK pathway is activated by EGF signalling. The MAP2K5 and PEAK1 proteins might be involved in specific arms of the EGFR signalling pathway involved in endosomal release.

NUCKS1 is a kinase located in the nucleus, and therefore is likely to have an effect on gene transcription rather than a direct effect on endosomal release. As NUCKS1 is likely to have an indirect effect on endosomal release we decided to focus or validation on PEAK1, IRAK-M and MAP2K5 initially. However, the effect of NUCKS1 on delivery could be studied in a future project to try to ascertain which protein expression levels change due to NUCKS1 silencing.

6.7.6 Confirmation of the degree of knockdown achieved by siRNA.

q-PCR analysis confirmed knockdown of Peak1 and MEK5 using the relevant siRNAs. We could not show a reduction with IRAK-M siRNA, largely because the Ct values obtained were often very high indicting low amplification of signal. This could be due to low expression levels of IRAK-M in the A431 cell line that make detection difficult. The primer pairs used to amplify IRAK-M may not have correctly identified the mRNA of IRAK-N leading to improper amplification. We tested two different IRAK-M primer pairs to try to resolve the issue but could not observe good amplification. Potentially an alternative splicing event occurs in the IRAK-M gene in A431 cells preventing detection using our primer pairs. Due to time limitations, we were not able to solve these challenges but in the future we would either optimise the q-PCR for the IRAK-M gene or attempt detection of the protein levels using western-blot analysis.

6.7.7 Knockdown of the identified hits does not affect macropinocytosis

We initially performed the macropinocytosis screen to compare with hits identified in the endosomal release screen. An increase in endosomal delivery of either HRP or LNP could be simply due to an increase the rate of endocytosis, which translates into a greater signal observed. All of the hits identified from the endosomal release screen showed Z-scores between $-2 < x > 2$ in the macropinocytosis screen, indicating they do not affect macropinocytosis to a large extent. The macropinocytosis screen was performed under PMA

stimulation and further experiments measuring macropinocytosis following knockdown of the hits confirmed that EGF stimulated macropinocytosis was not affected. This confirmed that the increase in endosomal release observed was not due to an increase in the uptake of macropinocytosis marker.

6.7.8 Increased endosomal release does not result from direct membrane damage

A route of endosomal release is via direct membrane damage to the endosomal membrane. Several virus proteins and potentially the membranes of LNP particles disrupt cellular membranes by destabilising the membrane. These membrane disruptions could either be small and result in low-scale leakage of endosomal content or they could rupture the entire endosome structure, releasing the entire content. We wanted to ascertain the level of damage to the endosomes upon silencing of our hits. The galectin proteins are recruited to localised areas of membrane damage and form puncta at membrane damage which can be observed by immunofluorescence. The galectin assay has been utilised to detect endosomal rupture by *Salmonella* infection as well as loss of permeability detected in lysosomal disorders (251,252). LLOME, a chemical that ruptures lysosomes, resulted in galectin punctate forming whereas cells treated with the identified siRNA had no effect. This result indicated the hits were not directly causing endosomal rupture to occur. This could indicate the mechanism of endosomal escape is via a non-membrane damaging system. The galectin-punctate assay has been used to study the endosomal escape of several viruses (253). The infection of adenovirus caused galectin-puncta recruitment indicating direct damage. Adenovirus is an enveloped virus and is thought to cause direct membrane damage via a lytic protein. During the same experiment, a non-enveloped virus, reovirus did not cause galectin puncta to form. It is known reovirus forms small pore structures in the endosomal membrane to promote endosomal release (267). This suggested that the endosomal release we had identified might be via a mechanism of transfer across the membrane, potentially via a pore protein.

6.7.9 Investigation into the NF-kB pathway as a signalling pathway involved in EGF stimulated release

Some of the hits were known to be involved in the regulation of innate immune signalling. Irak-M is involved in the regulation of immune signalling via Toll-like receptors and there is evidence that NUCKS1 plays a role in the regulation of innate immune system signalling, including the NF-kB signalling pathway (268). We also identified a subunit of the NF-KB transcription factor RELA to be a strong negative regulator of endosomal release in the HRP release screen. The NF-kB pathway is known to be activated by EGF signalling and therefore we decided we should investigate NFkB signalling as a potential explanation for EGF inducing endosomal release in A431 cells. Our data from the galectin assay indicated the type of endosomal release caused was likely via a mechanism which is intrinsic to normal cellular function rather than global destabilisation of the endosomal membrane. One cellular process which requires delivery of material from the endosome into the cytosol is antigen cross presentation. The process entails release of endocytosed antigens to the cytosol for presentation onto MHC-1 proteins. The process of cross presentation is closely aligned with regulation of the immune response and therefore we were especially interested in the links to NF-kB signalling.

6.7.10 EGF stimulation activates NF-kB signalling in A431 cells

We first confirmed that EGF can stimulate NFkB signalling in A431 cells. The NFKB complex is sequestered in the cytosol until phosphorylation by upstream kinases. We were able to confirm nuclear translocation of the NFKB subunit, RELA, from the cytosol after stimulation with EGF in A431 cells. The nuclear translocation of RELA occurred after 20 minutes of EGF stimulation, with release of HRP being seen after 10 minutes. This indicated that a component of the NF-kB signalling pathway upstream of nuclear translocation might be responsible for increasing endosomal release rather than an effect of the RELA transcription factor affecting gene expression in the nucleus. We showed an earlier activation (10 minutes post EGF treatment) of NF kappa B signalling by measuring phosphorylation of p65 and degradation of IkK. This was consistent with the time course of endosomal release.

Ionomycin, a known strong activator of NF-kB signalling, treatment activate NFKB signalling in A431 cells to a level similar to the longest EGF stimulations indicating EGF could activate the pathway to the same extent as Ionomycin.

6.7.11 Treatment of A431 cells with IFN-y increased endosomal release observed with EGF stimulation

One function of NF-kB signalling is to regulate the production of cytokines such as interferons. It is known that cytokines can activate NF-kB signalling and we were able to show stimulation of A431 cells with interferon-Y for 16 hours increased the release of HRP to the cytosol. This again suggested the release stimulated by EGF signalling was in part connected to the immune response as a cytokine was able to increase the release observed. The treatment of interferon-y was a much greater time period than the EGF signalling and therefore it is likely the IFN-Y had a transcriptional change on the A431 cells to increase the release observed. Potentially the earlier stimulation of Ifn-Y promotes a stronger NF-kB signalling in response to EGF and therefore increases the release observed.

6.7.12 Pharmacological inhibitors of NF-kB have variable effects on EGF stimulated endosomal release.

We had identified NF-kB as a potential signalling pathway involved in the release of content from the endosomal system. We decided to utilise known pharmacological inhibitors of the NF-kB pathway to observe the effect on endosomal release. The Nf-kB pathway is complex and there are several routes of signalling and therefore we used several NF-kB inhibitors that target different components of the signalling pathway. Due to availability, we initially tested the drug BX795 as an inhibitor of the non-canonical NF-kB pathway. The inhibitor BX795 increased the amount of endosomal release observed in A431 cells. BX795 inhibits the IKKe protein that function by phosphorylating the IKB protein. However, BX795 is not specific to IKKe and does inhibit additional targets, such as inhibition of PDK-1. As mentioned previously PDK-1 is involved in macropinosome signalling and could be affecting macropinocytosis. The inhibitor BX-795 was additionally predicted as being able to bind to Irak-M in the screen performed to identify inhibitors of IRAK-M. Therefore, it is difficult to know if BX795's effect on endosomal release is due to inhibition of IKKe or via PDK-1/Irak-M.

As BX795 inhibition was inconclusive we utilised the more conventional NF-kB inhibitors, IKK-16 and Amlexanox that are known specific NF-kB inhibitors. The inhibitor IKK-16 targets the IKK complex, mainly inhibiting IKKa and IKKb and so mainly inhibits the canonical NF-kB pathway but can inhibit non-canonical signalling to a lesser extent. On the other hand, Amlexanox inhibits IKKe specificity and therefore is known as an inhibitor of the non-canonical NF-kB pathway. We were able to show inhibition of the canonical NF-kB pathway with IKK-16 prevented EGF stimulated endosomal release when preincubated with IKK-16 for 4 hours. Amlexanox treatment had no effect on endosomal release. The pharmacological inhibitor experiments directly linked the canonical NF-kB signalling to EGF stimulated endosomal release.

6.7.13 Activation of NF-kB using ionomycin does not increase endosomal release

To further explore the role of NF kappa B in regulating endosomal release, we wanted to know if activation of NF-kB independent of EGF signalling also increased endosomal release. We had demonstrated that activation of NF kappa B signalling with Ionomycin occurred in the same time frame as EGF-dependent release. Ionomycin treatment had no effect on endosomal release which suggested that a component of the EGF signalling pathway, additional to NFkappaB signalling might be important for stimulating release, rather than just activating NF-kB signalling. The NF-kB signalling may not play a direct role in endosomal release and our results could be due to correlation.

We had previously shown the HRP release was susceptible to the macropinocytosis inhibitor EIPA indicating the formation of macropinosomes may be important to promote release. The Ionomycin/PMA treatment activates NF-kB as Ionomycin is a calcium ionophore which activates calcium sensitive kinase and PMA activates PKC and so activates NF-kB in combination (We previously used PMA to activate macropinocytosis in chapter 4 but the concentration to activate NF-kB is a factor of 3 lower than previously used, and therefore does not induce macropinocytosis). The treatment of cells with Ionomycin and PMA is not known to promote macropinocytosis and could explain why it is not sufficient to increase HRP release as macropinocytosis is required.

The treatment of A431 cells with EGF and Ionomycin/PMA in combination did not increase the endosomal release observed compared to only EGF stimulation indicating there is no additive effect of NF-kB activation on release. We were able to show EGF and Ionomycin individually strongly activate the NF-kB pathway and it is likely to be close to the maximum activation.

6.7.14 The pre-treatment of cells with Ionomycin abolishes EGF stimulated release.

During experimentation into using Ionomycin as an activator of NF-kB signalling we discovered that preincubation of A431 cells with Ionomycin for an hour prior to HRP addition ablated any cytosolic release of HRP. The preincubation with the activator of NF-kB prevented endosomal release which indicated the temporal activation of the NF-kB signalling is important to promote endosomal release. The activation of NF-kB signalling occurs over a time period, and we previously showed the time course for phosphorylation of NF-kB, degradation of IKB and nuclear translocation. These events happened between 10-40 minutes post stimulation. We hypothesised that the activation of NF-kB has to occur at a similar time to uptake and the preincubation activates NF-kB signalling too early which then inhibits endosomal release later. We expect a recovery time is required before the signalling pathway can reset.

6.7.15 Preincubation with EGF prevents endosomal release

Similar to pre-treatment with ionomycin, preincubation with EGF prevented endosomal release. When cells were pre-treated with EGF we did not see endosomal release at all time points of pre-treatment between 10 minutes and 60 minutes. These experiments highlighted the short time frame for endosomal release to be triggered as EGF signalling 10 minutes prior to HRP addition completely prevented endosomal release. The duration of EGF signalling and NF-kB is longer than 10 minutes which indicates the effectors of endosomal release are activated early in the signalling pathway. This temporal regulation of endosomal release can suggest possible mechanisms. Our theory that endosomal release occurs from macropinosomes could indicate the macropinosomes formed initially due to EGF signalling are permeable and allow release to occur, whereas macropinosomes formed later are non-

permeable which would explain why EGF preincubation prevents release. In EGF signalling there are many negative feedback mechanisms that prevent overactivation of the system upon overstimulation of the receptors. A simple negative feedback is endocytosis of the receptor and degradation. A possibility for the effect of EGF preincubation is simply the availability of EGF receptor at the cell surface that prevents the necessary signalling to occur to stimulate endosomal release. The preincubation of cells with EGF will trigger endocytosis of EGFR receptors and desensitise the cells to further stimulation. To observe the recovery time of the cells after EGF stimulation, we performed experiments where cells were stimulated with EGF for 10 minutes followed by variable recovery time and a HRP uptake assay to assess endosomal release. We were able to show that while a recovery time of 2 hours was not sufficient to rescue the release observed, a longer recovery time of 11 hours was sufficient to allow stimulation of endosomal release in the cells. Interestingly the endosomal release observed after an 11-hour recovery time period was significantly greater than observed in the control cells without preincubation and cells left to recover for a longer period of time. This result was interesting as the pre-stimulation primed the cells to be more effective at stimulating endosomal release. This result could be transcriptional changes to the cells that increase the levels of the endosomal release machinery, or potentially leads to greater numbers of EGFR at the cell surface. The activation of cells with EGF and subsequent NF-kB activation could prime cells for increased endosomal release in a complementary mechanism to cells which experience pro-inflammatory signalling from NF-kB and are primed to increase presentation of antigens. To investigate this effect further, in a future experiment we could observe the changes to NF-kB activation following the preincubation with EGF. We may observe a change in the magnitude of NF-kB signalling however we previously showed Ionomycin could not stimulate endosomal release and there was no additive effect of ionomycin and EGF indicating that NF-kB signalling was saturated. We may see a difference in the kinetics of signalling which would increase our understanding in the requirements for endosomal release.

An obvious hypothesis is the pre-stimulation of cells with EGF alter the availability of EGFR at the cell surface and therefore affects the later EGF signalling preventing endosomal release from occurring. Further experiments could be performed to assess the quantity of cell surface EGFR utilising a surface biotinylation based approach. From the literature EGF stimulation of

macropinocytosis in A431 has been previously shown to result in recycling of macropinosomes to the cell surface rather than degradation (229). It has also been shown that the EGF receptor is recycled multiple times after internalisation to the cell surface rather than degradation in A431 cells(269), and studies into the rate of EGF degradation have shown each EGF receptor can internalise and degrade multiple EGF molecules via recycling back to the plasma membrane (270). Combined with the high-expression levels of EGFR on A431 cells it is unlikely the preincubation with EGF for 10 minutes could result in degradation of sufficient EGFR to prevent any EGF signalling occurring. This suggests that the ability of EGF to stimulate endosomal release depends on strong EGF signalling. During the optimisation experiments we generated a concentration curve of EGF to see if altering the EGF concentration had an effect on the endosomal release observed. We varied the concentration from 66ng/ml to 400 ng/ml but this had no effect on the levels of endosomal release seen. A high concentration of EGF is required to trigger macropinocytosis which has been shown to be important in endosomal release.

6.7.16 Stimulation of A431 cells with alternative EGFR ligands can also stimulate endosomal release

The stimulation of endosomal release using EGF has been shown to be dependent partly on the EGFR by siRNA silencing of the EGFR which decreases the level of EGF stimulated release. The EGFR signalling system is complex and multiple different ligands can interact with the signalling system by binding to the EGFR receptor as well as other members of the ErbB2 family of receptor tyrosine kinases. As there are four members of the ErbB2 family of receptors and an active receptor is a homo or hetero dimer of two receptors the system has built in complexity with a variety of signalling occurring. EGF is a high-affinity ligand for the EGFR and is the canonical activator of EGFR signalling. We also showed stimulation of A431 cells with some alternative ERBb2 ligands was able to stimulate endosomal release. The ligands B-cellulin and Heparin-binding epidermal growth factor were able to stimulate endosomal release in A431 cells whereas amphiregulin had less of a response and showed limited release only at very high concentrations. The ligand, Beta-cellulin is a high affinity ligand for EGFR and ERbB4 (201). The HB-EGF ligand also shows affinity for EGFR and ERBb4 which is similar to the binding of EGF(201). The amphiregulin ligand has a much lower affinity

(100 fold weaker) (271) which may explain the differences observed. These results indicate the ligands do not impart specificity to trigger the endosomal release observed and activation of the EGFR is sufficient. The different ligands of the Erb family have been shown to have variable effects in different cell types and promote different signalling outcomes. It is possible, as the A431 cells are cancerous cells that express the EGFR to a high degree that is not naturally observed, the signalling from the ligands is altered from normal biological functions of the EGFR ligands. The ability of other ERBb2 receptor ligands to stimulate endosomal release suggests a key pathway of EGFR signalling is being required.

6.7.17 Endosomal release triggered by EGF is not damaging to the cells

An important consideration in increasing cytosolic delivery of therapeutic molecules is the potential for cell toxicity. The release of endosomal content to the cytosol can be damaging for the cell. Cell penetrating peptides have been linked to induced apoptosis and therefore the concentration needs to be limited to prevent damage to the cell (272). From our recovery experiments we were able to observe the cells were healthy and not noticeably damaged by the EGF treatment and induced endosomal release. The EGF signalling promoted growth and more cells were observed rather than apoptosis. This indicated the endosomal release was selective and did not cause damage to the cell. This could be as the endosomal release is a natural mechanism to release content, rather than an artificial release such as a CPP. This has advantages in lower cytotoxicity and immunogenicity but could provide problems in the quantity and size of protein that can be delivered.

6.7.18 Endosomal release occurs from a subset of endosomal vesicles

From our experiments we could deduce only a subsection of endosomes/macropinosomes can release content as preincubation prevented release, even 10 minutes prior to HRP addition. This suggested that macropinosomes formed after the initial signalling event did not release their content. It is possible the EGF signalling induces endosomal wide release and as our HRP signal is added at the same time as the EGF we did not observe the release from already formed endosomes. A possible experiment to observe this would be to load the

endosomal system initially by incubation of cells with the HRP for a period of time to allow HRP uptake followed by the EGF stimulation without HRP to see if the release occurs from current endosomal populations as well as newly formed macropinosomes(6).

6.7.19 Pharmacological inhibitors validation of hits from the siRNA screen

The inhibition of proteins using siRNA occurs over a period of 3 days, we therefore wanted to show acute inhibition of the identified hits as a method of validation.

A challenge however with using pharmacological inhibitors is the specificity for the correct target. Many kinase inhibitors target the binding pocket of kinases and therefore many pharmacological inhibitors can function on multiple kinases that contain conserved regions. We first had to identify pharmacological inhibitors of the proteins which was challenging for the pseudo-kinases IRAK-M and peak1 as without an active binding site these proteins are difficult to inhibit with conventional protein-kinase inhibitors. We were able to identify a pharmacological inhibitor of MEK5, bix-02189 which however only caused a marginal increase in endosomal release. As pharmacological inhibitors act more quickly than siRNA interference it is possible that MEK5 knockdown affects endosomal release by altering the EGF signalling pathway, in a similar fashion to EGF preincubation priming the cells for release and requires sustained inhibition than the more transient pharmacological inhibitor. Potential optimisation of the concentration and incubation time of bix-02189 could increase the release observed.

We were unable to find pharmacological inhibitors that target Peak1. To inhibit Irak-M we used some preliminary data from an indirect binding assay that identified tak-901 and BX-912 as potential inhibitors of IRAK-M (Unpublished data from Stefan Knapp). These potential inhibitors were unvalidated and untested in a cellular system and therefore we did not know if they functioned to inhibit IRAK-M in our system. The inhibitor BX-912 had a strong effect on endosomal release and an increase in endosomal release was observed after a 4-hour pre-treatment. Treating cells with the inhibitor tak-901 causes a slight but not significant increase in endosomal release. The effect on endosomal release from BX-912 could be due to inhibition of IRAK-M but could additionally be due to inhibition of an alternative kinase, such as PDK1 which Bx912 is known to inhibit strongly. Phosphoinositide-dependent kinase-1 (PDK1) is known to be involved in macropinosome signalling and therefore inhibition of PDK1

may slow the maturation of macropinosomes, therefore increasing the duration for endosomal release to occur.

6.7.20 Inhibition of the proteasome prevents endosomal release from occurring

The pharmacological inhibitor MG132 inhibits the proteasome complex. We showed MG132 prevented EGF from stimulating endosomal release indicating degradation of proteins are required in the process. This result can not directly point to a pathway as many cellular processes require proteasomal degradation to function correctly and therefore MG132 will have wide-ranging effects. The EGF signalling pathway itself requires the proteasome and MG132 has been shown to prolong EGFR phosphorylation (273). However, MG132 has been utilised as an inhibitor of NF-kB signalling as it prevents degradation of the IkB protein which usually inhibits the translocation of the transcription factor to the nucleus (274). The effect on endosomal release could be due to preventing NF-kB signalling from occurring.

6.7.21 Antigen cross presentation as a potential mechanism involved in endosomal release.

We can elucidate certain characteristics of the endosomal release from experiments performed. The releasing cells did not recruit Galectin-3 punctate indicating the membrane was not physically damaged. Additionally, stimulation with EGF did not apparently have any toxic effect on the cells. Together this suggested that we had uncovered a release mechanism which might occur under physiological conditions. We had also identified that NF-kB signalling was playing a role in stimulating endosomal release. We looked for biological systems connected to immune response signalling that requires transport of material from the endosomal system to the cytosol. A potential system is antigen cross presentation where endocytosed antigens are released from the endosomal system to the cytosol where they can be presented by the MHC1 process. Cross presentation usually occurs in professional immune cells such as dendritic cells and macrophages.

As our experiments were in a cancerous cell line the normal biological process may be altered to provide benefits to the cancer cell. The machinery that enables endosomal release in antigen cross presentation is currently unknown. Two possible mechanisms have been suggested, retro-translocation through a protein pore or membrane damage and rupture of

the endosomes. We began experimentation into antigen cross presentation using a SIINFEKL uptake experiment in the A431 cells. If antigen-cross presentation occurs, the SIINFEKL peptide is cross-presented to the cell surface by MHC-1 receptors that can be detected by flow cytometry with a specific antibody to the MHC-1-SIINFEKL peptide complex. We were not able to show direct SIINFEKL cross-presentation in A431 cells using this assay. We could show MHC-1 on the cell surface but could not show SIINFEKL release. It is possible the mechanism of endosomal release is similar to antigen cross-presentation but the machinery for loading cross-presented antigens onto MHC-1 is not present in A431 cells. In future work we will investigate if the identified hits are able to increase antigen-cross presentation in professional immune cells. We are planning on extracting bone marrow-derived dendritic cells from mice so we can perform experiments to see if our proteins of interest have an effect on antigen presentation in these cells. This would confirm if our identified proteins are having an effect on the process of antigen-cross presentation to increase the delivery of material from the endosomal system to the cytosol.

6.8 Future directions

The work completed for this thesis has identified several exciting protein candidates that could increase our understanding of endosomal release as a route to enhancing the cytosolic delivery of endocytosed therapeutics. We were also able to identify some exciting regulators of macropinocytosis that need validation and further study to discover their role in macropinocytosis. We have been able to implicate the NF-kB signalling pathway and the innate immune response as having a role in the endosomal release we have observed. To directly observe if antigen-cross presentation is the mechanism involved in the endosomal release observed we will perform antigen-cross presentation assays in professional immune cells, mouse bone-marrow derived dendritic cells. We will be able to use this model to observe if silencing our identified hits is able to increase antigen-cross presentation in these cells. We could not show antigen-cross presentation using the SIINFEKL uptake assay in the A431 cells, but it is possible these cells do not have the correct mechanism for cross presentation onto MHC-1 after antigen release from the endosome and are only able to release content in a pathway similar to antigen cross presentation due to cancerous manipulation of cellular processes. If we could show increased antigen-cross presentation

with silencing of our proteins of interest than we could further study how our proteins are affecting endosomal release. IRAK-M is involved in regulation of NF-kB signalling from cytokine receptors and therefore may modulate the kinetics of NF-kB signalling. We could investigate the role IRAK-M has in NF-kB signalling and which downstream proteins are affected by IRAK-M silencing using proteomics to identify key effectors of endosomal release. The proteins PEAK-1 and MAP2K5 are likely to effect endosomal release by effecting EGF signalling. We can investigate the downstream signalling from these proteins and identify effectors that directly allow endosomal release. Potentially the signalling pathway leads to activation of sec61 to allow retro-translocation of proteins or recruitment of an unknown protein to form a proteinaceous pore to allow endosomal escape to occur. As several of the hits are pseudo-kinases, we could investigate their role in signalling, either by discovering their mechanism of phosphorylation or understanding their scaffolding functions. Many pseudo-kinases function as scaffold proteins and can form multimeric complexes. A multimeric complex could also form a pore and therefore the pseudo-kinases might be able to form a pore. We could investigate the structural role in endosomal release.

Once a mechanism of release is identified, future work could look to utilise this mechanism as a route for delivering endocytosed therapeutics to the cytosol.

Chapter7: Appendix

7.1 HRP analysis-high throughput analysis

HRP assay high-throughput image analysis

1) load images

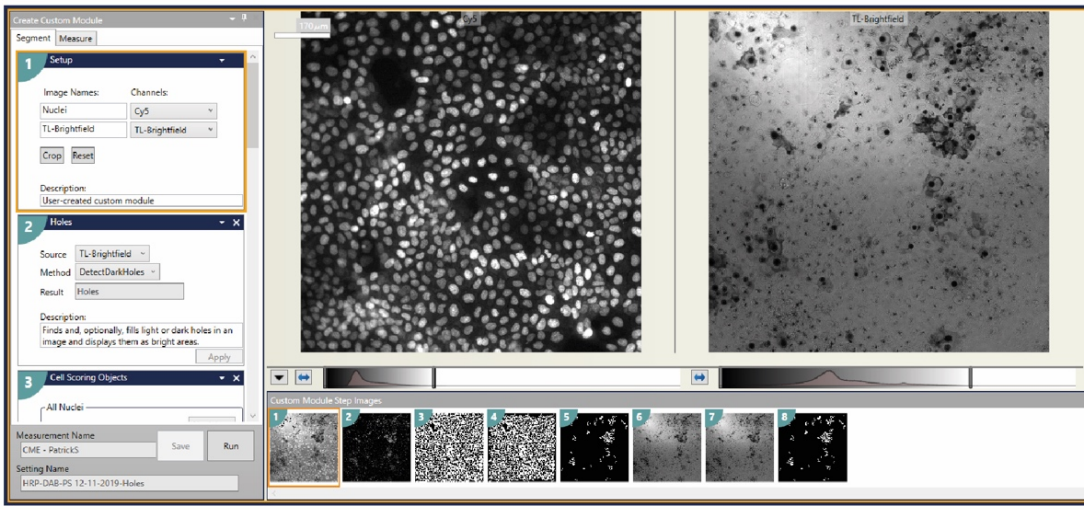

2) Identify dark regions

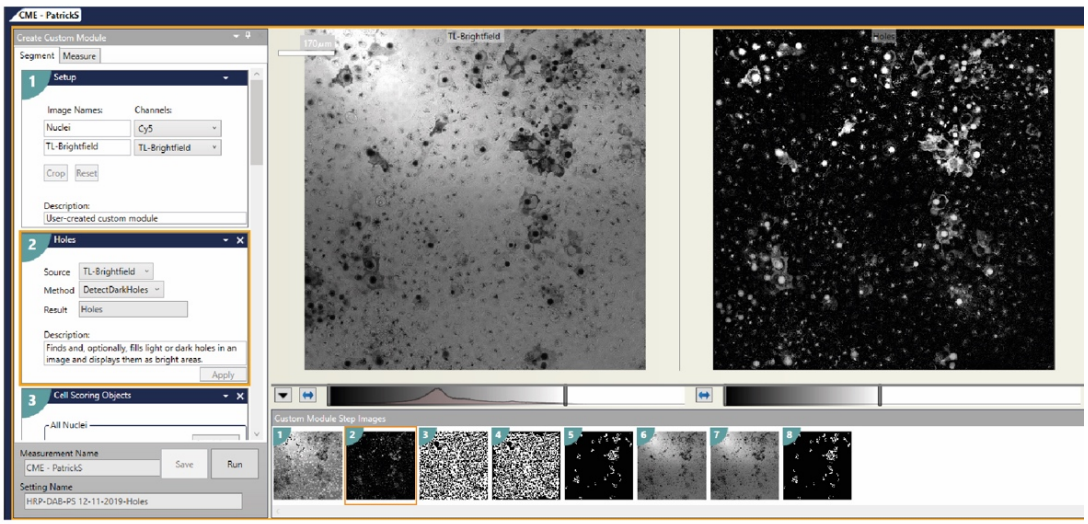

3) Identify nuclei and cytoplasm

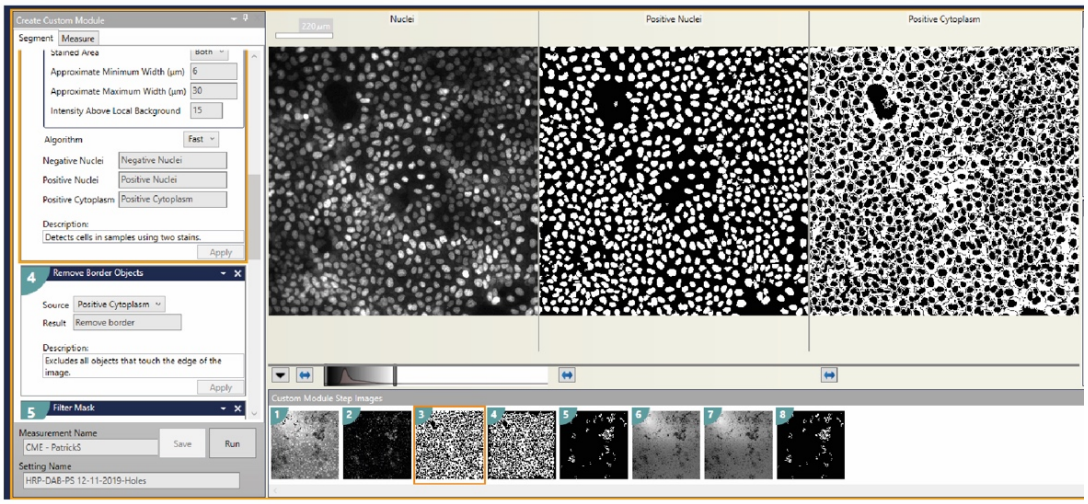

4) Remove border objects

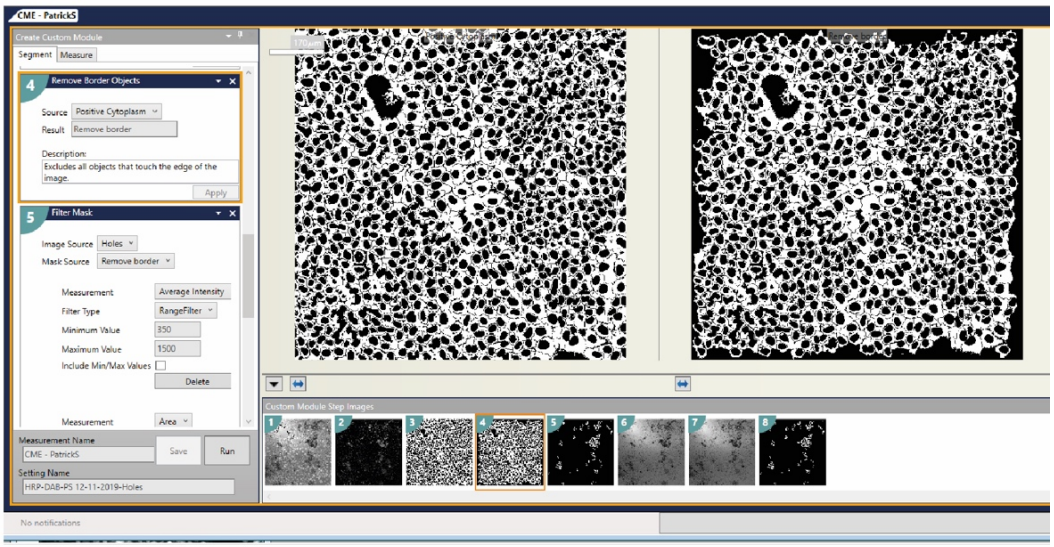

5) Filter cells based on intensity

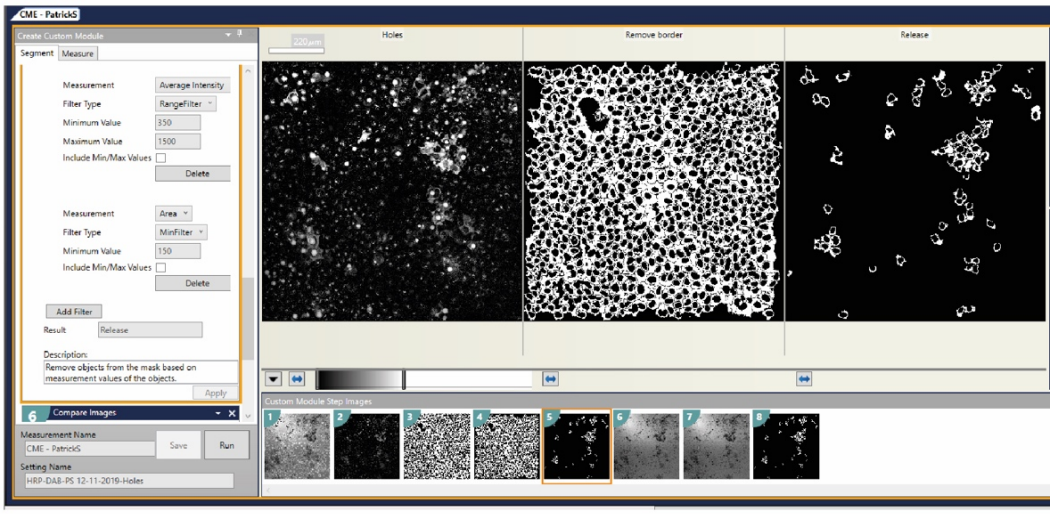

6) Identified cells

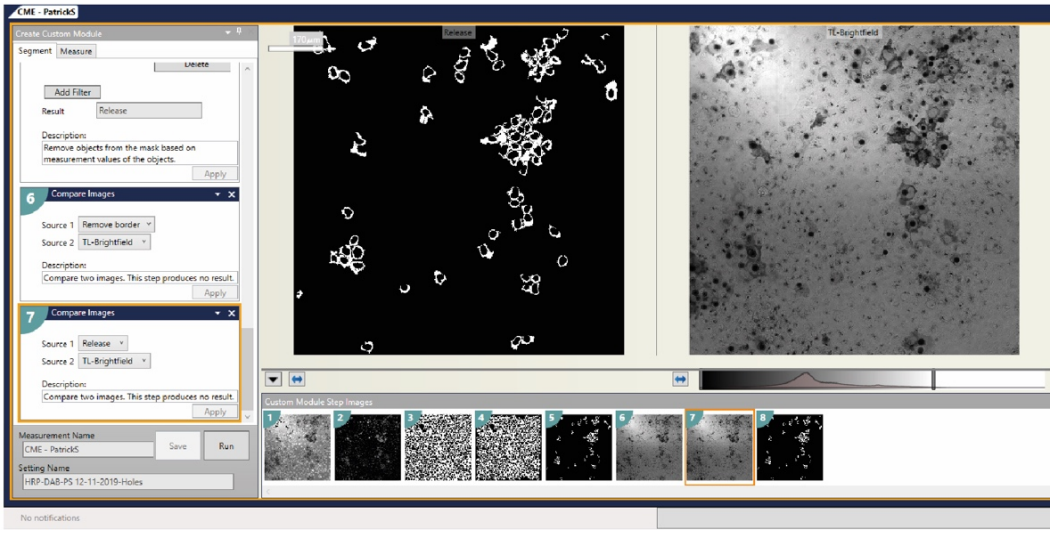

7.2 Macropinocytosis analysis high-throughput analysis

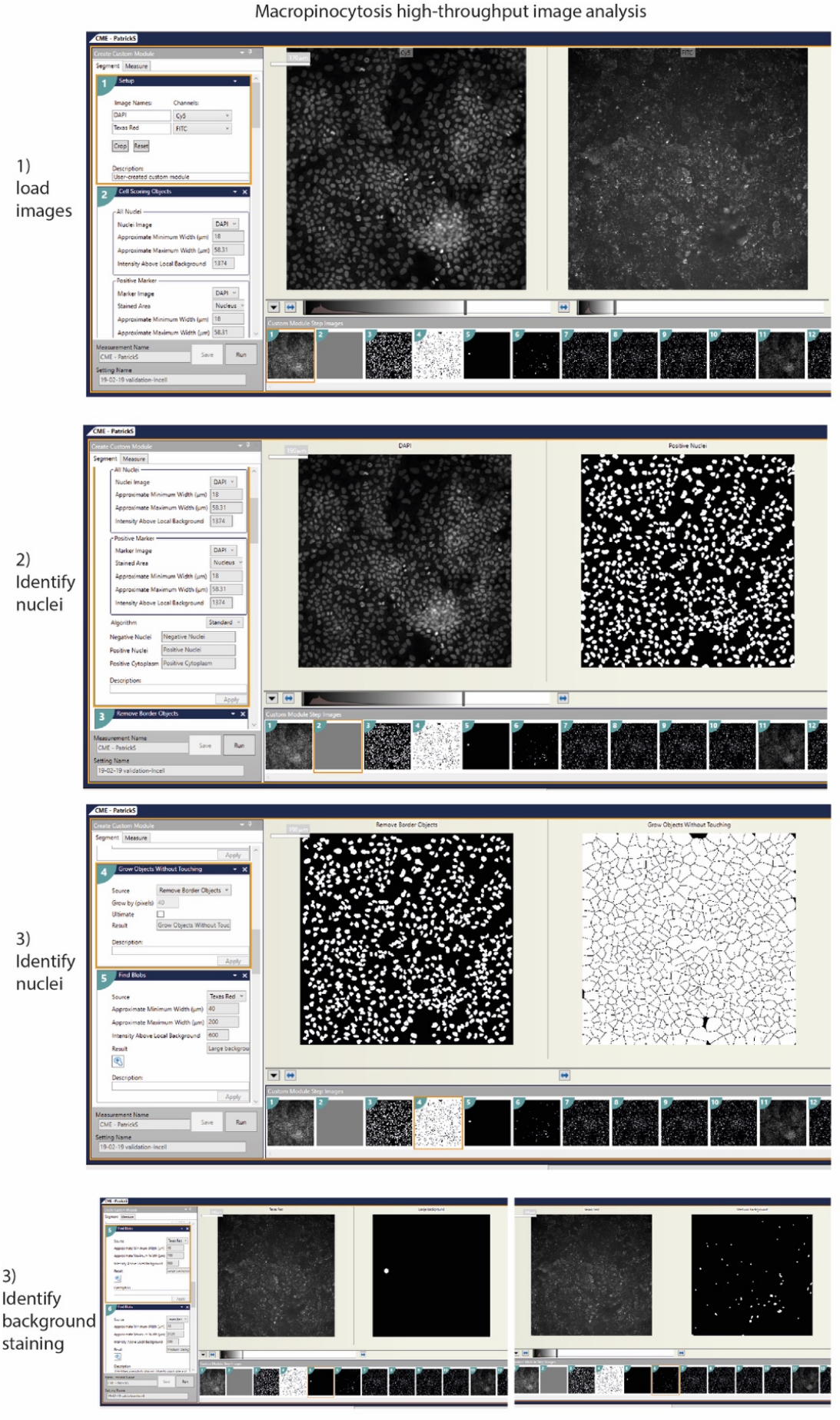

4) Identify macro-pinosomes

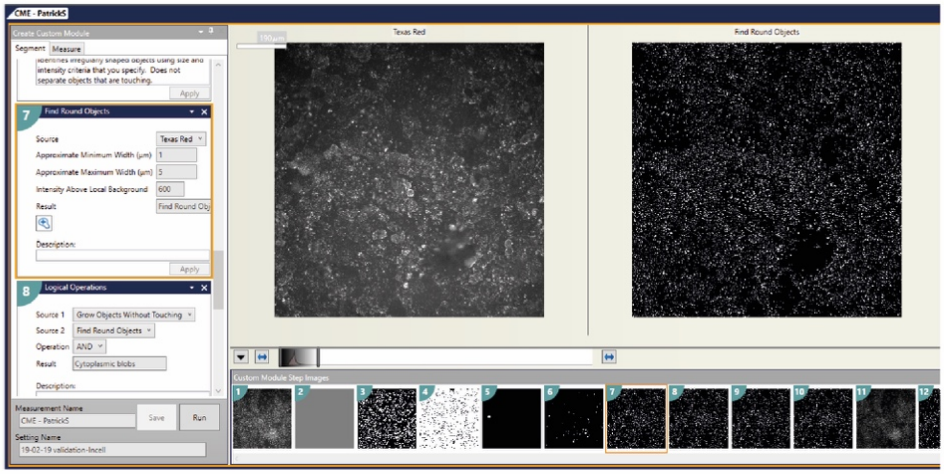

5) Combine masks

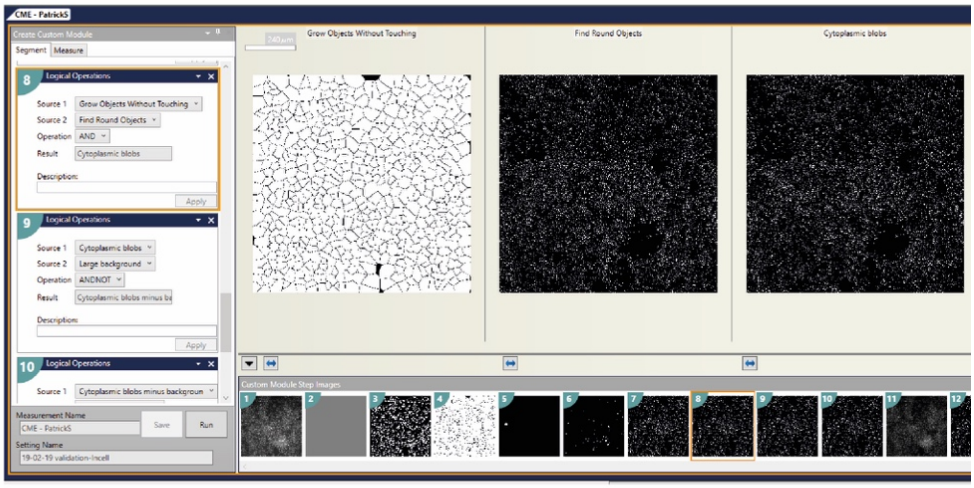

6) Remove background

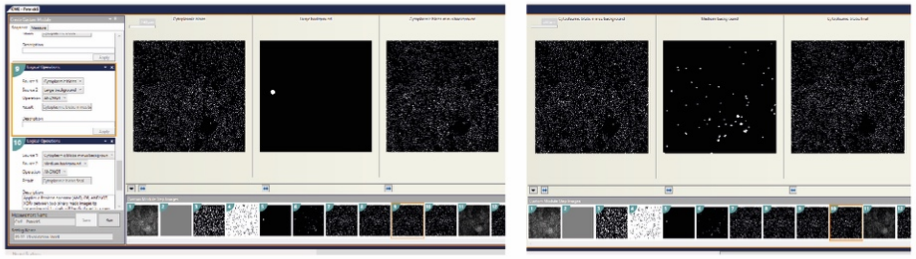

7) Measure Macro-pinosomes per cell

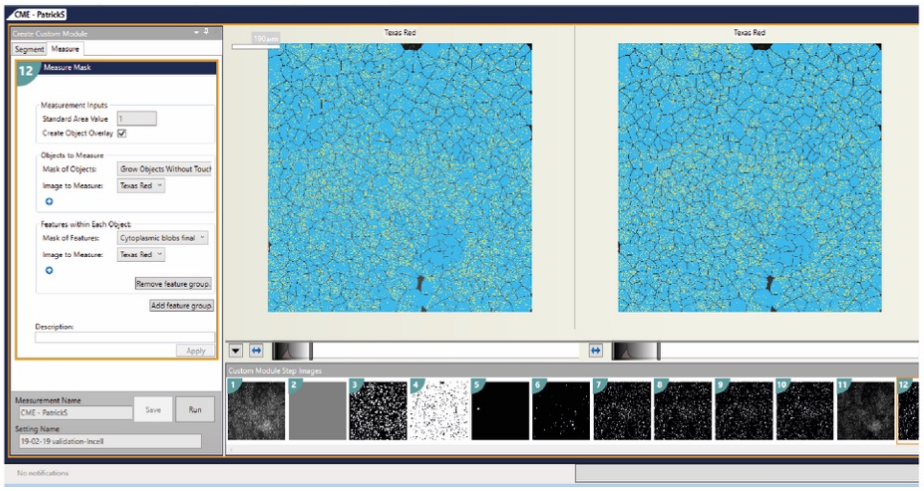

7.3 HRP analysis script-low throughput

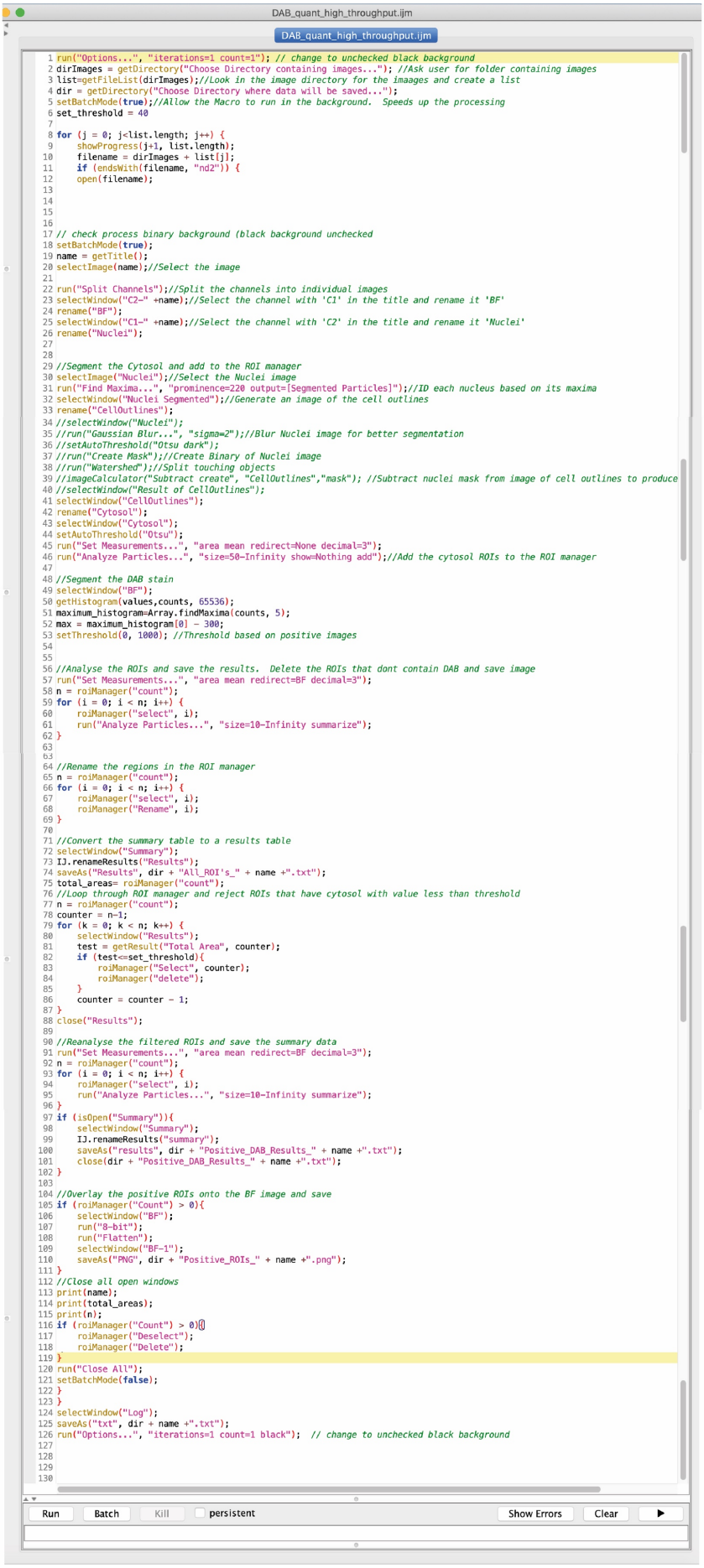


```
run("Options...", "iterations=1 count=1"); // change to unchecked black background
dirImages = getDirectory("Choose Directory containing images..."); //Ask user for folder containing images
list=getFileList(dirImages);//Look in the image directory for the imaages and create a list
dir = getDirectory("Choose Directory where data will be saved...");
setBatchMode(true);//Allow the Macro to run in the background.  Speeds up the processing
set_threshold = 40

for (j = 0; j<list.length; j++) {
    showProgress(j+1, list.length);
    filename = dirImages + list[j];
    if (endsWith(filename, "nd2")) {
    open(filename);



// check process binary background (black background unchecked
setBatchMode(true);
name = getTitle();
selectImage(name);//Select the image

run("Split Channels");//Split the channels into individual images
selectWindow("C2-" +name);//Select the channel with 'C1' in the title and rename it 'BF'
rename("BF");
selectWindow("C1-" +name);//Select the channel with 'C2' in the title and rename it 'Nuclei'
rename("Nuclei");


//Segment the Cytosol and add to the ROI manager
selectImage("Nuclei");//Select the Nuclei image
run("Find Maxima...", "prominence=220 output=[Segmented Particles]");//ID each nucleus based on its maxima
selectWindow("Nuclei Segmented");//Generate an image of the cell outlines
rename("CellOutlines");
//selectWindow("Nuclei");
//run("Gaussian Blur...", "sigma=2");//Blur Nuclei image for better segmentation
//setAutoThreshold("Otsu dark");
//run("Create Mask");//Create Binary of Nuclei image
//run("Watershed");//Split touching objects
//imageCalculator("Subtract create", "CellOutlines","mask"); //Subtract nuclei mask from image of cell outlines to produce
//selectWindow("Result of CellOutlines");
selectWindow("CellOutlines");
rename("Cytosol");
selectWindow("Cytosol");
setAutoThreshold("Otsu");
run("Set Measurements...", "area mean redirect=None decimal=3");
run("Analyze Particles...", "size=50-Infinity show=Nothing add");//Add the cytosol ROIs to the ROI manager

//Segment the DAB stain
selectWindow("BF");
getHistogram(values,counts, 65536);
maximum_histogram=Array.findMaxima(counts, 5);
max = maximum_histogram[0] - 300;
setThreshold(0, 1000); //Threshold based on positive images


//Analyse the ROIs and save the results.  Delete the ROIs that dont contain DAB and save image
run("Set Measurements...", "area mean redirect=BF decimal=3");
n = roiManager("count");
for (i = 0; i < n; i++) {
    roiManager("select", i);
    run("Analyze Particles...", "size=10-Infinity summarize");
}


//Rename the regions in the ROI manager
n = roiManager("count");
for (i = 0; i < n; i++) {
    roiManager("select", i);
    roiManager("Rename", i);
}

//Convert the summary table to a results table
selectWindow("Summary");
IJ.renameResults("Results");
saveAs("Results", dir + "All_ROI's_" + name +".txt");
total_areas= roiManager("count");
//Loop through ROI manager and reject ROIs that have cytosol with value less than threshold
n = roiManager("count");
counter = n-1;
for (k = 0; k < n; k++) {
    selectWindow("Results");
    test = getResult("Total Area", counter);
    if (test<=set_threshold){
        roiManager("Select", counter);
        roiManager("delete");
    }
    counter = counter - 1;
}
close("Results");

//Reanalyse the filtered ROIs and save the summary data
run("Set Measurements...", "area mean redirect=BF decimal=3");
n = roiManager("count");
for (i = 0; i < n; i++) {
    roiManager("select", i);
    run("Analyze Particles...", "size=10-Infinity summarize");
}
if (isOpen("Summary")){
    selectWindow("Summary");
    IJ.renameResults("summary");
    saveAs("results", dir + "Positive_DAB_Results_" + name +".txt");
    close(dir + "Positive_DAB_Results_" + name +".txt");
}

//Overlay the positive ROIs onto the BF image and save
if (roiManager("Count") > 0){
    selectWindow("BF");
    run("8-bit");
    run("Flatten");
    selectWindow("BF-1");
    saveAs("PNG", dir + "Positive_ROIs_" + name +".png");
}
//Close all open windows
print(name);
print(total_areas);
print(n);
if (roiManager("Count") > 0){
    roiManager("Deselect");
    roiManager("Delete");
}
run("Close All");
setBatchMode(false);
}
}
selectWindow("Log");
saveAs("txt", dir + name +".txt");
run("Options...", "iterations=1 count=1 black");  // change to unchecked black background
```

7.4 Macropinocytosis analysis script low throughput

Macropinosome coutnin with dapi save with summary together .ijm

```
macro "batch test [F9]"
  {

dir1 = getDirectory("Choose Source Directory ");
dir2 = getDirectory("Choose Destination Directory ");
list = getFileList(dir1);
setBatchMode(false);

for (i=0; i<list.length; i++) {
showProgress(i+1, list.length);
filename = dir1 + list[i];
if (endsWith(filename, "nd2")) {
open(filename);


IJ.deleteRows(0, 10000);
title = getTitle(); // TRITC
run("RGB Split");
selectImage("C1-"+title);
run("Z Project...", "projection=[Max Intensity]");
run("Duplicate...", " ");
run("8-bit");
run("Subtract Background...", "rolling=50");


run("Threshold...");
setThreshold(220,255);
setOption("BlackBackground", true);
run("Convert to Mask");

run("Fill Holes");
run("Watershed");
run("Create Selection");
run("Add to Manager");
run("Analyze Particles...", "size=0.2-20 circularity=0.00-1.00 show=Masks display clear summarize add slice");

saveAs("TIFF", dir2+list[i]+" mask");

//selectWindow("Summary");
//saveAs("Results", dir2+list[i]+"TRitc.xls");


selectImage("C2-"+title); //dapi image
run("Z Project...", "projection=[Max Intensity]");
run("Duplicate...", " ");
run("8-bit");
run("Auto Threshold", "method=Default white");
run("Fill Holes");
run("Watershed");
run("Analyze Particles...", "size=6-Infinity display clear summarize add");
//selectWindow("Summary");
//saveAs("Results", dir2+list[i]+"DAPI.xls");
roiManager("Delete");
run("Close All");


}
}
selectWindow("Summary");
saveAs("Results", dir2+"Results.xls");
}

}


```

Run | Batch | Kill | persistent | Show Errors | Clear | ▶

Chapter8:References

1. Maxfield FR, McGraw TE. Endocytic recycling. Vol. 5, Nature Reviews Molecular Cell Biology. Nature Publishing Group; 2004. p. 121–32.
2. Lim JP, Gleeson PA. Macropinocytosis: an endocytic pathway for internalising large gulps. Immunol Cell Biol [Internet]. 2011 Nov 22 [cited 2016 Oct 26];89(8):836–43. Available from: http://www.nature.com/doifinder/10.1038/icb.2011.20
3. Varkouhi AK, Scholte M, Storm G, Haisma HJ. Endosomal escape pathways for delivery of biologicals. Vol. 151, Journal of Controlled Release. Elsevier; 2011. p. 220–8.
4. Gurevich E V., Gurevich V V. Therapeutic potential of small molecules and engineered proteins. Handb Exp Pharmacol. 2014;219:1–12.
5. Lönn P, Kacsinta AD, Cui XS, Hamil AS, Kaulich M, Gogoi K, et al. Enhancing Endosomal Escape for Intracellular Delivery of Macromolecular Biologic Therapeutics. Sci Rep. 2016 Sep 8;6.
6. Gilleron J, Querbes W, Zeigerer A, Borodovsky A, Marsico G, Schubert U, et al. Image-based analysis of lipid nanoparticle-mediated siRNA delivery, intracellular trafficking and endosomal escape. Nat Biotechnol [Internet]. 2013 Jul 23 [cited 2021 Jan 19];31(7):638–46. Available from: https://www.nature.com/articles/nbt.2612
7. Swinney DC, Anthony J. How were new medicines discovered? Nat Rev Drug Discov. 2011 Jul 24;10(7):507–19.
8. Sahay G, Querbes W, Alabi C, Eltoukhy A, Sarkar S, Zurenko C, et al. Efficiency of siRNA delivery by lipid nanoparticles is limited by endocytic recycling. Nat Biotechnol. 2013 Jul;31(7):653–8.
9. Gong N, Chen S, Jin S, Zhang J, Wang PC, Liang X-J. Effects of the physicochemical properties of gold nanostructures on cellular internalization. Regen Biomater. 2015;2(4):273.
10. Yang NJ, Hinner MJ. Getting across the cell membrane: an overview for small molecules, peptides, and proteins. Vol. 1266, Methods in molecular biology (Clifton, N.J.). NIH Public Access; 2015. p. 29–53.
11. Lipinski CA, Lombardo F, Dominy BW, Feeney PJ. Experimental and computational approaches to estimate solubility and permeability in drug discovery and development settings. Vol. 23, Advanced Drug Delivery Reviews. Elsevier Science B.V.; 1997. p. 3–25.

12. Imai K, Takaoka A. Comparing antibody and small-molecule therapies for cancer. Nat Rev Cancer [Internet]. 2006 Sep [cited 2016 Dec 2];6(9):714–27. Available from: http://www.nature.com/doifinder/10.1038/nrc1913
13. Gao M, Skolnick J. A Comprehensive Survey of Small-Molecule Binding Pockets in Proteins. Singh M, editor. PLoS Comput Biol [Internet]. 2013 Oct 24 [cited 2020 May 14];9(10):e1003302. Available from: https://dx.plos.org/10.1371/journal.pcbi.1003302
14. Arkin MR, Tang Y, Wells JA. Small-molecule inhibitors of protein-protein interactions: Progressing toward the reality. Vol. 21, Chemistry and Biology. Elsevier Ltd; 2014. p. 1102–14.
15. Hopkins AL, Groom CR. The druggable genome. Nat Rev Drug Discov. 2002;1(9):727–30.
16. Lu RM, Hwang YC, Liu IJ, Lee CC, Tsai HZ, Li HJ, et al. Development of therapeutic antibodies for the treatment of diseases. Vol. 27, Journal of Biomedical Science. BioMed Central Ltd.; 2020. p. 1–30.
17. Liu JKH. The history of monoclonal antibody development - Progress, remaining challenges and future innovations. Vol. 3, Annals of Medicine and Surgery. 2014. p. 113–6.
18. Morrison SL, Johnson MJ, Herzenberg LA, Oi VT. Chimeric human antibody molecules: Mouse antigen-binding domains with human constant region domains. Proc Natl Acad Sci U S A. 1984 Nov 1;81(21 I):6851–5.
19. Antibody therapeutics approved or in regulatory review in the EU or US - The Antibody Society [Internet]. [cited 2020 May 14]. Available from: https://www.antibodysociety.org/resources/approved-antibodies/
20. Klapper LN, Waterman H, Sela M, Yarden Y. Tumor-inhibitory Antibodies to HER-2/ErbB-2 May Act by Recruiting c-Cbl and Enhancing Ubiquitination of HER-2 1. Vol. 60, CANCER RESEARCH. 2000.
21. Weidanz JA, Hildebrand WH. Expanding the targets available to therapeutic antibodies via novel disease-specific markers. Int Rev Immunol. 2011 Oct;30(5–6):312–27.
22. Perera RM, Zoncu R, Johns TG, Pypaert M, Lee F-T, Mellman I, et al. Internalization, intracellular trafficking, and biodistribution of monoclonal antibody 806: a novel anti-epidermal growth factor receptor antibody. Neoplasia [Internet]. 2007 Dec [cited 2016

Dec 1];9(12):1099–110. Available from: http://www.ncbi.nlm.nih.gov/pubmed/18084617

23. Ruggiero FM, Vilcaes AA, Yuki N, Daniotti JL. Membrane binding, endocytic trafficking and intracellular fate of high-affinity antibodies to gangliosides GD1a and GM1. Biochim Biophys Acta - Biomembr. 2017 Jan 1;1859(1):80–93.
24. Meier O, Boucke K, Hammer SV, Keller S, Stidwill RP, Hemmi S, et al. Adenovirus triggers macropinocytosis and endosomal leakage together with its clathrin-mediated uptake. J Cell Biol [Internet]. 2002 Sep 16 [cited 2016 Oct 19];158(6):1119–31. Available from: http://www.ncbi.nlm.nih.gov/pubmed/12221069
25. Wang Y, Huang L. A window onto siRNA delivery. Nat Biotechnol [Internet]. 2013 Jul 9 [cited 2016 Dec 22];31(7):611–2. Available from: http://www.nature.com/doifinder/10.1038/nbt.2634
26. Chames P, Van Regenmortel M, Weiss E, Baty D. Therapeutic antibodies: successes, limitations and hopes for the future. Br J Pharmacol [Internet]. 2009 May [cited 2016 Nov 17];157(2):220–33. Available from: http://www.ncbi.nlm.nih.gov/pubmed/19459844
27. Tanaka T, Rabbitts TH. Intrabodies based on intracellular capture frameworks that bind the RAS protein with high affinity and impair oncogenic transformation. EMBO J. 2003;22(5):1025–35.
28. O'Bryan JP. Pharmacological targeting of RAS: Recent success with direct inhibitors [Internet]. Vol. 139, Pharmacological Research. Academic Press; 2019 [cited 2020 Dec 21]. p. 503–11. Available from: /pmc/articles/PMC6360110/?report=abstract
29. Hillig RC, Sautier B, Schroeder J, Moosmayer D, Hilpmann A, Stegmann CM, et al. Discovery of potent SOS1 inhibitors that block RAS activation via disruption of the RAS–SOS1 interaction. Proc Natl Acad Sci U S A. 2019 Feb 12;116(7):2551–60.
30. Visintin M, Settanni G, Maritan A, Graziosi S, Marks JD, Cattaneo A. The intracellular antibody capture technology (IACT): Towards a consensus sequence for intracellular antibodies. J Mol Biol. 2002 Mar 15;317(1):73–83.
31. Wittrup A, Lieberman J. Knocking down disease: a progress report on siRNA therapeutics. Nat Rev Genet [Internet]. 2015 Aug 18;16:543. Available from: https://doi.org/10.1038/nrg3978
32. Yin H, Kanasty RL, Eltoukhy AA, Vegas AJ, Dorkin JR, Anderson DG. Non-viral vectors for

gene-based therapy. Vol. 15, Nature Reviews Genetics. Nature Publishing Group; 2014. p. 541–55.

33. Kotterman MA, Schaffer D V. Engineering adeno-associated viruses for clinical gene therapy. Nat Rev Genet [Internet]. 2014 [cited 2020 Apr 20];15(7):445–51. Available from: http://www.ema.europa.eu/docs/en_GB/document_library/EPAR_-

34. Bagga S, Bracht J, Hunter S, Massirer K, Holtz J, Eachus R, et al. Regulation by let-7 and lin-4 miRNAs results in target mRNA degradation. Cell. 2005 Aug 16;122(4):553–63.

35. Carthew RW, Sontheimer EJ. Origins and Mechanisms of miRNAs and siRNAs. Vol. 136, Cell. NIH Public Access; 2009. p. 642–55.

36. Fire A, Xu S, Montgomery MK, Kostas SA, Driver SE, Mello CC. Potent and specific genetic interference by double-stranded RNA in caenorhabditis elegans. Nature. 1998 Feb 19;391(6669):806–11.

37. Kanellopoulou C, Muljo SA, Kung AL, Ganesan S, Drapkin R, Jenuwein T, et al. Dicer-deficient mouse embryonic stem cells are defective in differentiation and centromeric silencing. Genes Dev. 2005 Feb 15;19(4):489–501.

38. Rivas F V., Tolia NH, Song JJ, Aragon JP, Liu J, Hannon GJ, et al. Purified Argonaute2 and an siRNA form recombinant human RISC. Nat Struct Mol Biol. 2005 Mar 30;12(4):340–9.

39. Zamecnik PC, Stephenson ML. Inhibition of Rous sarcoma virus replication and cell transformation by a specific oligodeoxynucleotide (tridecamer deoxyribonucleotide/hybridization competitor/hybridon). Vol. 75. 1978.

40. Azad RF, Driver VB, Tanaka K, Crooke RM, Anderson KP. Antiviral activity of a phosphorothioate oligonucleotide complementary to RNA of the human cytomegalovirus major immediate-early region. Antimicrob Agents Chemother. 1993;37(9):1945–54.

41. Layzer JM, McCaffrey AP, Tanner AK, Huang Z, Kay MA, Sullenger BA. In vivo activity of nuclease-resistant siRNAs. RNA. 2004 May 1;10(5):766–71.

42. Bartlett DW, Davis ME. Insights into the kinetics of siRNA-mediated gene silencing from live-cell and live-animal bioluminescent imaging. Nucleic Acids Res. 2006 Jan;34(1):322–33.

43. Chiu YL, Rana TM. siRNA function in RNAi: A chemical modification analysis. RNA. 2003 Sep 1;9(9):1034–48.

44. Morrissey D V., Blanchard K, Shaw L, Jensen K, Lockridge JA, Dickinson B, et al. Activity of stabilized short interfering RNA in a mouse model of hepatitis B virus replication. Hepatology [Internet]. 2005 Jun 1 [cited 2020 May 14];41(6):1349–56. Available from: http://doi.wiley.com/10.1002/hep.20702

45. Morrissey D V., Lockridge JA, Shaw L, Blanchard K, Jensen K, Breen W, et al. Potent and persistent in vivo anti-HBV activity of chemically modified siRNAs. Nat Biotechnol. 2005 Aug;23(8):1002–7.

46. Meng Z, Lu M. RNA interference-induced innate immunity, off-target effect, or immune adjuvant? Vol. 8, Frontiers in Immunology. Frontiers Research Foundation; 2017. p. 331.

47. Nielsen MS, Madsen P, Christensen EI, Nykjær A, Gliemann J, Kasper D, et al. The sortilin cytoplasmic tail conveys Golgi-endosome transport and binds the VHS domain of the GGA2 sorting protein. EMBO J [Internet]. 2001 May 1 [cited 2021 Mar 23];20(9):2180–90. Available from: https://www.embopress.org/doi/full/10.1093/emboj/20.9.2180

48. Stroes ES, Nierman MC, Meulenberg JJ, Franssen R, Twisk J, Henny CP, et al. Intramuscular Administration of AAV1-Lipoprotein Lipase ^{S447X} Lowers Triglycerides in Lipoprotein Lipase–Deficient Patients. Arterioscler Thromb Vasc Biol [Internet]. 2008 Dec [cited 2020 Apr 20];28(12):2303–4. Available from: https://www.ahajournals.org/doi/10.1161/ATVBAHA.108.175620

49. Glybera | European Medicines Agency [Internet]. [cited 2020 Apr 20]. Available from: https://www.ema.europa.eu/en/medicines/human/EPAR/glybera

50. Shahryari A, Jazi MS, Mohammadi S, Nikoo HR, Nazari Z, Hosseini ES, et al. Development and clinical translation of approved gene therapy products for genetic disorders. Vol. 10, Frontiers in Genetics. Frontiers Media S.A.; 2019.

51. Calcedo R, Vandenberghe LH, Gao G, Lin J, Wilson JM. Worldwide Epidemiology of Neutralizing Antibodies to Adeno-Associated Viruses. J Infect Dis [Internet]. 2009 Feb 1 [cited 2020 Apr 20];199(3):381–90. Available from: https://academic.oup.com/jid/article-lookup/doi/10.1086/595830

52. De Jong WH, Borm PJA. Drug delivery and nanoparticles:applications and hazards. Int J Nanomedicine [Internet]. 2008 [cited 2017 Nov 28];3(2):133–49. Available from: http://www.ncbi.nlm.nih.gov/pubmed/18686775

53. Bangham AD, Standish MM, Watkins JC. Diffusion of univalent ions across the lamellae of swollen phospholipids. J Mol Biol. 1965 Aug 1;13(1):238–52.
54. Gregoriadis G. Homing of liposomes to target cells. Biochem Soc Trans. 1975 Oct 1;3(5):613–8.
55. Allen TM. Liposomes. Opportunities in drug delivery. Vol. 54, Drugs. Springer; 1997. p. 8–14.
56. Cullis PR, Mayer LD, Bally MB, Madden TD, Hope MJ. Generating and loading of liposomal systems for drug-delivery applications. Adv Drug Deliv Rev. 1989 May 1;3(3):267–82.
57. Haran G, Cohen R, Bar LK, Barenholz Y. Transmembrane ammonium sulfate gradients in liposomes produce efficient and stable entrapment of amphipathic weak bases. BBA - Biomembr. 1993 Sep 19;1151(2):201–15.
58. Avnir Y, Ulmansky R, Wasserman V, Even-Chen S, Broyer M, Barenholz Y, et al. Amphipathic weak acid glucocorticoid prodrugs remote-loaded into sterically stabilized nanoliposomes evaluated in arthritic rats and in a Beagle dog: A novel approach to treating autoimmune arthritis. Arthritis Rheum [Internet]. 2008 Jan 1 [cited 2020 Apr 22];58(1):119–29. Available from: http://doi.wiley.com/10.1002/art.23230
59. Bulbake U, Doppalapudi S, Kommineni N, Khan W. Liposomal formulations in clinical use: An updated review. Vol. 9, Pharmaceutics. MDPI AG; 2017.
60. Johnston MJW, Edwards K, Karlsson Gör, Cullis PR. Influence of Drug-to-Lipid Ratio on Drug Release Properties and Liposome Integrity in Liposomal Doxorubicin Formulations. J Liposome Res [Internet]. 2008 Jan 9 [cited 2020 Apr 22];18(2):145–57. Available from: http://www.tandfonline.com/doi/full/10.1080/08982100802129372
61. Papahadjopoulos D, Allen TM, Gabizon A, Mayhew E, Matthay K, Huang SK, et al. Sterically stabilized liposomes: Improvements in pharmacokinetics and antitumor therapeutic efficacy. Proc Natl Acad Sci U S A. 1991;88(24):11460–4.
62. Sharrow O, Terry Lee D Leserman WD, Weinstein JN, Blumenthal R. Liposomes to the Murine Myeloma Tumor Mopc Binding of Antigen-Bearing Fluorescent [Internet]. 1979 [cited 2020 Apr 22]. Available from: http://www.jimmunol.org/content/122/
63. Sayers EJ, Peel SE, Schantz A, England RM, Beano M, Bates SM, et al. Endocytic Profiling of Cancer Cell Models Reveals Critical Factors Influencing LNP-Mediated mRNA Delivery and Protein Expression. Mol Ther [Internet]. 2019 Nov 6 [cited 2021 Mar

23];27(11):1950–62. Available from: https://doi.org/10.1016/j.ymthe.2019.07.018.

64. Cullis PR, Hope MJ. Lipid Nanoparticle Systems for Enabling Gene Therapies [Internet]. Vol. 25, Molecular Therapy. American Society of Gene and Cell Therapy; 2017 [cited 2021 Mar 23]. p. 1467–75. Available from: /pmc/articles/PMC5498813/

65. Martins S, Sarmento B, Ferreira DC, Souto EB. Lipid-based colloidal carriers for peptide and protein delivery - Liposomes versus lipid nanoparticles. Vol. 2, International Journal of Nanomedicine. Dove Press; 2007. p. 595–607.

66. Sahay G, Alakhova DY, Kabanov A V. Endocytosis of nanomedicines. Vol. 145, Journal of Controlled Release. NIH Public Access; 2010. p. 182–95.

67. Sahay G, Kim JO, Kabanov A V., Bronich TK. The exploitation of differential endocytic pathways in normal and tumor cells in the selective targeting of nanoparticulate chemotherapeutic agents. Biomaterials. 2010 Feb;31(5):923–33.

68. Presley E, Maxfield FR. Sorting of Membrane Components from Endosomes and Subsequent Recycling to the Cell Surface Occurs by a Bulk Flow Process.

69. Wagner E. Application of membrane-active peptides for nonviral gene delivery. Adv Drug Deliv Rev. 1999 Aug 20;38(3):279–89.

70. Holland JW, Cullis PR, Madden TD. Poly(ethylene glycol)-lipid conjugates promote bilayer formation in mixtures of non-bilayer-forming lipids. Biochemistry. 1996 Feb 27;35(8):2610–7.

71. Ellens H, Bentz J, Szoka FC. H+- and Ca2+-Induced Fusion and Destabilization of Liposomes. Biochemistry. 1985 Jun 1;24(13):3099–106.

72. Hope MJ, Cullis PR. The bilayer stability of inner monolayer lipids from the human erythrocyte. FEBS Lett [Internet]. 1979 Nov 15 [cited 2020 Apr 24];107(2):323–6. Available from: http://doi.wiley.com/10.1016/0014-5793%2879%2980399-3

73. Yatvin MB, Weinstein JN, Dennis WH, Blumenthal R. Design of liposomes for enhanced local release of drugs by hyperthermia. Science (80-). 1978 Dec 22;202(4374):1290–3.

74. Hu Q, Katti PS, Gu Z. Enzyme-responsive nanomaterials for controlled drug delivery. Nanoscale. 2014 Nov 7;6(21):12273–86.

75. Fechheimer M, Boylan JF, Parker S, Sisken JE, Patel GL, Zimmer SG. Transfection of mammalian cells with plasmid DNA by scrape loading and sonication loading. Proc Natl Acad Sci U S A. 1987 Dec 1;84(23):8463–7.

76. Tharkar P, Varanasi R, Wong WSF, Jin CT, Chrzanowski W. Nano-Enhanced Drug

Delivery and Therapeutic Ultrasound for Cancer Treatment and Beyond. Vol. 7, Frontiers in Bioengineering and Biotechnology. Frontiers Media S.A.; 2019.

77. Amstad E, Kohlbrecher J, Müller E, Schweizer T, Textor M, Reimhult E. Triggered release from liposomes through magnetic actuation of iron oxide nanoparticle containing membranes. Nano Lett. 2011 Apr 13;11(4):1664–70.

78. Oliveira RR, Carrião MS, Pacheco MT, Branquinho LC, de Souza ALR, Bakuzis AF, et al. Triggered release of paclitaxel from magnetic solid lipid nanoparticles by magnetic hyperthermia. Mater Sci Eng C. 2018 Nov 1;92:547–53.

79. Gilleron J, Querbes W, Zeigerer A, Borodovsky A, Marsico G, Schubert U, et al. Image-based analysis of lipid nanoparticle-mediated siRNA delivery, intracellular trafficking and endosomal escape. Nat Biotechnol. 2013 Jul 23;31(7):638–46.

80. Huotari J, Helenius A. Endosome maturation. EMBO J [Internet]. 2011 Aug 31 [cited 2016 Oct 26];30(17):3481–500. Available from: http://www.ncbi.nlm.nih.gov/pubmed/21878991

81. Christoforidis S, Miaczynska M, Ashman K, Wilm M, Zhao L, Yip SC, et al. Phosphatidylinositol-3-OH kinases are Rab5 effectors. Nat Cell Biol. 1999 Jul 15;1(4):249–52.

82. Horiuchi H, Lippé R, McBride HM, Rubino M, Woodman P, Stenmark H, et al. A novel Rab5 GDP/GTP exchange factor complexed to Rabaptin-5 links nucleotide exchange to effector recruitment and function. Cell. 1997 Sep 19;90(6):1149–59.

83. Kamentseva R, Kosheverova V, Kharchenko M, Zlobina M, Salova A, Belyaeva T, et al. Functional cycle of EEA1-positive early endosome: Direct evidence for pre-existing compartment of degradative pathway. Marjomaki VS, editor. PLoS One [Internet]. 2020 May 1 [cited 2020 Dec 22];15(5):e0232532. Available from: https://dx.plos.org/10.1371/journal.pone.0232532

84. D KW, McGraw TE, Maxfield FR. Iterative Fractionation of Recycling Receptors from LysosomaUy Destined Ligands in an Early Sorting Endosome.

85. Mayor S, Presley JF, Maxfield FR. Sorting of membrane components from endosomes and subsequent recycling to the cell surface occurs by a bulk flow process. J Cell Biol. 1993;121(6):1257–69.

86. Haglund K, Sigismund S, Polo S, Szymkiewicz I, Di Fiore PP, Dikic I. Multiple monoubiquitination of RTKs is sufficient for their endocytosis and degradation. Nat Cell

Biol. 2003 May 1;5(5):461–6.

87. Haglund K, Dikic I. The role of ubiquitylation in receptor endocytosis and endosomal sorting. Vol. 125, Journal of Cell Science. The Company of Biologists Ltd; 2012. p. 265–75.

88. Poteryaev D, Datta S, Ackema K, Zerial M, Spang A. Identification of the switch in early-to-late endosome transition. Cell. 2010 Apr 30;141(3):497–508.

89. Babst M, Katzmann DJ, Estepa-Sabal EJ, Meerloo T, Emr SD. ESCRT-III: An endosome-associated heterooligomeric protein complex required for MVB sorting. Dev Cell. 2002 Aug 1;3(2):271–82.

90. Balla T. Phosphoinositides: Tiny lipids with giant impact on cell regulation. Vol. 93, Physiological Reviews. 2013. p. 1019–137.

91. McMahon HT, Boucrot E. Molecular mechanism and physiological functions of clathrin-mediated endocytosis. Nat Rev Mol Cell Biol [Internet]. 2011 Jul 22 [cited 2016 Oct 26];12(8):517–33. Available from: http://www.nature.com/doifinder/10.1038/nrm3151

92. Wideman JG, Leung KF, Field MC, Dacks JB. The cell biology of the endocytic system from an evolutionary perspective. Cold Spring Harb Perspect Biol. 2014;6(4).

93. Antonescu CN, Aguet F, Danuser G, Schmid SL. Phosphatidylinositol-(4,5)-bisphosphate regulates clathrin-coated pit initiation, stabilization, and size. Mol Biol Cell. 2011;22(14):2588–600.

94. Pelkmans L. Secrets of caveolae- and lipid raft-mediated endocytosis revealed by mammalian viruses. Vol. 1746, Biochimica et Biophysica Acta - Molecular Cell Research. 2005. p. 295–304.

95. PALADE, GE. The fine structure of blood capillaries. J Appl Phys [Internet]. 1953 [cited 2020 Dec 23];24:1424. Available from: https://ci.nii.ac.jp/naid/10019993056

96. Mirre C, Monlauzeur L, Garcia M, Delgrossi MH, Le Bivic A. Detergent-resistant membrane microdomains from Caco-2 cells do not contain caveolin. Am J Physiol - Cell Physiol [Internet]. 1996 [cited 2020 Dec 23];271(3 40-3). Available from: https://pubmed.ncbi.nlm.nih.gov/8843719/

97. Kovtun O, Tillu VA, Ariotti N, Parton RG, Collins BM. Cavin family proteins and the assembly of caveolae [Internet]. Vol. 128, Journal of Cell Science. Company of Biologists Ltd; 2015 [cited 2021 Mar 24]. p. 1269–78. Available from:

https://jcs.biologists.org/content/128/7/1269

98. Schnitzer JE, Oh P, Pinney E, Allard J. Filipin-sensitive caveolae-mediated transport in endothelium: Reduced transcytosis, scavenger endocytosis, and capillary permeability of select macromolecules. J Cell Biol [Internet]. 1994 Dec 1 [cited 2020 Dec 23];127(5):1217–32. Available from: http://rupress.org/jcb/article-pdf/127/5/1217/1264059/1217.pdf

99. Herreros J, Ng T, Schiavo G. Lipid rafts act as specialized domains for tetanus toxin binding and internalization into neurons. Mol Biol Cell [Internet]. 2001 Oct 13 [cited 2020 Dec 23];12(10):2947–60. Available from: https://www.molbiolcell.org/doi/abs/10.1091/mbc.12.10.2947

100. Shogomori H, Futerman AH. Cholera Toxin is Found in Detergent-insoluble Rafts/Domains at the Cell Surface of Hippocampal Neurons but is Internalized via a Raft-independent Mechanism. J Biol Chem [Internet]. 2001 Mar 23 [cited 2020 Dec 23];276(12):9182–8. Available from: http://www.jbc.org/

101. Anderson HA, Chen Y, Norkin LC. Bound simian virus 40 translocates to caveolin-enriched membrane domains, and its entry is inhibited by drugs that selectively disrupt caveolae. Mol Biol Cell [Internet]. 1996 Oct 13 [cited 2020 Dec 23];7(11):1825–34. Available from: https://www.molbiolcell.org/doi/abs/10.1091/mbc.7.11.1825

102. Swanson JA. Shaping cups into phagosomes and macropinosomes. Vol. 9, Nature Reviews Molecular Cell Biology. 2008. p. 639–49.

103. LEWIS, WH. Pinocytosis. Bull Johns Hopkins Hosp. 1931;49:17–26.

104. Bloomfield G, Kay RR. Uses and abuses of macropinocytosis. J Cell Sci [Internet]. 2016 [cited 2016 Oct 19];129(14):2697–705. Available from: http://www.ncbi.nlm.nih.gov/pubmed/27352861

105. Lim JP, Gleeson PA. Macropinocytosis: an endocytic pathway for internalising large gulps. Immunol Cell Biol [Internet]. 2011 Nov 22 [cited 2016 Oct 3];89(8):836–43. Available from: http://www.nature.com/doifinder/10.1038/icb.2011.20

106. Liu Z, Roche PA. Macropinocytosis in phagocytes: regulation of MHC class-II-restricted antigen presentation in dendritic cells. Front Physiol [Internet]. 2015 [cited 2016 Oct 19];6:1. Available from: http://www.ncbi.nlm.nih.gov/pubmed/25688210

107. Haigler HT, McKanna JA, Cohen S. Rapid stimulation of pinocytosis in human carcinoma cells A-431 by epidermal growth factor. J Cell Biol. 1979;83(1):82–90.

108. Yoshida S, Gaeta I, Pacitto R, Krienke L, Alge O, Gregorka B, et al. Differential signaling during macropinocytosis in response to M-CSF and PMA in macrophages. Front Physiol [Internet]. 2015 [cited 2018 Mar 28];6(JAN):8. Available from: http://www.ncbi.nlm.nih.gov/pubmed/25688212
109. Bloomfield G, Traynor D, Sander SP, Veltman DM, Pachebat JA, Kay RR. Neurofibromin controls macropinocytosis and phagocytosis in Dictyostelium. Elife. 2015 Mar 27;2015(4).
110. Buccione R, Orth JD, McNiven MA. Foot and mouth: Podosomes, invadopodia and circular dorsal ruffles. Vol. 5, Nature Reviews Molecular Cell Biology. 2004. p. 647–57.
111. Bernitt E, Koh CG, Gov N, Döbereiner HG. Dynamics of actin waves on patterned substrates: A quantitative analysis of circular dorsal ruffles. PLoS One [Internet]. 2015;10(1). Available from: http://www.
112. Hoon J-L, Wong W-K, Koh C-G. Functions and Regulation of Circular Dorsal Ruffles. Mol Cell Biol. 2012 Nov 1;32(21):4246–57.
113. Orth JD, Krueger EW, Weller SG, McNiven MA. A novel endocytic mechanism of epidermal growth factor receptor sequestration and internalization. Cancer Res. 2006 Apr 1;66(7):3603–10.
114. Legg JA, Bompard G, Dawson J, Morris HL, Andrew N, Cooper L, et al. N-WASP involvement in dorsal ruffle formation in mouse embryonic fibroblasts. Mol Biol Cell. 2007 Feb;18(2):678–87.
115. Suetsugu S, Yamazaki D, Kurisu S, Takenawa T. Differential roles of WAVE1 and WAVE2 in dorsal and peripheral ruffle formation for fibroblast cell migration. Dev Cell. 2003 Oct 1;5(4):595–609.
116. Egami Y, Taguchi T, Maekawa M, Arai H, Araki N. Small GTPases and phosphoinositides in the regulatory mechanisms of macropinosome formation and maturation: Gtpases and phosphoinositides in macropinocytosis [Internet]. Vol. 5, Frontiers in Physiology. 2014 [cited 2019 Oct 9]. p. 374. Available from: http://www.ncbi.nlm.nih.gov/pubmed/25324782
117. Terebiznik MR, Vieira O V., Marcus SL, Slade A, Yips CM, Trimble WS, et al. Elimination of host cell Ptdlns(4, 5)P2 by bacterial SigD promotes membrane fission during invasion by Salmonella. Nat Cell Biol [Internet]. 2002 [cited 2021 Jan 15];4(10):766–73. Available from: https://pubmed.ncbi.nlm.nih.gov/12360287/

118. Yoshida S, Gaeta I, Pacitto R, Krienke L, Alge O, Gregorka B, et al. Differential signaling during macropinocytosis in response to M-CSF and PMA in macrophages. Front Physiol [Internet]. 2015 [cited 2016 Nov 3];6:8. Available from: http://www.ncbi.nlm.nih.gov/pubmed/25688212
119. Erami Z, Khalil BD, Salloum G, Yao Y, LoPiccolo J, Shymanets A, et al. -----Rac1-Stimulated Macropinocytosis Enhances GbetaUpsilon Activation of PI3Kbeta. Biochem J [Internet]. 2017 Dec 1 [cited 2017 Dec 4];474(23):3903–14. Available from: http://www.ncbi.nlm.nih.gov/pubmed/29046393
120. Porat-Shliom N, Kloog Y, Donaldson JG. A unique platform for H-ras signaling involving clathrin-independent endocytosis. Mol Biol Cell. 2008 Mar;19(3):765–75.
121. Welliver TP, Swanson JA. A growth factor signaling cascade confined to circular ruffles in macrophages. Biol Open. 2012 Aug 15;1(8):754–60.
122. West MA, Bretscher MS, Watts C. Distinct endocytotic pathways in epidermal growth factor-stimulated human carcinoma A431 cells. J Cell Biol. 1989;109(6 I):2731–9.
123. Lee SW, Zhang Y, Jung M, Cruz N, Alas B, Commisso C. EGFR-Pak Signaling Selectively Regulates Glutamine Deprivation-Induced Macropinocytosis. Dev Cell. 2019 Aug 5;50(3):381-392.e5.
124. Canton J. Macropinocytosis: New insights into its underappreciated role in innate immune cell surveillance. Vol. 9, Frontiers in Immunology. 2018.
125. Fey P, Kowal AS, Gaudet P, Pilcher KE, Chisholm RL. Protocols for growth and development of Dictyostelium discoideum. Nat Protoc. 2007 Jun 24;2(6):1307–16.
126. Normanno N, De Luca A, Bianco C, Strizzi L, Mancino M, Maiello MR, et al. Epidermal growth factor receptor (EGFR) signaling in cancer. Gene. 2006;366(1):2–16.
127. Park KA, Byun HS, Won M, Yang KJ, Shin S, Piao L, et al. Sustained activation of protein kinase C downregulates nuclear factor-κ B signaling by dissociation of IKK-γ and Hsp90 complex in human colonic epithelial cells. Carcinogenesis [Internet]. 2007;28(1):71–80. Available from: https://academic.oup.com/carcin/article-abstract/28/1/71/2476200
128. Mackay HJ, Twelves CJ. Targeting the protein kinase C family: Are we there yet? [Internet]. Vol. 7, Nature Reviews Cancer. Nature Publishing Group; 2007 [cited 2021 Mar 27]. p. 554–62. Available from: www.nature.com/reviews/cancer
129. Amyere M, Payrastre B, Krause U, Van Der Smissen P, Veithen A, Courtoy PJ. Constitutive macropinocytosis in oncogene-transformed fibroblasts depends on

sequential permanent activation of phosphoinositide 3-kinase and phospholipase C. Mol Biol Cell [Internet]. 2000 [cited 2021 Mar 27];11(10):3453–67. Available from: https://pubmed.ncbi.nlm.nih.gov/11029048/

130. Czikora A, Lundberg DJ, Abramovitz A, Lewin NE, Kedei N, Peach ML, et al. Structural basis for the failure of the C1 domain of ras guanine nucleotide releasing protein 2 (RasGRP2) to bind phorbol ester with high affinity. J Biol Chem [Internet]. 2016 May 20 [cited 2021 Mar 27];291(21):11133–47. Available from: http://www.jbc.org/article/S0021925820408579/fulltext
131. Nakase I, Niwa M, Takeuchi T, Sonomura K, Kawabata N, Koike Y, et al. Cellular uptake of arginine-rich peptides: Roles for macropinocytosis and actin rearrangement. Mol Ther [Internet]. 2004 Dec [cited 2016 Oct 5];10(6):1011–22. Available from: http://www.nature.com/doifinder/10.1016/j.ymthe.2004.08.010
132. Koivusalo M, Welch C, Hayashi H, Scott CC, Kim M, Alexander T, et al. Amiloride inhibits macropinocytosis by lowering submembranous pH and preventing Rac1 and Cdc42 signaling. J Cell Biol. 2010;188(4).
133. Kim GHE, Dayam RM, Prashar A, Terebiznik M, Botelho RJ. PIKfyve inhibition interferes with phagosome and endosome maturation in macrophages. Traffic [Internet]. 2014 Oct 1 [cited 2020 Mar 23];15(10):1143–63. Available from: http://doi.wiley.com/10.1111/tra.12199
134. Lim JP, Gleeson PA. Macropinocytosis: An endocytic pathway for internalising large gulps. Vol. 89, Immunology and Cell Biology. 2011. p. 836–43.
135. Racoosin EL, Swanson JA. Macrophage colony-stimulating factor (rM-CSF) stimulates pinocytosis in bone marrow-derived macrophages. J Exp Med. 1989;170(5):1635–48.
136. Racoosin EL, Swanson JA. Macropinosome maturation and fusion with tubular lysosomes in macrophages. J Cell Biol. 1993;121(5):1011–20.
137. Hamasaki M, Araki N, Hatae T. Association of Early Endosomal Autoantigen 1 with Macropinocytosis in EGF-Stimulated A431 Cells. Anat Rec - Part A Discov Mol Cell Evol Biol [Internet]. 2004 Apr 1 [cited 2020 Mar 23];277(2):298–306. Available from: http://doi.wiley.com/10.1002/ar.a.20027
138. Kerr MC, Lindsay MR, Luetterforst R, Hamilton N, Simpson F, Parton RG, et al. Visualisation of macropinosome maturation by the recruitment of sorting nexins. J Cell Sci. 2006 Oct 1;119(19):3967–80.

139. Buckley CM, Gopaldass N, Bosmani C, Johnston SA, Soldati T, Insall RH, et al. WASH drives early recycling from macropinosomes and phagosomes to maintain surface phagocytic receptors. Proc Natl Acad Sci U S A. 2016 Oct 4;113(40):E5906–15.
140. Buckley CM, King JS. Drinking problems: mechanisms of macropinosome formation and maturation [Internet]. Vol. 284, FEBS Journal. 2017 [cited 2017 Dec 4]. p. 3778–90. Available from: http://doi.wiley.com/10.1111/febs.14115
141. Kaczmarek JC, Kowalski PS, Anderson DG. Advances in the delivery of RNA therapeutics: from concept to clinical reality.
142. Xitong D, Xiaorong Z. Targeted therapeutic delivery using engineered exosomes and its applications in cardiovascular diseases. Vol. 575, Gene. Elsevier B.V.; 2016. p. 377–84.
143. Fawell S, Seery J, Daikh Y, Moore C, Chen LL, Pepinsky B, et al. Tat-mediated delivery of heterologous proteins into cells. Vol. 91. 1994.
144. Lord JM, Smith DC, Roberts LM. Toxin entry: How bacterial proteins get into mammalian cells [Internet]. Vol. 1, Cellular Microbiology. Blackwell Publishing Ltd.; 1999 [cited 2020 Apr 29]. p. 85–91. Available from: http://doi.wiley.com/10.1046/j.1462-5822.1999.00015.x
145. Tortorella D, Sesardic D, Dawes CS, London E. Immunochemical Analysis of the Structure of Diphtheria Toxin Shows All Three Domains Undergo Structural Changes at Low pH* [Internet]. 1995 [cited 2020 Apr 29]. Available from: http://www.jbc.org/
146. Hazes B, Read RJ. Accumulating evidence suggests that several AB-toxins subvert the endoplasmic reticulum-associated protein degradation pathway to enter target cells. Vol. 36, Biochemistry. American Chemical Society ; 1997. p. 11051–4.
147. Harburger DS, Calderwood DA. Integrin signalling at a glance. J Cell Sci. 2008;122(2).
148. Meier O, Greber UF. Adenovirus endocytosis. J Gene Med [Internet]. 2004 Feb [cited 2016 Nov 14];6(S1):S152–63. Available from: http://doi.wiley.com/10.1002/jgm.553
149. Green M, Loewenstein PM. Autonomous functional domains of chemically synthesized human immunodeficiency virus tat trans-activator protein. Cell. 1988 Dec 23;55(6):1179–88.
150. Frankel AD, Pabo CO. Cellular uptake of the tat protein from human immunodeficiency virus. Cell. 1988 Dec 23;55(6):1189–93.
151. Mishra A, Gordon VD, Yang L, Coridan R, Wong GCL. HIV TAT Forms Pores in Membranes by Inducing Saddle-Splay Curvature: Potential Role of Bidentate Hydrogen

Bonding. Angew Chemie Int Ed [Internet]. 2008 Apr 7 [cited 2020 Apr 28];47(16):2986–9. Available from: http://doi.wiley.com/10.1002/anie.200704444

152. Herce HD, Garcia AE. Molecular dynamics simulations suggest a mechanism for translocation of the HIV-1 TAT peptide across lipid membranes. Vol. 26, PNAS December. 2007.

153. Habault J, Poyet JL. Recent advances in cell penetrating peptide-based anticancer therapies. Molecules. 2019;24(5).

154. Luisoni S, Suomalainen M, Boucke K, Tanner LB, Wenk MR, Guan XL, et al. Co-option of membrane wounding enables virus penetration into cells. Cell Host Microbe [Internet]. 2015 Jul 8 [cited 2018 Feb 12];18(1):75–85. Available from: https://www.sciencedirect.com/science/article/pii/S1931312815002541?via%3Dihub#bib61

155. Akishiba M, Takeuchi T, Kawaguchi Y, Sakamoto K, Yu HH, Nakase I, et al. Cytosolic antibody delivery by lipid-sensitive endosomolytic peptide. Nat Chem [Internet]. 2017 May 22 [cited 2017 Nov 30];9(8):751–61. Available from: http://www.ncbi.nlm.nih.gov/pubmed/28754944

156. Patel S, Ryals RC, Weller KK, Pennesi ME, Sahay G. Lipid nanoparticles for delivery of messenger RNA to the back of the eye. J Control Release. 2019 Jun 10;303:91–100.

157. Shi B, Abrams M. Technologies for investigating the physiological barriers to efficient lipid nanoparticle-siRNA delivery [Internet]. Vol. 61, Journal of Histochemistry and Cytochemistry. Histochemical Society; 2013 [cited 2020 Dec 23]. p. 407–20. Available from: /pmc/articles/PMC3715328/?report=abstract

158. Puri A, Loomis K, Smith B, Lee JH, Yavlovich A, Heldman E, et al. Lipid-based nanoparticles as pharmaceutical drug carriers: From concepts to clinic. Vol. 26, Critical Reviews in Therapeutic Drug Carrier Systems. Begell House Inc.; 2009. p. 523–80.

159. Dunlap DD, Maggi A, Soria MR, Monaco L. Nanoscopic structure of DNA condensed for gene delivery. Vol. 25, Nucleic Acids Research. Oxford University Press; 1997.

160. Rejman J, Bragonzi A, Conese M. Role of clathrin- and caveolae-mediated endocytosis in gene transfer mediated by lipo- and polyplexes. Mol Ther. 2005 Sep 1;12(3):468–74.

161. von Gersdorff K, Sanders NN, Vandenbroucke R, De Smedt SC, Wagner E, Ogris M. The Internalization Route Resulting in Successful Gene Expression Depends on both Cell Line and Polyethylenimine Polyplex Type. Mol Ther. 2006 Nov 1;14(5):745–53.

162. Vermeulen LMP, De Smedt SC, Remaut K, Braeckmans K. The proton sponge hypothesis: Fable or fact? 2018 [cited 2020 May 5]; Available from: https://doi.org/10.1016/j.ejpb.2018.05.034
163. Haensler J, Szoka FC. Polyamidoamine Cascade Polymers Mediate Efficient Transfection of Cells in Culture. Bioconjug Chem. 1993 Sep 1;4(5):372–9.
164. Behr JP. The proton sponge: A trick to enter cells the viruses did not exploit. In: Chimia. 1997.
165. Tang MX, Redemann CT, Szoka FC. In vitro gene delivery by degraded polyamidoamine dendrimers. Bioconjug Chem. 1996 Nov;7(6):703–14.
166. Benjaminsen R V., Mattebjerg MA, Henriksen JR, Moghimi SM, Andresen TL. The possible "proton sponge " effect of polyethylenimine (PEI) does not include change in lysosomal pH. Mol Ther. 2013;21(1):149–57.
167. Sonawane ND, Szoka FC, Verkman AS. Chloride Accumulation and Swelling in Endosomes Enhances DNA Transfer by Polyamine-DNA Polyplexes. J Biol Chem. 2003 Nov 7;278(45):44826–31.
168. Lu Y, Xiong X, Helm A, Kimani K, Bragin A, Skach WR. Co- and posttranslational translocation mechanisms direct cystic fibrosis transmembrane conductance regulator N terminus transmembrane assembly. J Biol Chem. 1998 Jan 2;273(1):568–76.
169. Mothes W, Prehn S, Rapoport TA. Systematic probing of the environment of a translocating secretory protein during translocation through the ER membrane. EMBO J [Internet]. 1994 Sep [cited 2020 Jun 9];13(17):3973–82. Available from: http://doi.wiley.com/10.1002/j.1460-2075.1994.tb06713.x
170. Qi L, Tsai B, Arvan P. New Insights into the Physiological Role of Endoplasmic Reticulum-Associated Degradation. Vol. 27, Trends in Cell Biology. Elsevier Ltd; 2017. p. 430–40.
171. Römisch K. A Case for Sec61 Channel Involvement in ERAD. Vol. 42, Trends in Biochemical Sciences. Elsevier Ltd; 2017. p. 171–9.
172. Nowakowska-Gołacka J, Sominka H, Sowa-Rogozińska N, Słomińska-Wojewódzka M. Toxins utilize the endoplasmic reticulum-associated protein degradation pathway in their intoxication process. Vol. 20, International Journal of Molecular Sciences. MDPI AG; 2019.
173. Norbury CC, Hewlett LJ, Prescott AR, Shastri N, Watts C. œ. Immunity [Internet]. 1995 Dec 1 [cited 2018 Nov 22];3(6):783–91. Available from:

https://www.sciencedirect.com/science/article/pii/1074761395900675?via%3Dihub

174. Yoshimura S, Bondeson J, Foxwell BMJ, Brennan FM, Feldmann M. Effective antigen presentation by dendritic cells is NF-κB dependent: coordinate regulation of MHC, co-stimulatory molecules and cytokines. Vol. 13, International Immunology. 2001.

175. Gros M, Amigorena S. Regulation of antigen export to the cytosol during cross-presentation. Vol. 10, Frontiers in Immunology. Frontiers Media S.A.; 2019.

176. Wieczorek M, Abualrous ET, Sticht J, Álvaro-Benito M, Stolzenberg S, Noé F, et al. Major histocompatibility complex (MHC) class I and MHC class II proteins: Conformational plasticity in antigen presentation. Vol. 8, Frontiers in Immunology. Frontiers Research Foundation; 2017. p. 292.

177. Agrawal S, Reemtsma K, Bagiella E, Oluwole SF, Braunstein NS. Role of TAP-1 and/or TAP-2 antigen presentation defects in tumorigenicity of mouse melanoma. Cell Immunol. 2004 Apr 1;228(2):130–7.

178. Hewitt EW. The MHC class I antigen presentation pathway: Strategies for viral immune evasion. Vol. 110, Immunology. Wiley-Blackwell; 2003. p. 163–9.

179. ten Broeke T, Wubbolts R, Stoorvogel W. MHC class II antigen presentation by dendritic cells regulated through endosomal sorting. Cold Spring Harb Perspect Biol. 2013 Dec;5(12).

180. Kato Y, Kajiwara C, Ishige I, Mizukami S, Yamazaki C, Eikawa S, et al. HSP70 and HSP90 Differentially Regulate Translocation of Extracellular Antigen to the Cytosol for Cross-Presentation. Artic ID. 2012;2012.

181. Singh R, Cresswell P. Defective cross-presentation of viral antigens in GILT-free mice. Science (80-). 2010 Jun 11;328(5984):1394–8.

182. Ackerman AL, Giodini A, Cresswell P. A Role for the Endoplasmic Reticulum Protein Retrotranslocation Machinery during Crosspresentation by Dendritic Cells. Immunity. 2006 Oct 1;25(4):607–17.

183. Zehner M, Marschall AL, Bos E, Schloetel JG, Kreer C, Fehrenschild D, et al. The Translocon Protein Sec61 Mediates Antigen Transport from Endosomes in the Cytosol for Cross-Presentation to CD8+ T Cells. Immunity. 2015 May 19;42(5):850–63.

184. Grotzke JE, Kozik P, Morel JD, Impens F, Pietrosemoli N, Cresswell P, et al. Sec61 blockade by mycolactone inhibits antigen cross-presentation independently of endosome-to-cytosol export. Proc Natl Acad Sci U S A. 2017 Jul 18;114(29):E5910–9.

185. Ye Y, Meyer HH, Rapoport TA. Function of the p97-Ufd1-Npl4 complex in retrotranslocation from the ER to the cytosol: Dual recognition of nonubiquitinated polypeptide segments and polyubiquitin chains. J Cell Biol. 2003 Jul 7;162(1):71–84.
186. Ackerman AL, Giodini A, Cresswell P. A Role for the Endoplasmic Reticulum Protein Retrotranslocation Machinery during Crosspresentation by Dendritic Cells. Immunity. 2006 Oct 1;25(4):607–17.
187. Dingjan I, Verboogen DRJ, Paardekooper LM, Revelo NH, Sittig SP, Visser LJ, et al. Lipid peroxidation causes endosomal antigen release for cross-presentation. Sci Rep. 2016 Feb 24;6(1):1–12.
188. Dingjan I, Paardekooper LM, Verboogen DRJ, von Mollard GF, ter Beest M, van den Bogaart G. VAMP8-mediated NOX2 recruitment to endosomes is necessary for antigen release. Eur J Cell Biol. 2017 Oct 1;96(7):705–14.
189. Wong-Ekkabut J, Xu Z, Triampo W, Tang IM, Tieleman DP, Monticelli L. Effect of lipid peroxidation on the properties of lipid bilayers: A molecular dynamics study. Biophys J. 2007 Dec 15;93(12):4225–36.
190. Zehner M, Chasan AI, Schuette V, Embgenbroich M, Quast T, Kolanus W, et al. Mannose receptor polyubiquitination regulates endosomal recruitment of p97 and cytosolic antigen translocation for cross-presentation. Proc Natl Acad Sci U S A. 2011 Jun 14;108(24):9933–8.
191. Skowyra ML, Schlesinger PH, Naismith T V., Hanson PI. Triggered recruitment of ESCRT machinery promotes endolysosomal repair. Science (80-). 2018 Apr 6;360(6384).
192. Akishiba M, Takeuchi T, Kawaguchi Y, Sakamoto K, Yu HH, Nakase I, et al. Cytosolic antibody delivery by lipid-sensitive endosomolytic peptide. Nat Chem [Internet]. 2017 May 22 [cited 2017 Nov 24];9(8):751–61. Available from: http://www.nature.com/doifinder/10.1038/nchem.2779
193. Rust A, Hassan HHA, Sedelnikova S, Niranjan D, Hautbergue G, Abbas SA, et al. Two complementary approaches for intracellular delivery of exogenous enzymes. Sci Rep. 2015 Jul 24;5.
194. Sayers EJ, Peel SE, Schantz A, England RM, Beano M, Bates SM, et al. Endocytic Profiling of Cancer Cell Models Reveals Critical Factors Influencing LNP-Mediated mRNA Delivery and Protein Expression. Mol Ther [Internet]. 2019 Nov 6 [cited 2021 Mar 25];27(11):1950–62. Available from: https://doi.org/10.1016/j.ymthe.2019.07.018.

195. D'Astolfo DS, Pagliero RJ, Pras A, Karthaus WR, Clevers H, Prasad V, et al. Efficient intracellular delivery of native proteins. Cell. 2015 Apr 23;161(3):674–90.
196. Cabantous S, Waldo GS. In vivo and in vitro protein solubility assays using split GFP. Nat Methods [Internet]. 2006 Oct [cited 2021 Mar 29];3(10):845–54. Available from: https://pubmed.ncbi.nlm.nih.gov/16990817/
197. Cabantous S, Terwilliger TC, Waldo GS. Protein tagging and detection with engineered self-assembling fragments of green fluorescent protein. Nat Biotechnol [Internet]. 2005 Jan 1 [cited 2021 Mar 29];23(1):102–7. Available from: https://www.nature.com/articles/nbt1044
198. Singh B, Carpenter G, Coffey RJ. EGF receptor ligands: Recent advances [version 1; referees: 3 approved]. Vol. 5, F1000Research. Faculty of 1000 Ltd; 2016.
199. Ferguson KM, Berger MB, Mendrola JM, Cho HS, Leahy DJ, Lemmon MA. EGF activates its receptor by removing interactions that autoinhibit ectodomain dimerization. Mol Cell. 2003 Feb 1;11(2):507–17.
200. Olayioye MA, Neve RM, Lane HA. The ErbB signaling network: heterodimerization in development and cancer. EMBO J [Internet]. 2000 [cited 2020 Jun 12];19(13):3159. Available from: http://www.pubmedcentral.nih.gov/articlerender.fcgi?artid=313958&tool=pmcentrez&rendertype=abstract
201. Jones JT, Akita RW, Sliwkowski MX. Binding specificities and affinities of egf domains for ErbB receptors. FEBS Lett. 1999 Mar 26;447(2–3):227–31.
202. Oda K, Matsuoka Y, Funahashi A, Kitano H. A comprehensive pathway map of epidermal growth factor receptor signaling. Mol Syst Biol. 2005 Jan;1(1):2005.0010.
203. Karunagaran D, Tzahar E, Beerli RR, Chen X, Graus-Porta D, Ratzkin BJ, et al. ErbB-2 is a common auxiliary subunit of NDF and EGF receptors: implications for breast cancer. EMBO J. 1996 Jan;15(2):254–64.
204. Ben-Levy R, Paterson HF, Marshall CJ, Yarden Y. A single autophosphorylation site confers oncogenicity to the Neu/ErbB-2 receptor and enables coupling to the MAP kinase pathway. EMBO J. 1994;13(14):3302–11.
205. Orth JD, Krueger EW, Weller SG, McNiven MA. A novel endocytic mechanism of epidermal growth factor receptor sequestration and internalization. Cancer Res. 2006 Apr 1;66(7):3603–10.

206. Tanaka T, Zhou Y, Ozawa T, Okizono R, Banba A, Yamamura T, et al. Ligand-activated epidermal growth factor receptor (EGFR) signaling governs endocytic trafficking of unliganded receptor monomers by non-canonical phosphorylation. J Biol Chem. 2018 Feb 16;293(7):2288–301.
207. Swanson JA. Phorbol esters stimulate macropinocytosis and solute flow through macrophages. J Cell Sci [Internet]. 1989 Sep [cited 2017 Nov 14];94 (Pt 1):135–42. Available from: http://www.ncbi.nlm.nih.gov/pubmed/2613767
208. Sun SC, Chang JH, Jin J. Regulation of nuclear factor-κB in autoimmunity. Vol. 34, Trends in Immunology. 2013. p. 282–9.
209. Liu T, Zhang L, Joo D, Sun SC. NF-κB signaling in inflammation. Vol. 2, Signal Transduction and Targeted Therapy. Springer Nature; 2017.
210. Napetschnig J, Wu H. Molecular Basis of NF-κB Signaling. Annu Rev Biophys [Internet]. 2013 [cited 2020 May 6];42(1):443–68. Available from: www.annualreviews.org
211. Sun L, Carpenter G. Epidermal growth factor activation of NF-κB is mediated through IκBα degradation and intracellular free calcium. Oncogene [Internet]. 1998 [cited 2020 May 8];16(16):2095–102. Available from: http://www.stockton-press.co.uk/onc
212. Jiang T, Grabiner B, Zhu Y, Jiang C, Li H, You Y, et al. CARMA3 is crucial for EGFR-induced activation of NF-κB and tumor progression. Cancer Res [Internet]. 2011 [cited 2020 May 8];71(6):2183–92. Available from: http://cancerres.aacrjournals.org/
213. Sun L, Carpenter G. Epidermal growth factor activation of NF-kB is mediated through IkBa degradation and intracellular free calcium [Internet]. 1998 [cited 2020 May 7]. Available from: http://www.stockton-press.co.uk/onc
214. Zandi E, Rothwarf DM, Delhase M, Hayakawa M, Karin M. The IκB kinase complex (IKK) contains two kinase subunits, IKKα and IKKβ, necessary for Iκb phosphorylation and NF-κB activation. Cell. 1997 Oct 17;91(2):243–52.
215. Pai S, Thomas R. Immune deficiency or hyperactivity-Nf-κb illuminates autoimmunity. J Autoimmun. 2008 Nov 1;31(3):245–51.
216. Wang N, Liang H, Zen K. Molecular mechanisms that influence the macrophage M1-M2 polarization balance. Vol. 5, Frontiers in Immunology. Frontiers Media S.A.; 2014.
217. Scheinman RI, Cogswell PC, Lofquist AK, Baldwin AS. Role of transcriptional activation of IκBα in mediation of immunosuppression by glucocorticoids. Science (80-). 1995 Nov 1;270(5234):283–6.

218. Huxford T, Ghosh G. A structural guide to proteins of the NF-kappaB signaling module. Vol. 1, Cold Spring Harbor perspectives in biology. Cold Spring Harb Perspect Biol; 2009.
219. Senftleben U, Cao Y, Xiao G, Greten FR, Krähn G, Bonizzi G, et al. Activation by IKKα of a second, evolutionary conserved, NF-κB signaling pathway. Science (80-). 2001 Aug 24;293(5534):1495–9.
220. Gilmore TD, Herscovitch M. Inhibitors of NF-κB signaling: 785 and counting. Vol. 25, Oncogene. Nature Publishing Group; 2006. p. 6887–99.
221. Trescher K, Bernecker O, Fellner B, Gyöngyösi M, Krieger S, DeMartin R, et al. Adenovirus-mediated overexpression of inhibitor kappa B-alpha attenuates postinfarct remodeling in the rat heart. Eur J Cardio-thoracic Surg. 2004;
222. Pahl HL. Activators and target genes of Rel/NF-κB transcription factors. Vol. 18, Oncogene. Nature Publishing Group; 1999. p. 6853–66.
223. Lawrence T. The nuclear factor NF-kappaB pathway in inflammation. [Internet]. Vol. 1, Cold Spring Harbor perspectives in biology. 2009 [cited 2020 Jan 8]. Available from: www.cshperspectives.org
224. Brockman JA, Scherer DC, Mckinsey TA, Hall SM, Qi X, Lee WY, et al. Coupling of a Signal Response Domain in IB to Multiple Pathways for NF-B Activation. Vol. 15, MOLECULAR AND CELLULAR BIOLOGY. 1995.
225. Bae YS, Kang SW, Seo MS, Baines IC, Tckle E, Chock PB, et al. Epidermal growth factor (EGF)-induced generation of hydrogen peroxide. Role in EGF receptor-mediated tyrosine phosphorylation. J Biol Chem. 1997 Jan 3;272(1):217–21.
226. Andreakos E, Williams RO, Wales J, Foxwell BM, Feldmann M. Activation of NF-B by the intracellular expression of NF-B-inducing kinase acts as a powerful vaccine adjuvant [Internet]. 2006 [cited 2020 May 8]. Available from: www.pnas.orgcgidoi10.1073pnas.0603493103
227. Koivusalo M, Welch C, Hayashi H, Scott CC, Kim M, Alexander T, et al. Amiloride inhibits macropinocytosis by lowering submembranous pH and preventing Rac1 and Cdc42 signaling. J Cell Biol. 2010;188(4):547–63.
228. Wang JTH, Teasdale RD, Liebl D. Macropinosome quantitation assay. MethodsX. 2014;1(1):36–41.
229. Hamasaki M, Araki N, Hatae T. Association of Early Endosomal Autoantigen 1 With Macropinocytosis in EGF-Stimulated A431 Cells.

230. Welliver TP, Chang SL, Linderman JJ, Swanson JA. Ruffles limit diffusion in the plasma membrane during macropinosome formation. J Cell Sci. 2011;124(23):4106–14.
231. Efremov YM, Dokrunova AA, Bagrov D V., Kudryashova KS, Sokolova OS, Shaitan K V. The effects of confluency on cell mechanical properties. J Biomech. 2013 Apr 5;46(6):1081–7.
232. Meier O, Boucke K, Hammer SV, Keller S, Stidwill RP, Hemmi S, et al. Adenovirus triggers macropinocytosis and endosomal leakage together with its clathrin-mediated uptake. J Cell Biol [Internet]. 2002 Sep 16;158(6):1119 LP – 1131. Available from: http://jcb.rupress.org/content/158/6/1119.abstract
233. van der Want JJ., Klooster J, Nunes Cardozo B, de Weerd H, Liem RS. Tract-tracing in the nervous system of vertebrates using horseradish peroxidase and its conjugates: tracers, chromogens and stabilization for light and electron microscopy. Brain Res Protoc [Internet]. 1997 Aug 1 [cited 2019 Feb 20];1(3):269–79. Available from: https://www.sciencedirect.com/science/article/pii/S1385299X96000426?via%3Dihub
234. Rosene DL, Mesulam MM. Fixation variables in horseradish peroxidase neurohistochemistry. I. The effect of fixation time and perfusion procedures upon enzyme activity. J Histochem Cytochem [Internet]. 1978 Jan 5 [cited 2019 Feb 20];26(1):28–39. Available from: http://www.ncbi.nlm.nih.gov/pubmed/413864
235. Repnik U, Borg Distefano M, Speth MT, Ng MYW, Progida C, Hoflack B, et al. L-leucyl-L-leucine methyl ester does not release cysteine cathepsins to the cytosol but inactivates them in transiently permeabilized lysosomes. J Cell Sci [Internet]. 2017 [cited 2018 Jun 19];130(18):3124–40. Available from: http://jcs.biologists.org/content/joces/early/2017/07/28/jcs.204529.full.pdf
236. Henriksen L, Grandal MV, Knudsen SLJ, van Deurs B, Grøvdal LM. Internalization Mechanisms of the Epidermal Growth Factor Receptor after Activation with Different Ligands. PLoS One. 2013 Mar 5;8(3).
237. Paterson H, Reeves B, Brown R, Hall A, Furth M, Bos J, et al. Activated N-ras controls the transformed phenotype of HT1080 human fibrosarcoma cells. Cell. 1987 Dec 4;51(5):803–12.
238. THE JOURNAL OF HISTOCHEMISTRY AND CYTOcHEMISTRY Letters to the Editor A COLORIMETRIC METHOD FOR MEASUREMENT OF THE. 1973.
239. DAPI (4’,6-Diamidino-2-Phenylindole, Dihydrochloride) [Internet]. [cited 2020 Mar 19].

Available from: https://www.thermofisher.com/order/catalog/product/D1306#/D1306

240. Holm PK, Eker P, Sandvig K, van Deurs B. Phorbol Myristate Acetate Selectively Stimulates Apical Endocytosis via Protein Kinase C in Polarized MDCK Cells. Exp Cell Res. 1995;217(1):157–68.
241. Fan QW, Cheng C, Knight ZA, Haas-Kogan D, Stokoe D, James CD, et al. EGFR signals to mTOR through PKC and independently of Akt in glioma. Sci Signal [Internet]. 2009 Jan 27 [cited 2020 Dec 1];2(55):ra4–ra4. Available from: www.SCIENCESIGNALING.org
242. Zhang Z, Guan N, Li T, Mais DE, Wang M. Quality control of cell-based high-throughput drug screening. Acta Pharm Sin B. 2012 Oct 1;2(5):429–38.
243. Maddox CB, Rasmussen L, White EL. Adapting Cell-Based Assays to the High-Throughput Screening Platform: Problems Encountered and Lessons Learned. J Lab Autom. 2008;13(3):168–73.
244. Lundholt BK, Scudder KM, Pagliaro L. A simple technique for reducing edge effect in cell-based assays. J Biomol Screen [Internet]. 2003 Oct 25 [cited 2020 May 21];8(5):566–70. Available from: http://www.ncbi.nlm.nih.gov/pubmed/14567784
245. What is the difference between siGENOME and ON-TARGETplus siRNA? [Internet]. [cited 2020 Mar 31]. Available from: https://horizondiscovery.com/FAQ/Horizon-Discovery/RNAi-Custom-RNA-Synthesis/siRNA/What-is-the-difference-between-siGENOME-and-ON-TARGETplus-siRNA
246. Shim G, Choi H-W, Lee S, Choi J, Yu YH, Park D-E, et al. Enhanced intrapulmonary delivery of anticancer siRNA for lung cancer therapy using cationic ethylphosphocholine-based nanolipoplexes. Mol Ther [Internet]. 2013 Apr [cited 2016 Dec 2];21(4):816–24. Available from: http://www.ncbi.nlm.nih.gov/pubmed/23380818
247. Sako M, Song F, Okamoto A, Koide H, Dewa T, Oku N, et al. Key determinants of siRNA delivery mediated by unique pH-responsive lipid-based liposomes. Int J Pharm. 2019 Oct 5;569.
248. Liu X, Ghosh D. Intracellular nanoparticle delivery by oncogenic KRAS-mediated macropinocytosis. 2019 [cited 2019 Dec 23]; Available from: http://doi.org/10.2147/IJN.S212861
249. Liu X, Erikson RL. Polo-like kinase (Plk)1 depletion induces apoptosis in cancer cells.

Proc Natl Acad Sci U S A. 2003 May 13;100(10):5789–94.

250. Leung ELH, Luo LX, Liu ZQ, Wong VKW, Lu LL, Xie Y, et al. Inhibition of KRAS-dependent lung cancer cell growth by deltarasin: Blockage of autophagy increases its cytotoxicity article. Cell Death Dis. 2018;9(2).

251. Aits S, Kricker J, Liu B, Ellegaard AM, Hämälistö S, Tvingsholm S, et al. Sensitive detection of lysosomal membrane permeabilization by lysosomal galectin puncta assay. Autophagy. 2015;11(8):1408–24.

252. Paz I, Sachse M, Dupont N, Mounier J, Cederfur C, Enninga J, et al. Galectin-3, a marker for vacuole lysis by invasive pathogens. Cell Microbiol [Internet]. 2010 Apr [cited 2016 Dec 6];12(4):530–44. Available from: http://doi.wiley.com/10.1111/j.1462-5822.2009.01415.x

253. Maier O, Marvin SA, Wodrich H, Campbell EM, Wiethoff CM. Spatiotemporal dynamics of adenovirus membrane rupture and endosomal escape. J Virol [Internet]. 2012 Oct [cited 2016 Dec 6];86(19):10821–8. Available from: http://www.ncbi.nlm.nih.gov/pubmed/22855481

254. Tatake RJ, O'Neill MM, Kennedy CA, Wayne AL, Jakes S, Wu D, et al. Identification of pharmacological inhibitors of the MEK5/ERK5 pathway. Biochem Biophys Res Commun [Internet]. 2008 Dec 5 [cited 2021 Mar 24];377(1):120–5. Available from: https://pubmed.ncbi.nlm.nih.gov/18834865/

255. Jiang T, Grabiner B, Zhu Y, Jiang C, Li H, You Y, et al. Molecular and Cellular Pathobiology CARMA3 is Crucial for EGFR-Induced Activation of NF-kB and Tumor Progression. 2011 [cited 2019 Nov 25]; Available from: http://cancerres.aacrjournals.org/

256. Trask OJ. Nuclear Factor Kappa B (NF-κB) Translocation Assay Development and Validation for High Content Screening [Internet]. Assay Guidance Manual. Eli Lilly & Company and the National Center for Advancing Translational Sciences; 2004 [cited 2020 Dec 8]. Available from: http://www.ncbi.nlm.nih.gov/pubmed/23035273

257. Maier O, Galan DL, Wodrich H, Wiethoff CM. An N-terminal domain of adenovirus protein VI fragments membranes by inducing positive membrane curvature. Virology [Internet]. 2010 Jun 20 [cited 2016 Dec 6];402(1):11–9. Available from: http://www.ncbi.nlm.nih.gov/pubmed/20409568

258. Wickham TJ, Mathias P, Cheresh DA, Nemerow GR. Integrins αvβ3 and αvβ5 promote adenovirus internalization but not virus attachment. Cell [Internet]. 1993 Apr 23 [cited

2020 Nov 2];73(2):309–19. Available from: http://www.cell.com/article/009286749390231E/fulltext

259. Dharmawardhane S, Schurmann A, Sells MA, Chernoff J, Schmid SL, Bokoch GM. Regulation of macropinocytosis by p21-activated kinase-1. Mol Biol Cell [Internet]. 2000 [cited 2020 Nov 11];11(10):3341–52. Available from: /pmc/articles/PMC14996/?report=abstract

260. Naughtin MJ, Sheffield DA, Rahman P, Hughes WE, Gurung R, Stow JL, et al. The myotubularin phosphatase MTMR4 regulates sorting from early endosomes. J Cell Sci [Internet]. 2010 Sep 15 [cited 2020 Nov 11];123(18):3071–83. Available from: https://pubmed.ncbi.nlm.nih.gov/20736309/

261. Hao F, Itoh T, Morita E, Shirahama-Noda K, Yoshimori T, Noda T. The PtdIns3-phosphatase MTMR3 interacts with mTORC1 and suppresses its activity. FEBS Lett [Internet]. 2016 Jan 1 [cited 2020 Nov 11];590(1):161–73. Available from: https://pubmed.ncbi.nlm.nih.gov/26787466/

262. Chang B, Partha S, Hofmann K, Lei M, Goebl M, Harper JW, et al. SKP1 connects cell cycle regulators to the ubiquitin proteolysis machinery through a novel motif, the F-box. Cell [Internet]. 1996 Jul 26 [cited 2020 Nov 11];86(2):263–74. Available from: https://pubmed.ncbi.nlm.nih.gov/8706131/

263. Xiong X, Rao G, Roy RV, Zhang Y, Means N, Dey A, et al. Ubiquitin-binding associated protein 2 regulates KRAS activation and macropinocytosis in pancreatic cancer. FASEB J [Internet]. 2020 Sep 21 [cited 2020 Nov 12];34(9):12024–39. Available from: https://onlinelibrary.wiley.com/doi/10.1096/fj.201902826RR

264. Chang B, Partha S, Hofmann K, Lei M, Goebl M, Harper JW, et al. SKP1 connects cell cycle regulators to the ubiquitin proteolysis machinery through a novel motif, the F-box. Cell. 1996 Jul 26;86(2):263–74.

265. Wang D, Ma L, Wang B, Liu J, Wei W. E3 ubiquitin ligases in cancer and implications for therapies. Cancer Metastasis Rev [Internet]. 2017 Dec 1 [cited 2021 Mar 24];36(4):683–702. Available from: https://pubmed.ncbi.nlm.nih.gov/29043469/

266. Tomas A, Futter CE, Eden ER. EGF receptor trafficking: Consequences for signaling and cancer [Internet]. Vol. 24, Trends in Cell Biology. Elsevier; 2014 [cited 2021 Jan 15]. p. 26–34. Available from: /pmc/articles/PMC3884125/?report=abstract

267. Agosto MA, Ivanovic T, Nibert ML. Mammalian reovirus, a nonfusogenic nonenveloped

virus, forms size-selective pores in a model membrane. Proc Natl Acad Sci U S A [Internet]. 2006 Oct 31 [cited 2020 Nov 21];103(44):16496–501. Available from: /pmc/articles/PMC1637610/?report=abstract

268. Huang P, Cai Y, Zhao B, Cui L. Roles of NUCKS1 in Diseases: Susceptibility, Potential Biomarker, and Regulatory Mechanisms. Vol. 2018, BioMed Research International. Hindawi Limited; 2018.
269. Sorkin A, Krolenko S, Kudrjavtceva N, Lazebnik J, Teslenko L, Soderquist AM, et al. Recycling of Epidermal Growth Factor-Receptor Complexes in A431 Cells: Identification of Dual Pathways.
270. Masui H, Castro L, Mendelsohn J. Consumption of EGF by A431 Cells: Evidence for Receptor Recycling.
271. Macdonald-Obermann JL, Pike LJ. Different epidermal growth factor (EGF) receptor ligands show distinct kinetics and biased or partial agonism for homodimer and heterodimer formation. J Biol Chem [Internet]. 2014 Sep 19 [cited 2020 Nov 25];289(38):26178–88. Available from: /pmc/articles/PMC4176247/?report=abstract
272. Qiu Y, Yu Q, Shi K, Zhang M, Zhou X, Yang Y, et al. Cell-penetrating peptides induce apoptosis and necrosis through specific mechanism and cause impairment of Na+–K+-ATPase and mitochondria. Amino Acids [Internet]. 2017 Jan 1 [cited 2020 Nov 25];49(1):75–88. Available from: https://link.springer.com/article/10.1007/s00726-016-2327-8
273. Longva KE, Blystad FD, Stang E, Larsen AM, Johannessen LE, Madshus IH. Ubiquitination and proteasomal activity is required for transport of the EGF receptor to inner membranes of multivesicular bodies. J Cell Biol [Internet]. 2002 Mar 4 [cited 2020 Nov 26];156(5):843–54. Available from: /pmc/articles/PMC2173306/?report=abstract
274. Nakajima S, Kato H, Takahashi S, Johno H, Kitamura M. Inhibition of NF-κB by MG132 through ER stress-mediated induction of LAP and LIP. FEBS Lett [Internet]. 2011 Jul 21 [cited 2020 Nov 26];585(14):2249–54. Available from: http://doi.wiley.com/10.1016/j.febslet.2011.05.047